UNIVERSITEIT VAN PRETORIA
UNIVERSITY OF PRETORIA
YUNIBESITHI YA PRETORIA

UNIVERSITEIT VAN PRETORIA
UNIVERSITY OF PRETORIA
YUNIBESITHI YA PRETORIA
Department of Materials Science and
Metallurgical Engineering

Sulphidation of Copper Coolers in PGM Smelters

By

BM Thethwayo

A dissertation submitted in partial fulfilment
of the requirements for the degree of

MSc (Applied Sciences) Metallurgy

DEPARTMENT OF MATERIALS SCIENCE AND METALLURGICAL ENGINEERING

University of Pretoria

2010

Abstract

Corrosion problems of copper waffle coolers are experienced in Platinum Group Metals (PGM's) smelting furnaces. The copper cooler wear mechanism was studied through a post-mortem analysis of the refractory corrosion products that were removed from a PGM smelter. Post-mortem samples were characterised using Scanning Electron Microscopy (SEM), X-Ray Fluorescence Spectroscopy (XRF) and X-Ray Powder Diffraction (XRD). On visual inspection of the refractory wall it was observed that at the slag-feed interface the front refractory (mag-chrome) brick was completely corroded and only the freeze lining (frozen slag) formed a barrier between the copper cooler and the feed. At the bottom section of the slag zone the front refractory brick was still intact. Base metal sulphides and element sulphur were the major phases observed at the copper cooler-freeze lining interface while at the copper cooler-front brick interface only covellite (CuS) and element sulphur were observed. It was concluded that wear proceeded through two mechanisms: Reaction of copper with base metal sulphides which infiltrated the freeze lining and gaseous attach of copper by sulphur forming covellite. Front mag-chrome refractory bricks are replaced by graphite blocks in the latest furnace wall designs. A post-mortem graphite block was analysed with SEM, XRD and Inductively Coupled Plasma (ICP) to determine the phases associated with copper cooler corrosion. Base metal sulphides were observed at the copper cooler-graphite block (cold face) interface. Good agreement was found between the phases in the graphite block and the phases in the post-mortem sample where the refractory brick was used.

Laboratory experiments were carried out to determine the effect of corrosive gas composition and copper cooler surface temperature on the corrosion rate and morphology of the corrosion products. Tests were performed on copper foils at temperatures from 80°C to 140°C. Corrosive gases included H_2S, S_2 and S_2 with HCl. It was found that when a copper foil is exposed to sulphur the sulphides that form are covellite at 80°C, covellite and yarrowite (Cu_9S_8) at 110°C, yarrowite and digenite ($Cu_{1.8}S$) at 140°C. Linear corrosion rate behaviour was observed between 80°C and 110°C since the sulphide scales

are not passivating and they poorly adhere to the copper foil. Average corrosion rates of copper foil by sulphur vapour was 54 mm/y at 80°C and 80 mm/y at 110°C, above 112°C the corrosion rate decreased to 5 mm/y. Additions of HCl enhance the corrosion rate at temperatures above the melting point of sulphur (112°C). Chalcocite (Cu_2S) forms when copper is exposed to H_2S. It was concluded that the corrosion rate and the morphology of the corrosion product are functions of temperature and the corrosive gas composition.

Keywords: *sulphidation, copper waffle coolers, PGM smelters, corrosion, graphite block*

Sulphidation of copper coolers in PGM smelters

Table of contents

UNIVERSITEIT VAN PRETORIA
UNIVERSITY OF PRETORIA
YUNIBESITHI YA PRETORIA Sulphidation of copper coolers in PGM smelters

Sulphidation of copper coolers in PGM smelters

List of figures

Sulphidation of copper coolers in PGM smelters

Sulphidation of copper coolers in PGM smelters

Sulphidation of copper coolers in PGM smelters

Sulphidation of copper coolers in PGM smelters

List of tables

Sulphidation of copper coolers in PGM smelters

UNIVERSITEIT VAN PRETORIA
UNIVERSITY OF PRETORIA
YUNIBESITHI YA PRETORIA Sulphidation of copper coolers in PGM smelters

Sulphidation of copper coolers in PGM smelters

Sulphidation of copper coolers in PGM smelters

ACKNOWLEDGMENTS

The author wishes to express her gratitude to the people who made this research a success:

UNIVERSITEIT VAN PRETORIA
UNIVERSITY OF PRETORIA
YUNIBESITHI YA PRETORIA Sulphidation of copper coolers in PGM smelters

1. INTRODUCTION

Corrosion problems of copper coolers are experienced in all platinum group metals (PGMs) smelting furnaces that treat uncalcined concentrates with unstable sulphur [Nelson et al. 2006]. Corrosion is not limited to water-cooled copper coolers; conventional cooled or un-cooled magnesia refractories undergo significant corrosion by different mechanisms. Copper cooler corrosion rates of greater than 60 mm/y were observed on the slag-charge interface level of a PGM smelter [Nelson et al. 2006; Hundermark et al. 2006; Pistorius 2004].

Sulphidation of copper coolers by sulphur gas, coupled with chlorination by HCl gas, was characterised as the main cause of copper cooler corrosion from the analysis of post-mortem refractory samples and thermodynamic calculations [Nelson et al. 2006; Hundermark et al. 2006]. Copper sulphidation is the corrosion of copper by reduced sulphur species such as sulphur liquid, sulphur vapour (S_2) and hydrogen sulphide gas (H_2S) [Larson 2002; Tran et al. 2003]. The evolution of unstable sulphur and chlorides from the feed is expected at the slag-charge interface zone [Nelson et al. 2006]. It is not known how the copper cooler surface temperature and the composition of the corrosive gases affect the corrosion rate and the morphology of the corrosion product.

There are virtually no published data on the mechanism involved in the corrosion of copper coolers in PGM smelters. Data on the phenomenon of corrosion is vital in understanding the wear mechanism of copper coolers and in shaping future cooling system designs.

Prolonging the life of the furnace refractory walls through copper cooling technology is still a challenge (Nelson et al. 2006; Hundermark et al. 2006); however, a graphite block has been installed in recent smelter designs and its efficiency will be highlighted in this work [Van Manen 2008]. The graphite block replaces the front refractory brick, which was lined in front of the copper cooler to protect the copper coolers from the corrosive furnace melt.

The objective of this project was to determine how the surface temperature of the copper cooler and the composition of the corrosive gas affect the copper cooler corrosion rate and morphology of the corrosion product.

Sulphidation of copper coolers in PGM smelters

The first phase of this investigation was the phase chemical analysis of the post-mortem samples collected from a PGM smelter. Detailed analysis of the post-mortem refractory samples is presented in this report and a comparison is made with the sulphide compounds detected on the graphite block that was used in the smelter's latest design. The analysis results of the post-mortem samples formed the basis of the laboratory test work.

The second phase of this investigation was the laboratory test work, which focused on simulating the conditions on the copper cooler surface in order to determine the conditions under which the copper sulphides determined in the post-mortem samples form. The test work included reactions of copper foil with hydrogen sulphide, sulphur vapour, sulphur with HCl additions and sulphur vapour with water vapour addition. Tests were performed at a range of temperatures (80°C to 140°C) and comparisons were made between corrosion rates observed at high and at low temperatures. The morphologies of the corrosion products produced at different temperatures and gas compositions were compared.

This study theorises that when a copper foil is exposed to sulphurous corrosive gases, the rate of corrosion and the phase composition of a corrosion product is a function of temperature. Correlation between temperature and the rate of corrosion of copper were investigated where a copper foil was exposed to corrosive gases such as S_2, H_2S, HCl and water vapour. A quantitative research technique in the form of simulated experiments was used to understand the correlations between these variables.

UNIVERSITEIT VAN PRETORIA
UNIVERSITY OF PRETORIA
YUNIBESITHI YA PRETORIA Sulphidation of copper coolers in PGM smelters

2. BACKGROUND

2.1. Smelter feed

PGMs geologically associate with base metal sulphides such as copper, nickel and iron sulphide [Jones 1999]. There are three main ore deposits in Southern Africa, i.e. Merensky reef, UG2 and Plat reef. Merensky reef and Plat reef are similar in composition, while UG2 has a higher chrome oxide content than the other two ore bodies. A chrome content of more than 1% in the smelter feed causes operational problems such as higher operating temperatures, more viscous slag and PGM losses, which are aggravated by a low level of base metal sulphides (matte), which serve as PGM collector. Consequently, UG2 concentrate is normally blended with Merensky or Plat reef ore to achieve the desired matte output, which has a chrome content of 1% or less [Jones 1999; Cramer 2001; Cramer 2008].

The Merensky reef ore typically consists of 45% pyrrhotite ($Fe_{(1-x)}S$), 36% pentlandite (($Fe,Ni)_9S_8$), 12% chalcopyrite ($CuFeS_2$), 2-4% pyrite (FeS_2) and millerite (NiS) in small amounts [Jones 1999]. Less common base metal sulphides are mackinawate (FeS), vallerite ($Cu_3Fe_4S_7$), cubanite ($CuFe_2S_3$) and pyrite (FeS_2) [Cramer 2001]. UG2 has extremely low amounts of base metal sulphides, especially nickel and copper [Misra 1999, Cramer 2002]. A typical PGM content in a UG2 ore is 3-8 g/t, while Merensky ore has 3-9 g/t PGM [Cramer 2001].

Prior to smelting, the mined PGM-containing ore is milled and treated in floatation cells to upgrade the PGM content of the ore [Jones 1999]. The industrial water and chemical reagents used in the flotation cells and mills may introduce undesirable elements, such as chlorides, to the smelter feed. The smelter feed (PGM concentrate from the floatation cells) is dried in flash driers [Jones 1999] to decrease its moisture content to approximately 0.5% [Mabiza 2006].

Sulphidation of copper coolers in PGM smelters

2.2. Sulphides smelting

For smelting purposes of sulphides, submerged-arc electric furnaces are employed. In a submerged-arc furnace electrodes are buried on the resistive slag such that when the electric current is applied through the electrodes, thermal energy is generated. The concentrate floats on top of the hot resistive slag and melts gradually owing to the high temperatures generated around the electrodes [Fereday 1996; Woollacott et al. 1994].

In sulphide smelting two immiscible fluids, matte and slag, are formed. Typical PGM furnace slag and matte compositions are depicted in Table 1. Matte is composed of the valuable sulphides of copper, nickel, cobalt and iron. These sulphides serve as PGM collector, while the slag is mostly silicates, which are discarded. Silicates of magnesium, iron and calcium form the bulk of a typical furnace slag composition, with minor amounts of alumina and chromium (III) oxide.The matte has higher specific gravity than the slag, which is why separation is achieved by matte settling to the bottom of the furnace and the slag forming a top layer. A layer of concentrate normally floats on top of the slag to maintain a 'black top' [Woollacott et al. 1994].

Table 1: Chemical analysis of a typical PGM smelting furnace slag and matte

	Ni	Cu	Cr_2O_3	FeO	Co	Al_2O_3	MgO	CaO	S	SiO_2	Reference
*Slag	0.3	0.12	2.05	14.74	0.03	4.46	21.05	8.46	0.41	47.64	*Sarvinis et al 1999
Slag	0.07	0.06	2	11	0.001	5	23	5	0.3	52	Hundermark et al. 2006
Matte	15	9	$_{Cr}2^{\#}$	$_{Fe}40^{\#}$	0.35				30		Hundermark et al. 2006
*No corresponding matte composition was reported by Sarvinis et al. 1999. #Cr and Fe are present in the matte as sulphides.											

Typical operating conditions in PGM smelting furnaces are reducing conditions [P_{O_2}~ 9.869x10^{-9} atm] at temperatures of approximately 1550°C [Nell 2004]. The operating temperature depends on the ore that is being treated and ranges from 1550°C to above 1600°C. UG2 ore requires a higher smelting temperature, since it has higher concentrations of MgO, SiO_2, Cr_2O_3, and Al_2O_3 compared to Merensky ore. These compounds are associated with high slag liquidus temperatures. The liquidus temperature of the UG2 slag can

Sulphidation of copper coolers in PGM smelters

exceed 1600°C, while the liquidus temperature of the Merensky slag is typically 1350°C [Jones 1999 and Nell 1994].

2.3. Gases associated with PGM smelting

- Sulphur

Simulations done on the FactSage software (Reaction model) [Dale 2002] indicated that the smelting of base metal sulphides under reducing conditions at 1550°C produces mainly sulphur vapour (Table 2). It was also reported by Andrews (2008) that sulphur vapour is one of the gases which are given off during PGM smelting. Sulphur can also be contained in the raw material as metastable sulphur, which vaporises at 445°C [Andrews 2008]. The FactSage prediction in Table 2 shows that the breaking down of chalcopyrite, pyrite and millerite will give off mainly sulphur vapour as a gaseous species.

Table 2: Predicted reactions of base metal sulphides at 1550°C

Phases in PGM concentrate	Predicted reaction during melting
Pyrrhotite _Fe$_{(1-x)}$ S	$FeS(s) \rightarrow FeS(l)$
Pentlandite _ (Fe,Ni)$_9$S$_8$	$(Fe, Ni)_9 S_8(s) \rightarrow 7Fe(l) + 3Ni_3 S_2 + 2FeS(l)$
Chalcopyrite_CuFeS$_2$	$5CuFeS_2(s) \rightarrow 4FeS(l) + Cu_5 FeS_4(l) + S_2(g)$
Pyrite_FeS$_2$	$FeS_2(s) \rightarrow FeS(l) + \frac{1}{2}S_2(g)$
Millerite _ NiS	$3NiS(s) \rightarrow Ni_3 S_2 + \frac{1}{2}S_2(g)$

- Sulphur dioxide

Above the concentrate layer (freeboard zone) the presence of excess oxygen is expected. Sulphur can react with oxygen to form sulphur dioxide at 260°C (Equation 1). If there is excess oxygen, sulphur trioxide (SO$_3$) can form from the reaction of sulphur dioxide with oxygen (Equation 2) [Patnik 2003].

$$\tfrac{1}{2}S_2(g) + O_2(g) \rightarrow SO_2(g) \qquad\qquad\qquad \textit{Equation 1}$$

$$SO_2(g) + \tfrac{1}{2}O_2(g) \rightarrow SO_3(g) \qquad\qquad\qquad \textit{Equation 2}$$
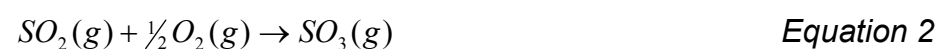
- Water vapour

The feed from the drier potentially has up to 0.5% moisture content, which at high temperature is given off as water vapour [Mabiza 2006]. The water vapour molecules dissociate further to form hydrogen gas and oxygen. The oxygen can react with the concentrate to form the oxides, while hydrogen can react with other gases evolving from the smelting process. An additional amount of water vapour in uncalcined concentrates evolves from thermal decomposition of chemically bound water when the concentrate is exposed to high smelting temperatures [Woollacott 1994].

- Hydrogen sulphide

Hydrogen can react with sulphur at temperatures between 260°C and 350°C to form hydrogen sulphide (Equation 3) [Patnik 2003]. Sulphur dioxide is reduced to sulphur and water when heated with hydrogen sulphide at 300°C (Equation 4) [Patnik 2003]. The reaction of sulphur trioxide and water forms sulphuric acid (Equation 5) [Patnik 2003], therefore the presence of sulphuric acid can be envisaged in the freeboard zone.

$$\tfrac{1}{2}S_2(g) + H_2(g) \rightarrow H_2S(g)$$ *Equation 3*

$$SO_2(g) + 2H_2S(g) \rightarrow \tfrac{3}{2}S_2(g) + 2H_2O(g)$$ *Equation 4*

$$SO_3(g) + H_2O(g) \rightarrow H_2SO_4(g)$$ *Equation 5*
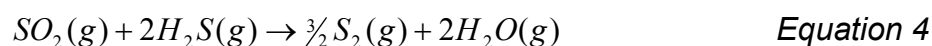
- Hydrogen chloride

The mined ore may contain halides such as $KClMg(SO_4)$ and $KMgCl_3$, which can dissociate and release chlorine gas [Hopt et al. 2006]. Chlorine can react with hydrogen gas to form a hydrogen chloride gas (Equation 6). This reaction is rapid in the presence of light [Patnik 2003]. Chlorine can oxidise hydrogen sulphide to sulphur (Equation 7) [Patnik 2003].

$$Cl_2(g) + H_2(g) \rightarrow 2HCl(g)$$ *Equation 6*

$$Cl_2(g) + H_2S(g) \rightarrow \tfrac{1}{2}S_2 + 2HCl(g)$$ *Equation 7*

Sulphidation of copper coolers in PGM smelters
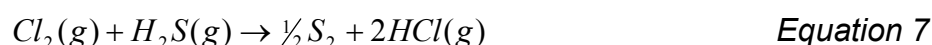
High temperatures associated with the resistive slag drive these gases towards a cooler place, which is in front of the copper coolers [Hopt et al. 2006].

2.4. Smelter cooling system

A typical PGM smelter refractory wall is lined with plate copper coolers in the freeboard zone, the slag zone has refractory bricks at the hot face and the waffle copper cooler at the cold face, while the hearth (containing the matte) is lined with refractory bricks (Figure 1). The cross-section of the furnace refractory wall is shown in Figure 1. The encircled area is the slag/concentrate interface where severe corrosion is typically observed.
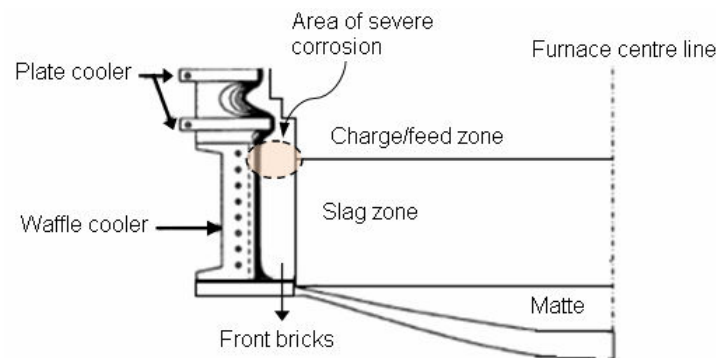
Figure 1: Schematic diagram of the cross-section of the refractory wall [Voermann et al. 1999].

To contain the high temperature melts, the smelter needs intense cooling to facilitate the formation of a frozen layer at the hot face of the refractory wall. Uchechukwu [2000] reported that there are several ways in which the cooling systems protect the furnace refractory wall, namely:
- The cooling system can significantly lower the refractory wall temperatures such that the hot furnace melt may freeze and maintain a residual thickness on the hot face (i.e. form a freeze lining) or,
- It can cool the refractory wall such that the chemical reactions slow down significantly or cease.
Refractory bricks used as furnace lining (in contact with the furnace melt) erode until a layer of slag freezes on the hot face of the refractory. To promote

Sulphidation of copper coolers in PGM smelters

the formation of the frozen layer, furnaces are equipped with cooling elements made of conductive copper with high cooling water velocity through these elements [Van Manen 2008; Uchechukwu 2000; Voermann et al. 1999].

 Copper has high thermal conductivity and can therefore remove heat from the furnace wall efficiently. Its efficiency in extracting heat is complemented by its comparatively high melting point (1083°C) and relatively low cost [Verscheure et al. 2006].

There are different types of copper coolers, namely waffle coolers, plate coolers and finger coolers. These copper coolers differ in their ability to extract heat from the furnace, with waffle coolers being the most efficient and finger coolers being the least efficient [Plascencia et al. 2005]. A copper waffle cooler has knobs, which extend from the copper base panel through which the cooling water circulates. The grooves between the base and the knobs facilitate the bonding between rammable refractory material and the copper cooler, forming a refractory-cooler composite at the hot face. This composite enhances the solidification of slag (freeze lining formation) on the hotter side of the copper cooler [Voermann et al. 1999; De Kieviet 2004]. The high cooling efficiency of copper makes it possible to increase the campaign life of the smelting furnace refractory wall [Hopt et al. 2006] from two to three years to five to seven years [Matyas et al. 1993]. The disadvantage of using copper in electric matte smelting furnaces is its susceptibility to corrosion by gases such as sulphur. This limitation of copper results in undesired occurrences of premature failure of copper coolers in furnace applications [Kammlott 1984].

Sulphidation of copper coolers in PGM smelters

3. PREVIOUS WORK

3.1. Introduction

Very little has been published on the mechanism involved in corrosion of copper coolers in PGM smelters. The references found report that the corrosion of copper coolers is due to sulphidation by sulphur assisted by chlorination involving hydrogen chloride gas (HCl) [Hundermark et al. 2006].

Test work done at the University of Pretoria on this subject [Pistorius 2006] included comparing the corrosion rate of clean copper foil and chlorinated copper foil by S_2 gas. The temperature of the copper foil varied between 80°C and 140°C. The following main observations were made:

- The corrosion rate was found to be greater than 100 mm/y
- Chlorinated foil was found to react at a higher rate than copper foil that was not exposed to HCl fumes.

3.2. Sulphidation of copper by sulphur

Various authors have studied phase relations in the copper-sulphur system at low temperatures. Blachnik et al. (2001) studied the formation of chalcocite (Cu_2S) from copper foils in the temperature range of 25°C to 600°C. They observed that below 128°C covellite (CuS) and $Cu_{1.1}S$ form, while between 128°C and 150°C covellite forms an outer layer (at the gas interface) while $Cu_{1.8}S$ forms near the copper foil surface. High sulphur concentrations and low temperature conditions favour the formation of covellite, while at high temperatures and low sulphur concentrations a copper-rich sulphide ($Cu_{2-x}S$) forms [Blachnik et al. 2001].

Bartkowicz et al. 1986 studied the kinetics of sulphidation on a copper block at temperatures below 850°C, using Wagner's pellet method. In Wagner's pellet method the sulphide pellet (pressed sulphide powder) is placed on a metal block and pressed by a glass tube with a diameter the same as that of the metal block. The sulphur gas is then applied at the open end of the glass tube. It was observed that copper sulphidation between 97°C and 507°C is complicated by the formation of hexagonal chalcocite, regular (monoclinic)

chalcocite and CuS. It was reported that the scale layer that formed was porous and had poor adherence to the metallic core.

3.2.1. Phase relations

Chemical interactions between copper and sulphur can be predicted by considering phase relations in the Cu-S phase diagram (Figure 2). Vaughan et al. (1978) reported that the sulphide phase in equilibrium with pure sulphur at temperatures less than 507°C is covellite. Regular (monoclinic) chalcocite is in equilibrium with pure copper below 103.5°C and hexagonal chalcocite is in equilibrium with pure copper between 103.5°C and 435°C. It was reported that digenite can form when sulphur reacts with chalcocite and covellite can form when sulphur reacts with digenite (Cu_9S_5) [Vaughan et al. 1978]. For this reason it can be expected that when a copper foil is exposed to sulphur at temperatures below 150°C, covellite and chalcocite may form. Covellite is expected to form at the gas scale interface and chalcocite is expected to form at the copper surface.
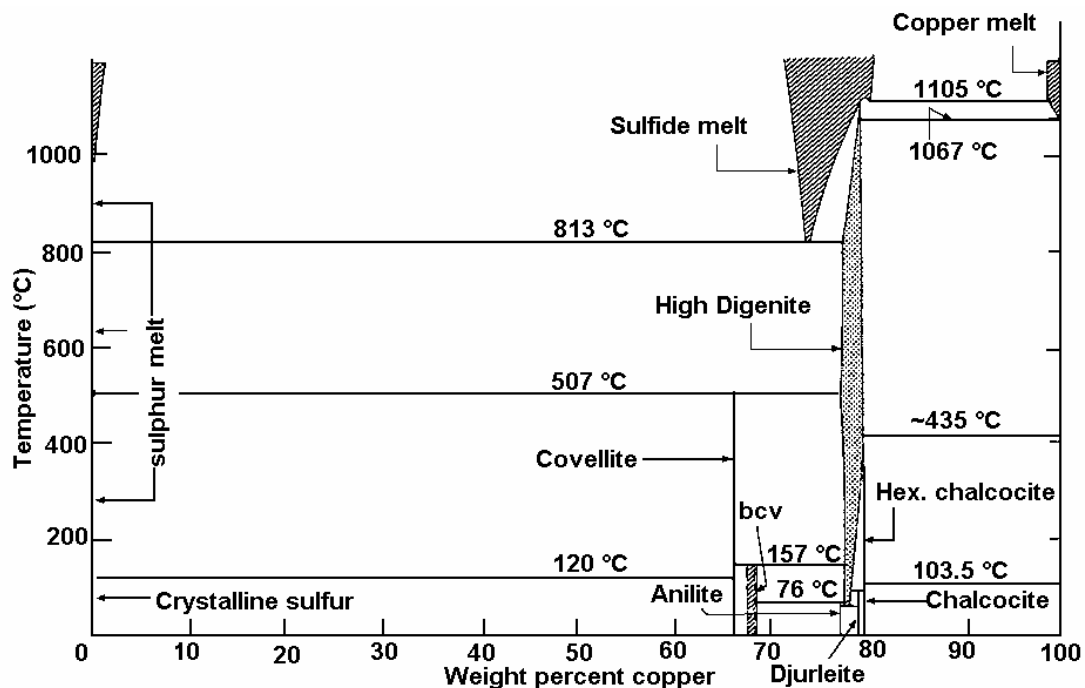
Figure 2: Temperature-composition diagram of condensed phases in the copper-sulphur system [Vaughan et al. 1978].

Sulphidation of copper coolers in PGM smelters

The mass transport through the hexagonal chalcocite is lower than in the regular (monoclinic) chalcocite [Bartkowicz et al. 1986]. The hexagonal chalcocite is more defected in structure than the monoclinic chalcocite, therefore hexagonal chalcocite can cause scale detachments and formation of a porous layer. Overall, the presence of the hexagonal chalcocite lowers the rate of corrosion [Furer et al. 1977; Bartkowicz et al. 1986].

3.3. Role of hydrogen chloride in sulphidation

When copper is exposed to a chlorine gas such as HCl, a copper chloride (CuCl) forms [Vracar et al. 1999; Sesselman et al. 1986]. In sulphidation, the presence of HCl gas facilitates the transition of corrosion kinetics from a parabolic rate to a linear rate at temperatures above 400°C [Brooks et al. 1985]. Blacknik (2001) observed that the copper foils cleaned with chlorine reacted faster at temperatures above the melting temperature of sulphur than the copper foils cleaned with alcohol.

It has been found that the chlorine has the ability to diffuse through the corrosion layer, providing a path for metal diffusion to the reaction surface, therefore chlorine increases the corrosion by physically disrupting the protective scale [Brooks et al. 1985; Sesselman et al. 1986; Reid et al. 2008].

3.4. Sulphidation of copper by hydrogen sulphide gas

Chalcocite (Cu_2S) forms when copper reacts with hydrogen sulphide (H_2S) [Larson 2002; Tran et al. 2003; Gesmundo et al. 1996; Tran et al. 2005]. The sulphide layer forms by the outward diffusion of copper ions from the metal core [Martinez et al. 1986; Gesmundo et al. 1996; Tran et al. 2003; Bartkowicz 1987].

The rate of growth of a sulphide layer is enhanced by an increase in temperature. This effect can be attributed to the increase in chemical, diffusion and electrochemical reaction rates [Tran et al. 2005].

The morphology of the sulphide scale is a function of exposure time and the H_2S concentration. At low concentrations and short exposure times, the layer

Sulphidation of copper coolers in PGM smelters

is uniform, coherent and small in grain size [Larson 2002]. At high exposure times and high gas concentrations, the scale is more granular and has high porosity, making access for corroding gas possible [Tran et al. 2003].

Tran et al. (2003) also noted that the corrosion rate kinetics in copper sulphidation by H_2S are irregular. There are three different stages of corrosion:

- The initial stage is a linear rate when diffusion is not rate-limiting.
- The second stage is parabolic; the corrosion slows down when the diffusion of the ions through a sulphide scale becomes rate-limiting.
- The third and final stage is the linear rate, which is faster than the initial rate. This rate is correlated to the scale thickness of more than 1micron and the porosity of the inner layer, which allows the gas ingress through the scale.

The occurrence of phases correlated to the gas concentration: at low gas concentration only the first two stages are observed, at high gas concentration only the last linear phase is observed [Tran et al. 2003].

Bartkowicz (1986) determined the parabolic rate constant (k) for sulphidation at temperatures between 570K and 780K to be:

$$k = 10.2 \exp\left(-70x10^{-3} \middle/ RT\right) \quad cm^2/s \qquad \qquad \textit{Equation 8}$$

From the parabolic rate law (Equation 9), the thickness (x) of the formed sulphide after a specified duration (t) can be estimated using Equation 9 which is the parabolic rate law, where C is a constant.

$$x^2 = 2kt + C \qquad \qquad \textit{Equation 9}$$

It would, however, be inaccurate to estimate the thickness loss using this rate constant, since the temperature range used in this study (80°C to 140°C) is lower than the range Bartkowicz used.

Sulphidation of copper coolers in PGM smelters

4. ANALYTICAL TECHNIQUES

X-Ray diffraction (XRD), X-ray fluorescence (XRF) and scanning electron microscopy (SEM) are the techniques that were used to analyse the post-mortem samples and the laboratory test samples.

4.1. Scanning Electron Microscopy

The phase compositions and morphologies of the samples were characterised with a SEM (Jeol JSM 6300) using energy-dispersive spectrometry (EDS). The samples were cut to approximately 30 mm in diameter and mounted in silicone resin. SiC paper was used to polish the sample mechanically to achieve a smooth surface. An MD-Nap supplied by Struers was used for the final polish. The atomic percentage of elements (excluding oxygen) was used to calculate the stoichiometry of the different phases. The compositions of the oxides were calculated from the elemental analysis as determined by EDS by assuming that aluminium (Al) is present as Al_2O_3, chrome (Cr) as Cr_2O_3, silicon (Si) as SiO_2, calcium (Ca) as CaO and iron (Fe) as FeO. The stoichiometries of the sulphide phases were calculated by working out the sulphur to other element atomic ratios.

4.2. X-Ray powder diffraction

XRD was used to determine the crystalline phases present in the samples. The samples were crushed to less than 10 mm in diameter in a jaw crusher followed by a cone crusher. The samples were further milled to less than 75 micron using a tungsten carbide milling pot.

The samples were analysed with a PANalytical X'Pert Pro powder diffractometer with X'Celerator detector and variable divergence and receiving slits with Fe filtered Co-Kα radiation. The phases were identified using X'Pert Highscore plus software. The machine was operated at 35 kV, 50 mA and 25°C. Quantification was done using the Autoquan software (BGMN® program). The semi-quantitative phase amounts (weight percentage) were

estimated using the reference intensity method in the X'Pert Highscore plus software.

4.3. X-Ray fluorescence spectroscopy

XRF was used to determine the bulk chemical compositions of the samples. The samples were prepared as for XRD. Trace elements were analysed using pressed powder briquettes. The values were normalised, as no percentage loss on ignition (LOI) was carried out to determine crystal water and oxidation state changes. Samples analysed on fused beads were further dried at 110°C and roasted at 1000°C to determine the LOI.

An ARL 9400XP Wavelength dispersive XRF spectrometer with rhodium tube and PET analysing crystal with a scintillation detector was used. WinXRF and UniQuant software were used for data reduction of the pressed powder program, while fused beads briquettes were analysed using the Quantas software. The software analyses for all elements in the periodic table between Na and U, but only elements found above the detection limits were reported. The pressed powder program is calibrated for oxides, whereby copper is expressed as CuO, and $CuSO_4$ as CuO and SO_3 [Loubser et al, 2008]. All elements were expressed as oxides, except for Zn, Fe, Pb, Mn, Cu and Cd, which are usually associated with sulphur as sulphides.

5. POST-MORTEM ANALYSIS OF THE REFRACTORY WALL OF A PRIMARY PGM SMELTER

5.1. Introduction

This section depicts the visual observations and phase chemical analysis of post-mortem refractory samples that were collected from a PGM smelter after 12 months of operation. The refractory samples were collected during the furnace maintenance shutdown and the pictures of the refractory wall were also taken then. Samples were submitted for analysis with the aim of identifying the phases associated with the corrosion of copper coolers in PGM smelters.

5.2. Sampling

Sampling was done three days after the furnace shutdown. Samples were classified by the area (A to F) in which they were collected, as indicated in Figure 3. The furnace refractory wall consists of top bricks, a waffle copper cooler, rammable refractory material and front bricks. The picture depicting the front view of the furnace refractory wall is shown in Figure 3.

A: Top brick

B: Build-up between the copper cooler and the top brick

C: Copper waffle cooler knobs

D: Corrosion product

E: Freeze lining

F: Front refractory brick (behind freeze lining)
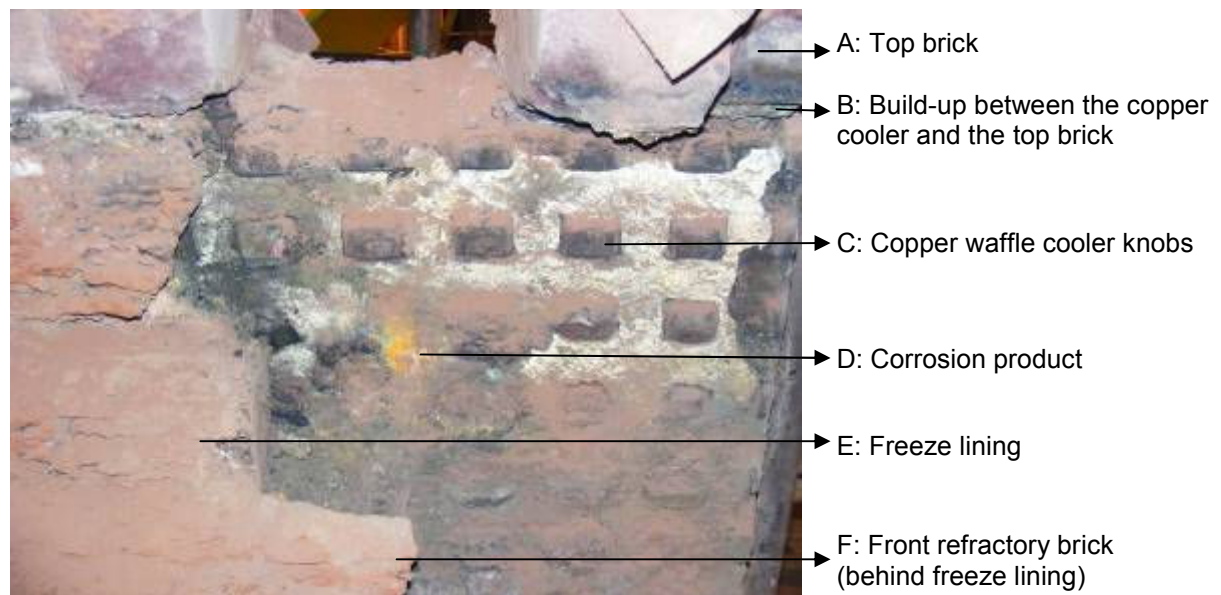
Figure 3: Front view of the furnace refractory wall, showing the top brick, copper waffle cooler knobs covered with corrosion product and the freeze lining.

Sulphidation of copper coolers in PGM smelters

Samples were collected from the following positions on the refractory wall:

- o Between the top brick and the copper cooler (TBC)
- o The freeze lining (FL)
- o Between the freeze lining and the copper cooler (FLC)
- o Between the front brick and the copper cooler (FBC)

Samples were kept in a dessicator prior to sample preparation for analysis. This was done in order to prevent the samples from reacting further with moisture. The refractory bricks and the copper cooler were not sampled for analysis.

5.3. Sample analysis and discussion

This section discusses the observations made on the furnace lining when the post-mortem samples were collected and the EDS, XRD and XRF analyses were performed on the corrosion products.

FL, FLC, and FBC were analysed using all three analytical techniques, while the TBC sample was only analysed by XRF and XRD because the preparation of a polished section for SEM analysis was not successful as this sample is too friable. The ramming refractory material was alumina-chrome-based, hence the presence of corundum (Al_2O_3) and eskolaite (Cr_2O_3) in all the corrosion products that were analysed.

5.3.1. Copper waffle coolers [C]

A copper waffle cooler is made of two sections, a base panel through which the cooling water circulates and the waffle knobs, which extend from the copper base panel. Waffle knobs facilitate bonding with the refractory layer (rammable) and enhance solidification of slag on the hotter side of the copper cooler [De Kieviet et al. 2004]. The waffle knobs behind the freeze lining were mostly covered with layers of corrosion products as well as the ramming refractory material (data sheet in Table A 1, Appendix A) which is used to fill the gaps between the waffle knobs. The ratio of corundum to eskolaite in the

ramming material is 1:0.44. A detailed view of the waffle knobs and corrosion products is shown in Figure 4. The copper waffle knobs appeared to be entirely covered with the corrosion product; where the corrosion product was removed the waffle knobs' surface seemed to be uneven, as if pitting corrosion had taken place.

Figure 4: Detailed view of the copper waffle knobs; C = copper waffle knob; D = corrosion product with ramming material; E = freeze lining (FL).

5.3.2. Refractory bricks [A and F]

Magnesia-chrome bricks were used as lining at the top and front of the copper cooler (composition of bricks is given in Table A 2, Appendix A). Top bricks separate the plate copper cooler (freeboard) from the waffle cooler. No significant wear of the bricks was noted. An alumina-chrome-based rammable refractory material was used to fill the space between the bricks and the waffle

cooler. A build-up of approximately 30 mm was found between the cooler and the top brick. This build-up is referred to as B in Figure 3.

The furnace was initially lined with magnesia-chrome bricks in front of the copper coolers. The main function of the front bricks was to protect the waffle cooler from the hot furnace contents during operation. The zone where severe corrosion occurred was at the slag-concentrate interface. In this area it was observed that the entire refractory brick had corroded and only the freeze lining remained in front of the copper cooler. The thickness of the remaining brick increased from the slag zone to the matte zone. The side view of the refractory wall is depicted in Figure 5 with typical furnace content levels marked with brackets.
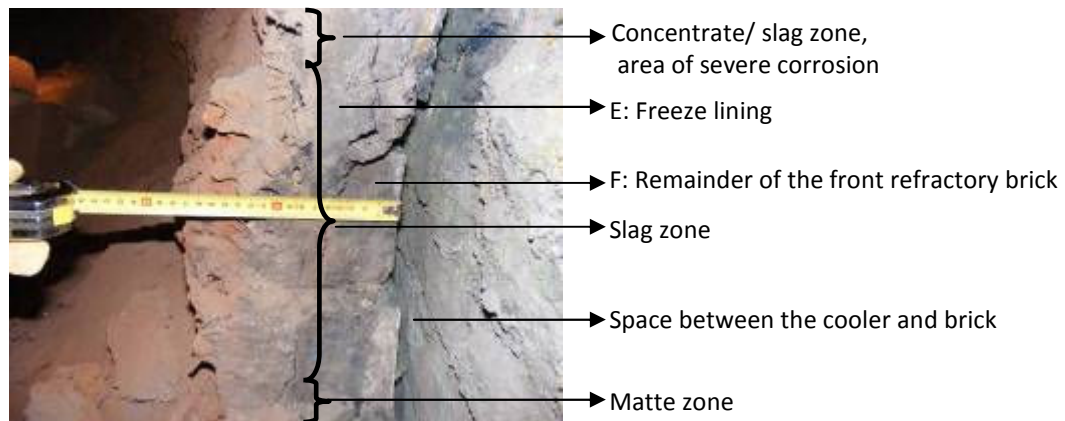
Figure 5: Side view of the freeze lining and the remaining refractory brick.

5.3.3. Sample collected between the top brick and the cooler (TBC)

A mixture of blue crystals, with white and black soft material, formed the bulk of the corrosion product between the cooler and the top brick. The top brick seemed to have been pushed upward as this layer formed. A top brick-copper cooler interface is depicted in Figure 6a. The detailed view of a build-up observed between the top brick and the copper cooler TBC is shown in Figure 6b. The build-up consisted of two horizontal layers, a blue layer formed adjacent to the copper cooler and a black layer mixed with small blue crystals was in contact with the top brick (Figure 6b).

Sulphidation of copper coolers in PGM smelters
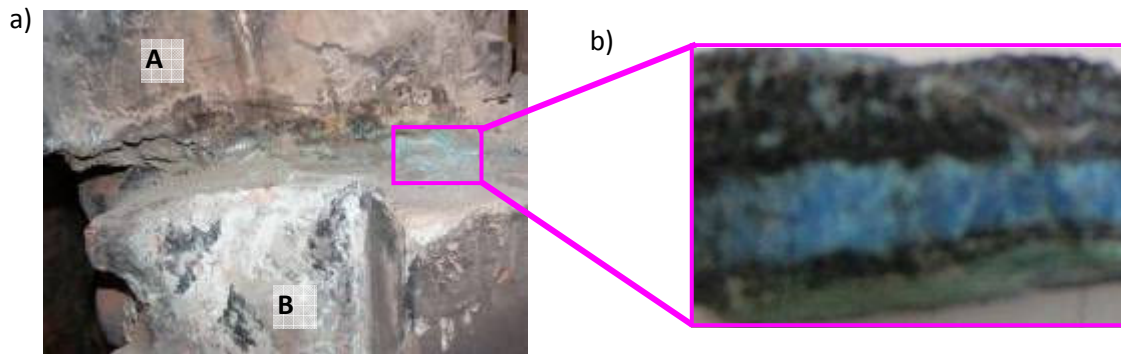
Figure 6: a) Detailed view of the TBC (A-top brick, B-waffle cooler), b) build-up between the cooler and the top brick.

Blue, black and white layers were analysed separately. The summaries of the XRD and XRF results are given in respectively Tables 3 and 4. Bonattite ($CuSO_4.3H_2O$), copper sulphate anhydrous ($CuSO_4$), chalcanthite ($CuSO_4.5H_2O$) and corundum were detected by XRD as major phases in the friable crystals collected on top of the copper cooler (Table 3). Minor phases detected were nantokite ($CuCl$) and alpha sulphur (S). No eskolaite was detected by XRD in this sample. Copper sulphate with different degrees of hydration was the most abundant phase in the sample collected on top of the cooler.

Copper and sulphur trioxide were detected as the major elements by XRF with no elemental sulphur. These results confirmed the presence of a sulphate and not a sulphide, which complemented the XRD results. A minor amount of corundum, eskolaite and chlorine was also detected by XRF. A loss on ignition value was not determined; however, the values reported in Table 4 were normalised, and the total before normalisation is also reported.

Sulphur, sulphur dioxide and sulphur trioxide are among the gases which report to the off gas during PGM smelting [Andrews 2008]. Sulphur trioxide can react with water to form sulphuric acid, which is very corrosive to copper at high temperatures (Equation 10) [Behrens 1991].

UNIVERSITEIT VAN PRETORIA
UNIVERSITY OF PRETORIA
YUNIBESITHI YA PRETORIA Sulphidation of copper coolers in PGM smelters

Table 3: Quantitative XRD analysis of the sample collected between the top brick and copper cooler (TBC) (%)

Crystalline phases	Bonattite	Chalcanthite	CuSO$_4$	Corundum	Nantokite	Sulphur alpha
	CuSO$_4$.3H$_2$O	CuSO$_4$.5H$_2$O	CuSO$_4$	Al$_2$O$_3$	CuCl	S
Black layer	0.00	96.07	0	0	3.93	0
Blue layer	74.69	0	22.76	0	0	2.56
White layer	49.59	1.51	34.5	12.79	1.62	0

Table 4: XRF analysis of the sample collected between the top brick and the copper cooler (TBC) (mass %)

Elements	Al$_2$O$_3$	Cl	Cr$_2$O$_3$	Cu	SO$_3$	S	Total before normalisation (%)
Black layer	2.44	3.16	0.77	48.41	45.22	0	94.4
Blue layer	1.79	0.88	5.23	42.57	49.53	0	93.4
White layer	15.07	1.42	0.03	36.89	46.58	0	92.1
Std Err	0.15	0.06	0.09	0.17	0.33	0.19	

$$2H_2SO_4(l) + Cu(s) \rightarrow CuSO_4(s,l) + SO_2 + 2H_2O \qquad \text{Equation 10}$$
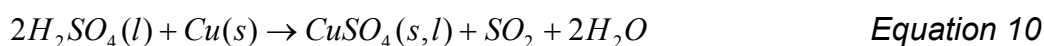
Based on these arguments it can be assumed that the build-up between the copper and the top brick was formed as a result of copper reacting with the sulphuric acid, since the phases identified on this sample include copper sulphate compounds with different degrees of hydration.

5.3.4. Freeze lining (FL)

The freeze lining is a layer of frozen slag that solidifies on the furnace refractory. The cooling effect of the copper cooler maintains the temperature of the furnace lining below the solidus temperature of the melt, thereby forming a chemically inert, frozen layer on the furnace refractory wall hot side [De Kieviet et al. 2004 and Marx et al. 2007].

The morphology of the freeze lining varied from the hot (front) face in contact with the furnace contents to the cold (back) face in contact with the cooler denoted as (front) and (back) in Figure 7. The cold face was denser with inclusions of corrosion product, while the hot face had cracks and seemed very porous.
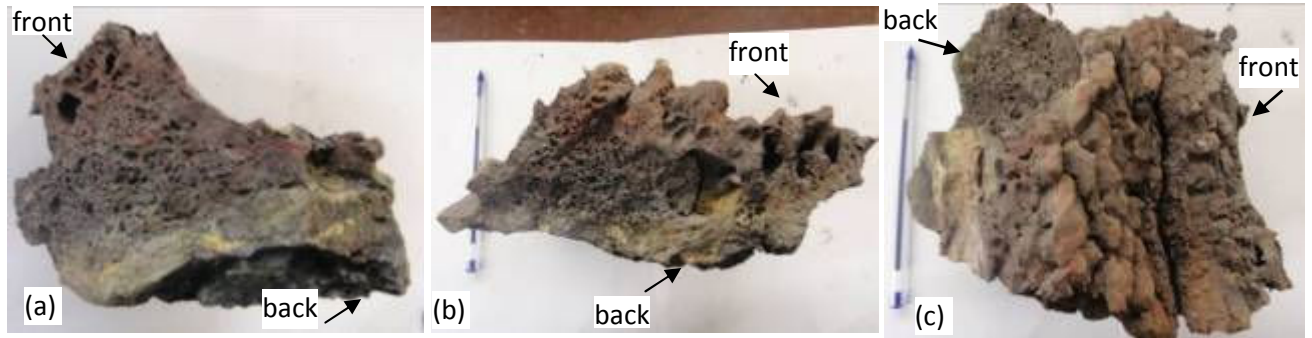
Figure 7: (a, b) Side view and (c) front view of the freeze lining (E).

Detail of the freeze lining is shown in Figure 8, with (i) indicating the gap between the freeze lining and the bulk of the corrosion product which covered the waffle cooler. During the lining of the furnace (pre-operation) there was virtually no gap between the waffle cooler and the front brick; the ramming refractory material filled the space denoted as (i) in Figure 8. A gap of approximately 2cm (parallel to the cooler) was observed at the copper cooler-front brick or freeze lining interface after shutdown of the furnace. The gap could have formed owing to thermal cycling of the furnace during operation or to refractory wall contraction during the furnace shutdown. If this gap formed during operation, a channel through which oxygen and off gases from the freeboard could reach the surface of the copper coolers was provided. Gaps can lead to contact resistance between the coolers and the refractory, which results in a decrease in cooling efficiency [Plascencia 2005].

For phase chemical analysis the sample of freeze lining was separated into three parts:

    a) Front or hot face

    b) Middle portion

    c) Back or cold face,
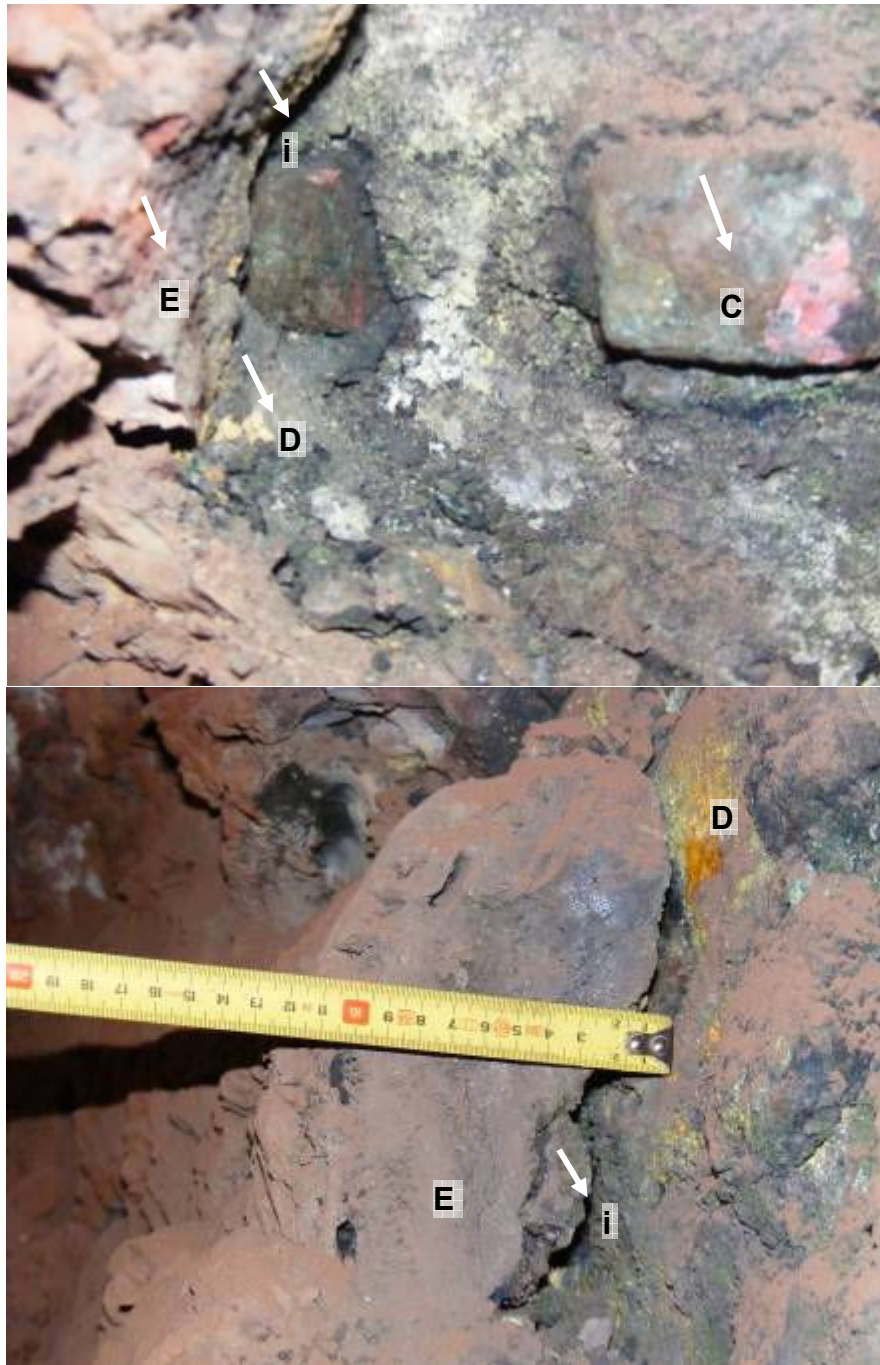
Figure 8: Detailed view of the freeze lining and the copper cooler (waffle knobs) interface, C is a copper waffle knob, D is the corrosion product, E is the freeze lining and (i) is the air gap between the freeze lining and the copper cooler.

5.3.4.1. SEM analysis of the freeze lining

(i) Front or hot face

The BSE images of the freeze lining are depicted in Figure 9. The microstructure of the hot face of the freeze lining is shown as a backscattered electron (BSE) image with the EDS spectra of each annotated point in Figure 9a. Diopside ($Ca(Mg,Fe)(Si,Al)_2O_6$), augite ($CaMgFe(Si,Al)_2O_6$), and forsterite (($MgFe)_2(SiO_4)$) were identified by EDS as the main constituents of the hot face of the freeze lining (Table 5) with base metal sulphides as minor white phases.

Table 5: EDS analyses of the hot face of the freeze lining (wt %)

Figure 9a	Description of phase	Al$_2$O$_3$	CaO	Cr$_2$O$_3$	FeO	MgO	SiO$_2$	Phase	Mineral name
1	Light grey	2.0	23.8	1.1	7.8	13.9	51.2	CaMgFe(Si,Al)$_2$O$_6$	Diopside
2	Grey	14.2	9.7		20.0	0.4	52.7	CaMgFe(Si,Al)$_2$O$_6$	Augite
3	Dark grey				14.5	40.7	42.2	(MgFe)$_2$(SiO$_4$)	Forsterite

(ii) Middle portion

Silicates identified in the hot face (diopside, augite and forsterite) were also present in the middle portion of the freeze lining with the inclusion of chromite (($Mg,Fe)(Cr,Al)_2O_4$)) and base metal sulphides such as iron sulphide ($Fe_{1.19}S$), digenite ($(Cu,Fe)_9S_5$), villamaninite ($(Cu,Ni,Fe)_xS_2$) and chalcopyrite ($(Cu_{0.8}Fe_{1.6})S_2$) (Figure 9b, Table 6).

Table 6: EDS analyses of the middle layer of the freeze lining (wt %)

Figure 9b	Description of phase	Al$_2$O$_3$	CaO	Cr$_2$O$_3$	*Cu	FeO/*Fe	MgO	*Ni	*S	SiO$_2$	Phase	Mineral name
4	Grey	6.1	0.2	66.5		13.3	11.8			0.3	(Mg,Fe)(Cr,Al)$_2$O$_4$	Chromite
	Area analysis 1				1.6	*52.1		1.2	43.8		Fe$_{1.2}$S	Iron sulphide
5	Area analysis 2		14.1		33.9	*5.6		2.8	22.2	18.6	(Cu,Fe)$_9$S$_5$	Digenite
	Area analysis 3				17.8	*30.2		13.8	36.5		(CuNi$_{0.8}$Fe$_{1.7}$)S$_2$	Villamaninite
6	Bright				19.4	*34.5			43.6		(Cu$_{0.8}$Fe$_{1.6}$)S$_2$	Chalcopyrite
	*Cu, Fe, Ni and S are reported as element atom %.											

UNIVERSITEIT VAN PRETORIA
UNIVERSITY OF PRETORIA
YUNIBESITHI YA PRETORIA Sulphidation of copper coolers in PGM smelters
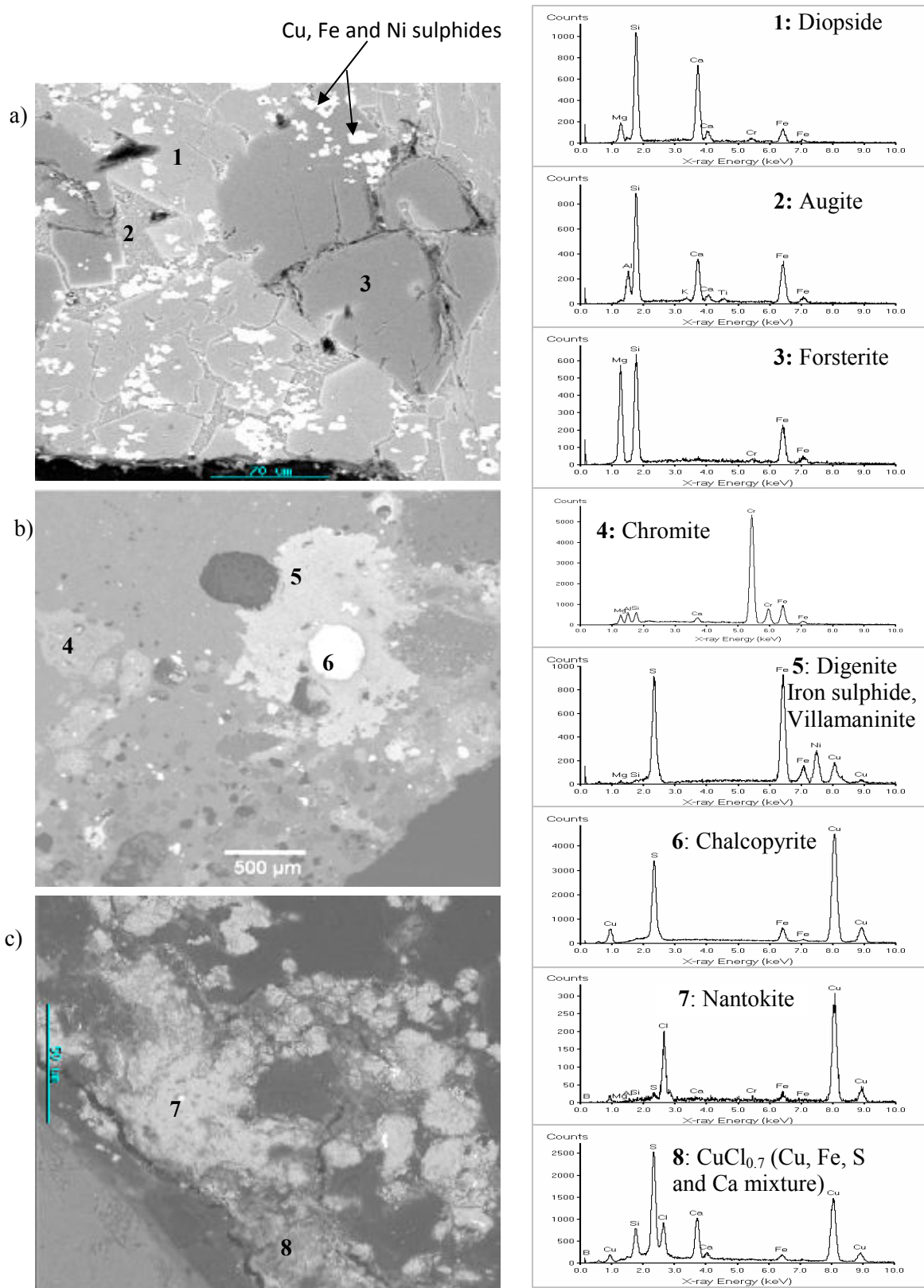
Figure 9: BSE image of a freeze lining sample (Section E), with EDS spectra for the annotated points. a) Front (hot) face b) middle and c) back (cold) face of the freeze lining.

(iii)   Back or cold face

Diopside formed the bulk of the cold face of the freeze lining. At the edge of the diopside (copper cooler interface) was a light grey phase (Figure 9c point 7) which was detected as copper chloride ($CuCl_{0.7}$). Adjacent to copper chloride was a mixture of copper, sulphur, iron and calcium. A summary of the phases identified by EDS in the freeze lining cold face is shown in Table 7 and Figure 9c. Al was taken as Al_2O_3 and Si as SiO_2.

5.3.4.2.   XRD analysis (FL)

Quantitative XRD analyses of the hot face, middle and cold face of the freeze lining are shown in Table 8. Diopside ($CaMgFe(Si_2O_6)$), forsterite ($(Mg,Fe)_2(SiO_4)$), enstatite ($(Mg,Fe)_2Si_2O_6$) and chromite ($(Mg,Fe)(Cr,Al)_2O_4$) were major phases detected by XRD in the hot face of the freeze lining sample. No augite was detected in the freeze lining hot face sample but it should be noted that diopside and augite have the same crystal structure (monoclinic), hence the XRD patterns for these phases are similar, which may affect the accuracy of the XRD analyses of these two phases. Augite ($(Ca,Mg,Fe)_{1.86}(Si,Al)_2O_6$), diopside, forsterite and chromite were the major phases in the middle portion of the sample. Augite, diopside, forsterite and corundum were the major phases in the cold face of the sample with minor amounts of eskolaite, chromite and millerite.

Table 7: EDS analyses of the cold face of the freeze lining (atom %)

Figure 9c	Description of phase	Al	Ca	Cl	Cu	Fe	Mg	S	Si	Stoichiometry
7	Light grey	0.0	0.0	22.0	58.0	3.0	0.0	15.0	0.0	$CuCl_2$, CuS
	Area analysis 1	0.0	0.0	7.0	41.0	25.0	0.0	23.0	0.0	$Cu_{1.8}S$, Fe, Cl
8	Area analysis 2	0.0	51.9	0.0	2.1	0.3	0.0	43.6	0.0	Ca, S
	Area analysis 3	2.9	2.1	40.6	11.5	2.1	0.0	20.6	17.0	Cl, S, Cu and Si
	Area analysis 4	5.6	0.0	0.0	49.8	0.0	5.1	36.0	2.4	$Cu_{1.4}S$

Table 8: Quantitative XRD analyses of the freeze lining sample (front, middle and back face) (%)

Stoichiometry	Augite $(Ca,Mg,Fe)_{1.86}(SiO_3)_2$	Chromite $MgCr_2O_4$	Corundum Al_2O_3	Diopside $CaMgFe(Si_2O_6)$	Enstatite $(Mg,Fe)_2(Si_2O_6)$	Eskolaite Cr_2O_3	Forsterite $(Mg,Fe)_2(SiO_4)$	Millerite NiS
Front	0.0	7.1	0.0	45.7	18.7	0.0	28.5	0.0
Middle	40.6	5.0	0.0	23.8	0.0	0.0	30.7	0.0
Back	39.2	1.0	9.1	29.4	0.0	3.7	16.4	1.1

The phases detected by XRD and EDS are in good agreement except that millerite was the only base metal sulphide detected by XRD in the freeze lining cold face sample. Copper iron sulphide, chloride phases and elemental sulphur were not detected by XRD in the freeze lining sample. However, copper iron sulphides, elemental sulphur and clinoatacamite (were observed in the XRD analysis of a sample collected between the copper cooler and the freeze lining. This can be due to the concentration effect. The XRD scans of the freeze lining sample (front, middle and back) are depicted in Figures B1 to B3, Appendix B.

5.3.4.3. XRF analysis (FL)

The XRF analyses of the freeze lining sample is depicted in Table 9. Fused beads were used to determine the bulk chemical composition (major elements) in the sample. The ratios of SiO_2 to other oxides were used to determine the correlation between the XRF analysis of the freeze lining and the typical slag composition (Table 1). The ratios of SiO_2 to other oxides in the freeze lining sample are similar to the ratios of SiO_2 to other oxides in a typical slag composition. The exception is iron, copper and nickel content, which is much higher in the XRF analysis than in the typical slag composition. This observation confirms the presence of matte in especially the hot face. The CuO content of the freeze lining increases from the hot face to the cold face. This observation confirms possible chemical reactions between the copper cooler and furnace gases or liquid constituents.

Table 9: XRF analyses of the freeze lining (hot, middle and cold face) (wt %)

	*FLA (hot face)	*FLA (middle)	*FLA (cold face)	**FLB (hot face)	**FLB (cold face)
SiO₂	39.76	37.84	34.83	38.45	31.18
TiO₂	0.37	0.26	0.23	0.26	0.24
Al₂O₃	3.95	5.02	14.48	4.17	16.64
Fe₂O₃	20.83	17.03	13.22	20.85	11.86
MnO	0.23	0.26	0.21	0.19	0.14
MgO	16.71	16.26	12.91	14.95	11.46
CaO	6.29	8.78	7.07	7.19	6.80
K₂O	0.00	0.20	0.00	0.00	0.00
P₂O₅	0.00	0.00	0.00	0.00	0.17
Cr₂O₃	3.76	5.28	9.23	5.07	10.53
NiO	3.01	2.52	1.17	2.88	1.05
SO₃	0.44	0.46	0.46	0.53	0.43
Cl	0.03	0.54	0.27	0.51	0.41
CuO	1.79	1.42	3.34	1.69	5.13
ZnO	0.06	0.00	0.04	0.32	0.06
LOI	2.29	3.32	3.32	1.77	3.43
Total	99.52	99.19	100.8	98.83	99.52

Two different freeze lining samples were submitted for analysis, Freeze Lining A (FLA) and Freeze Lining B (FLB). *FLA was divided into three portions (hot, middle and cold) face. **FLB was divided into two portions (hot face and cold face). An average of FLA and FLB was used in the text.

5.3.4.4. Discussion

Silicates in the freeze lining sample are associated with the furnace slag since the freeze lining analysis and the typical slag composition (Table 1) are comparable. Typical furnace slag and matte compositions are depicted in Table 1 [Sarvinis et al.1999; Hundermark et al. 2006]. The freeze lining commonly has pores and cracks, which result from thermal shocks [Hopt et al. 2006]. It is through these pores and cracks that the furnace gases and matte can permeate through to the copper cooler surface. Schacht [2004] argued that metal can sometimes be seen penetrating the refractory along with slag. Electromagnetic and natural convective forces in the submerged furnaces move the slag around the electrodes outwards (counter-clockwise) towards the furnace walls [Haywood et al. 2003; Matyas et al. 1992].

Matte entrainment in slag has been studied by Andrews [2008] who reported that loss of base metals to slag is due to the unsettled entrained sulphide matte. Pentlandite $(Fe,Ni)_9S_8$, triolite (FeS), pyrrhotite $(Fe_{1-x}S)$ and copper iron

sulphides are the phases identified in the entrained matte [Andrews 2008]. Small matte droplets (prills) float on top of the slag surface owing to the surface tension or they are suspended as droplets below small gas bubbles [Andrews 2008]. Gas bubbles leaving the furnace through the freeze lining as a result of the high temperatures of resistant slag may serve as matte carriers to the copper cooler surface. It was reported that the physically entrapped matte in the slag can arise from sulphide phases in the feed, dispersion of fine matte in regions of large temperature gradients such as the freeze lining, and the matte can be carried by the gas bubbles rising through the slag-matte interface [Andrews 2008]. The deposition of matte prills in the freeze lining is evident in the BSE image of the freeze lining middle portion (Figure 9b). At the feed-slag interface a very high temperature gradient is also envisaged, which enhances the dispersion of fine matte.

5.3.5. Sample collected between the freeze lining and the copper cooler (FLC)

The corrosion product between the cooler and the freeze lining consisted of yellow, grey, whitish, black and green material, which was attached to the cooler as shown in Figures 3, 4, 8 and 10. The corrosion product between the front brick and copper cooler was less (in volume) but looked similar to the material found behind the freeze lining. Pictures of corrosion product collected behind the freeze lining are shown in Figure 10. In some areas a mixture of black and green product was covered with a yellow product, while in other areas a pale yellow-whitish material covered the black and green mixture.
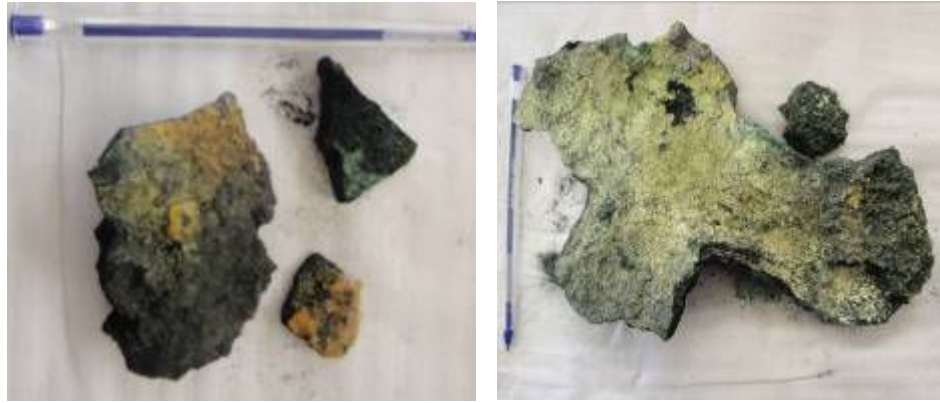
Figure 10: Corrosion product collected between the copper cooler and the freeze lining.

5.3.5.1. SEM analysis (FLC)

EDS analyses were performed on the FLC sample to determine the phase composition of this sample. Corundum, eskolaite, digenite $(Cu,Fe)_9S_5$, chalcocite (Cu_2S), covellite, arsenic (As) and nickel sulphide (NiS) are the phases detected by EDS in the FLC sample. The relationship between the corrosion products (base metal sulphides) and the ramming refractory material (corundum and eskolaite) is shown in Figures 11 and 12 as BSE images. The sulphides characterised as phases with high average atomic numbers (white colour) appear to form between the eskolaite and corundum (Figure 11 points 11, 12 and 13). The detail on the coexistence of copper sulphide, nickel sulphide and the refractory material is shown in Figure 12. Digenite (point 14) and nickel sulphide (point 16) formed between the eskolaite (point 15) and corundum (point 17). The morphology of this corrosion product suggests the possibility of matte penetration through the rammable refractory material. A summary of the EDS analyses is depicted in Table 10.

Sulphidation of copper coolers in PGM smelters
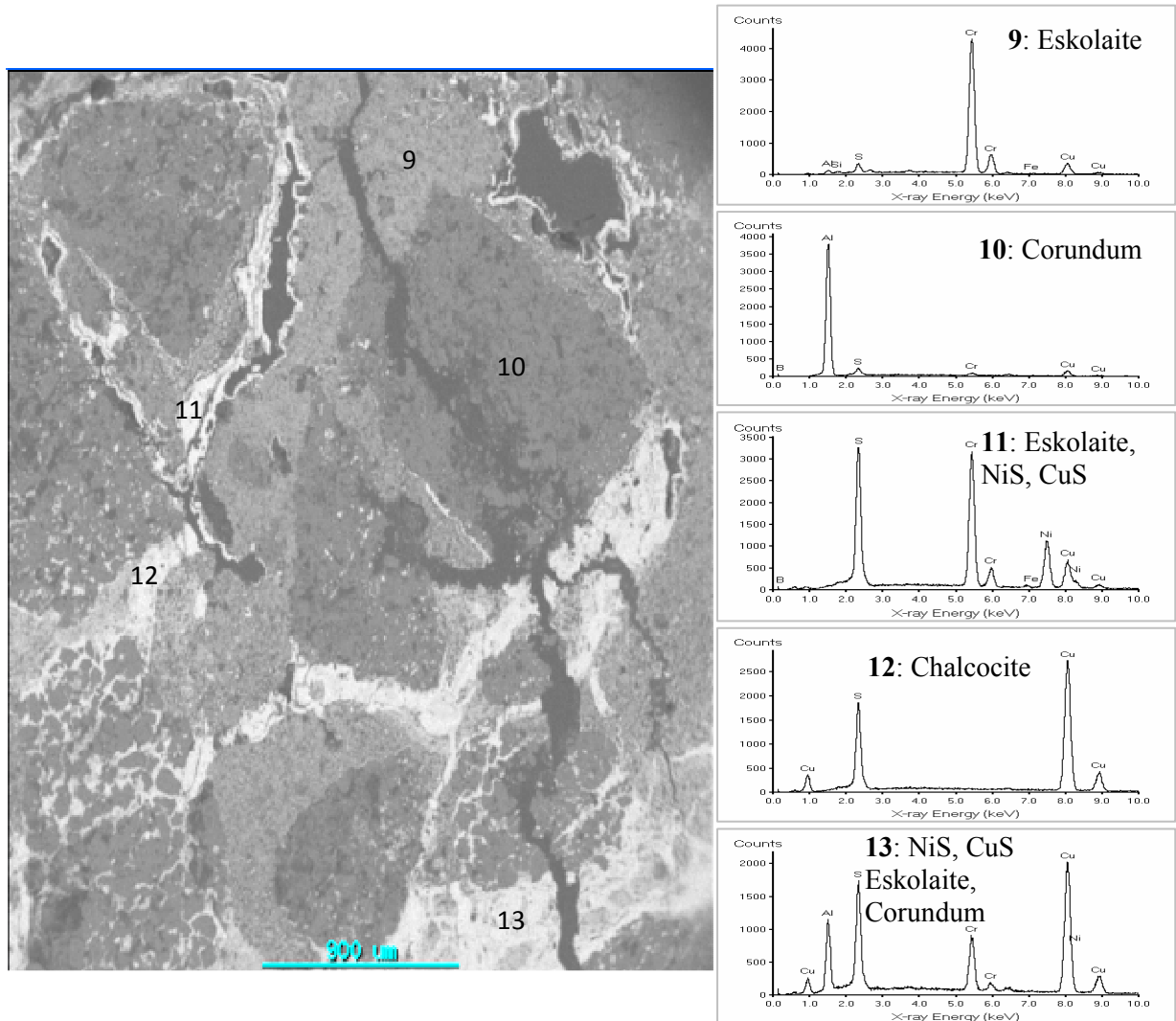
Figure 11: BSE image of the corrosion product collected between the copper cooler and the freeze lining (FLC) with the EDS spectra of the annotated points.

Table 10: EDS analyses of FLC (Atom %)

Figure 11 and 12	*Al	As	*Cr	Cu	Fe	Ni	S	stoichiometry	Mineral name
Points 9 and 15			95.6	2.2	0.5		1.3	Cr_2O_3	Eskolaite
Points 10 and 17	99.2			0.3	0.1			Al_2O_3	Corundum
Points 11 and 16						47.9	49.5	$(Ni)_{0.97}S$	Millerite
Points 12 and 18				68.2			31.4	$Cu_{2.17}S$	Chalcocite
Points 13 and 14				60.2	5.8		33.3	$(Cu_9Fe_{0.9})S_5$	Digenite
Point 13				57			41.4	$Cu_{1.4}S$	Spioncopite
Point 13		9.1		46.4			38.3	$Cu_{1.21}S$, As	Copper sulphide, arsenic
*Al and Cr are taken as oxides i.e. Al is Al_2O_3 and Cr is Cr_2O_3									

UNIVERSITEIT VAN PRETORIA
UNIVERSITY OF PRETORIA
YUNIBESITHI YA PRETORIA Sulphidation of copper coolers in PGM smelters
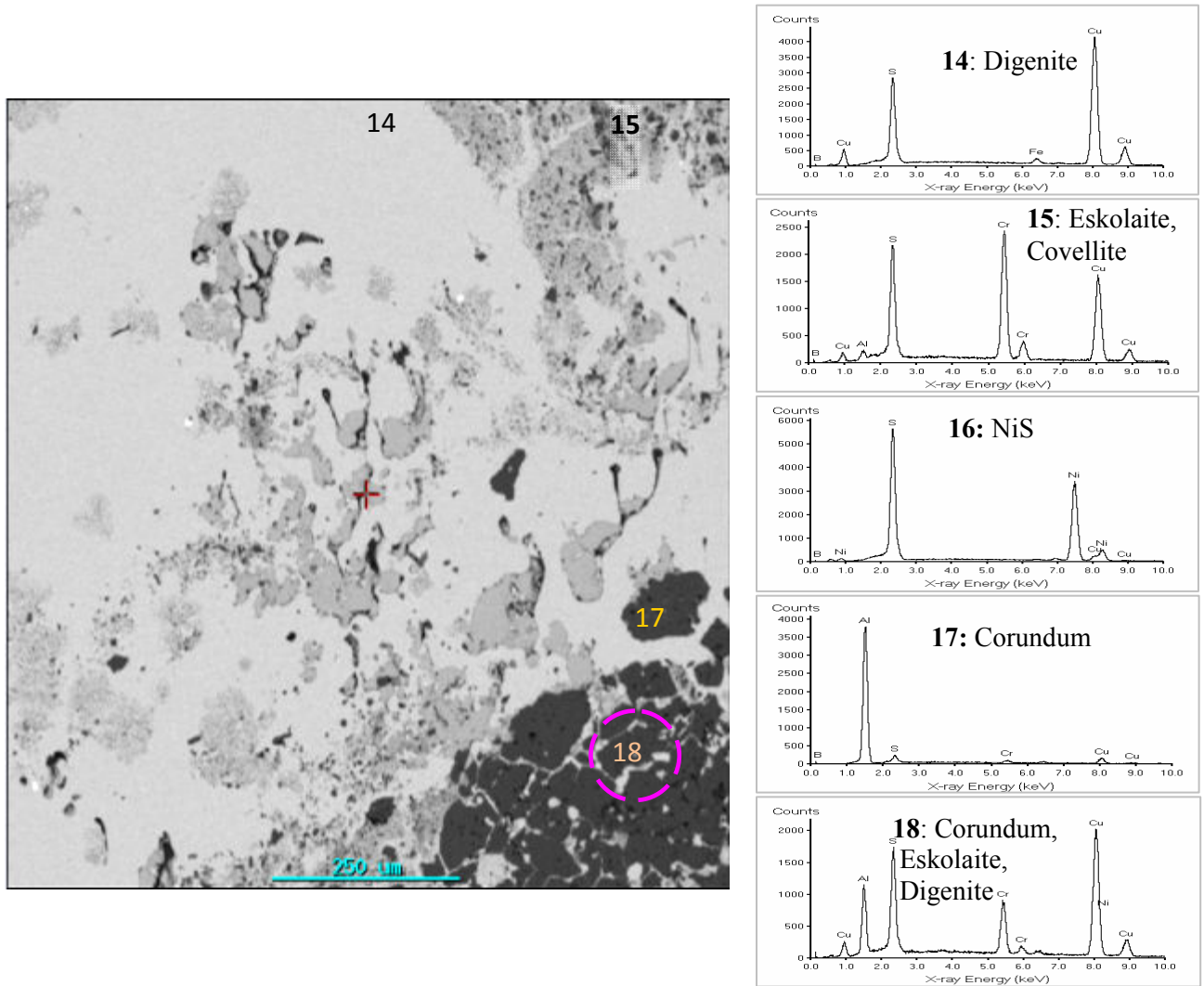
Figure 12: Detailed view of Point 13 in Figure 11 with the EDS spectra of the annotated points.

EDS analyses were performed on the corrosion product from the side that was in contact with the freeze lining up to 20mm towards the copper cooler surface. The profile across the corrosion product is depicted in Figure 13 as a BSE image. A layer of sulphur (S) formed the outer layer of the corrosion product. This layer is identified as a yellow substance in Figures 3, 4, 8 and 10. Arsenic (As) and Tellurium (Te) were observed adjacent to the sulphur layer, characterised by a white layer (As in Figure 13); this phase is arsenic sulphide with tellurium inclusions. A mixture of covellite (CuS), tellurium and arsenic was detected next to the arsenic sulphide (cv-As in Figure 13). This phase can be a mixture of covellite and arsenic suphide or one of the arsenic

minerals (enargite-Cu_3AsS_4 or tennantite-$Cu_{12}As_4S_{13}$), which are known to associate with the base metal sulphides such as covellite, chalcocite and chalcopyrite [Fornasiero et al. 2001; Klein et al. 1937]. The stoichiometry of this covellite arsenic phase did not match that of enargite or tennantite. A thin continuous layer of non-stoichiometric copper sulphide ($Cu_{1.3}S$) (cs in Figure 13) was observed in contact with the cv-As layer. A chalcocite-digenite (cc-dg) solid solution formed the bulk of the layer in contact with covellite extending towards the copper cooler. The solid solution composition ranged from (Cu+Fe):S = 2:1 to 2.1:1, which is close to digenite-to-chalcocite stoichiometry. A copper sulphide with a copper-to-sulphur (Cu:S) atomic ratio ranging from 2.11 to 1.26 formed part of the solid solution (cc and cs in Figure 13). The copper sulphide became more dominant towards the copper cooler (no iron was detected). Nickel sulphide (ni) was dispersed in the solid solution, characterised by dark small phases. A non-stoichiometric copper sulphide (cs) was abundant closer to the copper cooler, with minor amounts of covellite (cv). The dark and light grey phases (cor and esk in Figure 13) are corundum and eskolaite respectively. A summary of the EDS analysis is depicted in Table 11. A detailed view of the cs-As phase in Figure 13 is depicted as an insert in Figure 13, where copper sulphide and arsenic formed layers which seem to be arranged in layers one after the other. The composition of the grey phase ranged from $Cu_{1.6}S$ to $Cu_{1.2}S$, while the light phase ranged from $Cu_{1.5}S$-As to $Cu_{1.2}S$-As.
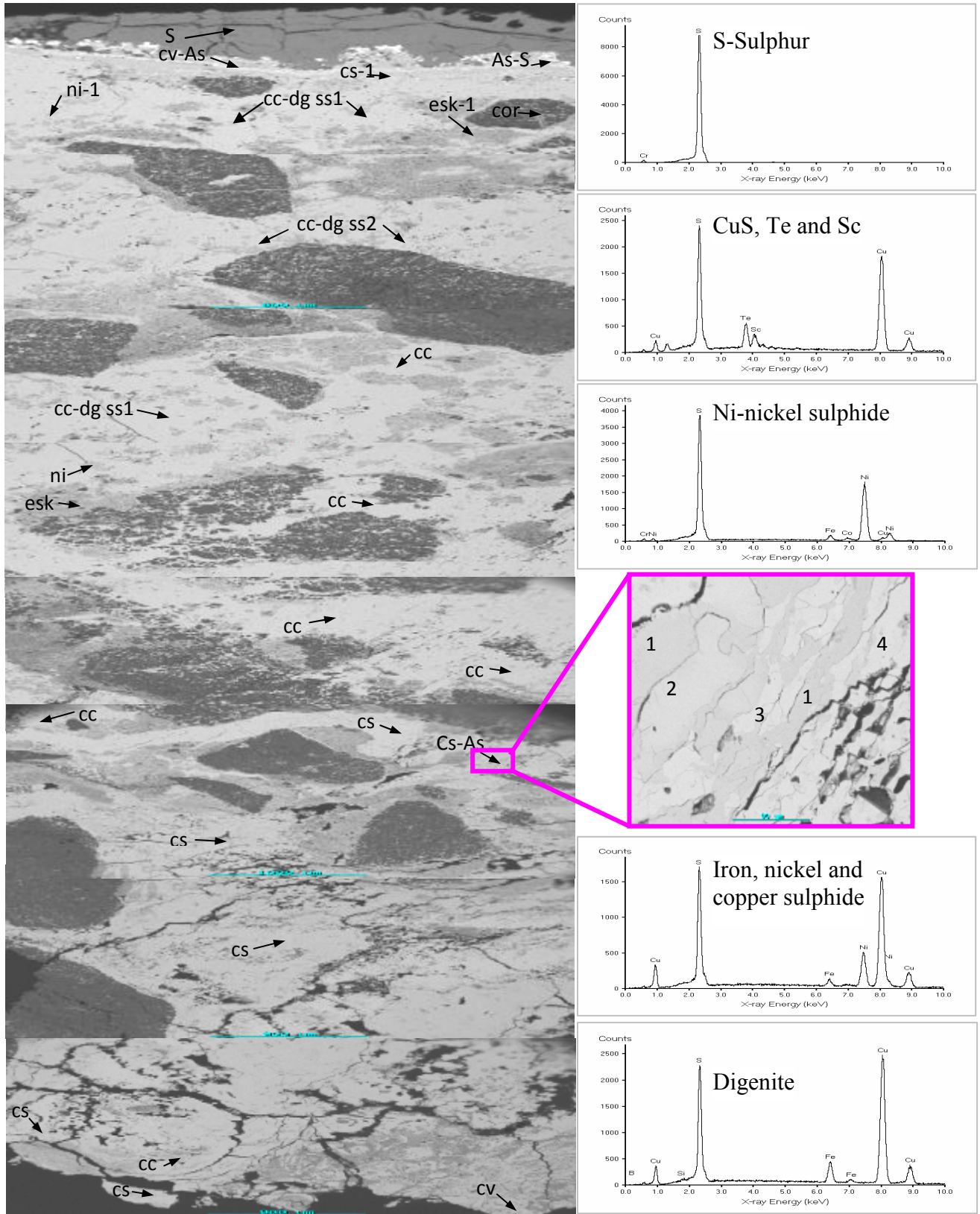
Figure 13: Profile across the corrosion product from the cold side of the freeze lining up to 20 mm towards the copper cooler surface. S-sulphur, cv_As-covellite and arsenic, cv-covellite, cc-chalcocite, ni-nickel, esk-eskolaite, cor-corundum, cs-copper sulphide, cv_S, covellite and sulphur, cc_dg-chalcocite-digenite solid solution.

Post mortem analysis of the refractory wall of a primary PGM smelter

Table 11: EDS analyses of the FLC profile from freeze lining to 20mm towards the copper cooler (atom %)

Figure 13	Description of phase	*Al	As	Cl	Co	*Cr	Cu	Fe	Ni	*Si	S	Te	Total	stoichiometry	Mineral name
S	Dark grey	0.0	0.0	0.2	0.0	0.0	0.1	0.0	0.0	0.5	99.2	0.0	100.0	S	Sulphur
As	white	0.2	22.3	0.0	0.1	0.0	0.4	0.0	0.1	0.7	71.6	4.8	100.2	AsS, S	Arsenic sulphide, sulphur
cv-As	Grey-white	0.2	4.9	0.0	0.0	0.1	44.5	0.0	0.0	0.5	40.6	9.3	100.1	CuS, As, Te	Covellite, arsenic, tellurium
cs-1	Light grey	0.0	0.0	0.9	0.0	0.0	55.9	0.0	0.1	0.4	42.8	0.0	100.1	$Cu_{1.3}S$	Copper sulphide
esk-1	Grey	0.8	0.0	0.0	0.0	47.0	30.6	0.0	0.0	0.3	21.1	0.0	99.8	$Cr_2O_3, Cu_{1.5}S$	Eskolaite, copper sulphide
cor	Dark	98.4	0.0	0.0	0.0	0.0	1.4	0.0	0.1	0.0	0.0	0.0	99.9	Al_2O_3	Corundum
ni-1	Small grey spots	0.0	0.1	0.0	1.1	0.2	0.9	4.5	46.4	0.5	46.4	0.0	100.1	$Ni_{0.9}S$	Millerite
cc-dg ss1	Light grey	0.0	0.0	0.0	0.0	0.0	64.0	2.9	0.0	0.4	32.7	0.0	100.0	$Cu_2Fe_{0.1}S$	&Chalcocite-digenite ss1
cc-dg ss2	Light grey	0.0	0.0	0.0	0.0	0.0	59.3	6.7	0.1	0.3	33.7	0.0	100.1	$Cu_{1.8}Fe_{0.2}S$	&Chalcocite-digenite ss2
cs-As 1	Light grey	0.4	0.1	0.1	0.0	0.0	54.5	0.0	0.0	0.4	44.6	0.0	100.1	$Cu_{1.2}S$	Copper sulphide
cs-As 2	Light grey	0.0	0.0	0.0	0.0	0.0	61.1	0.0	0.0	0.3	38.6	0.0	100	$Cu_{1.6}S$	Copper sulphide
cs-As 3	Light grey	0.0	12.9	0.0	0.0	0.0	46.8	0.0	0.6	0.3	39.6	0.0	100.2	$Cu_{1.2}S, As$	Copper sulphide, arsenic
cs-As 4	Light grey	0.0	3.8	0.0	0.0	0.0	57.2	0.0	0.0	0.3	38.6	0.0	99.9	$Cu_{1.5}S, As$	Copper sulphide, arsenic
cc	Light grey	0.0	0.0	0.0	0.2	0.0	67.0	0.8	0.1	0.4	31.2	0.1	99.8	$Cu_{2.1}S$	Chalcocite
Ni	Small grey spots	0.0	0.4	0.0	0.5	0.0	3.5	0.4	44.7	0.4	49.9	0.1	99.9	NiS	Millerite
esk	Grey	0.0	0.0	0.0	0.1	35.8	42.4	0.0	0.1	0.5	21.1	0.0	100	Cr_2O_3, Cu_2S	Eskolaite, chalcocite
cv	Light grey	0.0	0.0	2.1	0.0	0.0	47.0	0.0	0.0	3.1	47.8	0.0	100	CuS	Covellite

*Al, Cr and Si were taken as oxides i.e. Al is Al_2O_3, Cr is Cr_2O_3 and Si is SiO_2.

Sulphidation of copper coolers in PGM smelters

The findings from the FLC profile analysis imply that matte and gas diffuse through the freeze lining and permeate through the rammable refractory material as shown in Figures 11 and 12 to reach the copper cooler surface behind the rammable material, which may lead to reaction of copper coolers with the gases and the matte. Chloride phases were not detected by EDS.

5.3.5.2. XRD analysis (FLC)

Digenite $(Cu,Fe)_9S_5$, covellite (CuS), bornite (Cu_5FeS_4), corundum (Al_2O_3), eskolaite (Cr_2O_3) and clinoatacamite $(Cu_2(OH)_3Cl)$ were detected by XRD as major phases in this sample, with nukundamite $(Cu,Fe)_4S_4$ and brimstone (S) as minor phases. Quantitative XRD analyses are depicted in Table 12.

Table 12: XRD quantitative analyses for FLC (%)

Bornite	Corundum	Covellite	Digenite	Eskolaite	Brimstone	Clinoatacamite	Nukundamite
Cu_5FeS_4	Al_2O_3	CuS	Cu_9S_5	Cr_2O_3	S	$Cu_2(OH)_3Cl$	$(Cu,Fe)_4S_4$
10.9	5.9	16.4	55.3	3.6	1.5	4.5	1.9

5.3.5.3. XRF analysis (FLC)

XRF analysis of a sample collected behind the freeze lining is summarised in Table 13. Copper, arsenic, tellurium and thallium were detected by XRF with iron and chlorine in minor amounts. No SO_3 was detected behind the freeze lining which indicated that there were no sulphates present behind the freeze lining.

Table 13: XRF analyses for FLC (wt %)

S	SO_3	SiO_2	Fe	Al_2O_3	Cu	Cl	NiO	Cr_2O_3	As_2O_3	Tl_2O_3	TeO_2
23.1	0	0.7	3.4	20.19	39.69	2.27	1.47	7.51	0.84	0.48	0.27

5.3.5.4. Discussion (FLC)

The role of the freeze lining is to provide a chemically inert lining, which cannot be chemically corroded by the slag easily. However, the porosity of the

freeze lining and the cracks that were observed in the freeze lining provide a diffusion path for the furnace melt and gases to permeate through to the copper cooler surface. For this reason severe corrosion can be expected behind the freeze lining which can also be aggravated by higher rates of chemical reactions of copper with gases or matte behind the freeze lining than behind the brick. This can be supported by a higher temperature behind the freeze lining (150°C) than behind the brick (109 °C).

The matte transport mechanism from the furnace to the copper cooler surface can be through the gas bubbles which rise from the matte or the gas bubbles which are suspended in the slag. The slag movement can cause these gas bubbles to permeate easily through the pores of the freeze lining. The stages of a typical slag attack on refractory are depicted in Figure 14.

Schacht (2004) argues that corrosion of the refractory by a reactive component 'slag' begins where the slag comes into contact with the refractory hot face at elevated temperatures. Refractory maintains a degree of porosity and it is through these pores that the slag can penetrate the refractory. An illustration of the refractory attack by the slag is depicted in Figure 14 where a cross-section of the slag and refractory interface is considered. Slag penetrates the refractory until the refractory temperature is low enough for the slag to solidify, forming a freeze lining. Slag reacts with the refractory at the hot face and in the refractory pores. Metal can also be observed penetrating the refractory along with the slag. In stage I of slag attack the reactions occur at the immediate hot face. Where the refractory has small pores, full penetration of the refractory by the slag occurs in Stage II of slag attack. Stage III is a final stage of slag attack where the refractory bonding in the hot face is minimal [Schacht 2004]. From the visual observations and pictures depicted in Figures 5 and 8 it can be concluded that the slag attack illustrated by Schacht [2004] took place at the smelter refractory investigated in this study. After stage III of slag attack, penetration of matte and gases to the cold face of the refractory is inevitable since the freeze pane (freeze lining) is more porous than the mag-chrome brick and therefore can allow easy diffusion of the corrosive components.

UNIVERSITEIT VAN PRETORIA
UNIVERSITY OF PRETORIA
YUNIBESITHI YA PRETORIA Sulphidation of copper coolers in PGM smelters
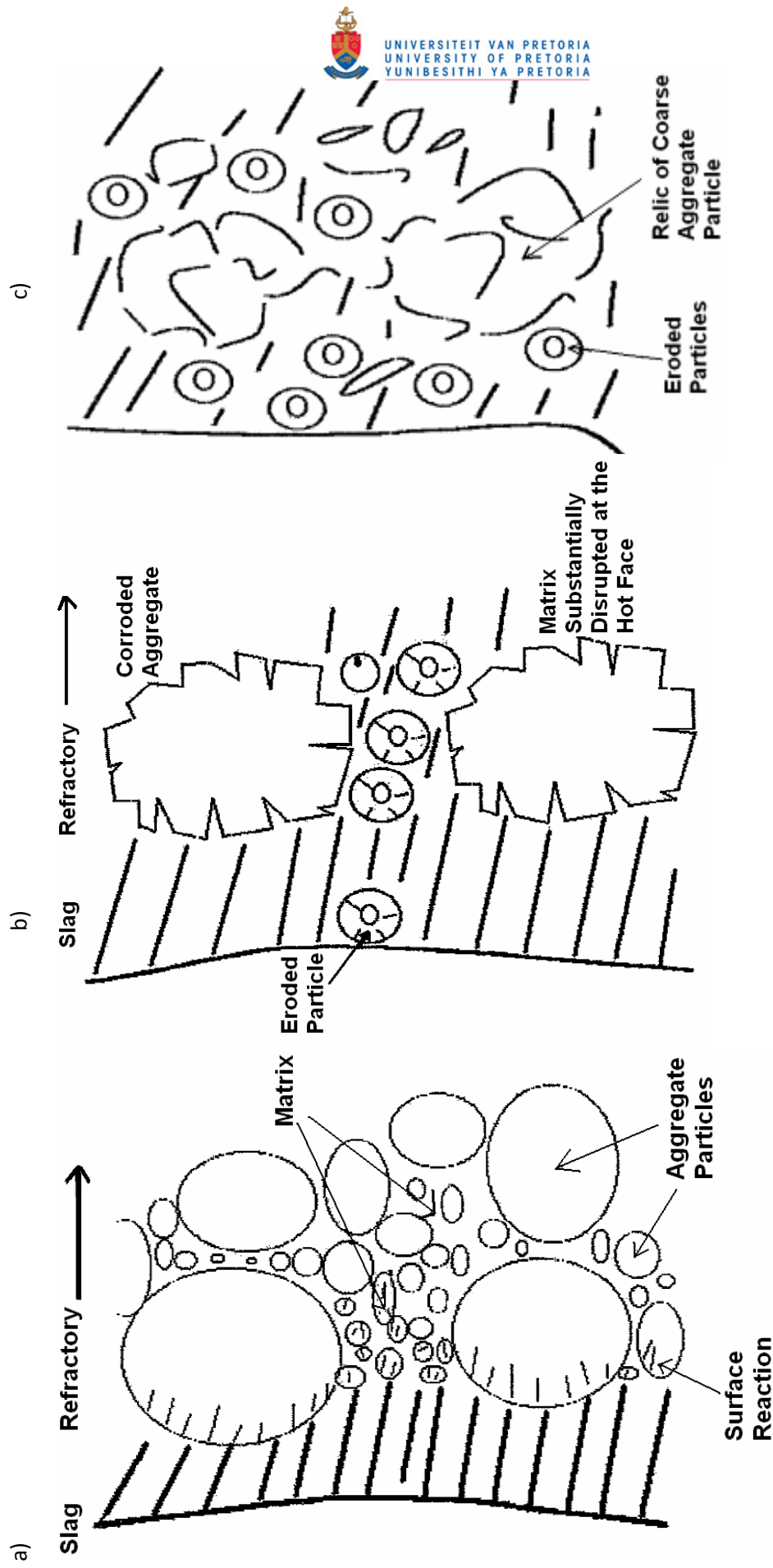
Figure 14: Stages of slag attack, a) Stage I of slag attack (showing a bonded refractory), b) Stage II of the corrosion process (showing a disrupted bonding in refractory), c) Stage III of the corrosion process (showing minimal refractory bonding) [Schacht 2004].

From the FLC profile it is evident that matte and gases penetrated the freeze lining and diffused through the rammable refractory material, since base metal sulphides and solidified sulphur were detected between the freeze lining and the copper cooler.

Sulphur vapour is one of the gases that are given off during PGM smelting [Andrews 2008]. Orthorhombic α-sulphur is stable at room temperature and it converts to monoclinic β-sulphur at 95.5°C. Orthorhombic sulphur melts at 110°C on rapid heating while monoclinic sulphur melts at 114°C [Vaughan et al. 1978]; other published melting points of sulphur are 115°C [Baker 1992] and 120°C [Vaughan et al. 1978]. This variability in the melting point of sulphur makes it a complex element. The temperature-pressure phase diagram of sulphur is depicted in Figure 15 with an insert showing the detail at low temperature and pressure. Sulphur vaporises at 445°C [Andrews 2008], while the temperatures at the feed-slag interface are expected to be above 500°C. Sulphur is expected to evolve at the feed-slag interface and it can be driven towards the furnace wall by the high heat and movement of the slag. Sulphur can further permeate through the refractory brick or freeze lining to reach the copper cooler surface.
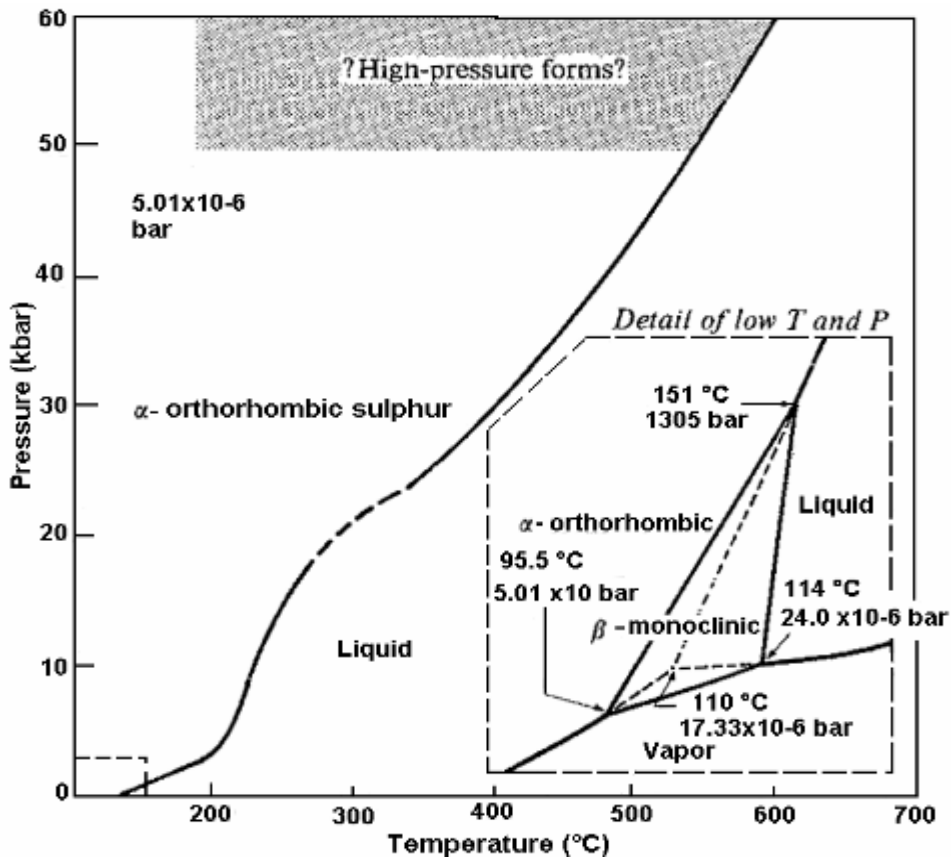
Figure 15: Temperature-pressure diagram for sulphur [Vaughan et al. 1978].

If the copper cooler surface is below 110°C sulphur will be deposited on the cooler surface as a solid. When the copper cooler surface temperature increases above 110°C the deposited sulphur will melt. Sulphur can further react with the copper cooler, forming covellite and chalcocite (Equations 11, 12 and 13). Covellite is in equilibrium with pure sulphur at temperatures below 507°C, while chalcocite is in equilibrium with pure copper at temperatures below 435°C, as shown in Figure 2. Covellite may also form as a result of the reaction of sulphur vapour with other sulphides, as shown in Equation 12. Digenite forms when sulphur reacts with chalcocite (Equation 14). At high sulphur partial pressures the following reactions can take place:

$$2Cu(s) + S_2(g) \rightarrow 2CuS(s) \qquad\qquad\qquad \textit{Equation 11}$$

$$Cu_{5.5}FeS_{6.5}(s) + S_2(g) \rightarrow CuS(s) + FeS_2 \qquad\qquad \textit{Equation 12}$$

$$2Cu(s) + \tfrac{1}{2}S_2(g) \rightarrow Cu_2S(s) \qquad\qquad\qquad \textit{Equation 13}$$

$$9Cu_2S(s) + \tfrac{1}{2}S_2(g) \rightarrow 2Cu_9S_5(s) \qquad\qquad \textit{Equation 14}$$
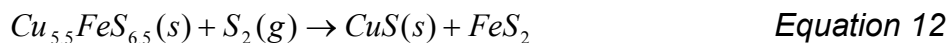
Bornite can form when sulphur reacts with chalcopyrite (Equation 15). In excess sulphur a reaction according to Equation 16 can occur. A solid solution of bornite-covellite-digenite and chalcocite occurs in a copper-iron sulphur system at low temperatures [Klein et al. 1937].

$$5CuFeS_2(s) + S_2(g) \rightarrow Cu_5FeS_4(s) + 4FeS_2 \qquad\qquad \textit{Equation 15}$$

$$Cu_5FeS_4(s) + S_2(g) \rightarrow Cu_{5.5}FeS_{6.5}(s) + FeS_2 \qquad\qquad \textit{Equation 16}$$
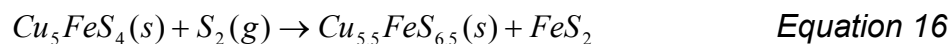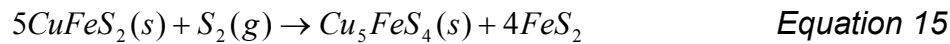
Arsenic sulphides (enargite Cu_3AsS_4 or tennantite $Cu_{12}As_4S_{13}$) geologically associate with bornite, covellite, chalcocite and chalcopyrite [Fornasiero et al. 2001, Klein et al. 1937]. For this reason arsenic and tellurium are expected to be present in the feed material and in the furnace melt. It can be concluded that the presence of these minerals in the corrosion product may be due to the infiltration of the furnace melt through the freeze lining wall to the copper cooler surface.

Millerite (NiS) is a constituent of the smelter feed. A metal-deficient form of millerite $Ni_{1-x}S$ is stable above 379°C [Vaughan et al. 1978].

The smelter concentrate consists of base metal sulphides such as chalcopyrite ($CuFeS_2$), pyrite (FeS_2), pentlhandite ($(FeNi)_9S_8$), pyrrhotite ($Fe_{1-x}S$) and millerite (NiS) as summarised in Table 2 [Jones 1999]. Predictions of the chemical reactions at typical slag temperatures through the use of FactSage are depicted in Table 2. From the predicted reactions the products consisted of sulphur vapour as gas species and the liquid phase had iron sulphide, copper iron sulphide and nickel sulphide. Therefore the presence of these phases can be expected in the furnace melt and consequently in the top portion of the furnace wall (freeze lining) where feed dissolution takes place.

Copper chloride can form when copper reacts with a chlorine-containing gas. Chlorine can be carried by the feed material as salts such as NaCl and $CaCl_2$. On dissociation the chlorine gas can react with the hydrogen gas released

when moisture carried by the smelter feed dissociates to hydrogen and oxygen at high temperatures. The reactions of copper and chlorine containing gas were investigated in the laboratory test work in order to determine the role of chlorine in sulphidation and are reported in Chapter 7.

5.3.6. Sample collected between the front brick and the copper cooler (FBC)

5.3.6.1. SEM analysis (FBC)

EDS analysis identified covellite, elemental sulphur, corundum and eskolaite as predominant phases in the corrosion product collected behind the front brick (FBC), The BSE image is shown in Figure 16. As in FLC, the corrosion products seem to form at the pores of the rammable. No digenite, nickel sulphide or chalcocite was detected in this sample. This observation suggests that the corrosion mechanism behind the front brick is different from the corrosion mechanism that occurs when the brick is totally consumed (and only a freeze lining exists).

5.3.6.2. XRD analysis (FBC)

Corundum, covellite, elemental sulphur and eskolaite were the major phases detected by XRD with atacamite as a minor phase. A summary of the EDS and XRD analyses of the sample FBC is shown in Tables 14 and 15 respectively.

Table 14: EDS analyses of FBC (wt %)

Figure 16	Al_2O_3	CaO	Cr_2O_3	*Cu	*S	SiO_2	SO_3	TiO_2	Phase
Point 19	99.4						0.3	0.2	Al_2O_3
Point 20	5.0	0.3	91.2			0.4	2.3		Cr_2O_3
Point 21			0.1	0.4	99	0.3			S
Point 22				53.6	44.3				CuS
*Cu and S are in atom %									

Table 15: XRD quantitative analyses for FBC (%)

XRD phase	Stoichiometry	XRD %
Corundum	Al_2O_3	29.29
Eskolaite	Cr_2O_3	18.65
Sulphur-alpha	S	21.81
Covellite	CuS	23.36
Atacamite	$Cu_2Cl(OH)_3$	6.89

5.3.6.3. XRF analysis (FBC)

Major elements in XRF analyses of FBC are copper, corundum, SO_3, eskolaite, sulphur and minor amounts of Cl and SiO_2 (Table 16). Iron and nickel were not detected in FBC. Arsenic, thallium and tellurium amounts were much less compared to the amounts of these elements that were detected in the corrosion product behind the freeze lining.

Table 16: XRF analyses for FBC (mass %)

S	SO_3	SiO_2	Fe	Al_2O_3	Cu	Cl	NiO	Cr_2O_3	As_2O_3	Tl_2O_3	TeO_2
20.2	6.45	1.13	0	21.8	28	3	0.1	12.01	0.18	0.02	0.08

UNIVERSITEIT VAN PRETORIA
UNIVERSITY OF PRETORIA
YUNIBESITHI YA PRETORIA Sulphidation of copper coolers in PGM smelters
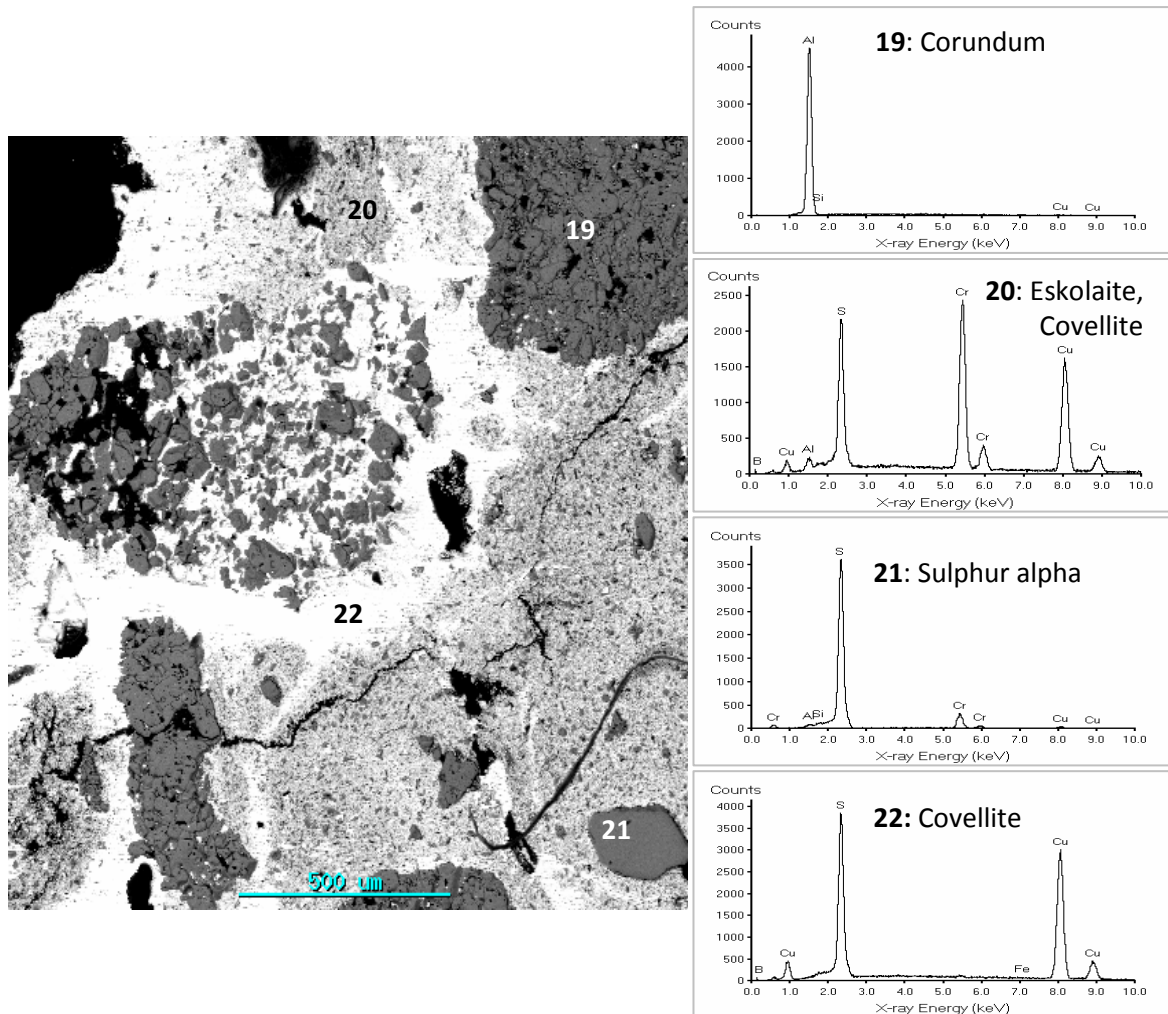
Figure 16: BSE image of the corrosion product collected between the copper cooler and the front brick (FBC) with EDS spectra of the annotated points.

5.3.6.4. Discussion (FBC)

The mag-chrome brick was completely corroded at the slag/feed interface while at the slag zone there was some brick left in front of the cooler. Slag attack and slag turbulence may result in refractory brick being completely eroded, as described by Shacht [2004] in Figure 14.

Wear of the copper cooler behind the front brick proceeded through chemical reaction between the copper cooler and the furnace off gases, which resulted in the deposition of sulphur and consequently the formation of covellite. This

was preceded by the penetration of the off gas through the refractory brick and the rammable material. Sulphur and water vapour carried by the feed are driven by the high heat of the slag to the cooler parts of the furnace, ie. the surface of the copper coolers [Hopt et al. 2006].

5.4. Summary of the main phases detected in the post-mortem samples

Eskolaite and corundum were present in all the corrosion products (the freeze lining sample, sample behind the freeze lining and sample behind the brick) because they are the main phases present in the ramming refractory material that was used to fill the waffle knob area. The significant finding from the FLC analysis is that there is a substantial amount of base metal sulphides at the freeze lining-copper cooler interface with a significant amount of sulphur associated with covellite and arsenide. Sulphate and oxide phases were not detected behind the freeze lining, but at the interface of the top brick and the copper cooler. Minor amounts of chlorine phases were detected by XRD and XRF. It can be concluded that the corrosion mechanism behind the freeze lining proceeds due to the presence of matte and element sulphur at the interface of the freeze lining and the cooler.

The significant findings on the FBC analysis are that only covellite and element sulphur formed the bulk of the corrosion product behind the front brick. Iron and nickel were not detected behind the front brick, which rules out the presence of base metal sulphides associated with feed or matte. Therefore the corrosion mechanism behind the front brick proceeds through gaseous attack whereby sulphur reacts with the copper cooler to form covellite. The possibility of this reaction was tested in the laboratory to determine under which conditions sulphur and copper can react to form covellite.

The EDS analyses detected higher (Cu+Fe):S atomic ratios in the corrosion products than the stoichiometric phases, e.g. the digenite (Cu+Fe):S atomic ratio is 9:1 but EDS detected a ratio of 10:1 and the covellite stoichiometric ratio is 1:1, but EDS detected an atomic ratio of 1.26:1, which was confirmed

by XRD as covellite. The copper content in the sample behind the brick was less than in the sample behind the freeze lining. The presence of base metal sulphides will also contribute significantly to the copper content. A summary of the phases detected in the corrosion products is shown in Table 17. Silicates, sulphides and copper chloride in small amounts were constituents of the freeze lining. Base metal sulphides, element sulphur and atacamite were observed behind the freeze lining. Covellite, element sulphur and atacamite were detected behind the front brick.

Table 17: Summary of phases detected in the corrosion products

Sample name	Phases
Freeze lining	Slag: augite, diopside, forsterite and chromite Sulphides: digenite, chalcopyrite, iron sulphide, $(Cu,Fe,Ni)_xS$ and millerite Other: $CuCl_2$
Behind freeze lining	S, CuS, Cu_9S_5, NiS, $(CuFe)_5S_4$, $(CuFe)_4S_4$, $Cu_2(OH)_3Cl$
Behind the front brick	S, CuS, $Cu_2(OH)_3Cl$

5.5. Conclusions

The wear mechanism of copper waffle coolers used in PGM smelters was studied through a post-mortem analysis of samples that were taken from the refractory wall of a primary PGM smelter. Two wear mechanisms were identified. In one the copper cooler reacted with the base metal sulphides such as NiS, digenite and bornite intermediate solid solution, which infiltrated the porous freeze lining. Chalcocite (Cu_2S), covellite (CuS) and a non stoichiometric copper sulphide ($Cu_{2-x}S$) were observed closer to the copper cooler.

The other corrosion mechanism was through the reaction of the copper cooler with gases evolving from the furnace, such as sulphur vapour. This led to the formation of copper sulphides, such as covellite and chalcocite, which resulted in the consumption of the copper cooler.

6. GRAPHITE BLOCK POST- MORTEM ANALYSES

6.1. Background

To address the corrosion problems associated with the copper cooler, a new copper cooler design was implemented in which the height of the copper cooler was divided into two, so that there is an upper and a lower cooler (Figure 17) [Van Manen 2008]. Different materials were tested to determine which material would effectively protect the top copper cooler from the corrosive environment [Nelson et al. 2006, Van Manen 2008]. Graphite blocks were installed on all the upper waffle coolers, since graphite appeared to be the most effective material to protect copper coolers [Van Manen 2008]. This chapter entails the SEM, ICP and XRD analysis of a post-mortem sample of a graphite block.

The schematic diagram of the new refractory wall design is depicted in Figure 17 [Van Manen 2008]. In the initial design a single waffle copper cooler was installed at the slag zone.
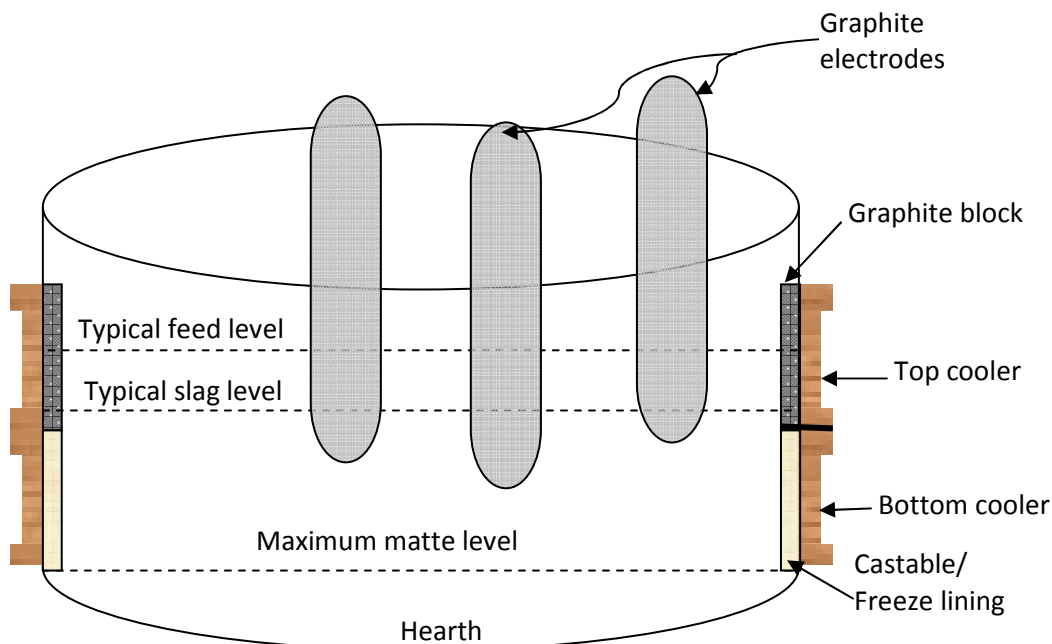
Figure 17: Schematic diagram of furnace cross-section with graphite block installed.

In the latest design the copper cooler has been split horizontally into two portions, the top cooler with the graphite in front and the lower cooler with the castable in front as shown in Figure 17 [Van Manen 2008]. The graphite block installation has minimised the corrosion substantially in the feed-slag zone, although severe corrosion is now observed at the graphite block-castable interface.

The graphite block was submitted for analysis with the aim of determining the phases involved in the corrosion of the copper cooler. It had been used as a lining in front of the copper coolers replacing the magnesia-chrome bricks which were initially used to line the furnace where corrosion problems were observed. The graphite block was received from the same smelter from which the post-mortem samples discussed in the previous chapter were collected. This particular graphite block was received after being in production for six months.

The sketch of the graphite block is depicted in Figure 18, where G-1 to G-bottom are the annotations used to identify where the samples were taken. G-1 is the top portion of the graphite block and G-bottom is the bottom (lower) portion of the graphite block in contact with the castable surface. The graphite block was 100mm in thickness, 105mm in width and 600mm in height, with grooves of 20mm in width on the hot surface to facilitate the slag retention and form a freeze lining. Carbon paste was used to fill in the gaps between the graphite blocks. The hot surface was denoted as (front) and the cold surface in contact with the cooler was denoted as (back). G-lid is the back portion of the graphite that was mechanically holding the graphite block and the cooler together.
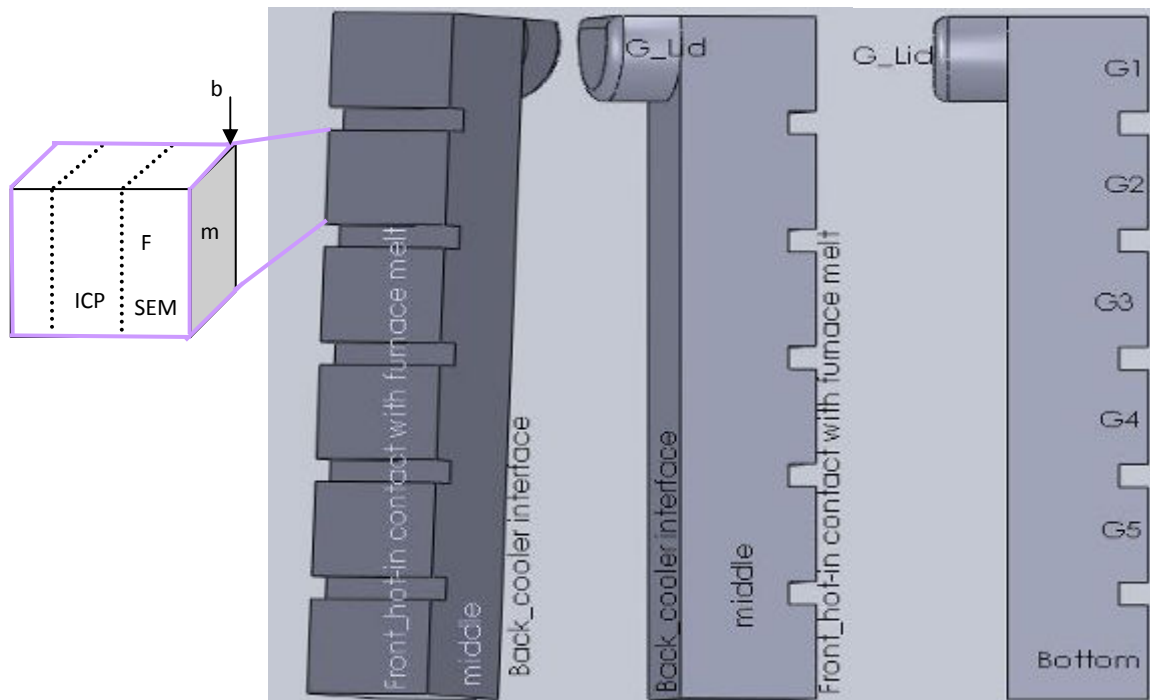
Figure 18: Schematic diagram of the graphite block.

The insert in the sketch depicts where the samples were taken for different analytical techniques. The edge marked SEM is where the SEM and the XRD sample was taken (where f = front, m = middle and b = back). The middle portion of the sketch marked ICP shows where the ICP samples were cut.

To investigate the copper cooler corrosion mechanism the phases in the hot face and the cold face of the graphite block were determined using SEM, XRD and ICP. These phases were then compared to the phases observed in the post-mortem sample that was collected when magnesia-chrome bricks were used as a front lining. The presence of similar phases, especially at the cold face of the graphite block, would confirm whether the copper cooler corrosion progressed through matte attack or gas attack or both. The comparison between the post-mortem samples of both the graphite and the magnesia-chrome bricks would assist in understanding the role of graphite in limiting the corrosion of copper cooler.

6.2. Analyses

The chemical compositions of the phases detected in the graphite block were acquired by SEM using EDS analysis. The micrographs in Figures 19 to 30 were obtained by the SEM using BSE analysis. The graphite portions examined in SEM were only G-1, G-3, G-5, G-bottom and G-lid. ICP was used to determine the elements present in the graphite G-1, G-2 and G-bottom portion. The ICP sample was cut in the middle of the block as indicated in the insert in Figure 18 in order to determine if the furnace constituents diffused through the block to the copper cooler or if they diffused through the graphite block interfaces.

6.2.1. SEM analyses

Pentlandite $(FeNi)_{8.7}S_8$, chalcopyrite $(CuFe_{1.4})S_2$ and a copper-rich chalcopyrite $(Cu_2Fe_{0.4})S_2$ could be identified in sample G-1 front (hot face) (Table 18, Figure 19). The freeze lining on G-1 front mostly had base metal sulphides with minor amounts of augite embedded in sulphides, as shown in Figure 19 (point E).

Pentlandite $(FeNi)_{9.7}S_8$, chalcopyrite $(Cu_{1.8}Fe_{0.6})S_2$, copper iron nickel sulphide and copper iron sulphide, similar to the sulphide in G-1 front, were distinguished in sample G-1 middle. Copper sulphide phase with no iron was observed in the graphite. Arsenide associated with covellite was observed as an inclusion in the slag in G-1 middle, as shown in Figure 20 and reported in Table 18. The material attached to the side of the graphite had matte closer to the hot face and slag furthest from the hot face (towards the copper cooler). The slag had arsenic-copper sulphides embedded in it.

The infiltration at the cold face of graphite was more pronounced than in the hot face. Sulphide phases observed in sample G-1 back consisted of a copper-rich sulphide $Cu_{2+x}S$ (x=0.32) associated with a copper iron nickel sulphide at the graphite-copper cooler interface respectively denoted as 0 and 1 in Figure 21. The copper-rich phase was not detected at the hot face (front). It is presumably a product of a reaction between the copper cooler and the furnace contents or gases.

Table 18: EDS area analyses of G-1 front, middle and back (atom %)

G-1 Front	As	Cl	*Ca	*Cr	Cu	Fe	*Mg	*Na	Ni	S	*Si	Total	Stoichiometry	Phase
1	0.0	0.0	0.0	0.0	0.0	24.0	0.0	0.0	27.0	47.0	0.0	98.6	$(Fe,Ni)_{8.7}S_8$	Pentlandite
2	0.0	0.0	0.0	0.0	22.4	32.0	0.0	0.0	1.2	45.0	0.0	99.8	$(CuFe_{1.4})S_2$	Chalcopyrite
3	0.0	0.0	0.0	0.0	45.5	9.2	0.0	0.0	0.0	45.0	0.0	99.4	$(Cu_2Fe_{0.4})S_2$	Chalcopyrite
D	0.0	0.0	11.0	1.8	0.0	16.0	23.0	0.0	0.0	0.0	47.3	98.8	$(Mg,Fe,Ca)_{2.1}Si_2O_6$	Augite
G-1 middle														
1	0.0	0.0	0.0	0.0	4.7	39.0	0.0	0.0	9.1	44.0	0.0	96.9	$(Cu,Fe,Ni)_{9.7}S_8$	Pentlandite
2	0.0	0.0	0.0	0.0	39.3	12.0	0.0	1.8	2.1	43.0	0.0	98.9	$(Cu_{1.8}Fe_{0.6})S_2$	Chalcopyrite
3	0.0	0.0	0.0	0.0	53.8	0.0	0.0	0.0	0.0	46.0	0.0	99.7	$Cu_{1.2}S$	Copper sulphide
D	0.0	1.0	0.0	0.0	0.0	0.0	0.0	0.0	0.0	11.0	85.1	96.8	Si, S	Si, S
E	11.0	0.0	0.0	0.0	39.2	1.8	0.0	3.4	0.0	42.0	2.3	99.6	$Cu_{0.9}S$, As	Covellite, arsenic
G-1 Back														
0	0.0	0.0	0.0	0.0	67.0	0.2	0.0	2.5	0.05	29.0	1.25	99.8	$Cu + Cu_2S$	Copper, chalcocite
1	0.0	0.0	0.0	0.0	9.4	38	0.0	0.0	12.3	38.0	1.3	99.7	$(Cu,Fe,Ni)_{1.54}S$	Copper iron nickel sulphide
2	0.0	0.0	0.0	0.0	66.3	0	0.0	3.1	0.1	28.9	1.6		$Cu + Cu_2S$	Copper, chalcocite

*Ca, Cr, Mg, Na and Si were taken as oxides i.e Ca=CaO, Cr=Cr_2O_3, Mg=MgO, Na=NaO and Si=SiO_2.
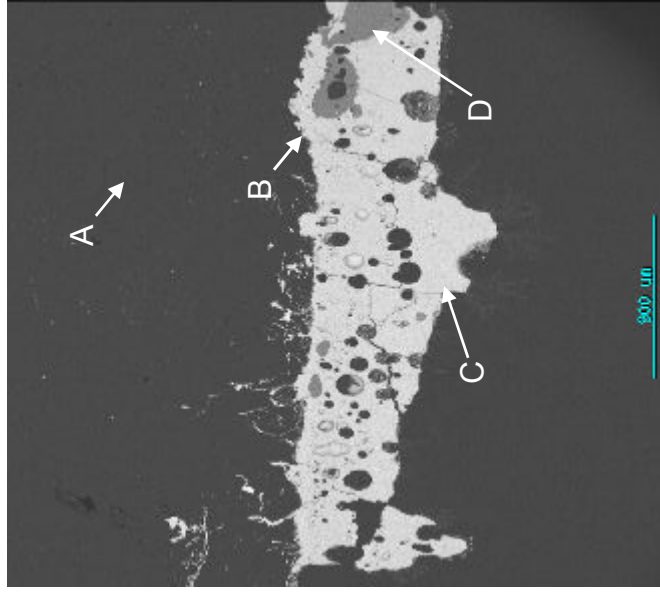
a) Freeze lining-graphite interface
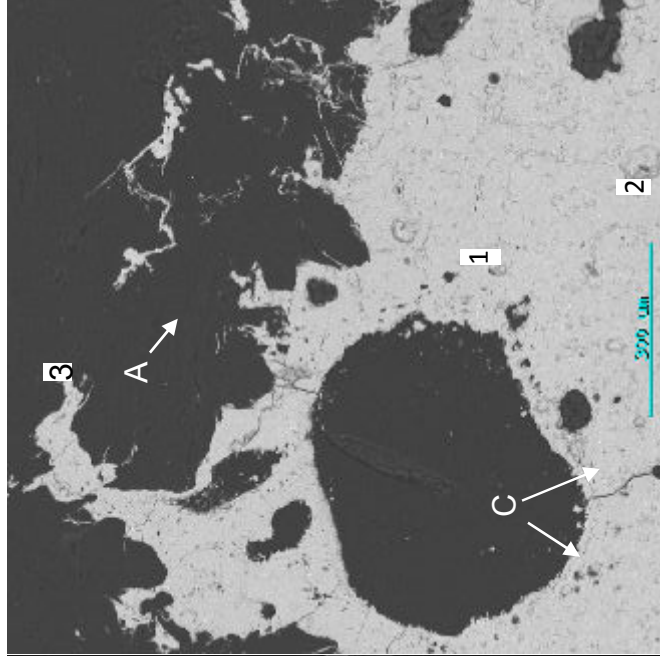
b) Detailed view of the freeze lining-graphite interface
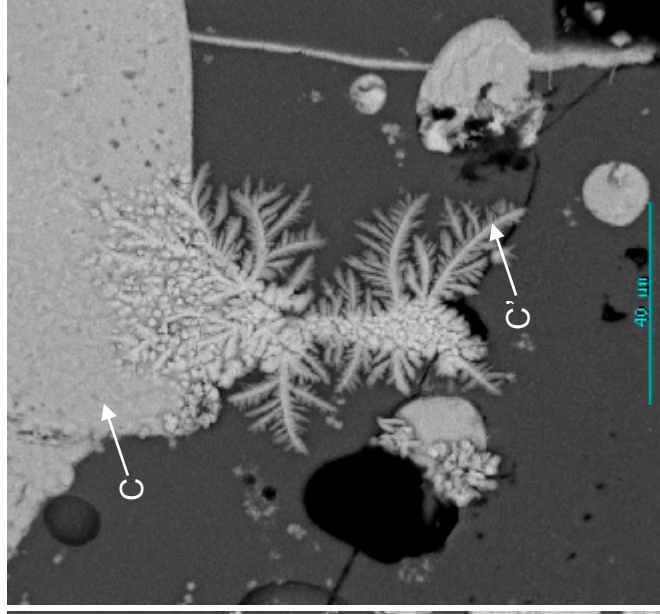
c) Detailed view of the sulphide infiltration in graphite

Figure 19: BSE image of the sample G-1 front, A = graphite block; B = interface between graphite and freeze lining; C = sulphides;

C' = dendrites extending from the sulphides; D = slag surrounded by sulphides.

Sulphidation of copper coolers in PGM smelters

a) Matte build-up on graphite-graphite interface   b) Slag build-up on graphite-graphite interface
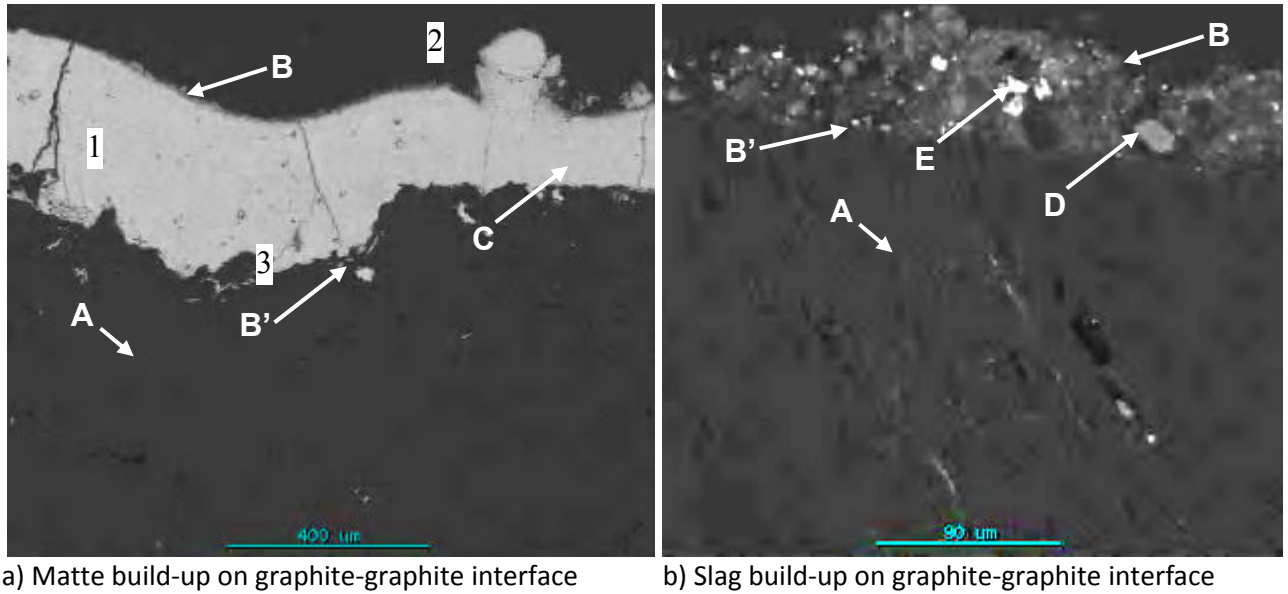
Figure 20: BSE image of the graphite-graphite interface of sample G-1 middle, A = graphite block; B = interface between two graphite blocks; B' = graphite-buildup interface; C = sulphides attached to the graphite block; D = slag; E = matte in slag.

The depth of infiltration of graphite by sulphides at the cold face can be attributed to the difference in pressure between the cold face and the hot face of graphite. When the furnace is operating at a positive pressure, the furnace contents, especially gases, are more prone to be escaping the furnace at higher rates, whereas if the operating pressure inside the furnace is slightly negative, the vacuum will suck the gases inwards from the colder face to the hotter face.
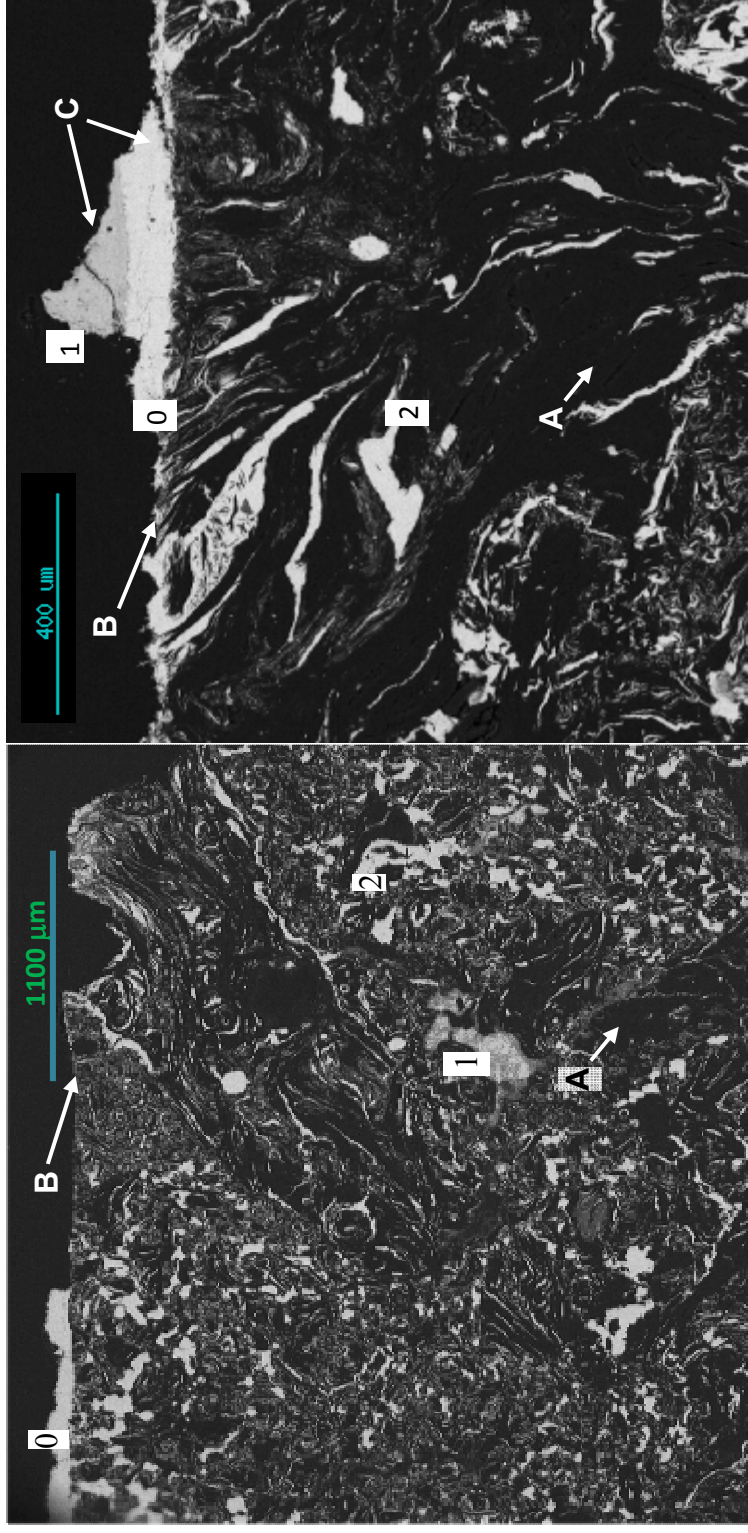
a) G-1 cold face

b) Detailed view of G-1 cold face

Figure 21: BSE image of sample G-1 back. A = graphite block; B = graphite-copper cooler interface; C = sulphides attached to the graphite block at the cooler interface; 0,1,2 = different types of sulphides in the graphite block.

Sulphidation of copper coolers in PGM smelters

Pentlandite $(FeNi)_{8.9}S_8$, chalcopyrite $(Cu_{1.1}Fe_{1.4})S_2$ and slag (augite) could be identified in sample G-3 front (hot face). G-3 hot face BSE image is depicted in Figure 22. G-3 middle was not examined by SEM. G-3 back (cold face) had a copper sulphide with a copper-to-sulphur atomic ratio of 1.2 and a copper-rich chalcocite $Cu_{2+x}S$ (x=0.6) and copper chloride $(CuCl_{0.7})$. BSE images of G-3 back are depicted in Figure 23. EDS area analyses of the phases distinguished in sample G-3 front and G-3 Back are depicted in Table 19.
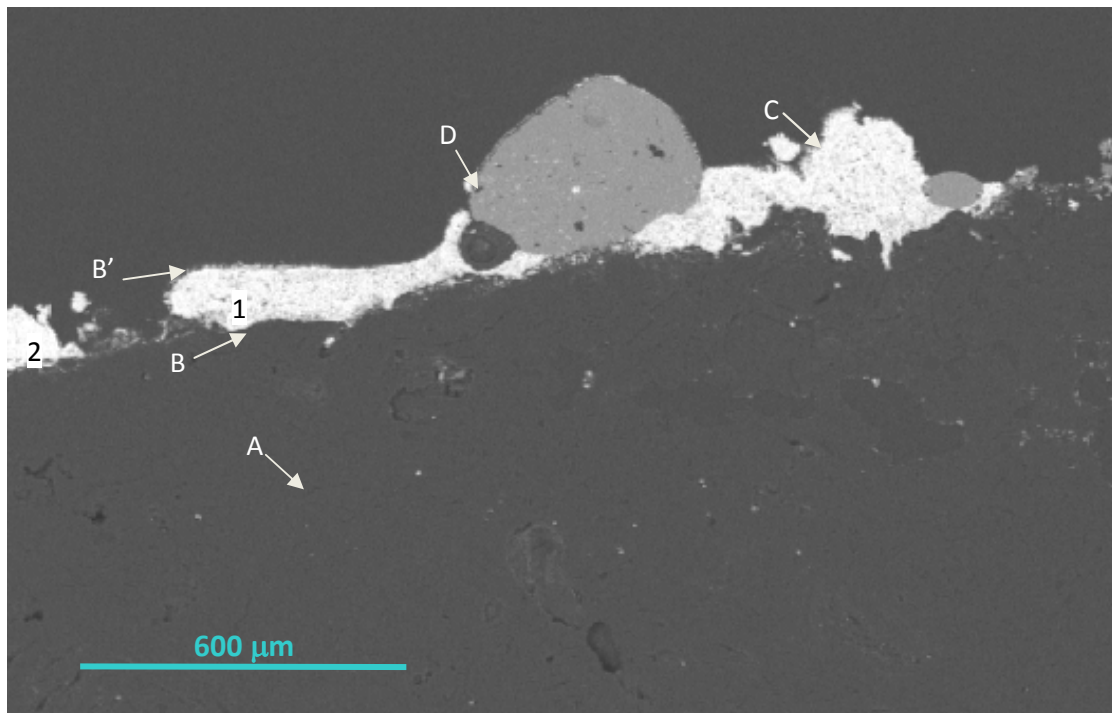
Figure 22: BSE image of sample G-3 hot. A = graphite block; B = graphite-freeze lining interface; B'=freeze lining-furnace melt interface; C = matte; D = slag; 1,2 = different types of sulphides in the graphite block.

Table 19: EDS area analyses of G-3 hot and cold face (Atom %)

G3_hot	Al	Ca	Cl	Cr	Cu	Fe	Mg	Na	Ni	S	Si	Total	Stoichiometry	Phase
1	0	0	0	0	22.8	31			1.4	43		98.6	$(Cu_{1.1}Fe_{1.4})S_2$	Chalcopyrite
2	0	0	0	0.9	22	20		1.8	9.3	46		99.5	$(Cu,Fe,Ni)_{8.9}S_8$	Pentlandite
D	4	11	0	2.1		17	18				46.9	98.5	$(Ca,Mg,Fe)_{1.8}(Si,Al)_2O_6$	Augite
G3_cold														
D			0		97	0		0		1.6		98.6	Cu	Copper
E			41		56.6					1.7		99.3	$CuCl_{0.7}$	Copper chloride
C			3.5		78.9	1.7		6.5		7.6		98.2	Cu	Copper
C'					54.4					45		98.9	$Cu_{1.2}S$	Copper sulphide
C''					71	0.9				27		99.1	$Cu + Cu_2S$	Copper+chalcocite
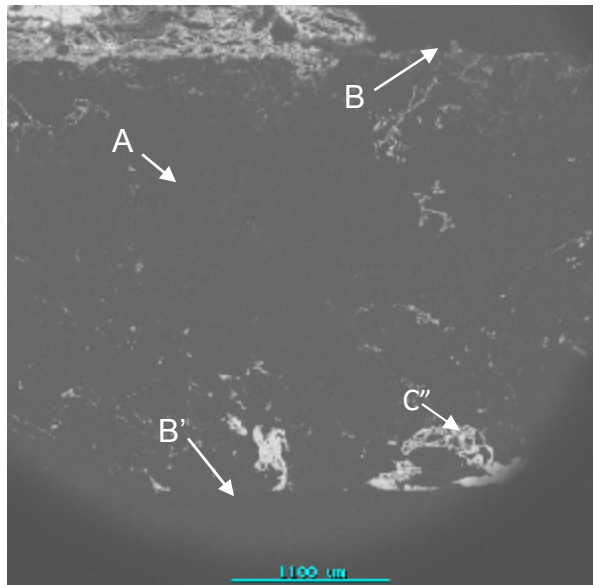
a) Graphite-copper cooler interface
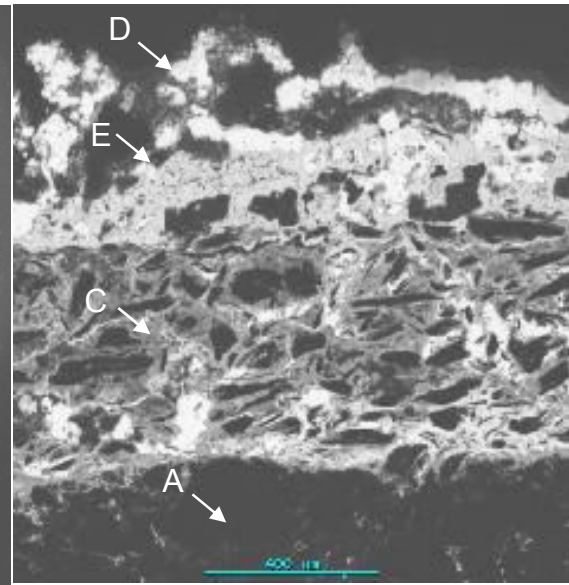
b) Detailed view of the graphite cooler interface
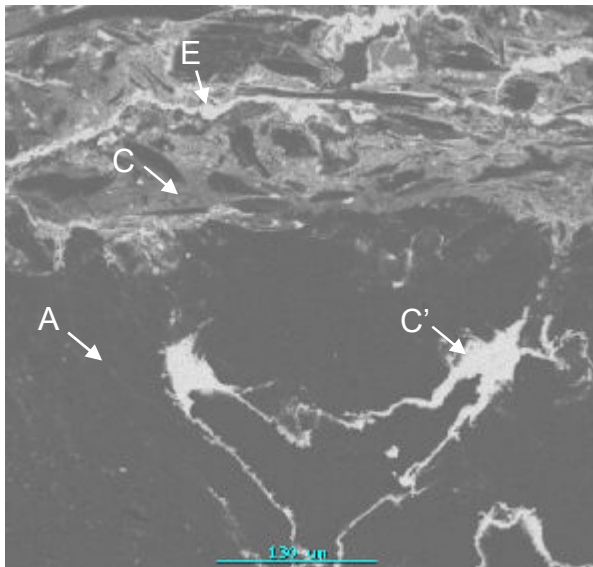
c) Sulphides penetrated in graphite
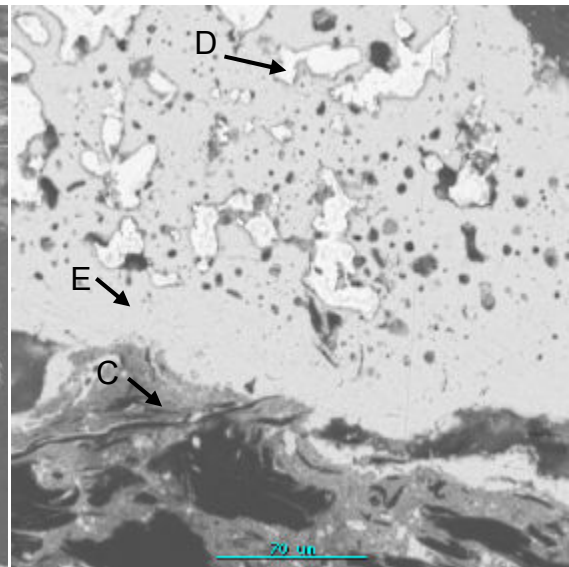
d) Detailed view of the corrosion product

Figure 23: BSE image of sample G-3 cold face. A = graphite block; B = copper cooler-graphite interface; B' = graphite-graphite interface; C = copper sulphide; C' = Cu$_{2.6}$S; D = copper; E = copper chloride.

Sample G-5 front has slag and matte at the freeze lining. The depth of infiltration of graphite by furnace contents is higher than in sample G-1 hot face. There is also slag penetration in the graphite whereas in G-1 front only matte was observed in the graphite. The furnace contents attached to G-5 front had a copper-rich digenite $(Cu,Fe)_{2.1}S$, chalcopyrite $Cu_{1.3}Fe_{1.3}S_2$, copper iron nickel sulphide $(Cu_{0.2}Fe_{0.4}Ni_{0.3}S)$ and slag, which consisted of the oxides of calcium, aluminium, silica and chlorine. Sample G-5 middle consisted of iron nickel sulphide and iron embedded in the graphite.

There were no large pieces of slag or matte attached to the graphite at the sample G-5 cold face. There was, however, infiltration of sulphides into the graphite up to a depth greater than 1 mm. Copper nickel sulphide $(Cu,Ni)_{2+x}S$ (x=0.4), chalcopyrite $(Cu_{1.2}Fe_{1.2}S_2)$, digenite $(Cu_{1.8}S)$ and a copper-rich chalcocite $Cu_{2+x}S$ (x=0.2) were the phases observed in the graphite (sample G-5 cold face). BSE images of G-5 hot face, middle and cold face are presented in Figures 24, 25 and 26 respectively. EDS area analyses of phases found in sample G-5 are presented in Table 20.

Table 20: EDS area analyses of G-5 front, middle and back (atom %)

G-5 front	Al	Ca	Cl	Cr	Cu	Fe	Mg	Na	Ni	S	Si	Te	Total	Stoichiometry	Phase
0	0.0	0.0	0.0	0.0	11.0	77.3	0.0	2.1	0.0	7.9	0.0	0.0	98.6	Fe	Iron
1	0.0	0.0	0.0	0.0	59.0	8.2	0.0	0.0	0.0	32.3	0.0	0.0	99.4	$Cu_{1.8}Fe_{0.3}S$	Digenite
2	0.0	0.0	0.0	0.0	28.0	27.5	0.0	1.5	0.0	42.5	0.0	0.0	99.4	$Cu_{1.3}Fe_{1.3}S_2$	Chalcopyrite
A0	1.2	40	15	0.0	0.0	0.0	0.0	0.0	0.0	0.0	38.0	5.0	98.9	Ca, Si, Al and Cl	Mixture of silicon, calcium, alumina and chlorine
A1	0.0	24	9	0.0	0.0	0.0	0.0	0.0	0.0	0.0	66.0	0.0	98.6	Si, Ca and Cl	Mixture of silicon, calcium and chlorine
A2	0.0	0.0	0.0	9.2	9.9	17.5	0.0	0.0	15.0	48.1	0.0	0.0	99.4	$(Cu_{0.2}Fe_{0.4}Ni_{0.3})S$	Copper iron nickel sulphide
G-5 middle															
0	0.0	0.0	0.0	0.0	0.0	34.3	0.0	0.0	16.0	47.2	0.0	0.0	97.7	$(Fe_{0.7}Ni_{0.3})S$	Iron nickel sulphide
1	0.0	0.0	0.0	0.0	2.8	84.1	0.0	0.0	3.0	7.55	0.0	0.0	97.4	Fe	Iron
G-5 back															
0	0.0	0.0	0.0	0.0	30.0	0.0	0.0	3.2	43.0	21.1	1.6	0.0	99.4	$(Cu_{1.4}Ni_2)S$	Copper nickel sulphide
1	0.0	0.0	2.0	0.0	49.0	0.0	0.0	5.8	9.8	31.1	0.6	0.0	98.4	$(Cu_{1.6}Ni_{0.32})S$	Copper nickel sulphide
2	0.0	0.0	0.0	0.0	27.0	27.4	0.0	0.0	0.0	44.2	0.0	0.0	98.1	$Cu_{1.2}Fe_{1.2}S_2$	Chalcopyrite
3	0.0	0.0	1.0	0.0	57.0	0.0	0.7	8.3	0.0	31.2	0.7	0.0	98.7	C_9S_5	Digenite
Shades on graphite	0.0	0.0	0.0	0.0	65.0	0.0	0.0	4.6	0.0	29.4	0.3	0.0	99.1	$Cu + Cu_2S$	Copper + chalcocite
Dark next to 0	0.0	0.0	0.0	0.0	75.0	0.0	2.3	0.0	0.0	18.8	3.4	0.0	99.3	$Cu + Cu_2S$	Copper + chalcocite
Slag	0.0	0.0	0.0	0.0	4.1	0.0	27	0.0	0.0	0.0	67	0.0	98.2	Si, Mg and copper	Mixture of silica, magnesium and copper
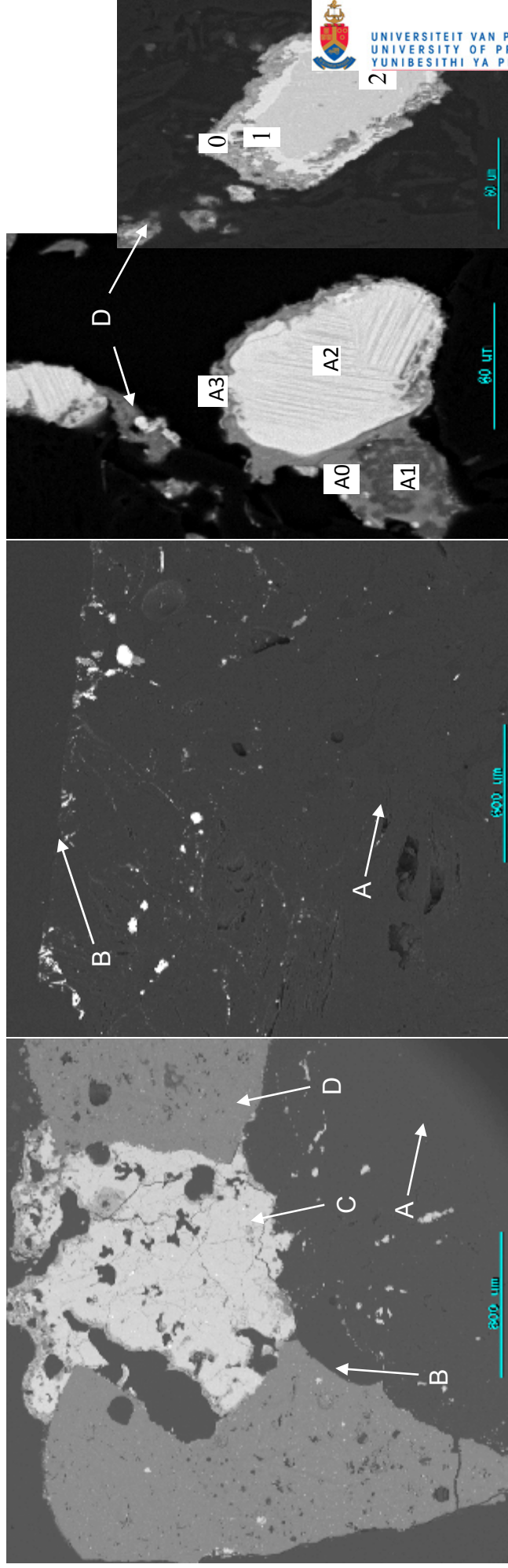
a) Graphite-freeze lining interface

b) Depth of penetration in graphite

c) Detailed view of slag/matte penetration

Figure 24: BSE image of sample G-5 front. A = graphite block; B = graphite-freeze lining interface; C = sulphides; D = slag; 0,1,2, A2 = different types of sulphides in the graphite block; A0, A1 = silicon, calcium, aluminium and chlorine.

Sulphidation of copper coolers in PGM smelters

a) Graphite-graphite interface   b) Detailed view of the penetration
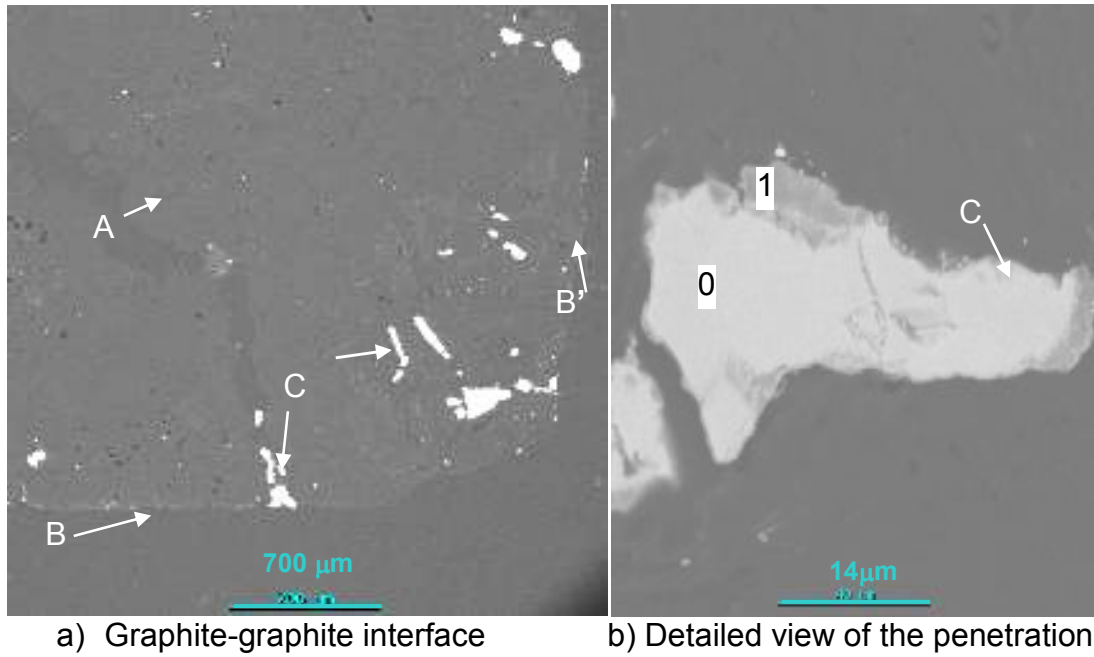
Figure 25: BSE image of sample G-5 middle. A = graphite block; B = graphite-freeze lining interface; B' = graphite-graphite interface; (C,0) = iron nickel sulphide; 1 = Iron.

Sulphidation of copper coolers in PGM smelters
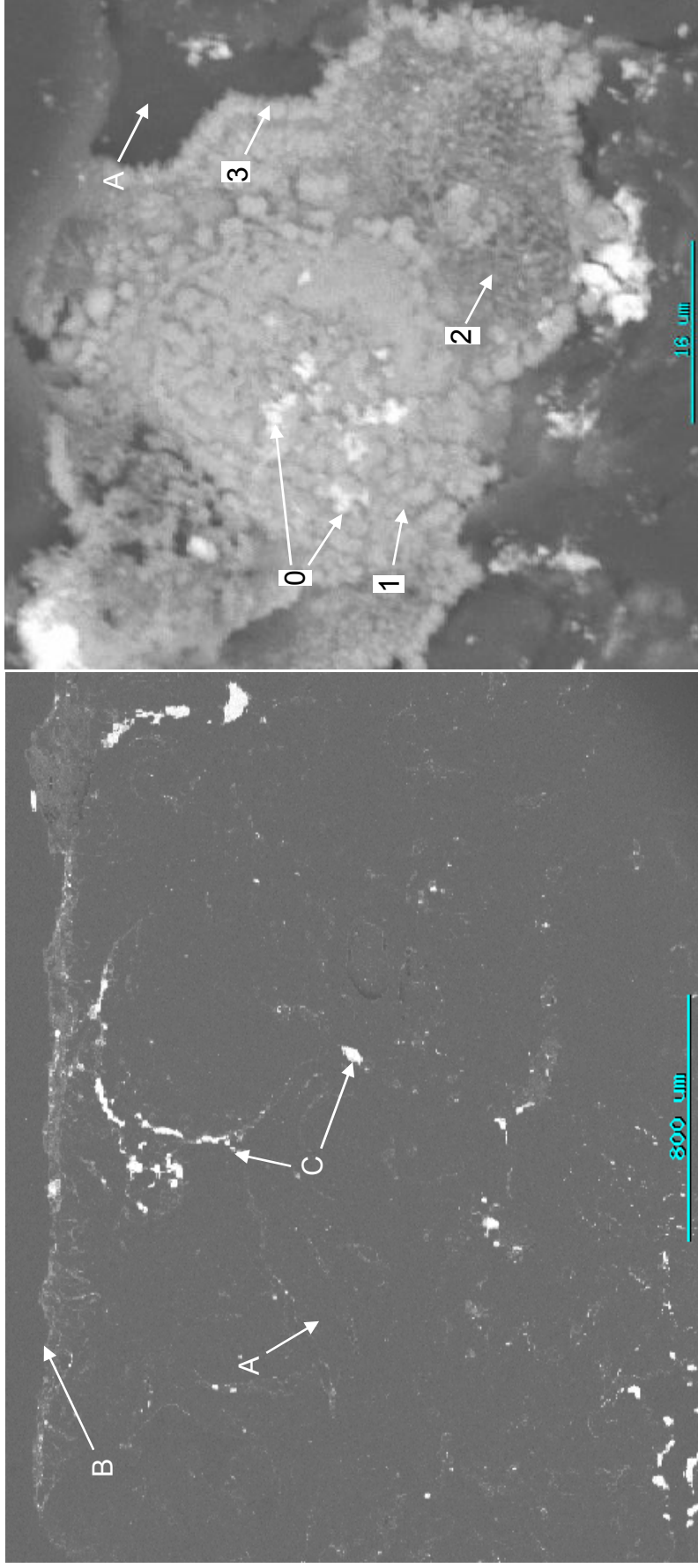
a) Graphite –copper cooler interface

b) Detailed view of the infiltration

Figure 26: BSE image of sample G-5 back. A = graphite block; B = copper cooler-graphite interface; C (0,1,2,3) = sulphides.

Sulphidation of copper coolers in PGM smelters

Sample G-bottom was taken at the graphite-castable interface, which is associated with the slag zone. There was a matte piece that remained attached to the front portion of sample G-bottom. The slag and matte infiltration depth into the graphite hot face was the highest compared to all the sections of the graphite. The infiltration consisted of pentlandite, enstatite, augite and iron adjacent to the slag. Sample G-bottom hot face had much more slag infiltration than the other samples; it had no copper sulphides either. BSE images of the G-bottom front and G-bottom-castable interface are depicted in Figures 27 and 28. EDS area analyses of phases identified in sample G-bottom are depicted in Table 21.

The slag and matte infiltration depth was more pronounced at the graphite-castable interface (middle). Pentlandite, iron sulphide ($Fe_{1.1}S$) and slag (calcium, alumina silicate) were observed in the sample G-bottom middle. No copper sulphides were detected. Chalcopyrite and digenite were the sulphide phases detected by EDS at the G-bottom cold face. The BSE image of G-bottom cold face is depicted in Figure 29.

Sulphidation of copper coolers in PGM smelters

Table 21: EDS area analyses of G-bottom hot face, castable interface and cold face

Hot face	Al	Ca	Cl	Cr	Cu	Fe	Mg	Ni	S	Si	Total	Stoichiometry	Phase
C,D	0.0	0.0	0.0	0.0	0.0	26.0	0.0	27.0	45.7	0.0	98.7	$(Fe,Ni)_{9.3}S_8$	Pentlandite
E-rim	0.0	0.0	0.0	0.0	0.0	96.0	0.0	2.1	0.0	0.0	97.8	Fe	Iron
E	2.0	7.0	0.0	0.0	0.0	13.0	29.0	0.0	0.0	47.0	99.2	$(Ca,Mg,Fe,Al)_2(Si,Al)_2O_6$	Enstatite
1	6.0	10.0	0.0	0.0	0.05	15.0	16.0	0.0	0.25	52.0	98.65	$(Ca,Mg,Fe,Al)_{1.41}(Si,Al)_2O_6$	Augite
2	0.0	0.0	0.0	0.0	0.0	40.0	0.1	11.0	46.8	0.0	98.3	$(Fe,Ni)_{8.7}S_8$	Pentlandite
2-rim	0.0	0.0	0.0	0.0	3.7	86.0	0.0	2.8	5.2	0.0	97.8	Fe	Iron
3	0.0	0.0	0.0	0.0	0.0	9.4	0.1	45.0	44.3	0.0	98.7	$(Fe,Ni)_{9.8}S_8$	Iron nickel sulphide

Castable interface	Al	Ca	Cl	Cr	Cu	Fe	Mg	Ni	S	Si	Total	Stoichiometry	Phase
1	0.0	0.0	0.0	0.0	0.0	52.0	0.0	0.0	47.3	0.0	98.9	$Fe_{1.1}S$	Iron sulphide
2	0.0	0.0	0.0	1.4	0.0	36.0	0.0	15.0	46.6	0.0	99.0	$(Fe,Ni)_{8.8}S_8$	Pentlandite
D	52.0	9.0	1.3	0.0	0.0	5.1	0.0	0.0	17.7	14.0	99.5	slag	Calcium,alumina silicate
D	13.0	12	1.6	0.2	0.0	0.7	8.0	0.0	1.1	62.0	98.9	$(Ca,Mg,Fe,Al)_{0.9}(Si,Al)_2O_6$	Augite

Cold face	Al	Ca	Cl	Cu	Fe	K	Ni	S	Si	Total	Stoichiometry	Phase
cp	1.1	1.0	1.0	42.1	7.3	3.0	3.9	38.8	1.6	99.8	$(Cu_{2.2}Fe_{0.4})S_2$	Chalcopyrite
dg	0.0	0.1	0.1	61.1	3.1	0.3	0.4	34.6	0.3	100	$(Cu,Fe)_{9.2}S_5$	Digenite

Graphite block post mortem analyses

a) G-bottom hot face

b) Matte that remained attached to the graphite hot face

c) Slag that remained attached to the graphite hot face

d) Detailed view of the particles embedded in graphite
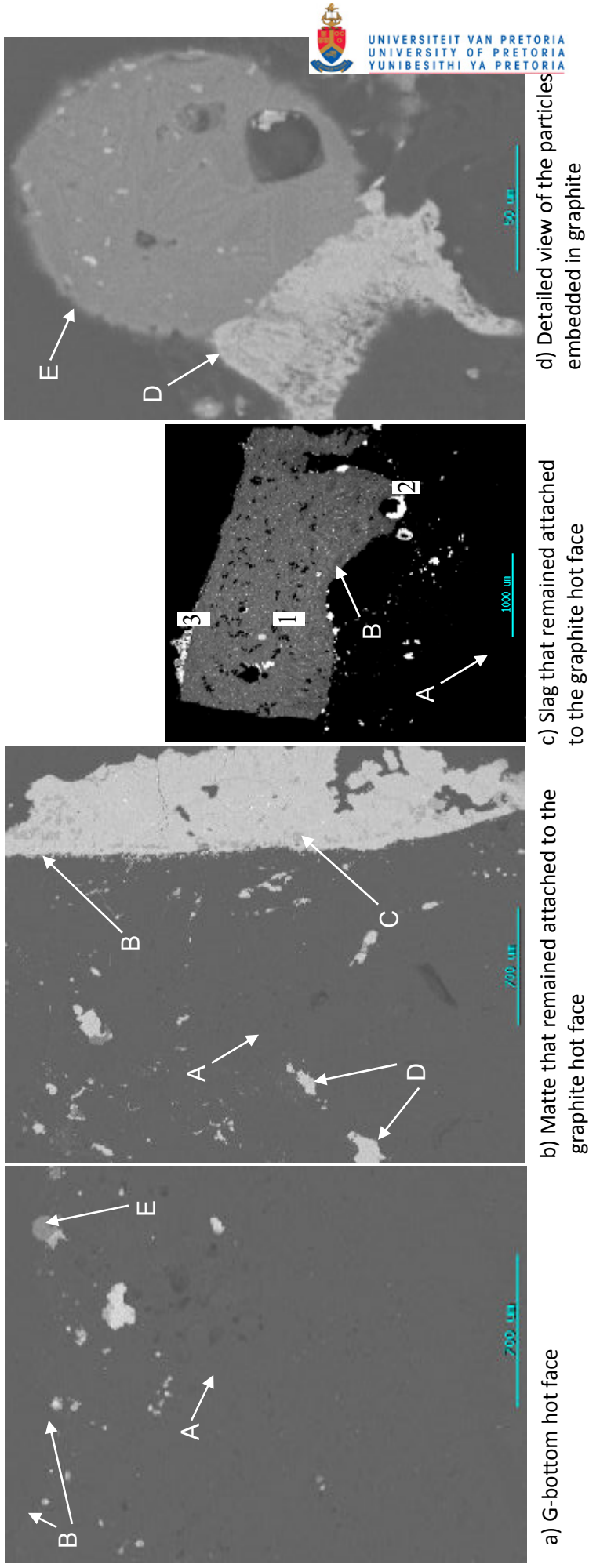
Figure 27: BSE image of sample G-bottom front. A = graphite block; B = freeze lining; C = freeze lining-graphite interface; D(2,3) = sulphides; E(1)=slag.

Sulphidation of copper coolers in PGM smelters
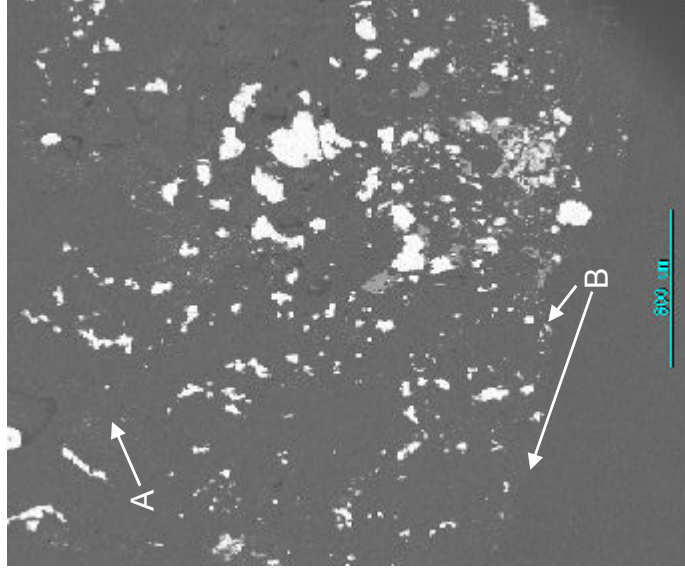
a) Interface of graphite and castable
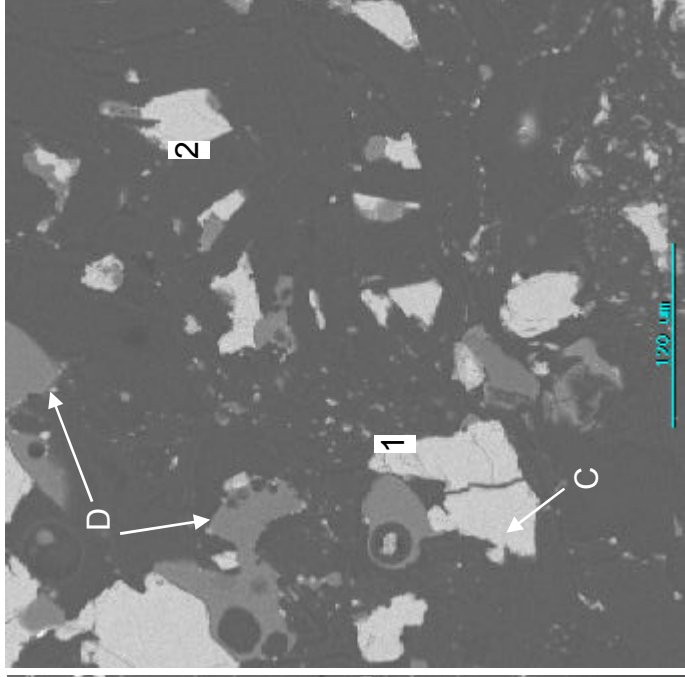
b) Detailed view of the graphite-castable interface
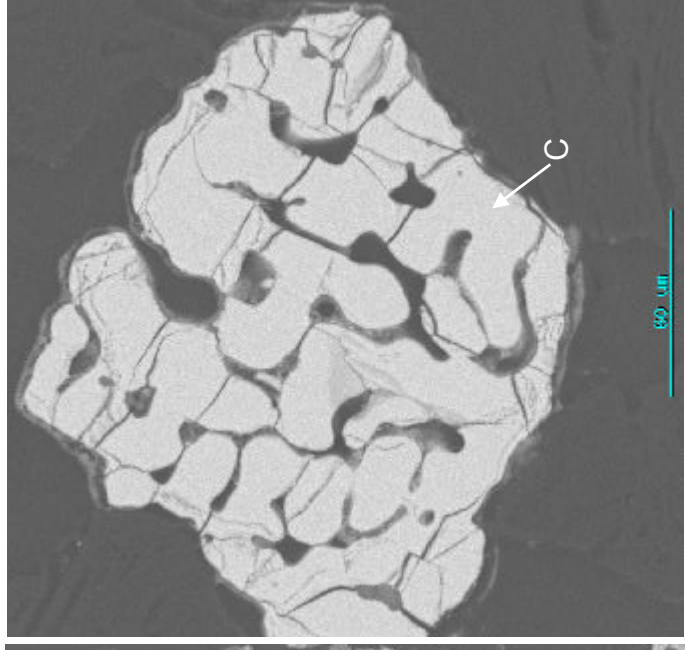
c) Detailed view of the matte particle in the graphite

Figure 28: BSE image of sample G-bottom. A = graphite block; B = copper cooler-graphite interface; C (1, 2) = sulphides; D = slag.
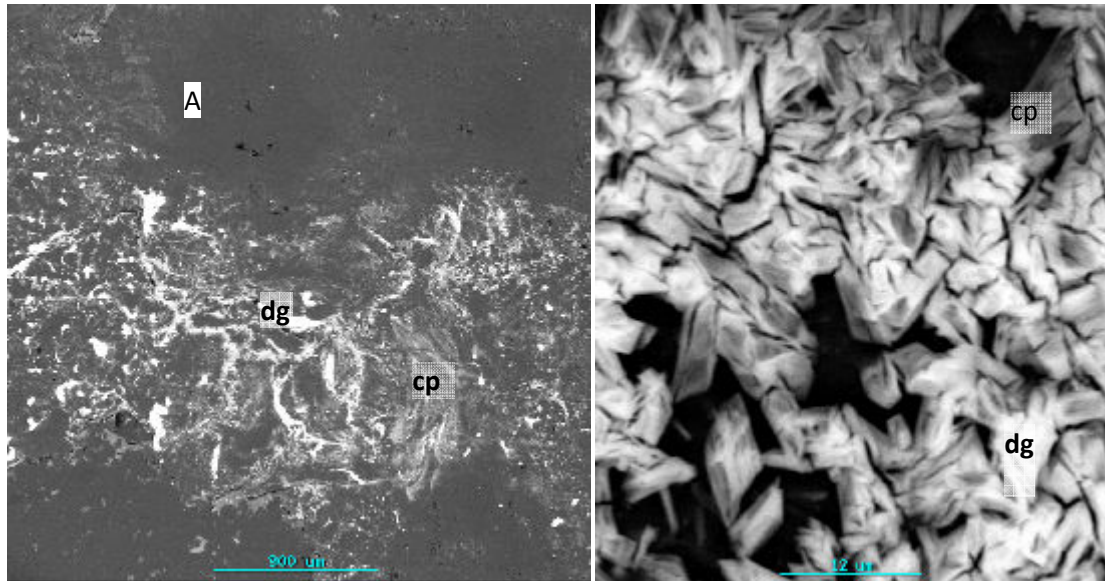
| a) G-bottom-copper cooler interface | b) Detailed view of the copper sulphide(s) in the G-bottom cold face |

Figure 29: BSE image of sample G-bottom cold face. A = graphite, cp = chalcopyrite, dg = digenite.

Copper, copper sulphide and copper chloride were the constituents of the material which was observed at the G-lid copper cooler interface (Table 22). Copper associated with chlorine and sodium was mostly in the edges of the lid. The presence of sodium suggests that the source of chlorine might be sodium chloride. Dendrites observed in Figure 30 grew from a copper sulphide base. Dendrites consisted of copper sulphide $Cu_{1.3}S$ while the base was a copper-rich chalcocite $Cu_{2+x}S$ (x=0.2 to 0.4) and digenite ($Cu_{1.8}S$) with small amounts of iron. The detection of the copper-rich sulphide confirmed the presence of elemental copper. Nickel phases were not detected. The BSE images of microstructures observed in sample G-lid are presented in Figure 30.

Sulphidation of copper coolers in PGM smelters

Table 22: EDS area analyses of G-lid (atom %)

G-lid	Cl	Cu	Fe	Na	S	Si	Total	Stoichiometry	Phase
0	1.3	54.0	0.0	11	31	2.9	100.85	$Cu_{1.3}S + Na$	Copper sulphide + sodium
1		66.0	0.0	2.5	30	0.5	99.45	$Cu + Cu_2S + Na$	Copper + chalcocite + sodium
2	13.6	49.0	7.0	7.2	20	0.8	98.2	$CuCl + Cu_{1.8}S + Na + Fe$	Copper chloride + digenite + sodium + iron
3		84		7.1	8.2	0.6	99.6	$Cu + Na + S$	Copper + sodium + chalcocite
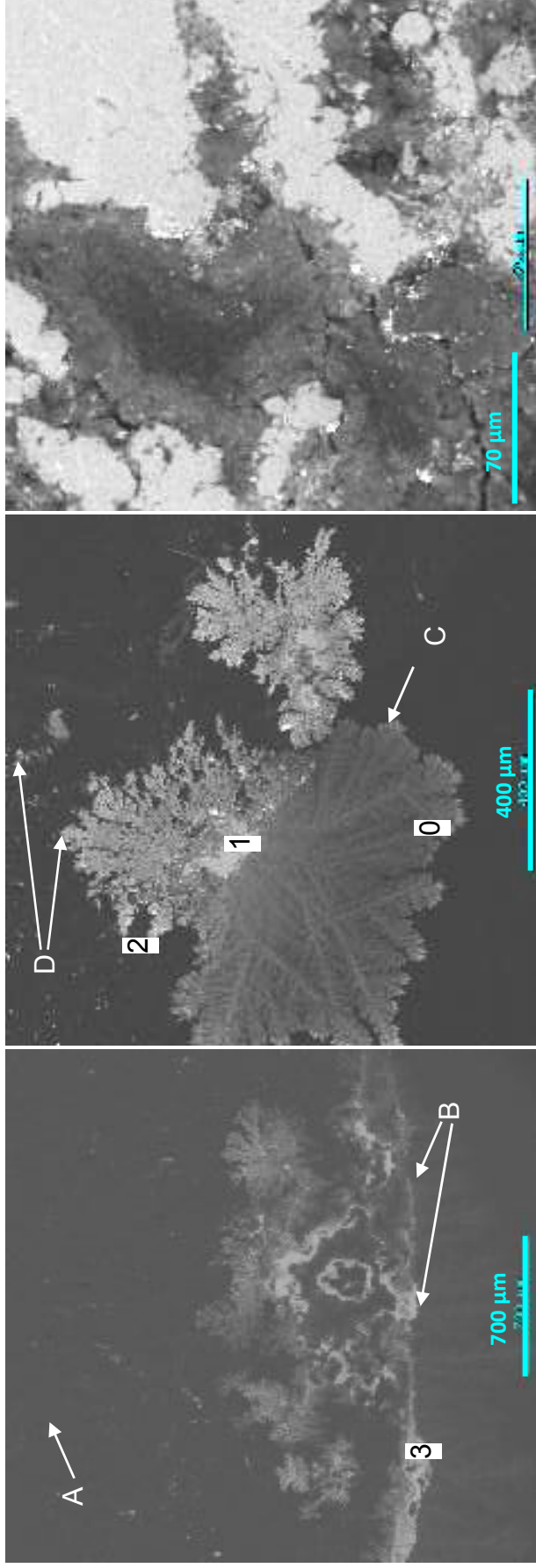
a) G-lid-copper cooler interface

b) G-lid edge

c) Detailed view of the corrosion product

Figure 30: BSE image of sample G-lid. A = graphite; B = G-lid-copper cooler interface; C = copper sulphide dendrites; D = copper sulphide penetration into graphite.

Sulphidation of copper coolers in PGM smelters

6.2.1.1. Discussion: SEM analyses

A very thin freeze lining was observed at the graphite hot face compared to the 10 cm thick freeze lining which was observed on the mag-chrome brick hot face. Pentlandite and chalcopyrite are constituents of the smelter feed and are therefore expected to form part of the furnace melt with augite, diopside and enstatite as slag. Chalcopyrite can deviate at high temperatures from the ideal $CuFeS_2$ to a metal-rich $Cu_{1+x}Fe_{1+x}S_2$ [Vaughan et al. 1978]. In a Cu-Fe-S system an intermediate solid solution (iss) is dominant at T>500°C. This solid solution extends from a sulphur atom % of 50 to 45, copper atom % of 33 to 15 and iron atom % of 20 to 25. The phases analysed by EDS deviated from the ideal stoichiometry. It is assumed that these phases were a mixture of the stoichiometric phase with intermediate solid solution. At the cold face the phases detected (chalcocite, digenite and copper chloride) were richer in copper than the ideal stoichiometry. Since these samples are at the interface of the graphite block with the copper cooler, the chemical reactions of copper cooler with gases and matte might have resulted in copper-rich compounds.

G-1 is the top portion of the graphite block which is in the feed-slag zone where severe corrosion was observed in the previous copper cooler design where the magnesia-chrome brick was completely worn away.

It is apparent that the phases present in the sample G-1 hot face are the same phases detected at the sample G-1 middle and G-1 cold face. From this observation it can be presumed that the base metal sulphides permeate the graphite-graphite interface until they reach the cold face of the graphite, which is in contact with the copper cooler.

Sample G-bottom is at the slag-matte interface and adjacent to the castable. Copper sulphide phases such as chalcocite or covellite were not detected in this sample but the depth of penetration by matte and slag was more pronounced. Chalcopyrite and digenite were observed at the cold face of the sample G-bottom.

Sample G-lid contained copper-deficient copper sulphide, chalcocite, copper chloride and copper. Iron and nickel containing sulphide phases were not observed.

The depth of infiltration of both slag and matte was higher at the bottom portion of the graphite block than at the top portion (G-1). It was also observed that the depth of sulphide infiltration at the graphite cold face (back) was much higher than in the hot face (front). This is unexpected, since the gas infiltration is expected to be higher at the hot face than at the cold face. A reasonable explanation would be that the gases diffuse in between the graphite blocks and reach the surface of the cooler where they react and form copper sulphide corrosion products, whereas at the hot face the freeze lining may limit infiltration and chemical reactions from taking place. Slag infiltration was more pronounced at the bottom portion (G-bottom) than at the top (G-1), while metal infiltration was higher at the top portion of the graphite block.

The permeation path is presumably through the interfaces between graphite blocks rather than through the graphite, since from the BSE images it was observed that the permeation from the hot face is not continuous and decreases towards the middle, whereas the permeation depth is higher from the cold face inwards.

6.2.1.2. Summary: SEM analyses

Pentlandite, chalcopyrite and augite were the major phases detected at the graphite block hot face, except that pentlandite was not detected at G-5 and chalcopyrite was not detected at G-bottom. No augite was detected on G-5 and G-bottom front but a non-stoichiometric calcium alumina silicate was observed, which is associated with chlorine. Digenite was only observed at the G-5 hot face, while enstatite was only detected at the G-bottom hot face. Pentlandite, copper sulphide(s), covellite with arsenic and iron were observed in the G-1 middle sample. At the cold face a copper-rich chalcocite was a major phase detected in the cold face of the graphite block, except in the G-bottom sample. Digenite and chalcopyrite were detected in samples G-5 and G-bottom. Copper chloride was observed in samples G-3 and G-lid.

6.2.2. XRD analysis of the graphite block

The graphite block was scraped on the surface of the hot face, middle and cold face to collect the samples which were submitted for XRD analysis. XRD samples were taken at the same positions on the graphite block (front, side and back edges) as the SEM samples so as to compare the elements determined in SEM with crystalline phases detected by XRD. Samples G-2, G-3 cold face, G-4 middle, G-4 cold face, G-5 middle and G-5 cold face were not analysed by XRD because enough sample could not be obtained. Graphite was detected in all the samples submitted.

6.2.2.1. Graphite block hot face

The graphite hot face from samples G-1 to G-bottom had slag consisting of augite $((Ca,Mg,Fe)_{1.86}(Si_2O_6))$, enstatite $(Mg,Fe(SiO_3))$ and forsterite $((Mg,Fe)_2(SiO_4))$ as major phases. Base metal sulphides such as chalcopyrite $(CuFeS_2)$, pentlandite $(Fe_9Ni_9S_{16})$, pyrrhotite $(Fe_{0.95}S_{1.05})$ and millerite (NiS) were detected in small amounts. XRD quantitative analyses are depicted in Table 23.

Table 23: Quantitative XRD analyses of the front (hot) faces of samples (G-1, G-3, G-4, G-5 and G-bottom) (%)

Stoichiometry	Phase	G-1	G-3	G-4	G-5	G-bottom
$(Ca_{0.61}Mg_{0.76}Fe_{0.49})(Si_2O_6)$	Augite	25.67	17.2	29.14	31.82	34.78
$CuFeS_2$	Chalcopyrite	2.46	0.00	3.34	3.37	4.63
$MgFeSiO_3$	Enstatite	10.34	20.71	24.79	18.64	7.47
$Mg_{1.8}Fe_{0.2}(SiO_4)$	Forsterite (Fe)	36.82	41.26	33.61	35.83	24.96
C	Graphite 2H	17.39	19.29	0.38	1.57	17.02
NiS	Millerite	0.63	1.53	0.79	1.17	0.38
$Fe_9Ni_9S_{16}$	Pentlandite	3.37	0.00	2.59	0.77	3.67
$Fe_{0.95}S_{1.05}$	Pyrrhotite 3T	3.31	0.00	5.35	6.83	7.08

6.2.2.2. Graphite block middle (graphite-graphite interface)

Base metal sulphides such as mooihoekite $(Cu_9Fe_9S_{16})$, pentlandite, pyrrhotite, chalcopyrite, troilite (FeS) and vaesite (NiS_2) were major phases detected in the sample G-middle with diopside $(Ca,Mg(Si_2O_6))$, forsterite

($MgFe(SiO)_4$), chalcocite (Cu_2S) and millerite (NiS) as minor phases. XRD quantitative analysis of sample G-middle is depicted in Table 24.

Table 24: Quantitative XRD analyses of the middle portions (graphite-graphite interfaces) of samples G-1, G-3 and G-4 (%)

Stoichiometry	Phase	G-1 middle	G-3 middle	G-4 middle
Cu_2S	Chalcocite M	0.0	0.0	2.33
$CuFeS_2$	Chalcopyrite	1.85	3.34	12.55
$(Mg_{0.857}Fe_{0.122})(Si_{1.877}Fe_{0.144})O_6$	Diopside	7.53	0.0	0.0
$CaMg(Si_2O_6)$	Diopside	0.0	7.71	11.38
$Mg_{1.48}Fe_{0.52}(SiO_4)$	Forsterite (Fe)	0.0	0.0	2.04
C	Graphite 2H	39.97	45.61	66.32
NiS	Millerite	0.0	0.23	0.5
$Cu_9Fe_9S_{16}$	Mooihoekite	23.5	20.92	0.0
$Fe_9Ni_9S_{16}$	Pentlandite	15.17	5.88	0.0
$Fe_{0.95}S_{1.05}$	Pyrrhotite 3T	5.61	16.31	0.0
$Fe_{0.94}S$	Troilite	6.39	0.0	0.0
NiS_2	Vaesite	0.0	0.0	4.88

6.2.2.3. Graphite block cold face

Atacamite, chalcanthite and digenite were major phases detected in the cold face of the graphite sample. Chalcocite (Cu_2S) and anilite (Cu_7S_4) were only observed in sample G-1. Copper was detected on samples G-1 and G-3 cold face; sample G-bottom had no copper. Covellite (CuS), chalcopyrite ($CuFeS_2$) and small amounts of nukundamite $(CuFe)_4S_4$ were only detected at sample G-bottom. Nantokite ($CuCl$) and antlerite ($Cu_3(SO)_4(OH)_4$) were only detected in sample G-3; only a small amount of nantokite was detected in sample G-1. XRD quantitative analysis of sample G-cold face is depicted in Table 25.

*Table 25: Quantitative XRD analyses of the back (cold) faces of samples G-1,
G-3 and G-bottom (%)*

Stoichiometry	Phase	G-1 back	G-3 back	G-bottom back
Cu_7S_4	Anilite	2.14	0	0
$Cu_3(SO_4)(OH)_4$	Antlerite	0	4.42	0
$Cu_2Cl(OH)_3$	Atacamite	9.99	12.72	0
$CuSO_4(H_2O)_5$	Chalcanthite	23.45	14.65	26.42
Cu_2S	Chalcocite M	19.51	0	0
$CuFeS_2$	Chalcopyrite	0	0	1.42
Cu	Copper	7.73	22.46	0
CuS	Covellite	0	0	10.64
Cu_9S_5	Digenite	9.86	0	6.31
C	Graphite 2H	26.58	27.1	54.59
$CuCl$	Nantokite	0.75	18.69	0
$Cu_{3.39}Fe_{0.61}S_4$	Nukundamite	0	0	0.61

6.2.2.4. Graphite block sample G-lid and a green growth

XRD analyses were performed four months after receiving the graphite sample. When the samples were prepared a green growth at the cold face of the graphite block was observed. This green growth was not present when the sample was received (when the ICP and SEM samples were submitted). The green growth associated with samples G-1 and G-lid was analysed to identify the crystalline phases. Atacamite ($Cu_2Cl(OH)_3$) and chalcanthite ($CuSO_4(H_2O)_5$) are major phases detected in this green growth (Table 26). Nantokite, covellite and copper are minor phases detected on G-lid green while G-1 green had eriochalcite ($CuCl_2(H_2O)_2$) and nantokite as minor phases. G-lid sample had similar phases as the G-lid green sample (Table 26), except that G-lid also contains digenite, which was not detected in the G-lid green sample.

*Table 26: Quantitative XRD analyses of sample G-lid and green growth (G-lid,
G-lid green and G-1 green) (%).*

Stoichiometry	Phase	G-1 back green	G-lid green	G-lid
$Cu_2Cl(OH)_3$	Atacamite	47.73	32.27	18.38
$CuSO_4(H_2O)_5$	Chalcanthite	32.61	25.9	27.64
Cu	Copper	0	3.1	13.47
CuS	Covellite	0	6.64	1.25
Cu_9S_5	Digenite	0	0	5.47
$CuCl_2(H_2O)_2$	Eriochalcite	3.8	0	0
C	Graphite 2H	14.7	23	27.92
$CuCl$	Nantokite_	1.19	9.09	5.86

6.2.2.5. Summary: XRD analyses

Augite, enstatite and forsterite were major phases detected in the hot face of the graphite block with minor phases constituted by pyrrhotite, pentlandite, chalcopyrite and millerite. Mooihoekite, pentlandite, troilite, pyrrhotite, chalcopyrite and diopside were major phases in the sample collected at the graphite-graphite interface (middle).

Chalcocite, covellite, digenite, atacamite, chalcanthite, nantokite and copper were detected at the cold face of the graphite block, with a minor amount of antlerite and anilite. Chloride containing phases were detected in the cold face samples, except in sample G-bottom. Chalcocite, covellite and digenite can form as a result of copper reacting with reduced sulphur such as elemental sulphur (S) or (H_2S). The iron-containing sulphides (nukundamite and chalcopyrite) were only detected in sample G-bottom cold face.

The green growth observed after four months of storing the sample is rich in atacamite and chalcanthite, which are hydrated phases of copper chloride and copper sulphate.

Sulphidation of copper coolers in PGM smelters

6.2.3. ICP analyses

ICP analysis was performed on the graphite samples and on the ashed graphite samples. The ashed graphite samples were prepared by heating the graphite samples to 1000°C; each graphite sample (G-1, G-2 and G-bottom) corresponds to the ash sample (G-1, G-2 and G-bottom). The ICP analyses of the graphite and ashed samples are depicted in Figures 31 to 36, as well as Tables 27 and 28. The data sheet for the unused graphite block is depicted in Table 29. The concentrations of the elements (impurities) reported in the data sheet are much less than the concentrations of the impurities detected by ICP in the used graphite block. This suggests that the post-mortem graphite block was contaminated with the furnace contents. This was also confirmed by the BSE images of the graphite block discussed in the section 6.2.1.

6.2.3.1. Ash content of the graphite sample

The ash content of graphite samples G-1 and G-bottom decreased from the hot face to the middle and increased from the middle to the cold face. The ash content of sample G-2 decreased from the hot face to the middle and it remained constant from the middle to the cold face. The graph of ash content versus depth into the graphite block (i.e. from the hot face to the cold face) of samples G-1, G-2 and G-bottom is depicted in Figure 31.
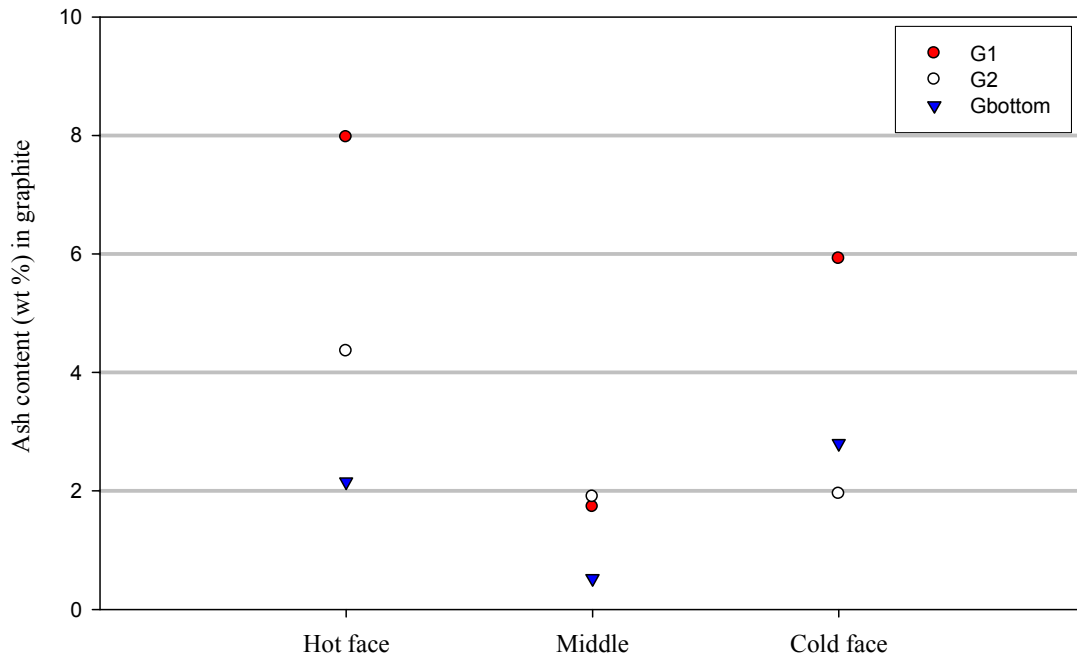
Figure 31: Ash content (wt %) in the graphite block.

6.2.3.2. Sulphur

Since sulphur volatilises at 444.6°C [Andrews 2008], it could not be detected in the ashed sample; it was only detected in the graphite sample. The sulphur content reported by ICP is the total sulphur, including the sulphur present as sulphides, sulphates and elemental sulphur. It should be noted that no element sulphur was detected by EDS and XRD in the graphite sample. The sulphur content in sample G-1 decreased from the hot face to the middle, and again increased from the middle to the cold face as shown in Figure 32. Sulphur content in sample G2 linearly decreased from the hot face to the cold face. The sulphur content in sample G-bottom remained constant from the hot face to the middle, but increased towards the cold face.
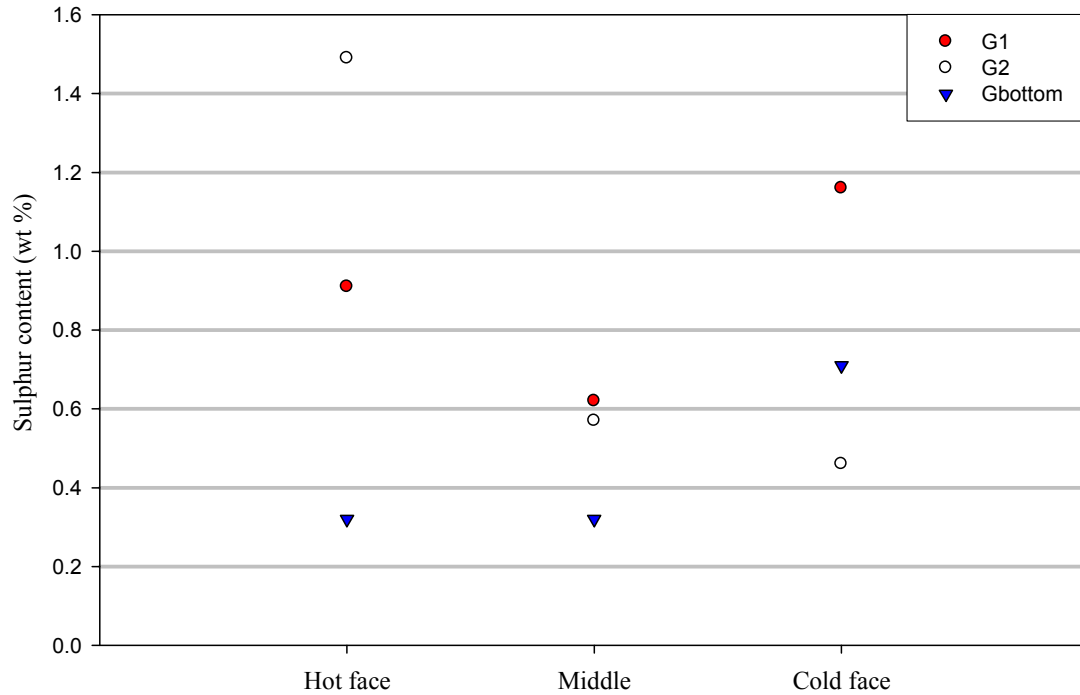
Figure 32: Sulphur content (wt %) in the graphite block.

6.2.3.3. Copper

The copper content in graphite samples G-1 and G-2 decreased from the hot face to the middle and increased from the middle to the cold face (Figure 33). In the G-bottom sample, the copper content was the same in the front and middle portions and increased towards the cold face. The copper content in the cold face for all the samples was higher than the amount detected in the hot face of the graphite sample. There was no correlation between the sulphur and the copper contents in all the graphite samples analysed. The copper contents in the ashed samples followed the same trend as in the graphite samples (Figure 34).

Sulphidation of copper coolers in PGM smelters
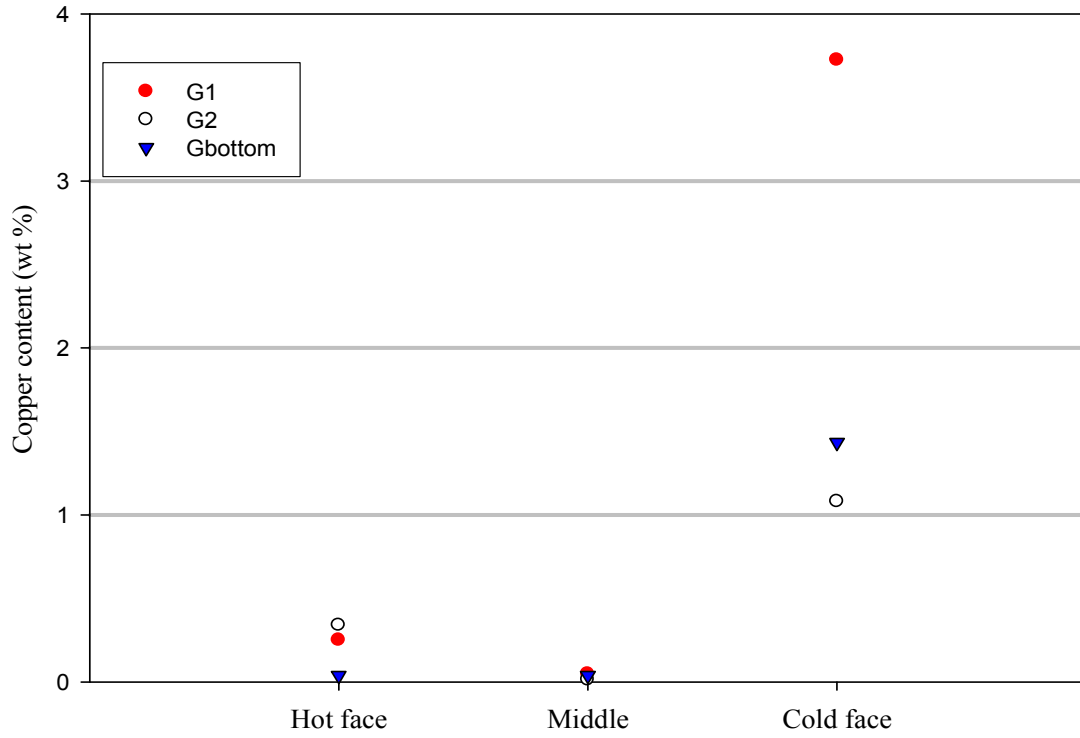
Figure 33: Copper content (wt %) in the graphite block.
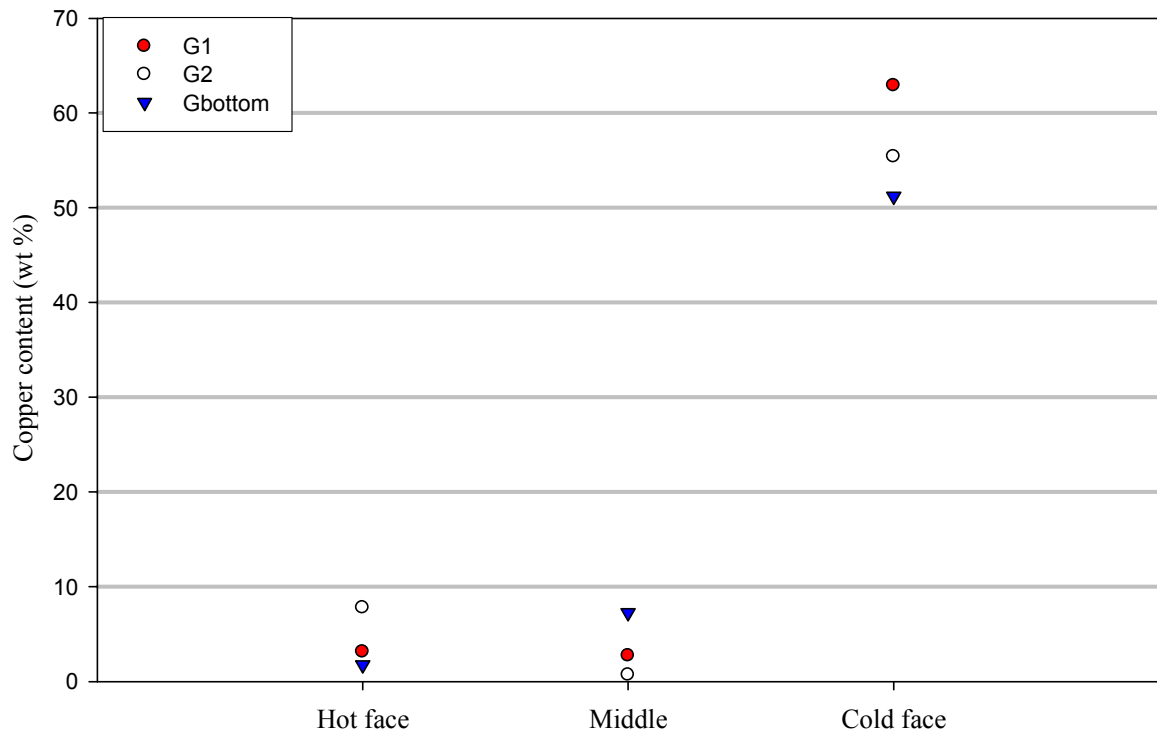
Figure 34: Copper content (wt %) in the ashed samples.

6.2.3.4. Nickel

The nickel content decreased from the hot face to the cold face of samples G-1 and G-2. The nickel content of sample G-bottom was very low at less than 0.1 wt% (Figure 35). There was no correlation between the sulphur, copper and nickel contents of the graphite samples analysed.

Nickel content in the ashed samples followed the same trend as in the graphite samples (Figure 36).
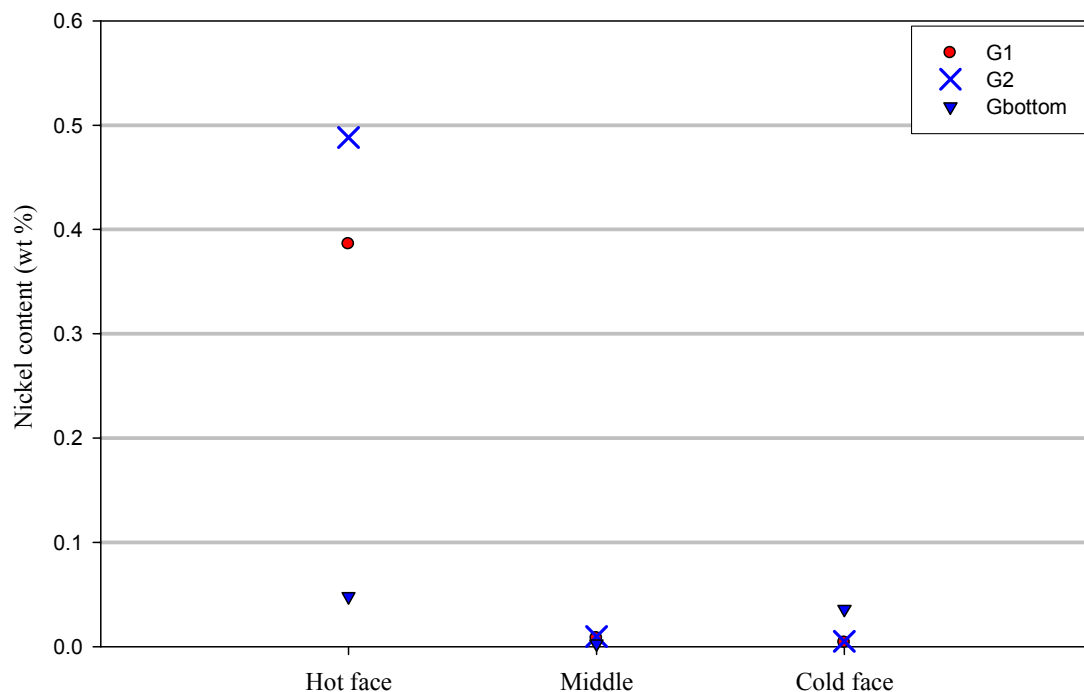
Figure 35: Nickel content (wt %) in the graphite block.

Sulphidation of copper coolers in PGM smelters
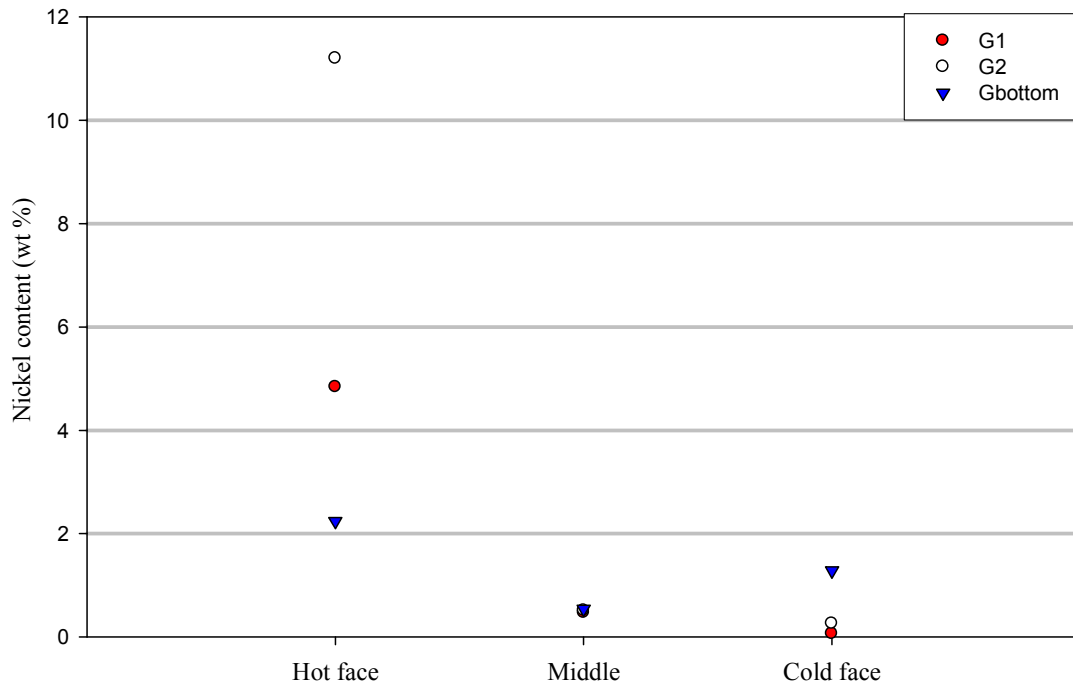
Figure 36: Nickel content (wt %) in the ashed sample.

6.2.3.5. Fe, MgO and SiO$_2$

Iron, CaO and SiO$_2$ were the impurities present in the unused graphite block, as listed in the data sheet (Table 29). Iron, MgO and SiO$_2$ in the graphite sample followed a trend similar to the nickel content (Figure D 7 to D 12: Appendix D).

Iron in the ashed samples increased from the hot face to the middle and decreased from the middle to the cold face. The iron content from G-1 to G-bottom (vertically) increased, which can be associated with the slag content of the freeze lining as observed in the EDS analyses.

The SiO$_2$ contents in samples G-1 and G-bottom decreased from the hot face to the cold face, while in sample G-2 the silica content was constant from the hot face to the middle and decreased from the middle to the cold face.

UNIVERSITEIT VAN PRETORIA
UNIVERSITY OF PRETORIA
YUNIBESITHI YA PRETORIA

Table 27: ICP analyses of the graphite samples G-1, G-2 and G-bottom (wt %)

Graphite sample	SiO₂	Al₂O₃	Fe(total)	Fe₂O₃	TiO₂	CaO	MgO	Na₂O	K₂O	MnO	P	Cr	Cu	Ni	Pb	V	C	Ash	S	L.O.I.
G-1 Front	2.821	0.433	2.008	2.872	0.026	0.307	1.355	0.0088	0.0183	0.0151	0.003	0.111	0.249	0.386	0.003	0.005	92.0	7.97	0.910	94.2
G-1 Middle	0.280	0.169	0.865	1.237	0.043	0.054	0.010	0.0017	0.0265	0.0078	<0.001	0.001	0.047	0.008	<0.001	0.011	98.3	1.73	0.620	99.5
G-1 Back	0.240	0.096	0.284	0.406	0.035	0.026	0.013	0.0018	0.0124	0.0021	0.001	0.001	3.724	0.004	0.007	0.006	94.1	5.92	1.160	96.9
G-2 Front	0.484	0.140	1.753	2.506	0.016	0.073	0.177	0.0022	0.0126	0.0061	0.001	0.044	0.339	0.488	0.004	0.005	95.6	4.36	1.490	96.5
G-2 Middle	0.211	0.227	1.051	1.503	0.012	0.023	0.007	0.0016	0.0163	0.0030	<0.001	0.001	0.013	0.010	0.000	0.007	98.1	1.90	0.570	99.0
G-2 Back	0.117	0.087	0.238	0.340	0.009	0.007	0.013	0.0012	0.0088	0.0014	0.001	0.001	1.080	0.005	0.002	0.002	98.1	1.95	0.460	97.6
G-bottom/Front	0.596	0.460	0.802	1.147	0.025	0.048	0.018	0.0024	0.0252	0.0018	0.001	0.011	0.038	0.048	0.002	0.006	97.9	2.15	0.320	98.7
G-bottom/Middle	0.072	0.081	0.236	0.337	0.003	0.005	0.006	0.0006	0.0037	0.0004	<0.001	0.001	0.038	0.003	0.000	0.002	99.5	0.52	0.320	98.9
G-bottom/Back	0.142	0.102	0.423	0.605	0.008	0.009	0.049	0.0020	0.0073	0.0010	0.002	0.006	1.434	0.036	0.004	0.003	97.2	2.80	0.710	97.4

Table 28: ICP analyses of the ashed samples G-1, G-2 and G-bottom (wt %)

Ash sample	SiO₂	Al₂O₃	Fe(total)	Fe₂O₃	TiO₂	CaO	MgO	Na₂O	K₂O	MnO	P	Cr	Cu	Ni	Pb	V
G-1 Front	35.4	5.43	25.2	36.0	0.33	3.85	17.0	0.11	0.23	0.19	0.03	1.39	3.13	4.84	0.040	0.065
G-1 Middle	16.2	9.77	50.0	71.5	2.48	3.15	0.59	0.10	1.53	0.45	<0.01	0.082	2.72	0.47	<0.001	0.63
G-1 Back	4.06	1.63	4.8	6.8	0.59	0.44	0.22	0.03	0.21	0.035	0.02	0.018	62.9	0.06	0.120	0.093
G-2 Front	11.1	3.21	40.2	57.5	0.37	1.68	4.07	0.05	0.29	0.14	0.02	1.01	7.77	11.2	0.082	0.105
G-2 Middle	11.1	11.9	55.3	79.1	0.65	1.21	0.36	0.09	0.86	0.16	<0.01	0.072	0.68	0.51	0.017	0.350
G-2 Back	6.00	4.47	12.2	17.4	0.44	0.35	0.65	0.06	0.45	0.073	0.03	0.048	55.4	0.26	0.089	0.077
G-bottom/Front	27.7	21.4	37.3	53.3	1.14	2.24	0.84	0.11	1.17	0.085	0.03	0.49	1.76	2.24	0.072	0.300
G-bottom/Middle	13.9	15.7	45.3	64.8	0.52	0.94	1.25	0.12	0.72	0.069	<0.01	0.20	7.26	0.54	0.008	0.330
G-bottom/Back	5.08	3.66	15.1	21.6	0.28	0.33	1.74	0.07	0.26	0.035	0.07	0.23	51.2	1.28	0.150	0.100

Table 29: Chemical composition of unused graphite block as reported in data sheet from the supplier (Ucar South Africa) (wt %)

Fe %	Ca %	Si %	Ti %	Mo %	V %	Cl %	Cr %	Cu %	Ash %	C %
0.1955	0.005	0.0045	0.0013	0.0008	0.0005	0.0002	0.0002	0.0001	0.15	99.64
Al, Pb, Mn, Ni, P, K, Sr, S, Y, Zn, and Zr were not detectable. Elements in the ash content of the graphite exist as oxides, ash is mostly silica and some alumina (no specific data)										

6.2.3.6. Summary of ICP results

It was observed that the copper content at the cold face for all samples was much higher compared to the corresponding hot face samples. The sulphur content at the cold face is slightly higher than at the hot face for graphite samples G-1 and G-bottom.

From the ICP analyses it can be seen that the concentration of elements from the furnace melt do not increase or decrease linearly from the hot face to the cold face but there is a sharp decrease at the middle sample and a sudden increase at the cold face of the graphite block. This observation suggests that the permeation path is not through the graphite block but the gases, slag and matte diffuse through the gaps in between the graphite blocks, since matte and slag were observed on the BSE images of G-1 and G-5 middle.

6.3. Summary: graphite block post-mortem sample

The graphite block sample was analysed by SEM, XRD and ICP. SEM was used to determine the depth of infiltration using BSE images and to determine the impurities embedded in the graphite block by EDS analyses. XRD was used to determine the crystalline phases on the surface of the graphite block and ICP was used to examine the path of infiltration, whether the impurities diffuse through the graphite block or on the sides of the graphite block to reach the copper cooler surface. The ICP analysis was only used to determine whether there is a profile on the matte concentration from the cold face through the centre (middle portion) to the cold face of the graphite block therefore the data from ICP was not directly comparable to the data from SEM and XRD.

The depth of infiltration of the graphite block by furnace melt was higher at the cold face than at the hot face, according to the observation made on the BSE images. The filtration at the cold face seemed to be towards the hot face. Phases identified on the hot face by EDS and XRD are pentlandite, chalcopyrite, augite, enstatite, forsterite and small amounts of pyrrhotite and millerite. At the graphite-graphite interface mooihoekite, troilite, pyrrhotite,

chalcopyrite and diopside were observed. At the cold face were chalcocite, covellite, digenite and minor amounts of atacamite, chalcanthite and nantokite; G-bottom also had nukundamite and chalcopyrite at the cold face. Atacamite, chalcanthite and nantokite were observed at G-lid and in the green growth that was observed on the sample after being stored for four months.

The amount of impurities in the graphite block did not increase from the hot face to the cold face; the impurities decreased to almost zero in the graphite samples taken in the middle, not at the edge. The permeation path of the impurities from the hot face to the cold face is therefore not through the graphite but the gases, slag and matte diffuse through the gaps in between the graphite blocks and reach the copper cooler surface, since matte and slag were also observed on the BSE images of G-1 and G-5 middle (SEM analysis).

6.4. Concluding remarks

The following observations were made when comparing the Mag-chrome post-mortem sample and the graphite block post-mortem sample.

- No severe corrosion of the graphite block was observed at the slag/feed interface, compared to the mag-chrome brick which was totally consumed at the slag-feed interface.
- No element sulphur was detected in any of the graphite samples.
- The freeze lining on the graphite block was mostly made of matte and it was thin (2mm) compared to the freeze lining that was observed on the mag–chrome bricks, which was 10cm thick. The graphite block freeze lining was not as porous as the mag-chrome brick freeze lining and the cracks were not observed on the graphite block freeze lining.
- The base metal sulphides were only detected in sample G-bottom, according to the XRD results; base metal sulphides were also detected by EDS in samples G-1 to G-5 cold face. The amounts of base metal

sulphides at the graphite cold face were very low compared to the amounts detected behind the freeze lining and the mag-chrome brick.

- Chloride containing phases were observed at the cold face (G-3 and G-lid) of the graphite block where as in the mag-chrome brick post-mortem the chloride phases were detected at the sample on top of the cooler and between the copper cooler and the front brick.

- Atacamite and chalcanthite were observed on the G-lid and G-1 back after the sample had been stored for four months

It can be concluded that graphite plays a significant role in inhibiting the furnace corrosive gases from reaching the copper cooler surface since very low corrosion was observed at the slag-feed interface when the graphite block was used compared to when the mag-chrome brick was used. Graphite retards the rate at which the base metal sulphides reach the copper cooler, since the base metal sulphide penetration path is limited to the gaps between the graphite blocks and there is no linear gradient of penetration of sulphides through the copper block itself. The furnace operating pressure plays a significant role in the depth of infiltration of sulphides from the cold side of graphite. If the furnace can run at a negative pressure the gases at the cooler side of the refractory lining will be sucked in, towards the hot face, while the freeze lining may limit the penetration at the hot face to only the surface.

7. LABORATORY SCALE SULPHIDATION OF COPPER

Laboratory tests were performed on copper foil to investigate the mechanism involved in the corrosion of copper coolers in PGM smelters through gaseous attack. The conditions and parameters in the furnace were estimated from published data in the literature, that is, gases that evolve during smelting and slag temperature. These furnace conditions were simulated in the laboratory scale experiments. The cooler surface temperature was calculated from the thermal conductivity of the refractory lining, thickness of the refractory lining, estimated operating temperature in the furnace and cooling water temperatures.

7.1. Design concept of the experiment

The corrosion rate of the foil was determined by measuring the change in foil thickness over time. When corrosion takes place, the copper foil thickness decreases while the thickness of the corrosion product layer increases. Copper is a conductor and copper sulphide is a semiconductor. If copper is electrically connected in parallel with copper sulphide, the electrons will flow through the conductor, copper, as it has the lowest resistance. The formation of a sulphide layer should therefore not affect the electrical path. An open circuit is an indicator that the copper foil (conductor) has been totally consumed. For this reason, the electrical approach to corrosion rate measurement was employed. As the sulphide scale forms on copper foil owing to corrosion, the copper foil thickness decreases while the resistance of the foil increases. The resistance is inversely proportional to the conductor thickness, as indicated in Equation 17 [Steinhogl 2005].

$$R = \rho L / A \hspace{3cm} \textit{Equation 17}$$

where R is the resistance of a conductor (ohms), L is the electrical length (m), A is the cross-sectional area of the conductor (thickness x width) measured in (m^2) and ρ is resistivity of the conductor in ohm metres (Ω.m)

Based on Equation 17, at constant temperature, width and electrical length the resistance should increase proportionally as the foil thickness decreases.

Sulphidation of copper coolers in PGM smelters

The initial resistance of the foil is calculated from Ohm's law. Ohm's law states that if a potential difference, (V), is applied across a conductor with resistance (R), a current (I) will flow through the conductor (Equation 18). The voltage drop V, across a conductor with resistance R is therefore proportional to the current through the conductor [Schuster 2001].

$$V = IR \qquad\qquad\qquad \textit{Equation 18}$$

7.2. Factors considered during the experimental design
7.2.1. Surface temperature of the cooler

The temperature of the copper cooler varies depending on the level of the furnace contents. Van Manen (2008) observed the heat loss through the waffle copper coolers when the slag level was high and when the slag level was low. Van Manen discovered that at high slag levels the waffle copper coolers are exposed to higher temperatures and at low slag levels the coolers are exposed to lower temperature, since less heat is lost when the slag levels are low. To account for this thermal variability, the temperature of the copper foil was gradually raised from 80° to 140°C at 20°C intervals to determine the effect of varying temperature. Temperature control was achieved by attaching the foil to a heat sink (copper block). The temperature was regulated by circulating silicone oil through the heat sink.

A schematic diagram of the layers of refractory lining in a typical PGM smelter is shown in Figure 37. The copper waffle base indicated as Cu waffle is a portion of a cooling element through which the cooling water circulates. The rammable refractory layer is annotated as $R^{\#}$.

Sulphidation of copper coolers in PGM smelters
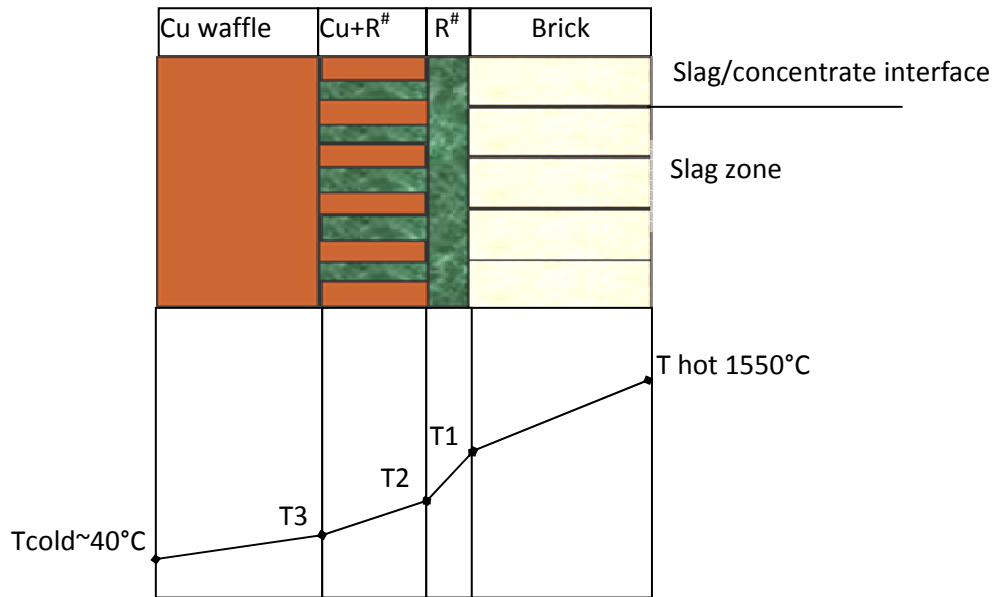
Figure 37: Schematic diagram of the furnace shell refractory lining.

The knobs extend from the base, forming the grooves in which the rammable refractory material sticks such that a composite of copper knobs and rammable material is formed. The rammable material used was alumina-chrome based with 68.3% Al_2O_3, 30% Cr_2O_3, with SiO_2 as the main impurity phase in this refractory (Table A 1, Appendix A). A magnesia- chrome refractory brick with 57% MgO, 23% Cr_2O_3, 12% Fe_2O_3, 6.5% Al_2O_3 and calcium oxide and silica as impurities was used to line the furnace in front and on top of the copper coolers. The front brick was in contact with the furnace melt. Its main function was to prevent direct contact of the copper coolers with the furnace melt until the freeze lining is formed. The thermal heat flux was calculated by implementing Fourier's law of one-dimensional heat transfer, Equation 19. Equation 20 is the expanded version of Equation 19.

$$Q = -kA\frac{\partial T}{\partial X}$$

Equation 19

The thermal conductivity values were taken from the supplier's data sheet (Table A 2, Appendix A). To estimate the heat loss through the refractory wall, the following assumptions were made:

- Cold (inlet cooling stream) temperature is approximately 40°C [Van Manen 2008].
- Waffle knob: rammable composite ratio is 1:1.
- The rammable thickness in front of the composite is 5 mm.
- The thermal conductivity of the magnesia-chrome brick is 2.8 W/m.K at 1550°C.

The refractory data used to calculate the heat loss through the furnace wall is shown in Table 30. The side view of the refractory wall post operation is depicted in Figure 38. The freeze lining thickness was measured from the furnace and was approximately 10cm. The freeze lining measurement was obtained using a measuring tape during the furnace shutdown as shown in Figure 38. XRD quantitative analyses were used to calculate the percentage contribution of each crystalline phase to the freeze lining. This phase composition was then used to calculate the thermal resistance of the freeze lining. The temperature profile through the refractory wall (T1, T2 and T3 in Figure 38) was calculated using Equation 21.

$$Q = \left(\frac{T_{hotface} - T_{coldface}}{\dfrac{l_{brick}}{k_{brick}} + \dfrac{l_{R^{\#}}}{k_{R^{\#}}} + \dfrac{l_{Cu+R^{\#}}}{k_{Cu+R^{\#}}} + \dfrac{l_{Cuwaffle}}{k_{Cuwaffle}}} \right)$$

<div align="right">*Equation 20*</div>

At steady state (temperature does not change with time): Q=q1=q2=q3 and

$$T_X = T_{(X-1)} - \left(\frac{T_{hotface} - T_{coldface}}{R} \right) R_x$$

<div align="right">*Equation 21*</div>

Where T_x = temperature of interface, °C

T_{x-1} = hot face temperature of previous layer, °C

R_x = thermal resistance of the layer = (*l*/k)

R = total thermal resistance through the wall

l = thickness of layer (cm)

k = thermal conductivity of the layer (W/m.k).

Table 30: Data for heat loss calculations through the refractory wall

Refractory brick (Fig 37)	Elements	Thickness (cm)	k (W/mK)	Resistance (Ω)	Q (kW/m^2)
*Cu waffle	Cu	3.5	360	0.01	
Cu + R$^{\#}$	Cu, Al$_2$O$_3$, Cr$_2$O$_3$	5	180.7	0.03	
R$^{\#}$	Al$_2$O$_3$, Cr$_2$O$_3$	0.5	1.4	0.36	
brick	MgO, Cr$_2$O$_3$, Fe$_2$O$_3$, Al$_2$O$_3$	23	2.8	8.21	
TOTAL		32	544.9	8.61	0.18
Freeze lining					
	Diopside	3.4	2.3	1.48*	
	Augite	4.6	1.5	3.07*	
	Enstatite	1.4	4.6	0.30*	
TOTAL		9.4	8.4	4.85	0.29

*Cu waffle is a copper waffle cooler base, R$^{\#}$ is a rammable refractory material, Cu + R$^{\#}$ is copper knobs, rammable composite. * [Verlag, 1995]

The furnace was initially lined with the refractory brick in front of the copper coolers. During the maintenance shutdown it was observed that at the slag/concentrate interface the front refractory brick was totally corroded; only the freeze lining remained in front of the copper cooler, as shown in Figure 38. The refractory wall interface temperatures were then calculated for both scenarios, namely with the refractory brick in front of the copper cooler and with the freeze lining in front of the copper cooler. Estimated temperature profiles of both scenarios are presented in Table 31.
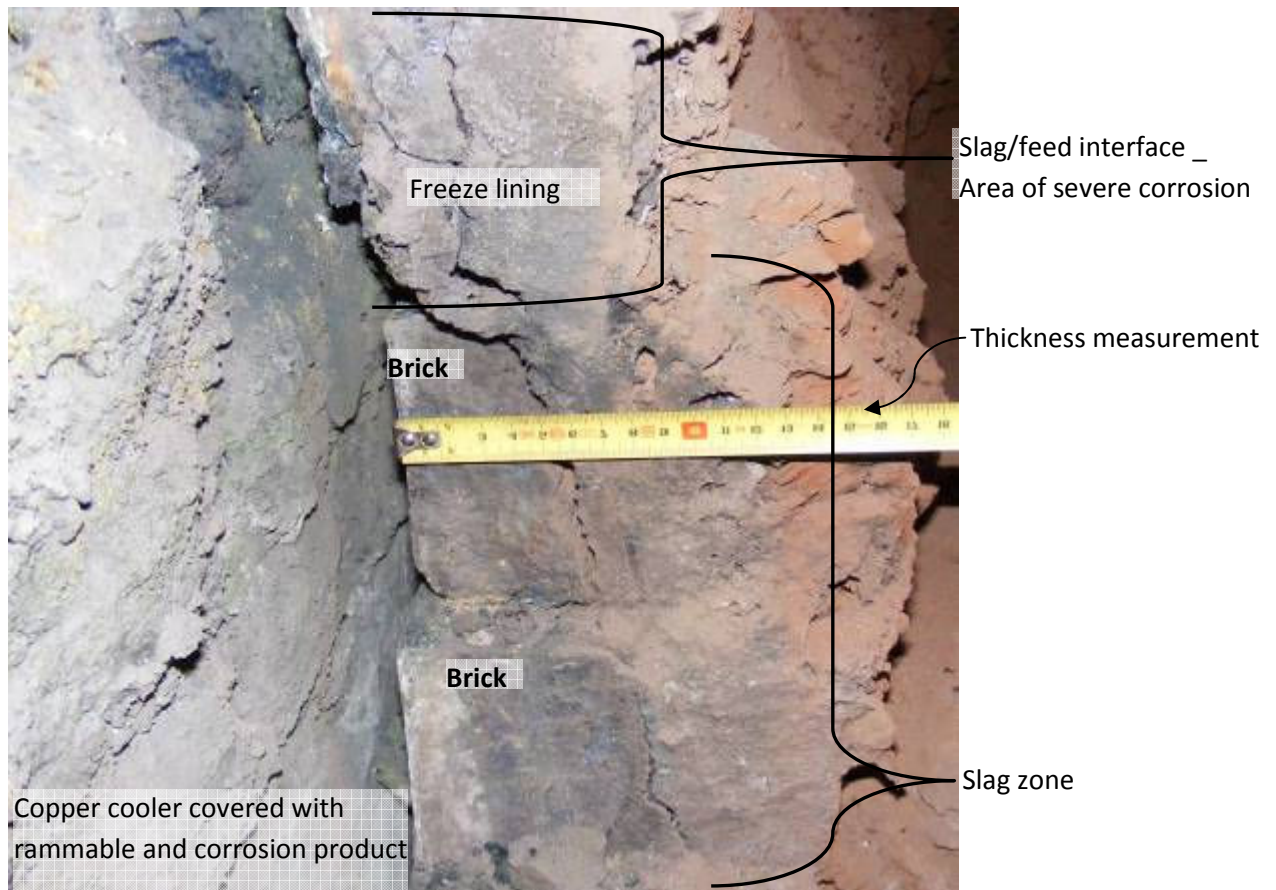
Figure 38: Side view of the furnace refractory lining taken during maintenance shutdown.

Table 31: Temperature profile of the refractory wall

Interface temperature (*Figure 37*)	Refractory brick (°C)	Freeze lining (°C)
T1	109.20	153.61
T2	46.56	50.77
T3	41.71	42.80

The total heat loss through the wall with the refractory brick was 0.18kW/m², while through the wall with 10 cm freeze lining the total heat loss was 0.29kW/m². The brick-rammable interface temperature (T1) is the critical temperature since it determines the reactions that can occur between the copper cooler and the corrosive material that can permeate through the brick or freeze lining. T1 was higher (153.61°C) for the wall with freeze lining and 109.2°C for the wall with a brick. During operations the refractory brick is exposed to different wear mechanisms due to chemical reactions with the melt, thermal cycling and erosion by furnace contents. The thickness of the brick decreases gradually until

it is completely consumed, as observed in Figure 38. The change in brick thickness was not considered during the calculations, but as the brick thickness decreases, the interface temperatures through the furnace lining at T1, T2 and T3 increase.

Initially the rammable thickness in front of the composite was estimated to be 5mm. Calculations indicate, however, that the change in thickness of this layer affects T1 significantly. The furnace lining profile was re-calculated, varying the rammable thickness. These calculated temperatures are shown in Table 32. The hot face temperature was kept constant at 1550°C. The rammable thickness had a limited effect on T2 and T3 while T_{cold} (inlet) temperature remained unchanged at 40°C.

Table 32: Temperature profile of the refractory wall as a function of the rammable thickness

Rammable thickness (mm)	Tcold (°C)	T3 (°C)	T2 (°C)	T1 (°C)	T hot (°C)
5	40	41.71	46.56	109.2	1550
3	40	41.73	46.67	84.9	1550
1	40	41.76	46.78	59.7	1550
0.5	40	41.77	46.81	53.3	1550
0.1	40	41.78	46.84	48.1	1550

According to these temperature profile calculations, the highest temperature at the refractory brick-rammable interface is 109.2°C and the coldest temperature is 48°C. When the brick is replaced with the freeze lining, temperatures at the rammable surface can exceed 150°C. The temperature range (80°C-140°C) assumed in this test work is therefore a good approximation of the copper cooler surface temperature, since it falls within the highest and the lowest range of the calculated temperatures.

7.2.2. Chemical composition of copper coolers

Sulphidation is a function of substrate composition. A copper foil with similar composition to the copper cooler was therefore used so that the results are comparable to the copper coolers. The copper cooler purity was approximately 99.7% as stated by the supplier data sheet.

7.2.3. Environment of the copper cooler surface

Nell (2004) reported that the typical smelter operating partial pressure of oxygen is 9.869×10^{-9} atmospheres at 1550°C. The experimental system was therefore constantly purged with an inert gas (argon) to simulate the oxygen-depleted atmosphere.

7.2.4. Most probable gases evolved during operation

The gases used as corrosive gases in this test work were estimated based on the corrosion product analysed on the copper cooler surface and from the published literature. Sulphur vapour, hydrogen chloride, water vapour and hydrogen sulphide are the gases that were used in this test work as corrosive gases. Corrosion by sulphur dioxide and sulphuric acid was not studied, since the formation of these gases is envisaged on the freeboard, while the area of interest for this study is the slag/feed interface.

7.3. Materials and apparatus

To simulate the corrosion of copper coolers in the laboratory, the experimental setup had to be designed in such a way that the conditions in the smelters can be simulated. The apparatus employed in the laboratory tests is depicted in Figures 39 and 40.

An annealed, 99.7%, 0.05mm thick copper foil, supplied by Goodfellow, was used as a substrate sample, which represents the waffle copper cooler. A copper block was used as a heat sink since it has a high thermal conductivity and helped regulate the foil temperature. The copper block also served as a support structure for the foil. The block was hollow and rectangular with 10mm inside diameters and sides measuring 70 x 20 x 20 mm (Figure 39).

A Pratley quickset clear high-strength epoxy was used to attach the foil to the heat sink for maximum contact. Epoxy has a maximum operating temperature of 150°C; it could therefore be used at all temperature ranges employed in this test work without causing non-adherence between the foil and the block.
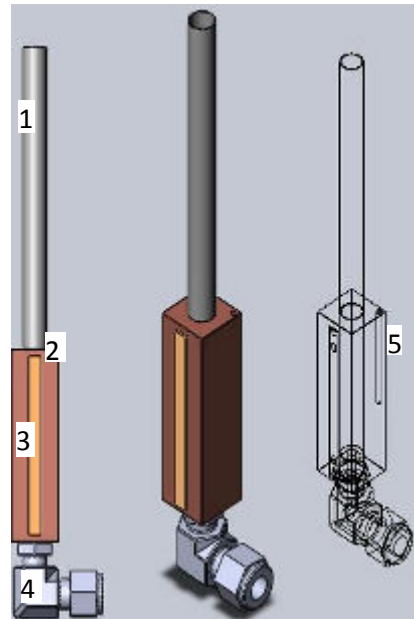
1: stainless steel pipe

2: heat sink (copper block)

3: copper foil sample

4: stainless steel fitting

5: thermocouple fitting

Figure 39: Detail of the copper block with attached copper foil.
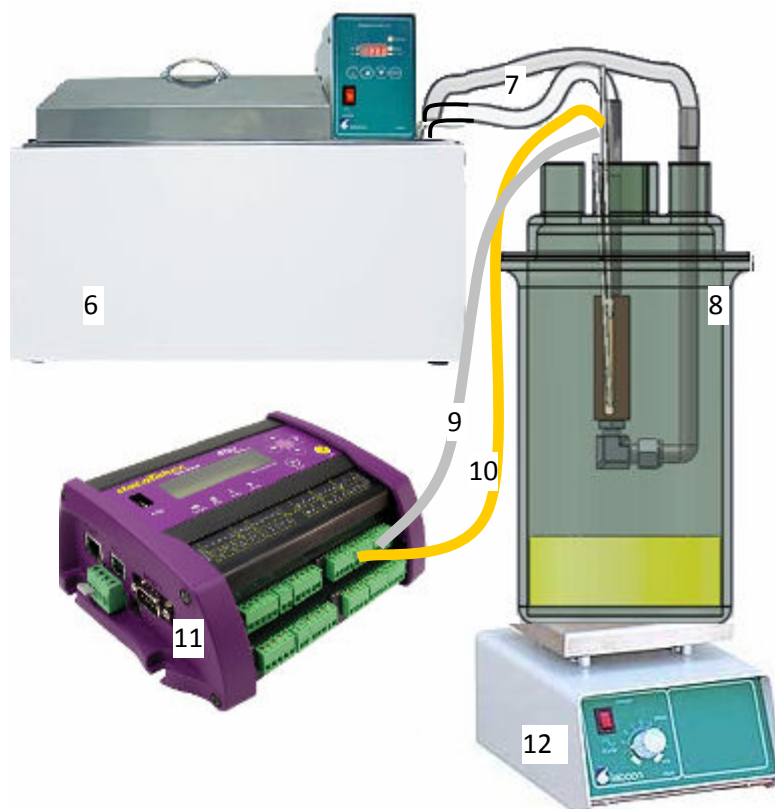
6: silicone bath oil

7: silicone flexible pipes

8: glass jar

9: shielded cables-voltage measurement

10: thermocouple wire

11: datataker

12: Hot plate

Figure 40: Experimental apparatus.

A silicone conformal coating (SCC3) was used to coat the heat sink for electrical insulation and for protection from the corrosive reactants. The SCC3 was supplied by RS Components.

Stainless steel pipe (SS-304) of 8mm inside diameter and 10mm outside diameter supplied by man-2-size was fitted at each end of the copper block using stainless steel fittings supplied by swagelok (Figure 39). Stainless steel pipes are highly resistant to corrosive gases and are easily available and affordable.

Flexible silicone pipes were connected between the stainless steel pipes and the oil bath to complete the oil circulation circuit as shown in Figure 40 number 7. These pipes have a high temperature tolerance and very low thermal conductivity, therefore they will efficiently carry the hot oil flow and prevent heat losses through the pipes.

A sealable glass jar was used as a reaction chamber (Figure 40 number 8). A glass reactor is inexpensive, it does not react with reactants used in this experiment, it is transparent and therefore allows visual examination of the experiment. Its softening point is in excess of 1000°C and it can therefore be used in a wide range of temperatures. It is also easy to seal for an air-tight operation [Vaughan et al. 1978].

Rubber seals were used as fittings for pipes on the reactor lid. The rubber seal can handle high temperatures without breaking and can also seal for air-tightness.

A silicone oil bath was used to regulate the substrate temperature of the copper block. A Labcon CPM 200 was used for its efficiency and specifications. Silicone oil has a high boiling point and the equipment could handle temperatures of up to 200°C, and therefore could comfortably regulate the required temperature.

A Heidolph MR2002 hot plate was used to bring the reactor temperature above the melting point of sublimed sulphur powder (supplied by Merck Chemical) to synthesise sulphur vapour.

A Goodwill power supply (GPR1850) with specifications, 0 to 18 Volts, 0 to 5 Amps, maximum ripple voltage of 0.5mV, and a 100 microsecond transient response was used as a constant current supply.

For data acquisition a datataker was used. A datataker (DT80) is a digital multimeter with built-in electronic sensors and data logger. The temperature and voltage drop were directly measured by the Datataker. The advantage of using the multimeter is its ability to reduce instrument connection errors and its higher precision and high reading speed, since the digits display voltage, resistance and temperature directly. It has a resolution of 2.5 microvolts for a voltage of +/-30 VDC; the voltage accuracy is 0.35% of the reading.

A tinned copper stranded conductor covered with silicone rubber and glass fibre braid supplied by RS Components was used for electrical connection on the foil. The maximum operating temperature of this copper cable is 150°C. These cables were extended to the electrical instruments (power supply and multimeter) by shielded cables. A shielded cable reduces the electrical noise so that the data measured is free of interference from the surroundings.

A type K thermocouple supplied by Lenton was fitted on the heat sink to measure the temperature of the foil. The temperature range for this thermocouple type is 0 to 1372°C. This thermocouple was calibrated against a calibrated thermocouple; the calibration curve is given in Figure C 2, Appendix C.

7.4. Apparatus construction

A copper foil of 50µm thick, 2.5mm in width and 60mm in length was cut from a copper sheet using scissors. The samples were polished mechanically using a silicone carbide paper up to size 400 micron [Graedel et al. 1987]. Foil geometry was of high importance since it was used to calculate the corrosion rate.

Fibreglass copper wires were soldered onto each end of the copper foil. Four wires were required per sample, since a four-wire resistance method was used in the voltage drop measurement. Two wires were for current input and output. The

other two wires were for voltage drop measurement across the foil as shown in Figure 41.

A foil was attached to the copper block using super glue. Epoxy was applied at each end of the foil below and above the soldered wires. The function of the epoxy was to ensure electrical insulation and to protect the wires from the corrosive gases. After curing the glue at room temperature the heat sink was fitted with the stainless steel pipes using the stainless steel fittings as shown in Figure 39. Teflon tape was used on the pipe threads to tighten the joints and prevent oil leakage. Choc blocks were used to connect the fibreglass wires from the sample to the shielded cables from the power supply and datataker.

The flexible silicone pipes were connected at the ends of the stainless steel pipes and extended to the oil bath, completing the oil circulation circuit as shown in Figure 40. The power supply and datataker were switched on 30 minutes before the experiment was started, to stabilise the readings of the instruments prior to data measurements.

7.5. The experimental procedure

7.5.1. Electrical connections

A four-wire resistance measurement was used because it measures resistance with high precision. This method eliminates resistance error due to the voltage drop through wire connections to the source and wire connections to the resistor. A voltmeter/datataker reads the voltage across the resistor; ideally no current flows into the voltmeter and thus there are no voltage drops over the leads or at contact points between the leads and resistor.

A wire of known resistance (shunt resistor) was connected between the current supply and the multimeter (datataker). The voltage drop across a shunt resistor was measured and the current was calculated from Ohm's law (Equation 18). The current is equal to the measured voltage drop divided by the value of the shunt resistor. The shunt resistor and the copper foil are connected in series such that the current through the shunt resistor is equal to the current through the copper foil, as shown in Figure 41.
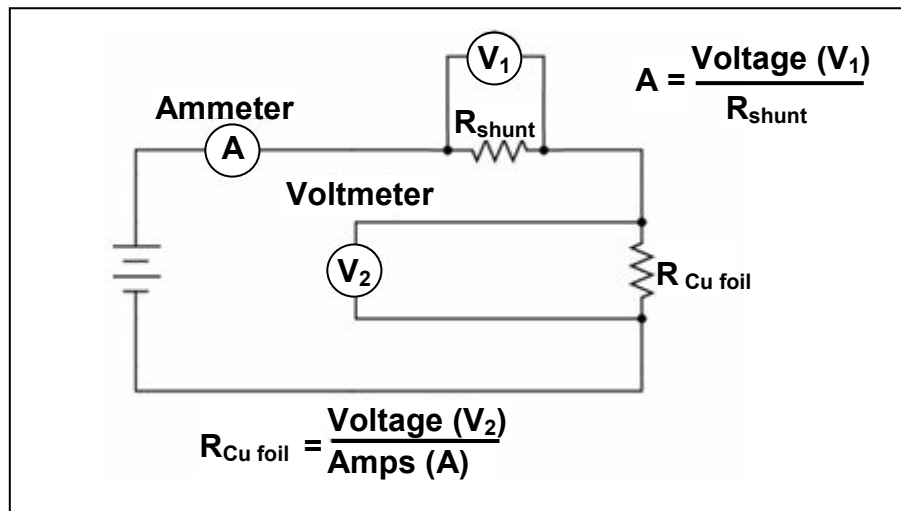
Figure 41: Electrical circuit diagram used for the foil resistance measurements.

The voltage drop across the foil was measured by a datataker. The initial resistance of the foil was calculated from the current through the foil and the voltage drop across the foil. Change in resistance was measured throughout the experiment in order to be able to calculate the change in foil thickness based on the original foil geometry and initial resistance.

The initial copper foil thickness was taken to be 50 microns as per supplier specification. Resistance is related to resistivity (ρ) of the material through Equation 17. From the measured temperature and published resistivity at 25°C, the ratio (length/width) can be calculated from Equation 17. Equations 22 and 23 are the expanded versions of Equation 17.

$$R = \frac{\rho L}{tw}$$

Equation 22

$$\left(\frac{Rt}{\rho}\right)_{initial} = \left(\frac{L}{w}\right)$$

Equation 23

From Equation 23 L is the electrical length in (m), tw is the cross-sectional area (thickness x width) measured in (m^2), ρ is the resistivity in ohm metres (Ω.m) [Steinhogl et al. 2005]. The change in foil thickness was not measured physically from the geometry of the sample but it was calculated using the change in

measured resistance. The change in resistance is directly proportional to the change in thickness.

The change in resistance due to temperature was taken into account by calculating the alpha (α), which is the temperature coefficient of resistivity (TCR). In the temperature range 20°C to 150°C, resistivity is linearly correlated to temperature [Schuster et al. 2001]. The TCR is almost constant in this temperature range. A slope of [R/R_o vs ΔT] = α was determined to be 0.0031K^{-1}, where:

R = Conductor resistance at temperature T

R_0 = Conductor resistance at reference temperature T_{ref}

α = TCR for the conductor material at reference temperature

T = conductor temperature in °C

T_{ref} = reference temperature that α is specified at for the conductor material (20°C).

The literature value of α at 20°C is 0.0044K^{-1} for pure copper [Steinhogl et al. 2005]. To determine the value of alpha, the foil was heated up to the maximum operating temperature (140°C) and cooled down to room temperature under argon atmosphere. At constant length, width and thickness, R/R_o = ρ/ $ρ_o$, change in resistivity with temperature can be calculated from the slope of [R/R_o vs ΔT]. The resistivity at a temperature is given by Equation 24 where:

ρ = conductor resistivity

$ρ_o$ = conductor resistivity at reference temperature

$$\rho = \rho_{25°C}\left[1 + \alpha(T - 25°C)\right]$$ *Equation 24*

ρ $_{25°C}$ = 1.70978X10^{-8} Ωm

Initial thickness = 50 X10^{-6} metres

$\alpha = 0.0031K^{-1}$.

Knowing the alpha of a foil, the resistivity at any temperature between 20°C and 150°C can be calculated from Equation 24 [Steinhogl et al. 2005; Schuster et al. 2001]. The change in copper foil thickness was calculated from Equation 23 using the initial value of a constant (L/w), a measured resistance of the copper foil and copper foil resistivity calculated from Equation 24.

7.5.2. Corroding gas synthesis

7.5.2.1. Sulphur vapour

Sublimed sulphur powder (98%) supplied by Merck was used to synthesise the sulphur vapour. It was purified by re-crystallisation where it was heated up to 200°C and cooled to room temperature. This step was essential in order to remove the moisture from the sublimed sulphur. To create the sulphur vapour, the re-crystallised sulphur was heated to 300°C. The reactor remained on the hot plate for the duration of the experiment to ensure the sulphur remained molten.

7.5.2.2. HCl vapour

A concentrated hydrochloric acid (32% v/v) was used to provide the HCl vapour. Argon gas was saturated with HCl vapour by passing the argon through a volumetric flask with 32% saturated HCl acid. The gas stream was introduced at the inlet in the reactor lid. The vapour pressure of chlorine gas was calculated using Antoinne's equation. Calculations are detailed in Appendix E. The calculated flow rate was 0.01 l/min and partial pressure was 0.04 atm.

7.5.2.3. H_2O vapour

Water vapour was introduced to the system by bubbling the argon gas through a volumetric flask with boiling distilled water. The stream temperature was monitored at 80°C to be able to calculate the humidity of the gas stream. The vapour pressure of water was calculated using Antoinne's equation; detail of the calculation is given in Appendix E. A vapour pressure of 0.47 atm and a flow rate of 0.22 l/min were used.

7.5.2.4. Hydrogen sulphide gas

Synthetic iron sulphide (FeS) and concentrated sulphuric acid (96% v/v) were used to synthesise hydrogen sulphide gas. FeS was received as sticks, 10mm in diameter; it was crushed with a jaw and cone crusher to +/-1 mm to increase the surface area. The reaction model of Factsage software [Bale et al. 2002] was used to predict the reaction suitable for H_2S synthesis (Equation 25). A total volume of 124ml of a dilute acid solution H_2SO_4 of 0.15mol/L was reacted with 50g FeS to produce 19.38g of H_2S.
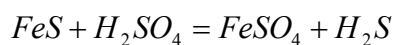
$$FeS + H_2SO_4 = FeSO_4 + H_2S \hspace{3cm} Equation\ 25$$

The method used to determine the amount of hydrogen sulphide gas evolved is indicated in Appendix E. The hydrogen sulphide gas evolved was bubbled through a potassium dichromate solution in which it oxidised to produce sulphate species. Redox titration of iron sulphate by Cr(VI) residue solution gives the concentration of Cr(III), which is equivalent to the amount of H_2S formed. Diphylamine indicator was used to determine the end point characterised by solution colour change from green to pink [Gudyanga et al. 1999, Lenahan et al. 2001].

7.5.2.5. Argon gas

Argon technical gas supplied by Afrox was used as a carrier gas for S_2, HCl and water vapour. It was also used to create an inert environment inside the reactor. The argon flow rate to the reactor was monitored by a rotameter. The flow rate was calculated from the equation obtained from the calibration curve in Figure C 1 Appendix C. The calculated argon flow rate was 0.25 l/min and it was kept constant for all the tests.

All the chemicals used for gas synthesis were supplied by Merck chemicals.

7.5.3. Temperature and corrosion rate measurement

The temperature at the surface of the foil was estimated using a K-type thermocouple, which was fitted on the heat sink; temperature measurements were taken using a datataker (Figure 40).

Corrosion is considered a rate of formation of another layer or substance on a substrate. The change in resistance of a foil (conductor) indicates the change in thickness at constant length and width. Resistance was calculated from measured amperes and voltage drop across the foil. The measured change in resistance (ohms) was converted to thickness loss (mm) using Equation 23. Change in foil thickness (micron per minute) was plotted against time at a constant temperature to determine the corrosion rate.

7.5.4. Copper foil heat-up and gas flow through the system

The sulphur and the copper foil sample were heated separately to avoid pre-sulphidation of the copper foil sample before it got to the operating temperature. The foil (sample) was heated to the operating temperature by circulating the silicone oil through the heat sink. The temperature set point of the oil bath was regulated accordingly to bring the foil temperature to the operating temperature. Argon was used to purge the system prior to introducing the corrosive gases to the foil. When the measured temperature of the sample reached the operating temperature, the glass reactor with the sulphur melt was assembled, with the reactor lid holding the sample as shown in Figure 40 number 8. A similar procedure was followed for the tests where HCl and water vapour were added. The carrier gas, argon with HCl or water vapour, was introduced to the system after the sulphur-containing reactor and the reactor lid had been assembled.

For the H_2S tests, the crushed FeS was fed into the reactor before the foil heat-up was started. Argon was bubbled through the acid for 20 minutes to purge oxygen on the acid prior to adding acid to the iron sulphide. The acid was added to the reactor only when the foil temperature had reached the operating temperature. The reactor was immediately sealed to prevent the gas from escaping from the reactor; only the vent valve remained open.

7.5.4.1. Corrosion at constant temperature

The operating temperature was kept constant for the duration of the test work. Experiments were performed at 65°C, 80°C, 90°C, 100°C, 110°C, 120°C, 130°C and 140°C where a copper foil was exposed to sulphur vapour for two hours, after which the sample was allowed to cool to 25°C under an argon atmosphere. For HCl additions, water vapour additions and H_2S tests, experiments were performed at 80°C, 110°C and 140°C. Each experiment was repeated three times to verify repeatability.

7.5.4.2. Corrosion at varying temperature (80°C to 140°C)

To determine the effect of thermal variability on corrosion rate and transition temperatures from fast to slow corrosion rates, the copper foil surface temperature was gradually raised from 80°C to 140°C at 20°C intervals every hour until the maximum operating temperature (140°C) was reached. These tests were done for all the gas compositions. After 140°C had been reached, the foil was cooled to 25°C under an argon atmosphere and prepared for analysis.

7.5.5. Phase composition and morphology of the corrosion product

Morphology is defined as the form and the structure of a substance. Chemical composition, chemical phases and layout of the corrosion product were the variables used in this work to describe morphology. SEM was used to obtain the back-scattered electron images of the foil and its EDS function was used to determine the composition of the corrosion products. XRD was used to determine the crystalline phases in the sample.

The copper foil residue and the corrosion products produced when the corrosion tests were performed were subjected to analysis to determine the effect of gas composition and copper foil temperature on the morphology of the corrosion product. SEM analysis required a polished surface of the mounted sample such that a cross-section of the foil could be examined.

7.6. Results

7.6.1. Effect of temperature on corrosion rate

Copper foil samples were exposed to corrosive sulphurous gases where their surface temperature was varied in order to determine the effect of temperature on corrosion rate. The corrosion rate was determined by calculating the thickness loss from the measured change in foil resistance as described in the previous chapter. The slope of thickness loss versus exposure time was determined by fitting a straight line through the curve. Where the data pattern did not fit a straight line, the curve was split to allow a straight line to be fitted and an average slope to be calculated. The data presented are an average of three tests performed at each temperature.

7.6.1.1. Sulphidation of copper by sulphur vapour

Copper foil samples were exposed to sulphur vapour at different temperatures in the range 65 to 140°C. Thickness loss as a function of exposure time up to one hour at various temperatures is shown in Figure 42. The slopes for the curves are summarised in Table 33. Time intervals used in Table 33 were selected based on durations where the slope of the curve seemed constant.

- *Corrosion at constant temperature*

The slope observed at 65°C operating temperature increased from 0.04 in the initial 15 minutes to 0.06 micron per minute in the final 35 minutes of the test. The overall corrosion rate behaviour was linear. To determine the average corrosion rate per year, a direct conversion from micron per minute to millimetres per year was used, since linear behaviour was assumed. The average corrosion rate after an hour of exposure was 0.05 micron per minute, which is equivalent to 25.2 mm/y.

At a copper foil temperature of 80°C the corrosion rate was also linear, where an initial slope of 0.07 in the first 15 minutes increased to 0.11 (micron loss per

minute) in the final 35 minutes of the test. An average slope of 0.09 micron loss per minute was observed after a total of 60 minutes exposure time.

At a copper foil operating temperature of 90°C the observed slope increased from 0.09µm/min after 15 minutes of exposure to 0.12µm/min in the final 40 minutes. The average thickness loss rate of 0.10µm/min was observed after 60 minutes exposure.

At a copper foil operating temperature of 100°C the observed thickness loss slope increased from 0.11µm/min after initial 15 minutes to 0.21µm/min in the final 40 minutes. The average thickness loss rate of 0.16µm/min was observed after 60 minutes exposure.
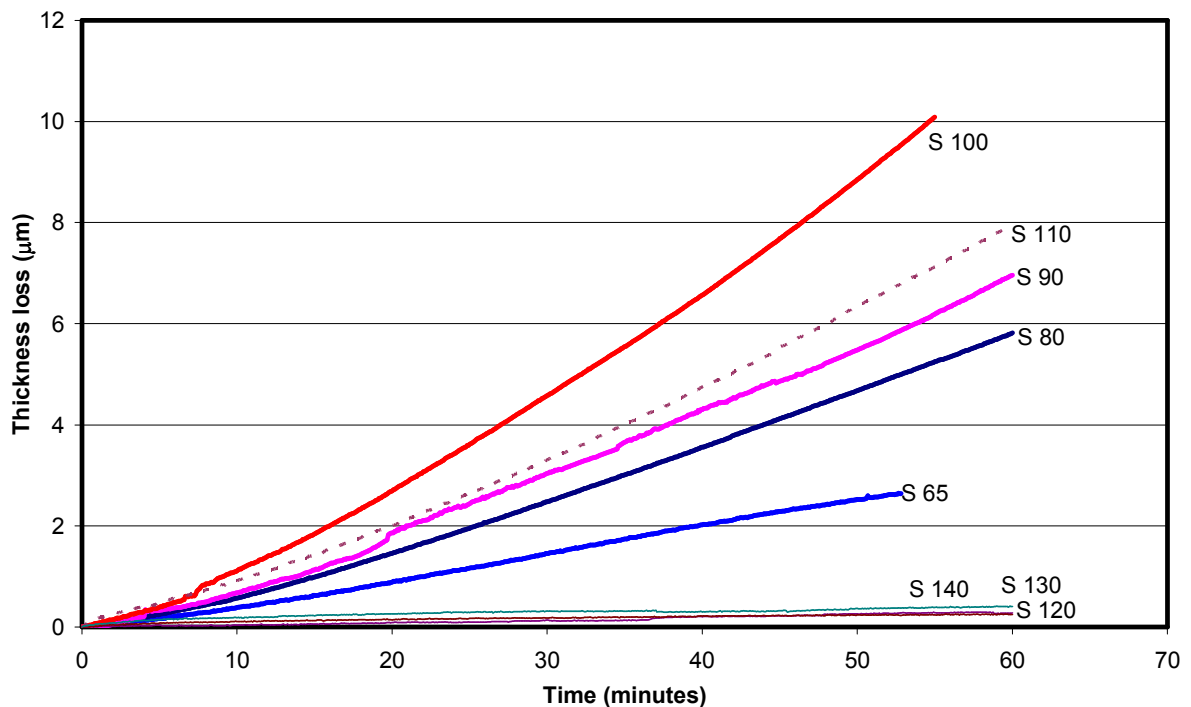
Figure 42: Thickness loss on copper foil as a function of exposure time for temperatures ranging from 65°C to 140°C (sulphidation by sulphur vapour).

Table 33: Summary of slope of thickness loss of copper foil exposed to sulphur vapour versus exposure time

Copper foil surface temperature °C	Slope (micron loss per minute)		
	0-15 minutes	20-55 minutes	0-60 minutes (average)
65	0.04	0.06	0.05
80	0.07	0.11	0.09
90	0.08	0.12	0.10
100	0.11	0.21	0.16
110	0.09	0.15	0.12
140		0.01	0.01

At a copper foil operating temperature of 110°C the observed slope of the thickness loss versus time graph increased from 0.09µm/min after 15 minutes of exposure to 0.15µm/min in the final 40 minutes. The average thickness loss rate of 0.12µm/min was observed after 60 minutes exposure.

An average thickness loss slope of 0.01µm/min was observed at operating temperatures from 120°C to 140°C.

The average corrosion rate as a function of temperature is depicted in Figure 43 and Table 34. The top and bottom bars in Figure 43 mark the maximum and the minimum corrosion rates observed.
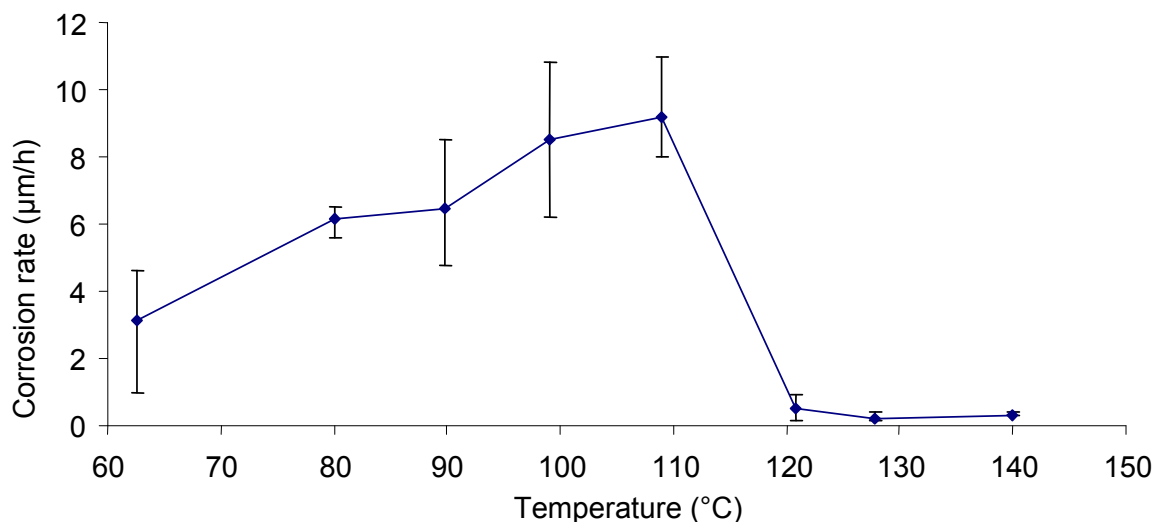
Figure 43: Average corrosion rate as a function of temperature when copper was exposed to sulphur vapour in a temperature range of 65°C to 140°C.

Table 34: Average corrosion rate of copper foil exposed to sulphur vapour at different temperatures

Average temperature °C	62.6	80.1	89.8	99.1	108.9	120.8	127.8	140.0
μm/h	3.1	6.2	6.5	8.5	9.2	0.5	0.2	0.3
mm/y	27.2	54.1	56.8	74.5	80.3	4.6	1.8	2.6

The corrosion behaviour of copper foil at temperatures from 65°C to 110°C follows a similar pattern, which is almost linear. Between 110°C and 120°C there seems to be a shift in the rate of thickness loss from an average of 0.12 μm per minute to 0.01 μm per minute. Experiments were performed where the copper foil surface temperature was varied from 80°C to 140°C to determine the transition temperature from a high corrosion rate observed at 110°C to slow corrosion rates observed from 120°C to 140°C. The results of these experiments are presented in Figure 45.

- *Discussion*

From 65°C to 110°C the corrosion rate increased with temperature. Although the corrosion rate seemed to increase at the later stage of the experiment, linear behaviour was implemented to simplify the calculations. Linear corrosion rate behaviour is observed when the scale layer formed is highly porous, poorly adherent or cracked, which causes the scale to be non-protective. The corrosion rate behaviour is expected to change from linear to parabolic with increasing sulphide thickness, but if the sulphide scale is not protective, the corrosion rate remains linear.

Tran et al. [2003] commented that tests performed under synthetic conditions cannot be extrapolated to longer times in plant conditions since different sulphidation phases are observed over time. Although the corrosion rate could be described by the linear rate law, there are other factors that influence the corrosion rate, including:

(i)   Morphology of the corrosion product

The corrosion product becomes porous, and the grain size may change with exposure time. Permeability of the corrosion product may change significantly during exposure, which may affect the corrosion rate.

(ii)   Loss of a protective layer

It was observed that the corrosion product at all temperatures was non-adherent and easily flaked off. Gesmundo et al. [1996] observed that the irregularity or change in corrosion rate from parabolic to linear is due to the loss of protectiveness of the corrosion layer. The corrosion layer can lose its protectiveness owing to the loss of adherence of the scale to the metal. The parabolic rate law assumes that the corrosion layer becomes passivating as the thickness increases, but if and when a new surface is exposed owing to a corrosion layer flaking off, that exposed surface will be corroded at a different rate compared to the surface that is covered with an intact corrosion product [Gesmundo et al. 1996].

(iii)   Stress

Tran et al. [2003] reported that internal stresses in the corrosion layer leads to cracks and porosity at long exposure times. Reid et al. [2008] also observed that when the thickness of a corrosion layer is above 1.2 microns, the growth rate of the film becomes parabolic, but internal stresses and defects in a corrosion layer allows access to corrosive gases, which induces linear rate growth of the corrosion layer [Reid et al. 2008].

Copper foil was exposed to sulphur vapour for eight hours to ascertain the effect of exposure time on corrosion rate at 140°C. Copper foil thickness loss as a function of time is depicted in Figure 44.
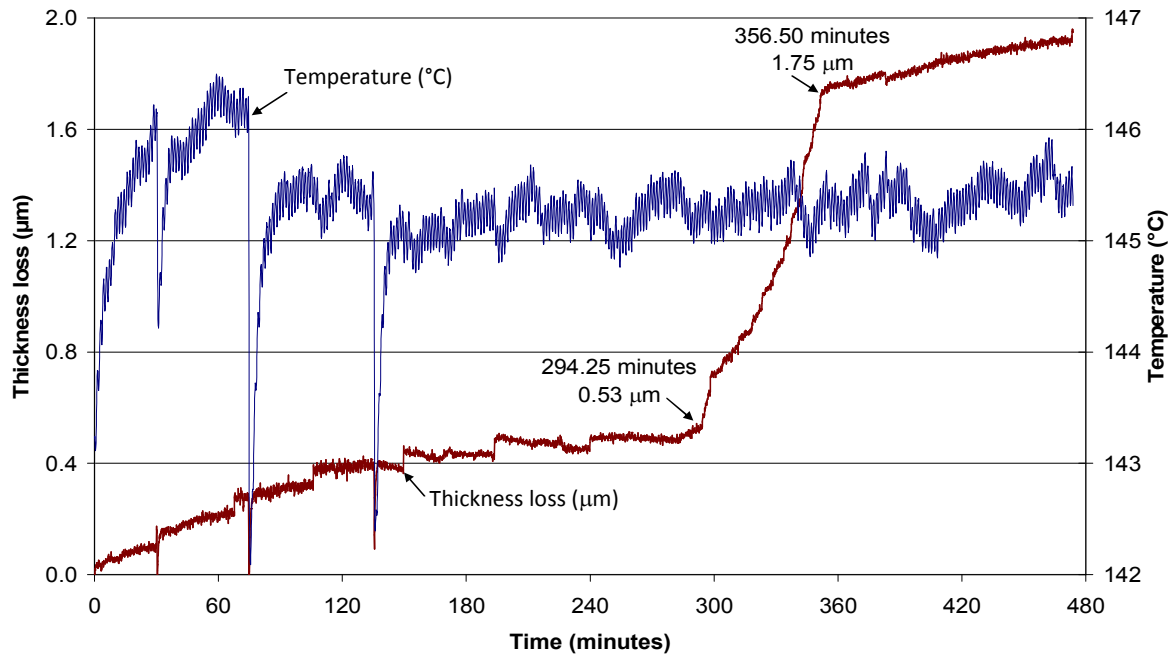
Figure 44: Thickness loss of a copper foil as a function of exposure time at 140°C in sulphur vapour.

Samples were taken at 30 minutes, 75 minutes and 135 minutes to examine the change in the scale thickness under the SEM. During sampling the heat sink was taken out of the reactor and the system was exposed to the colder environment for approximately 20 seconds while taking a sample, hence a sharp decrease in temperature observed at these intervals (Figure 44). Parabolic behaviour was observed initially where 0.53 micron of the foil thickness was lost in five hours. At five hours the corrosion rate suddenly increased sharply while the temperature remained constant. A linear rate was observed from 294.25 minutes to 356.5 minutes (Figure 44 arrowed points). During this period the total thickness lost was 1.22µm. The linear rate lasted an hour, after which a sharp decrease in thickness loss was observed, although the slope of the graph remained higher than the initial slope. After the test it was observed that the corrosion product had a crack.

The sudden increase in corrosion rate could be attributed to the crack in the sulphide surface, since there were no other defects in the corrosion product. Each experiment would display unique effects but this is a classic example of what might happen with long exposure times. Because of other uncontrollable

variables affecting the scale during corrosion, it would be inaccurate to apply the parabolic rate law to estimate the corrosion rate during long exposure times as in the smelter, hence the linear rate was assumed in estimating the corrosion rate depicted in Figure 42.

- *Corrosion at varying temperature (80°C to 140°C)*

To determine the transition temperature from a fast corrosion rate to a slow corrosion rate observed above 110°C, experiments were performed where the substrate temperature was increased from 80°C to 140°C. The operating temperature set point was raised by 20°C intervals every hour until 140°C was reached. The graph of the thickness loss as a function of exposure time from 80°C to 140°C is depicted in Figure 45. All three replicates are shown in order to compare the transition temperature in each test performed. In the first experiment the transition from high thickness loss rate to low was at 112.30°C when the thickness loss was 14.50μm. The transition temperature was 112.55°C at a total thickness loss of 20.20μm for the second experiment. In the last experiment the transition temperature was at 113.41°C with a total thickness loss of 11.45μm. Comparing the three experiments, there seems to be a strong correlation between the temperature and the corrosion rate behaviour. The total thickness loss value did not seem to have much effect on the transition from high corrosion rate to low corrosion rate, since in the first test the total thickness loss was 14.50 microns, while in the second test it was at 20.20 microns and in the last test it was at 11.45 microns.
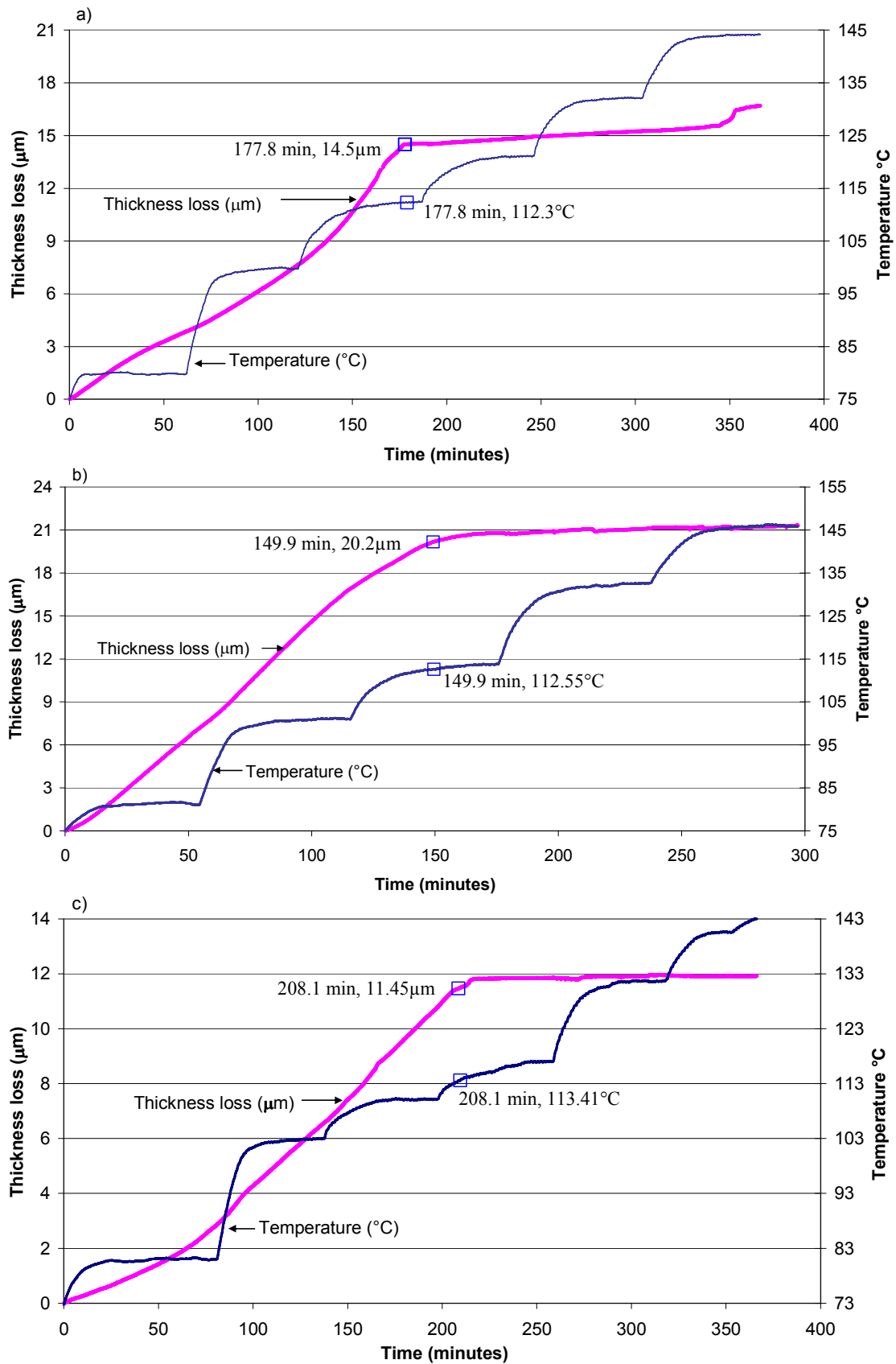
Figure 45: Thickness loss of copper foil as a function of exposure time in the temperature range 80°C to 140°C in sulphur vapour. a), b) and c) are three replicates of the same condition.

The transition from a high corrosion rate to a low corrosion rate took place at temperatures between 112°C and 114°C. The second effect observed in the first test (Figure 45a) at temperatures above 140°C is believed to be the same effect observed for long exposure times (Figure 44), which is presumably caused by the physical disruption of the foil.

The corrosion rate transition observed between 112°C and 114°C coincides with the melting temperature of sulphur, which is 110°C for orthorhombic sulphur and 114°C for monoclinic sulphur, according to Vaughan [1978]. In contrast, Patnik [2003] reported that orthorhombic beta-sulphur melts at 115°C while gamma-sulphur melts at 120°C. The corrosion rate transition can be attributed to sulphur that changed from a solid phase to a liquid phase. Vaughan et al. [1978] reported that a transition from monoclinic chalcocite (Cu_2S) to hexagonal chalcocite (Cu_2S) occurs at 103.5°C in the copper-sulphur system. Furer et al. [1977] observed that hexagonal chalcocite lowers the corrosion rate, since it is much more defective than monoclinic chalcocite, which implies that the transition in corrosion rate can also be attributed to the phase transformation from monoclinic chalcocite to orthorhombic chalcocite. Furer also observed that chalcocite causes a fragile area to occur on the metal surface, which may cause detachments and affect the protectiveness of the corrosion layer. Bartkowicz et al. [1986] observed that mass transport is slower in hexagonal chalcocite than in monoclinic chalcocite. Bartkowicz also noted that a porous layer on a metal surface causes poor adherence of the scale to the metal. If a porous layer or a non-adherent layer forms between the metal surface and the outer sulphide layer, the diffusion of copper species to the surface for reaction to proceed is retarded, which may lead to a slower corrosion rate.

7.6.1.2. Sulphidation of copper by sulphur vapour with HCl additions

The copper foil was exposed to both sulphur and HCl vapour to determine the effect of chlorine addition on the corrosion rate. The curve for thickness loss as a function of exposure time for copper foil exposed to sulphur vapour with HCl at 80°C, 110°C and 140°C is depicted in Figure 46. Different corrosion rate patterns

were observed for this gas composition at each temperature. A summary of the thickness loss versus time slopes is depicted in Table 35.

- *Corrosion at constant temperature*

Parabolic corrosion behaviour was observed when the copper foil surface temperature was at 80°C. The slope of thickness loss decreased from 0.07 micron per minute in the initial 55 minutes to 0.02 micron per minute after two hours of exposure. An average rate of 0.04 micron loss per minute was observed after the total exposure time of two hours. Parabolic behaviour was therefore assumed, which suggested that the corrosion layer formed was protective, unlike the corrosion behaviour observed when the copper foil was exposed to sulphur at the same temperature.
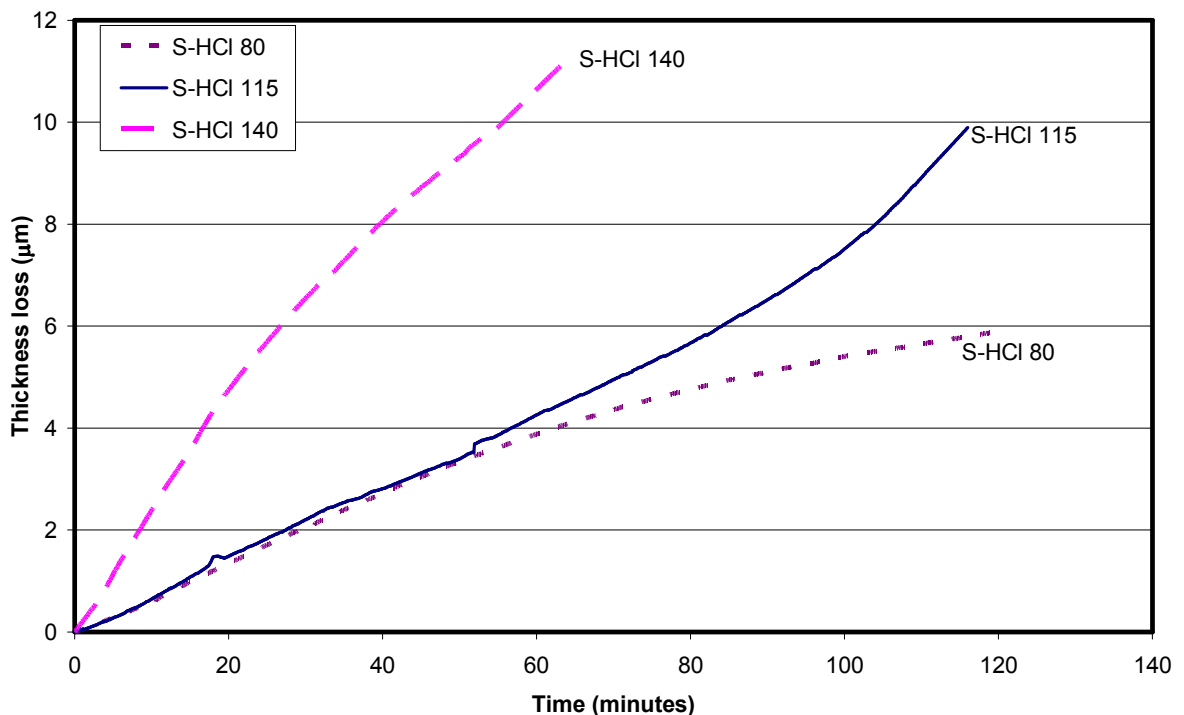
Figure 46: Thickness loss as a function of exposure time at 80°C, 115°C and 140°C when copper foil was exposed to sulphur and HCl vapour.

Table 35: Summary of slope of thickness loss of copper foil exposed to sulphur vapour with HCl additions

Copper foil surface temperature °C	Slope (micron loss per minute)				
	0-52min	52-82min	82-103min	103-116min	0-120min
80	0.07	0.05	0.03	0.02	0.04
115	0.07	0.07	0.10	0.16	0.09
	0-17min	20-65min			average
140	0.24	0.14			0.19

When copper foil was exposed to sulphur and HCl at 115°C a linear corrosion rate with a slope of 0.07µm/min was observed in the initial 96 minutes of exposure. At a total thickness loss of 6 µm the slope increased to 0.16 micron per minute in the final 10 minutes of a two-hour exposure test. It was noted that the initial slope for 80°C and 115°C operating temperatures was 0.07µm/min in the first hour.

The fastest thickness loss rate was observed when the copper foil surface temperature was at 140°C. An initial rate of 0.24 micron per minute was observed in 15 minutes of exposure, after which the rate dropped slightly to 0.14 micron per minute. Average corrosion of 0.19 micron per minute was observed after one hour of exposure.

- *Discussion*

Different corrosion rate behaviours were observed at the different operating temperatures. At 80°C a parabolic rate was observed while at 115°C the rate was almost linear for the first 90 minutes and at 140°C a faster parabolic rate was observed. The lowest corrosion rate (0.04 micron loss per minute) was observed at 80°C while the highest rate (0.19 micron loss per minute) was observed at 140°C (Table 35). The cause of the increase in corrosion rate after 90 minutes of operation at 115°C is not clear. A parabolic rate observed at 80°C can presumably be attributed to the difference in diffusion rate after the corrosion product reached a certain thickness, where the diffusion of ions through the corrosion product became rate-limiting. This observation was made by Reid et al. [2008] who reported that when the corrosion product reaches a critical thickness

Sulphidation of copper coolers in PGM smelters

of 1.2 microns the rate of film growth becomes parabolic, depicting that diffusion of copper species through the corrosion layer is rate-limiting. Swinbourne et al. [1979] reported that chlorine diffuses faster through chalcocite than through covellite, and covellite is expected to form when sulphur reacts with copper at low temperatures and high sulphur concentrations.

Brooks et al. [1985] observed that the role of chlorine in sulphidation is to induce the transition from parabolic to linear corrosion kinetics at high temperatures (400°C to 500°C). Reid et al. [2008] reported that it is the internal stresses and defects in structure that allow the corrosive gases to reach the metal surface, thereby inducing the transition from parabolic to linear corrosion kinetics, which is in contrast with the behaviour observed in Figure 46 where the corrosion rate changed from linear to parabolic. However, the observation is in agreement in the sense that the corrosion rate changed from slow to fast at 115°C.

Reid et al. [2008] and Brooks et al. [1985] observed that chlorine can penetrate through the entire corrosion film and metal, thereby creating a path for the copper species to diffuse to the reaction surface.

The increased thickness loss rate at 140°C can be attributed to the ability of chlorine to diffuse faster through chalcocite than in covellite, as reported by Swinbourne et al. [1979]. Brooks et al. [1985] also reported that the presence of HCl increases the porosity of the corrosion layer by physically disrupting any protective layer, creating a path for ion diffusion at higher temperatures. It can be concluded that the faster corrosion rate at 140°C compared to 80°Cand 115°C is due to the differences in morphology of the corrosion products that formed at these temperatures and the increased diffusion rate of ions.

- *Corrosion at varying temperature (80°C to 140°C)*

To determine the transition temperature from slow to fast thickness loss rate, experiments were performed where the temperature was varied from 80°C to 140°C in increments of 20°C. The resulting curves of thickness loss as a function of temperature are depicted in Figure 47 where a and b are the replicates of the same experiment. The transition from a slower to a faster corrosion rate occurred

at 112.08°C at a thickness loss of 10.74µm in the first experiment, whereas at the second experiment the transition was observed at 112.46°C at a thickness loss of 19.81µm. These temperatures are almost the same as the transition temperature from a faster corrosion rate to a slow corrosion rate observed when copper was exposed only to a sulphur vapour (Figure 45). Tran et al. [2003] reported that the foil cleaned with HCl reacted faster after the melting point of sulphur compared to the foil cleaned in alcohol. For this reason it can be concluded that the transition from a slower to a faster corrosion rate is associated with the sulphur phase transition and the ability of chlorine to permeate a thick layer of molten sulphur and sulphide phases.
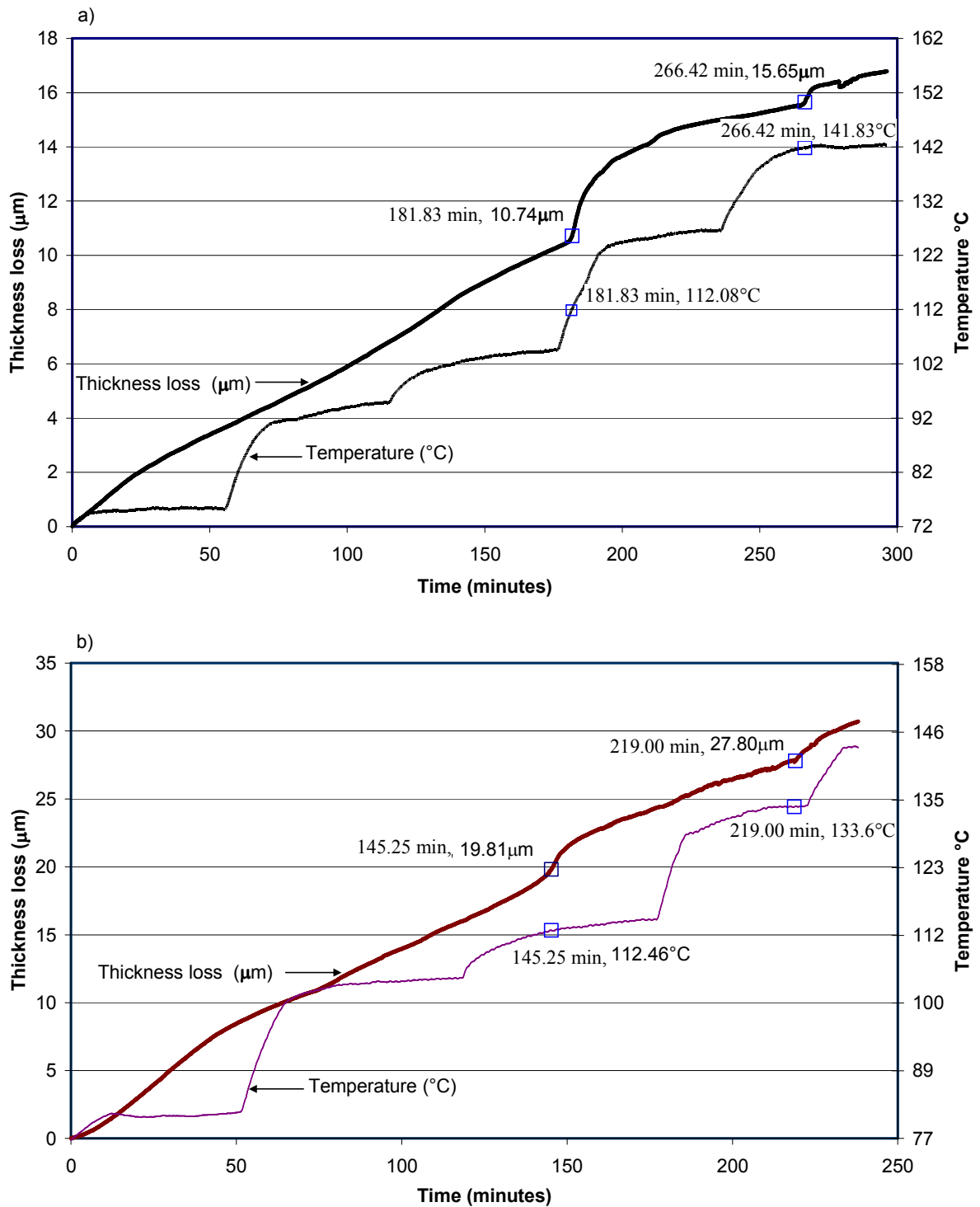
Figure 47: Thickness loss as a function of exposure time at varying temperatures (80°C to 140°C); when copper foil was exposed to sulphur and HCl vapour. a) and b) are two replicates of the same condition.

The increase in corrosion rate observed at temperatures greater than 130°C did not occur at the same temperature in both tests; one occurred at 141.8°C and the other was observed at 133.6°C (Figure 47). For this reason the increase in

corrosion rate could not be attributed to any phase transformations. It was assumed to be caused by cracks or defects in the foil due to the foil detachment from the heat sink, since these temperatures are close to the softening point (150°C) of the epoxy bonds.

7.6.1.3. Sulphidation of copper by sulphur vapour with H_2O additions

Addition of water vapour to the system presented challenges in determining the corrosion rate. The heat sink was coated with a conformal coating and an epoxy was used to attach the foil to the heat sink. The conformal coating is not suitable for high-humidity applications and the presence of moisture compromises the adhesion between the foil and the heat sink. Because of this problem the corrosion rate could not be accurately determined, since most of the time the system was disturbed when the foil had to be re-attached. However, the average thickness lost was estimated from the total change in foil resistance with time. It was observed that the addition of water vapour resulted in lower corrosion rates compared to the corrosion rate of copper foil when exposed to sulphur only. At a copper foil surface temperature of 80°C an average copper foil thickness loss of 0.35 micron per hour was observed with the addition of water compared to an average thickness loss rate of 6.2 micron per hour with sulphur only.

The determination of the corrosion rate of copper foil when exposed to sulphur vapour with water vapour was consequently discontinued, since a different setup would have to be used to achieve accurate data that can be compared to other gas compositions without water vapour.

7.6.1.4. Sulphidation of copper by hydrogen sulphide (H_2S)

Copper foil was exposed to hydrogen sulphide-containing gas to determine the corrosion rate of copper at 80°C, 110°C and 140°C. Thickness loss of copper foil as a function of exposure time at different temperatures is shown in Figure 48. A summary of the corrosion rate is depicted in Table 36.

- *Corrosion at constant temperature*

No corrosion was observed in the initial 30 minutes of copper foil exposure at 80°C. A slope of 0.003 micron per minute was observed in the final 80 minutes of the 110-minute run. An average corrosion rate of 0.01 micron per minute was observed after exposure of the copper foil for 110 minutes at 110°C. A linear corrosion rate of 0.08 micron per minute was observed after a total exposure of 110 minutes at 140°C.
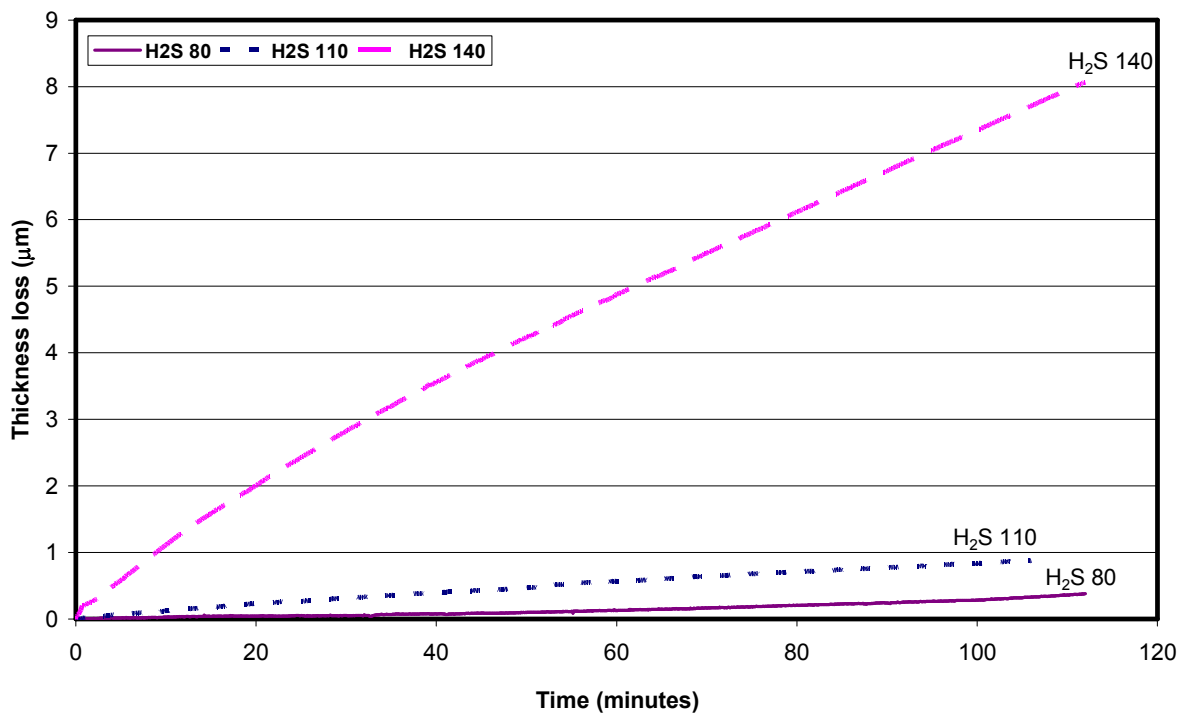
Figure 48: Thickness loss on copper foil as a function of exposure time for different temperatures in H_2S gas.

Table 36: Summary of slope of thickness loss of copper foil exposed to hydrogen sulphide (H_2S).

Copper foil surface temperature °C	Slope (micron loss per minute)
	0-110 minutes
80	0.003
110	0.008
140	0.078

Gesmundo et al. [1996] and Tran et al. [2005] observed that the corrosion rate of copper by hydrogen sulphide gas increases with temperature and it is also a function of gas concentration. These authors used H_2-H_2S mixtures from cylinders to provide H_2S for their system. H_2S from a cylinder could not be used in this study owing to the environmental regulations that H_2S may not be kept in a laboratory because of its toxicity. The gas synthesis procedure (Appendix E) in this study was kept the same for all the tests to minimise calculation errors and to keep the gas concentration constant in all the tests.

7.6.1.5. Summary: Sulphidation rate as a function of a corroding gas composition

The sulphidation rates of copper by S_2, S_2+HCl and H_2S at three different temperatures (80°C, 110°C and 140°C) are shown in Figures 49 to 51. A corrosion rate curve by a sulphur gas at 80°C depicted linear behaviour and hence a faster rate than the rate observed when HCl was added. An average corrosion rate over a period of 80 minutes was 0.09 micron per minute for S_2 only and 0.07 micron per minute where HCl was added (Figure 49). Based on the observation in Figure 49, it can be concluded that the addition of chlorine at 80°C retards the corrosion rate when copper is exposed to sulphur vapour. The corrosion by hydrogen sulphide occurred at the slowest rate of 0.003 micron loss per minute at 80°C. The summary of thickness loss rate for all the gases at 80°C is presented in Table 37.

Figure 49: Comparison of thickness loss as function of time for copper foil exposed to S_2 (S 80), S_2+HCl (S-HCl 80) and H_2S at 80°C.

Table 37: Summary of slope of thickness loss of copper foil exposed to various gases at 80°C (µm/min)

Figure 49	0-18min	18-77min	0-77 min
S80	0.07	0.115	0.0925
S-HCl80	0.068	0.067	0.068
H_2S80	0.003	0.003	0.003

The overall corrosion rates increased at 110°C but a similar trend was observed where the thickness loss rate was highest due to S_2(g) exposure (0.14 µm/min) while the chlorine addition retarded the corrosion rate by half from an average of 0.14 without HCl to 0.078 micron per minute with HCl after 110 minutes of S_2(g) exposure (Figure 50, Table 38). Corrosion due to hydrogen sulphide increased from 0.0032 micron per minute at 80°C to 0.008 micron per minute at 110°C.
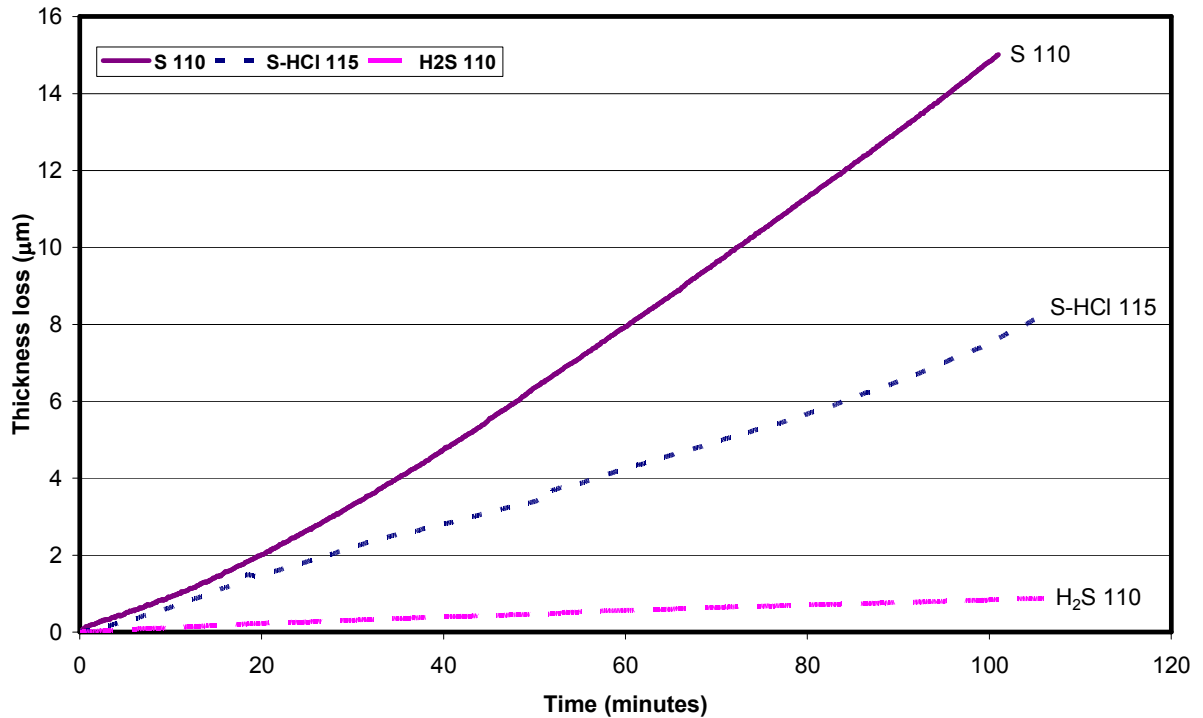
Figure 50: Comparison of thickness loss as function of time for copper foil exposed to S_2 (S 110), S_2+HCl (S-HCl 115) and H_2S at 110°C.

Table 38: Summary of slope of thickness loss of copper foil exposed to various gases at 110°C (µm/min)

Figure 50	0-30 minutes	30-100 minutes	0-100 minutes
S110	0.11	0.17	0.14
S-HCl 115	0.07	0.08	0.08
H_2S 110	0.01	0.01	0.01

Corrosion rates at 140°C depicted a different trend from the rates at 80°C and 110°C. $S_2(g)$ exposure had the lowest thickness loss rate while adding chlorine enhanced the corrosion significantly (Figure 51, Table 39). The rate of corrosion by hydrogen sulphide was also enhanced at 140°C. A summary of the slopes is presented in Table 39. Tran et al. [2005] reported that when copper is exposed to hydrogen sulphide, the rate of growth of a sulphide layer is enhanced by an increase in temperature, which can be attributed to the increase in chemical, diffusion and electrochemical reaction rates. It has been found that the chlorine

has the ability to diffuse through the corrosion layer providing a path for metal diffusion to the reaction surface. Chlorine therefore increases the corrosion by physically disrupting the protective scale [Brooks et al. 1985; Sesselman et al. 1986; Reid et al. 2008]. It is presumed that the layer that forms above 110°C is passivating to a sulphur gas, but the presence of chlorine enables the corrosive gases or the metal ions to diffuse to the reaction site, thereby enhancing the corrosion rate.
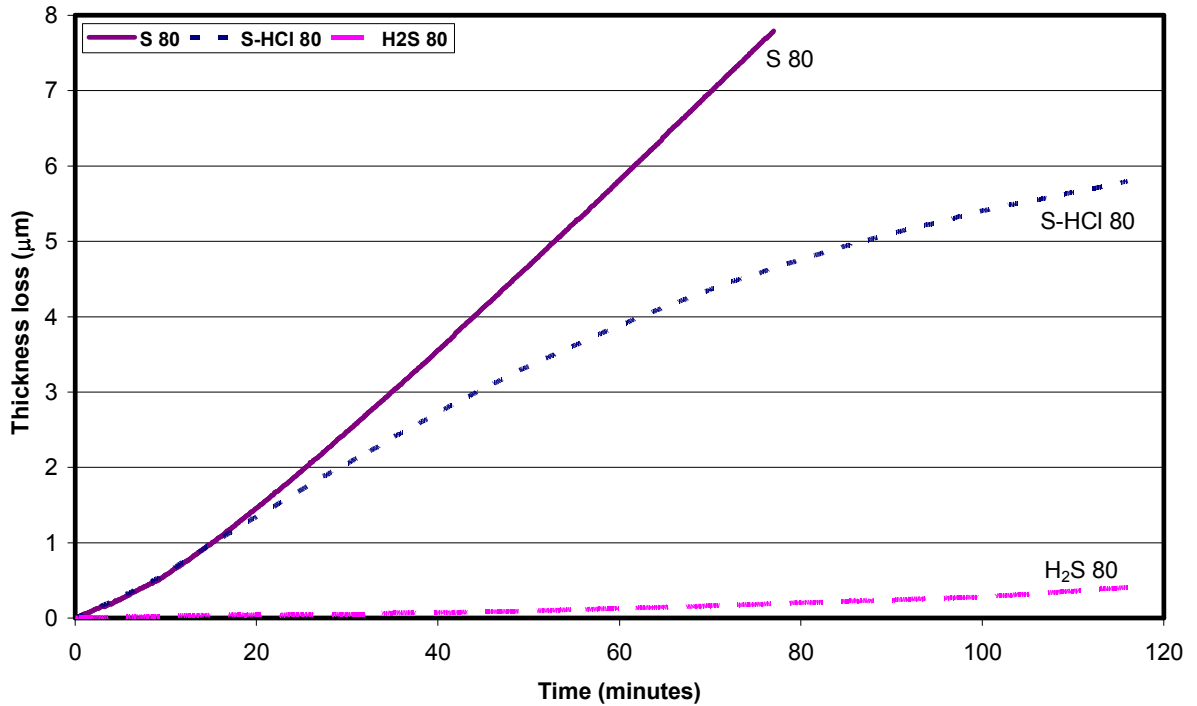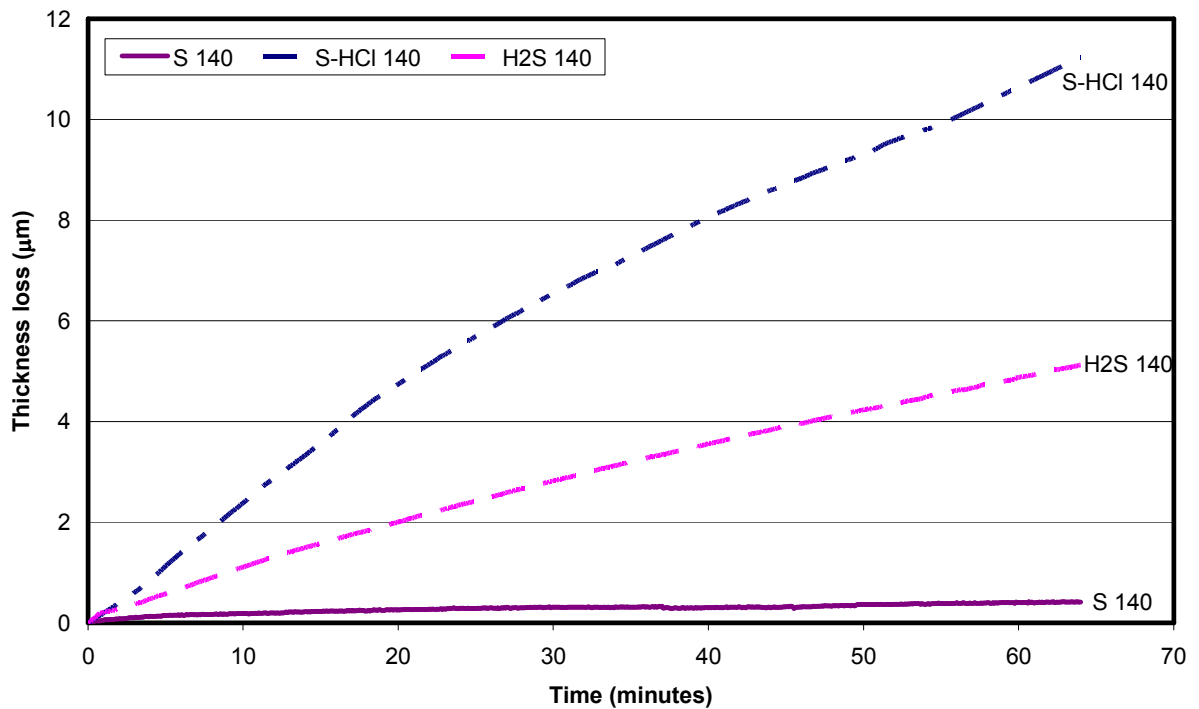

Figure 51: Comparison of thickness loss as a function of time for copper foil exposed to S_2 (S 140), S_2+HCl (S-HCl140) and H_2S at 140°C.

Table 39: Summary of slope of thickness loss of copper foil exposed to various gases at 140°C (µm/min)

Figure 51	0-17 minutes	20-65 minutes	0-65 minutes
S140		0.01	0.01
S-HCl 140	0.24	0.14	0.19
H_2S 140	0.10	0.071	0.09

An average corrosion rate of 54.1 mm/y to 80 mm/y was observed when copper foil with a surface temperature of 80°C and 110°C respectively was exposed to sulphur vapour. The copper cooler surface temperature (rammable composite)

ranges from 48°C to 109.2°C, based on the calculation done in Table 31. It can therefore be concluded that at high sulphur concentrations the copper cooler thickness loss can exceed 80 mm/y if the copper surface is operated at temperatures around 110°C. The corrosion rate of copper by sulphur can be enhanced to above 100 mm/y if the copper surface temperature is greater than 110°C and HCl vapour is present. At low temperatures (80°C and 110°C) addition of chlorine retards the corrosion rate of copper by sulphur.   The corrosion rate of copper by hydrogen sulphide is very slow at copper foil surface temperatures below 110°C; at higher temperatures (140°C) corrosion rates of 47.3 mm/y can be observed.

7.6.2. Effect of gas composition on morphology of corrosion product

7.6.2.1. *Phase composition and morphology of the corrosion product exposed to sulphur vapour*

The copper foil was exposed to sulphur vapour at 80°C, 110°C and 140°C to study the effect of temperature on the morphology of the corrosion product. The EDS area analyses and the XRD qualitative analyses are presented in Tables 40 to 47. The XRD patterns of the crystalline phases are presented in Appendix B. BSE images of the cross-section of the corrosion products formed on the copper foil after exposure to S_2 at 80°C, 110°C and 140°C are shown in Figure 52 (a, b and c respectively). The annotations used in the BSE images differentiate the corrosion layers:

M: the remainder of the copper foil after exposure

MS: the inner corrosion layer closer to or in contact with the foil

GS: the outer corrosion layer at the gas-scale interface

SS: the corrosion layer between MS and GS.

a) Phase composition and morphology at 80°C

Copper foil was exposed to sulphur vapour to determine the morphology of the corrosion product at 80°C. A thin black layer with fine yellow particles on top was

visually observed on the foil surface after exposure. Under the SEM three layers of the corrosion product could be observed, as shown in Figure 52a. A thin non-uniform layer (MS1-1) formed closer to the foil surface. EDS area analysis of this layer could not be performed since it was too thin. A dense, thicker sulphide layer (MS1) was observed adjacent to this thin layer. The composition of MS1 according to the EDS area analysis has a copper-to-sulphur ratio of 1. A layer of elemental sulphur (GS1) was observed at the gas-sulphide interface. Covellite (CuS) and synthetic sulphur were detected by XRD in the corrosion product. EDS analysis results are depicted in Table 40, semi-quantitative XRD analysis results are shown in Table 41.
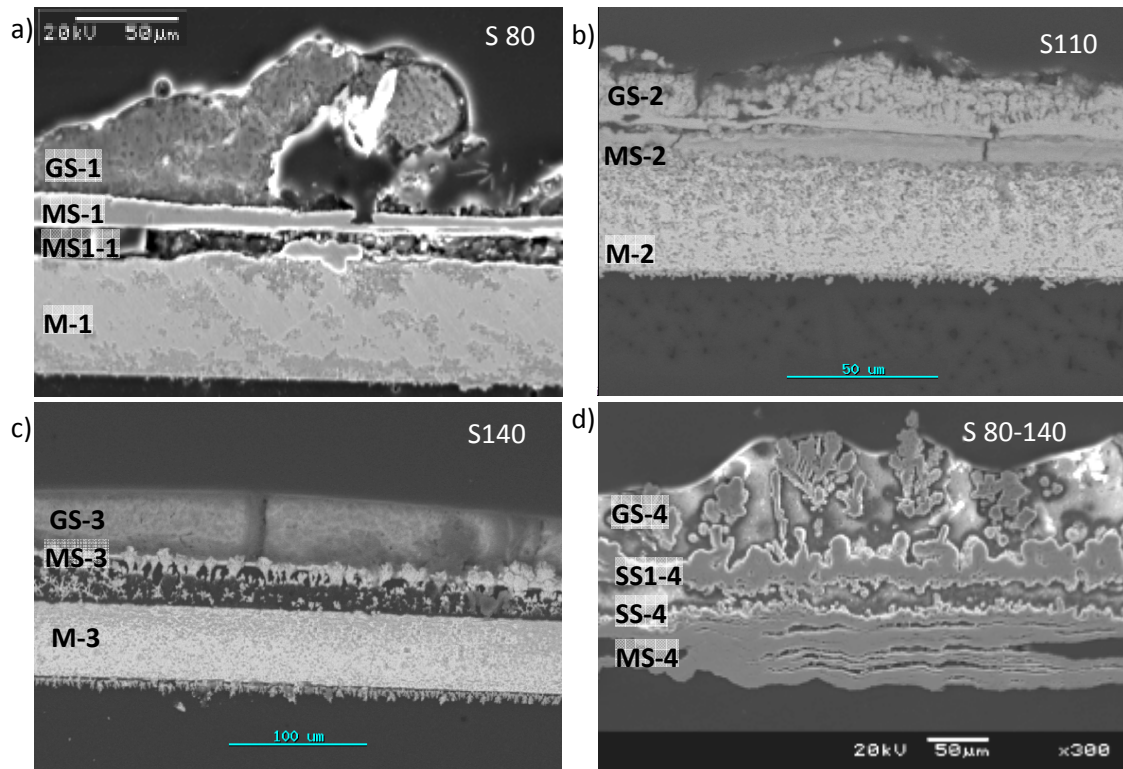
Figure 52: BSE image of the cross-section of the corrosion product formed during sulphidation with S_2 at a)80°C, b)110°C, c)140°C and d)80°C-140°C.

Table 40: EDS area analysis of corrosion layers observed at 80°C

Figure 52a	SEM composition (wt %)		
80°C	**S-K**	**Cu-K**	**Phases**
GS1	99.62	0.77	Sulphur
MS1	33.40	66.60	Covellite
M1	0.66	99.34	Copper

Table 41: XRD analysis of the corrosion product at 80°C

Structure	Stoichiometry	Semi-Quantitative (%)	Phase
Hexagonal	CuS	65	Covellite
Orthorhombic	S_8	35	Sulphur

b) Phase composition and morphology at 110°C

Copper foil was exposed to sulphur vapour to determine the morphology of the corrosion product at 110°C. A black non-adherent corrosion layer was observed at the copper foil surface after exposure. A BSE image of the cross-section of the corrosion product in Figure 52b indicates that two different scales formed during sulphidation at 110°C. A copper-rich thin layer (MS-2) was observed at the metal-scale interface. Meaningful EDS analyses of MS-2 could not be obtained owing to the thickness of this layer; however, the closest stoichiometric phase was yarrowite (Cu_9S_8). The outer layer at the gas-sulphide interface (GS-2) was a thick copper sulphide with a copper-to-sulphur atomic ratio of 1 according to EDS area analysis (Table 42). Covellite (CuS) and digenite (Cu_9S_5) were identified by XRD analysis as major phases. The XRD semi-quantitative analyses are presented in Table 43.

Table 42: EDS area analyses of the corrosion product at 110°C

Figure 52b	SEM composition (wt %)						
110°C	S-K	Cu-K	Ca-K	O-K	Al-K	Si-K	Phase
GS-2	33.84	66.16					Covellite
MS-2*	23.56	70.18	0.15	10.19	0.28	2.71	Yarrowite*
M2	0	100					Copper
*This phase was disregarded since the layer is too thin to be accurately analysed by EDS.							

Table 43: XRD analyses of a corrosion product at 110°C

Phase	Stoichiometry	Semi-Quantitative (%)	Structure
Covellite	CuS	60	Hexagonal
Digenite	Cu_9S_5	40	Rhombohedral

c) Phase composition and morphology at 140°C

Copper foil was exposed to sulphur vapour to determine the morphology of the corrosion product at 140°C. A thick molten deep red layer covered the copper foil surface after exposure of the copper foil to sulphur vapour at 140°C. A BSE image of a cross-section of the corrosion product is shown in Figure 52c. The corrosion product consisted of two layers, an outer layer (GS-3) that consisted of thick molten sulphur, and an inner copper sulphide layer (MS-3). The inner layer was very porous and non-adherent. The sulphide copper-to-sulphur atomic ratio of this layer was determined to be 1.3 (Table 44). Yarrowite, covellite and sulphur were detected by XRD as the major phases in this corrosion product, with digenite as a minor phase (Table 45).

Table 44: EDS area analyses of the copper foil after exposure to sulphur vapour at 140°C

Figure 52c	SEM composition (wt %)		
140°C	**S-K**	**Cu-K**	**Phase**
GS–3	99.12	0.88	Sulphur
*MS–3	28.96	71.04	Yarrowite*
M	7.11	92.56	Copper
*S-3 can be a mixture of covellite and chalcocite			

Table 45: XRD analyses of the copper foil after exposure to sulphur vapour at 140°C

Phase	Stoichiometry	Semi-quantitative (%)	Structure
Yarrowite	Cu_9S_8	64	Hexagonal
Covellite	CuS	20	Hexagonal
Sulphur	S_8	14	Orthorhombic
Digenite	$Cu_{1.95}S$	2	Cubic

d) Phase composition and morphology at varying temperature (80°C to 140°C)

Copper foil was exposed to sulphur vapour where its surface temperature was varied from 80°C to 140°C to examine the effect temperature variation (thermal cycles) may have on the morphology of the corrosion product. A multilayered corrosion product shown in Figure 52d was observed. The corrosion product was non-adherent, and the foil residue detached easily when the sample was taken

off the heat sink. The inner scale (MS-4) in contact with the foil was smooth, dense and uniform but it had cracks parallel to the foil surface. This sulphide layer had a copper-to-sulphur atomic ratio of 1 (Table 46). Adjacent to this sulphide layer was a sulphur layer (SS-4). Another sulphide layer (SS1-4) with minor amounts of chlorine was observed on top of the sulphur layer. This layer had dendrites that grew outward towards the gas interface. These dendrites had an almost similar composition as the sulphide layer, except that the dendrite was slightly higher in chlorine content. At the sulphide gas interface another layer of molten sulphur (GS-4) could be distinguished. Covellite and sulphur were detected by XRD as the major phases in this corrosion product, as summarised in Table 47. The chlorine detected by EDS in the intermediate scale layer (SS1 and dendrites) is associated with the resin and was therefore ignored.

Table 46: EDS area analyses of the corrosion product when copper foil was heated from 80°C to 140°C in the presence of sulphur vapour (wt %)

Figure 52d	SEM composition (wt %)				
80-140	**S-K**	**Cu-K**	**Cl-K**	**Si-K**	**Phase**
GS-4	96.5	3.5			Sulphur
Dendrite	30.36	64.86	4.11	1.36	Covellite
SS1- 4	31.62	65.65	2.73		Covellite
SS – 4	93.13	6.87			Sulphur
MS – 4	33.46	66.54			Covellite

Table 47: XRD analyses of the copper foil after exposure to sulphur vapour at 80°C to140°C (wt %)

Phase	Stoichiometry	Semi-Quantitative (%)	Structure
Covellite	CuS	27	Hexagonal
Sulphur	S_8	73	Orthorhombic

e) Discussion

In the copper–sulphur phase diagram, at temperatures below 507°C, covellite is in equilibrium with pure sulphur at sulphur concentrations above 66 wt% [Vaughan et al. 1978]. Covellite is therefore expected to form at high sulphur concentration and low copper concentrations in the studied temperature range

(80°C to 140°C). However, at copper concentrations above 80 wt% chalcocite is in equilibrium with pure copper. Monoclinic chalcocite is stable below 103.5°C while hexagonal chalcocite is stable between 103.5°C and 435°C. Chalcocite is therefore expected to form at the copper surface. Yarrowite (Cu_9S_8) and annilite ($Cu_{1.75}S$) are sulphide phases which form at low temperatures where copper concentrations range between 66 wt% and 80 wt% [Vaughan et al. 1978]. A layer of yarrowite and annilite may form between the covellite and the chalcocite layers.

Blacknik et al. [2001] observed that when copper is exposed to sulphur above 128°C, an outer layer of $Cu_{1.15}S$ and an inner layer of digenite ($Cu_{1.3}S$ to $Cu_{1.5}S$) form. In contact with pure copper they observed a thin layer of $Cu_{2-x}S$. At temperature ranges of 128°C to 150°C a thin outer layer of $Cu_{1.05}S$ and an inner thicker layer of $Cu_{2-x}S$ were observed near the copper foil surface. These findings are in agreement with the observations listed in Tables 40 to 47 where the bulk of the corrosion product formed at 80°C was covellite, at 110°C a mixture of covellite and a copper-rich sulphide was observed and at 140°C a non-stoichiometric sulphide was observed (MS-3).

Blacknik et al. [2001] explained that the deviation of phases from stoichiometric compositions occurs because these phases are a mixture of different sulphides such as digenite, covellite and yarrowite ($Cu_{1.1}S$). Layer MS-3 (Table 44) may therefore be a mixture of covellite and chalcocite.

The morphology of the corrosion product confirms the transition in phases between 110°C and 140°C from covellite to $Cu_{2-x}S$. This transition may have induced the transition from a high corrosion rate observed at low temperatures to a low corrosion rate observed from 120°C to 140°C. The formation of a porous layer (MS-3) at the metal-scale interface could have also contributed to slow corrosion rate observed at 140°C, this observation was also noted by Bartkowicz et al. [1986] who observed that if a porous layer or a non-adherent layer forms between the metal surface and the outer sulphide layer, the diffusion of copper species to the surface for reaction to proceed is retarded which slows down the overall corrosion rate.

f) Summary: phase composition and morphology of a corrosion product from copper foil exposed to sulphur

Copper foil at different surface temperatures of 80°C, 110°C and 140°C was exposed to sulphur vapour. The morphologies and compositions of the corrosion products differed as the surface temperature of the copper foil changed. Covellite and sulphur were major phases detected on the corrosion product where the copper foil surface temperature was 80°C. The sulphur observed in this corrosion product was powder (loose particles), which resulted from the sulphur vapour deposition. Yarrowite and covellite were detected in the corrosion product where the copper foil surface temperature was 110°C. No sulphur was detected in this sample. A corrosion product produced from the copper foil at a surface temperature of 140°C had yarrowite, sulphur, covellite and a small amount of digenite. The sulphur in this corrosion product was molten. These observations are in agreement with the phases expected at these temperatures, considering the phase relations in the copper-sulphur phase diagram depicted in Figure 2. The phase composition of the corrosion product is therefore a function of temperature.

Sulphur and covellite were the major phases in the corrosion product where the copper foil surface temperature was varied from 80 to 140°C; no digenite was observed. Varying the copper cooler surface temperature from the lower range (80°C) to a higher range (140°C) affects the morphology of the corrosion product, as can be seen in Figure 52. The corrosion product in Figure 52d is different in structure and in composition when compared to the corrosion products that formed respectively at 80°C, 110°C and 140°C (Figure 52 a to c).

7.6.2.2. Sulphidation of copper by sulphur vapour with HCl additions

HCl vapour was added together with the sulphur vapour to determine the effect of HCl on the morphology of the corrosion product. Dark blue powder was observed at the surface of the corrosion product. This powder could not be sampled for analysis since it was present in small amounts. The copper foil residue was perforated. The morphology of the sample is depicted in Figure 53. EDS and XRD analyses are given in Tables 48 and 49.

a) Phase composition and morphology at 140°C

A BSE image of the cross-section of the corrosion product of the copper foil after exposure to S_2 and HCl at 140°C is shown in Figure 53. Only one scale (GS-5) was observed in contact with the foil. This layer was composed of copper and sulphur at an atomic ratio of 1, according to the EDS area analysis (Table 48). No chlorides were detected by SEM (EDS). The remaining metal seemed to have pits, especially on the metal-sulphide scale interface. The analysis of the pitted foil showed small amounts of sulphur in the pits. The XRD analyses are summarised in Table 49 where it can be seen that covellite and sulphur were major phases detected by XRD.

Figure 53: BSE image of the cross- section of the copper foil after exposure to sulphur and HCl vapour at 140°C.

Table 48: EDS area analysis of the copper foil after exposure to sulphur and HCl vapour at 140°C (wt %)

Figure 53	SEM composition (wt%)		
S-HCl 140	**S-K**	**Cu-K**	**Phase**
GS- 5	31.79	68.21	covellite
Pits	16.63	83.37	Copper*
M- 5	3.7	95.99	Copper
Copper*: Copper with sulphur in the pits			

Table 49: XRD analysis of the corrosion product scale after copper foil exposure to sulphur and HCl vapour at 140°C (wt %)

Stoichiometry	Semi-Quantitative (%)	Structure	Phase
CuS	17	Hexagonal	Covellite
S_8	83	Orthorhombic	Sulphur

Reid et al. [2008] exposed copper to atmospheric gases containing HCl, and observed that no copper chloride compounds such as CuCl or atacamite ($Cu_2(OH)_3Cl$) were detected by XRD. A SIMS depth profile performed by Reid depicted that chlorine had penetrated the entire corrosion film without reacting and forming crystalline phases or chemical compounds [Reid et al. 2008]. This observation is in agreement with the results depicted in Figure 53, in which the foil was pitted without any chloride compound formation, as chloride phases were not detected by either EDS or XRD in this study. It could visually be observed that the foil was perforated after the exposure.

Chlorine addition to $S_2(g)$ at 140°C resulted in the formation of covellite, whereas when copper was exposed to a sulphur vapour at 140°C the major phase was yarrowite, i.e. S_2-HCl experiments yielded a corrosion product with lower Cu:S ratio while S_2 experiments yielded corrosion products with a higher Cu:S ratio.

b) Phase composition and morphology at varying temperature (80°C to 140°C)

Copper foil was exposed to S_2 and HCl vapour where temperature was gradually increased from 80°C to 140°C to determine the effect of thermal cycling on the morphology of the corrosion product. A BSE image of the resulting corrosion product is shown in Figure 54. The corrosion product spalled from the foil, therefore the BSE images in Figure 54 depict two corrosion product layers with no foil residue. An outer layer (GS-6) on the gas scale interface consisted of sulphur while an inner layer on the metal surface (MS-6) consisted of covellite with small amounts of chlorine, according to the EDS analysis depicted in Table 50.
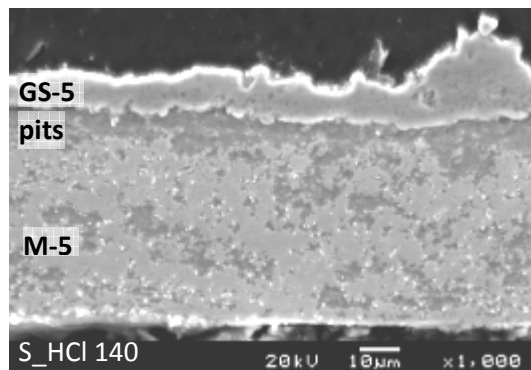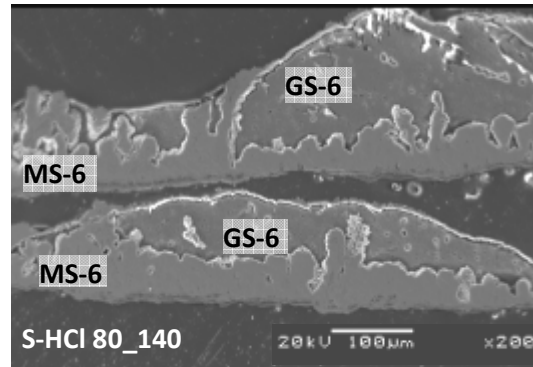
Figure 54: BSE image of the cross-section of the copper foil after exposure to sulphur and HCl vapour at 80-140°C.

Table 50: EDS area analysis of copper foil after exposure to sulphur and HCl vapour at temperatures from 80°C to 140°C

Figure 54	SEM composition (wt %)			
S-HCl 80-140	**S-K**	**Cu-K**	**Cl_K**	**Phase**
GS-6	98.54	1.94		Sulphur
MS-6	30.63	66.35	3.03	Covellite

Covellite and sulphur were major phases detected by XRD when copper foil was exposed to sulphur and HCl vapour at temperatures from 80°C to 140°C. A small amount of tolbachite ($CuCl_2$) was detected but no nantokite (CuCl) was detected by XRD in this corrosion product. The XRD analyses with the semi-quantitative amounts of phases are depicted in Table 51.

Table 51: XRD analysis of copper foil after exposure to sulphur and HCl vapour at 80°C to 140°C

Phase	Stoichiometry	Semi-quantitative (%)	Structure
Covellite	CuS	20	Hexagonal
Sulphur	S_8	75	Orthorhombic
Tolbachite	$CuCl_2$	5	Monoclinic

Covellite and sulphur are the major phases observed when the copper foil has been exposed to sulphur and HCl vapour. The morphology of a corrosion product at varied temperature is slightly different from the product exposed at 140°C in that neither the sulphur nor the copper chloride phase was detected on a sample

at 140°C. A small amount of tolbachite (5 wt%) was detected in the sample exposed at varied temperature (80°C to 140°C).

7.6.2.3. Sulphidation of copper by sulphur vapour with the addition of water vapour

a) Phase composition and morphology at varying temperature (80°C to 140°C)

Water vapour was added with the sulphur vapour to examine the effect of water vapour on the morphology of the corrosion product. The cross-section of the copper foil after exposure to sulphur and water vapour at 140°C is depicted in Figure 55 as a BSE image. Two types of structures were observed, a non-uniform copper-rich sulphide (MS-7) in contact with the foil and the outer scale (GS-7), consisting of dendrites growing outwardly from a thin sulphide base. The compositions of the base layer and the dendrites differ significantly (Table 52).
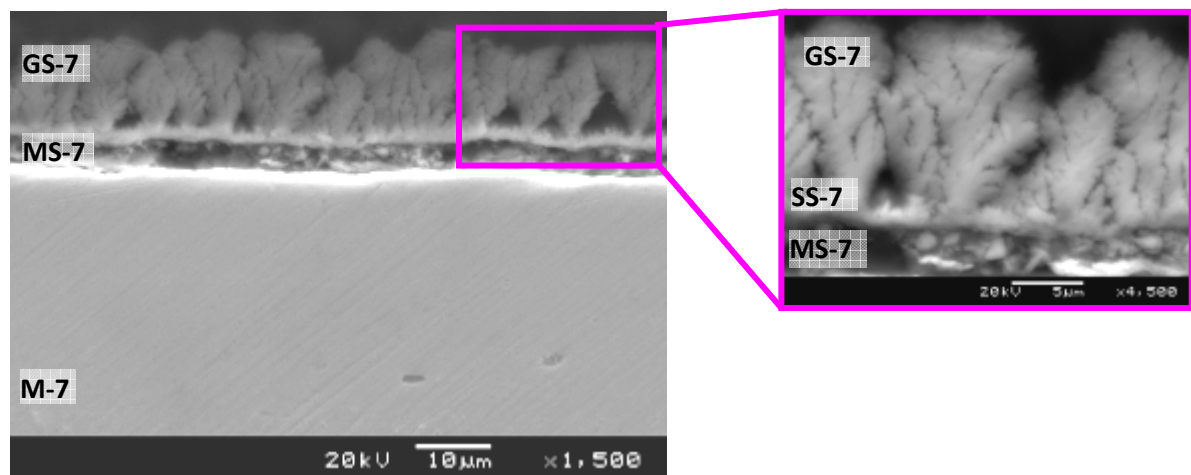
Figure 55: BSE image of the corrosion product produced at 80°C to 140°C with sulphur gas and water vapour.

The oxygen content of all three layers is different, with the top layer having the highest oxygen content. GS-7 seemed to be a mixture of covellite with 13 wt% oxygen. This stoichiometry does not fit any oxide or copper sulphate; it was assumed that it is a mixture of a copper sulphide with copper oxide or a sulphate. The sulphide forming SS-7 also has 4.4 wt% oxygen and a higher copper content. MS-7 is porous and non-uniform, therefore the EDS analysis for this layer may not be accurate and was therefore disregarded.

Table 52: EDS area analysis of copper foil after exposure to S_2 with H_2O additions at 80°C-140°C.

Figure 55	SEM composition (Wt %)				
S-H₂O 80_140	**S-K**	**Cu-K**	**O-K**	**Si-K**	**Ca-K**
GS –7	21.49	65.29	12.77	0.45	
SS –7	19.5	74.93	4.4	1.05	0.17
*MS –7	6.32	81.05	8.05	2.47	1.62
M –7		99.9	0.1		
*Because of the high porosity of this layer (MS-7) the EDS analysis was disregarded.					

Covellite, sulphur alpha and dolerophane ($Cu_2O(SO_4)$) were detected by XRD as major phases in the corrosion product (Table 53). Autoquan method was used to quantify the phase fractions present in this sample. Tezuka et al. [2007] reported that the role of water vapour in sulphidation is to disrupt a passivating sulphide layer whereby the reactant (metal) surface is exposed, allowing sulphidation to proceed. They observed that sulphur detected on the copper surface limits the sites for hydroxyl ions, which are required for the formation of the metal oxide.

Table 53: XRD analysis of copper foil after exposure to sulphur and H_2O vapour at 80°C to 140°C

Phase	Stoichiometry	Autoquan (wt %)
Copper	Cu	11.70
Covellite	CuS	19.50
Dolerophane	$Cu_2O(SO_4)$	6
Paramelaconite	Cu_4O_3	0
Sulphur alpha	S	62.80

Covellite and copper oxysulphate ($Cu_2O.SO_4$) were phases detected after the exposure of copper foil to sulphur and water vapour at 80°C to 140°C.

7.6.2.4. Sulphidation of copper by hydrogen sulphide (H_2S)

Copper was reacted with hydrogen sulphide at 140°C to determine the morphology of the corrosion product. The BSE image depicted in Figure 56 shows the cross-section of the corrosion product formed on the copper foil after exposure. EDS analyses are summarised in Table 54. A summary of XRD analyses is depicted in Table 55.

a) Phase composition and morphology at 140°C

EDS analysis of the thick layer MS-8 depicted a copper-to-sulphur atomic ratio of 2 (Figure 56, Table 54). It was observed that a thin outer layer (GS-8) with the same composition as the bulk of the corrosion layer was flaking off. At the sulphide-foil interface the foil was heavily pitted. The corrosion product was identified by XRD to be a mixture of high chalcocite (Cu_2S) and low chalcocite (Table 55). These analyses are in agreement with the literature observation that chalcocite is the sulphide phase which forms when copper is reacted with hydrogen sulphide.
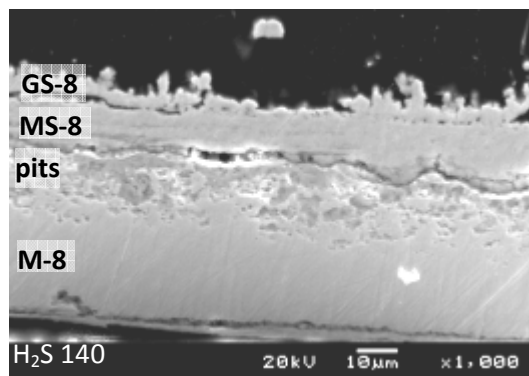
Figure 56: BSE image of the copper foil cross-section after exposure to H_2S at 140°C.

Table 54: EDS area analysis of copper foil after exposure to H_2S at 140°C

Figure 56	Composition (Wt %)			
140°C	**S-K**	**Cu-K**	**stoichiometry**	**Phases**
GS–8	20.79	79.21	Cu_2S	Chalcocite
MS–8	20.15	79.33	Cu_2S	Chalcocite
Pits*	3.87	96.1	*Cu	Copper*
M –8		100	Cu	Copper
*Pits in the copper foil residue with sulphur in the pits				

Table 55: XRD analysis of copper foil corrosion product after exposure to H_2S at 140°C (wt %)

Phase	Stoichiometry	Semi-Quantitative (%)	Structure
High chalcocite	Cu_2S	34	Hexagonal
Low chalcocite	Cu_2S	66	Monoclinic

b) Phase composition and morphology at varying temperature (80°C to 140°C)

Experiments were performed where the temperature was varied from 80°C to 140°C to determine if there is any difference in morphology that is caused by gradual change in temperature. BSE images of a cross-section of copper foil after exposure to H_2S at 80°C to 140°C are depicted in Figure 57 a and b. The images are of corrosion products of the same foil sampled at different positions. The corrosion product consisted of a dense layer of copper sulphide (Figure 57 a) GS-9, with a copper-to-sulphur atomic ratio of 1. This scale easily separated into two layers with an outer thicker layer (GS-9a) and a thinner layer (MS-9) in contact with the copper foil (Figure 57 b). EDS analysis indicated that the copper content of the outer layer (GS-9a) is equal to the composition of the bulk of the corrosion layer (GS-9), while the copper content of the inner layer is higher than that of an outer layer (Table 56). 50.5% low chalcocite (Cu_2S), 24.8% high chalcocite (Cu_2S), 14.9% copper (Cu) and 9.9% covellite (CuS) were the major phases detected by XRD in the corrosion product of copper foil exposed to H_2S at 80°C to 140°C. EDS and XRD analyses are summarised in Tables 56 and 57.

Figure 57: BSE image of the cross-section of the corrosion product produced when copper was exposed to H_2S at 80°C to 140°C. a) and b) are images of the same foil taken at different positions.
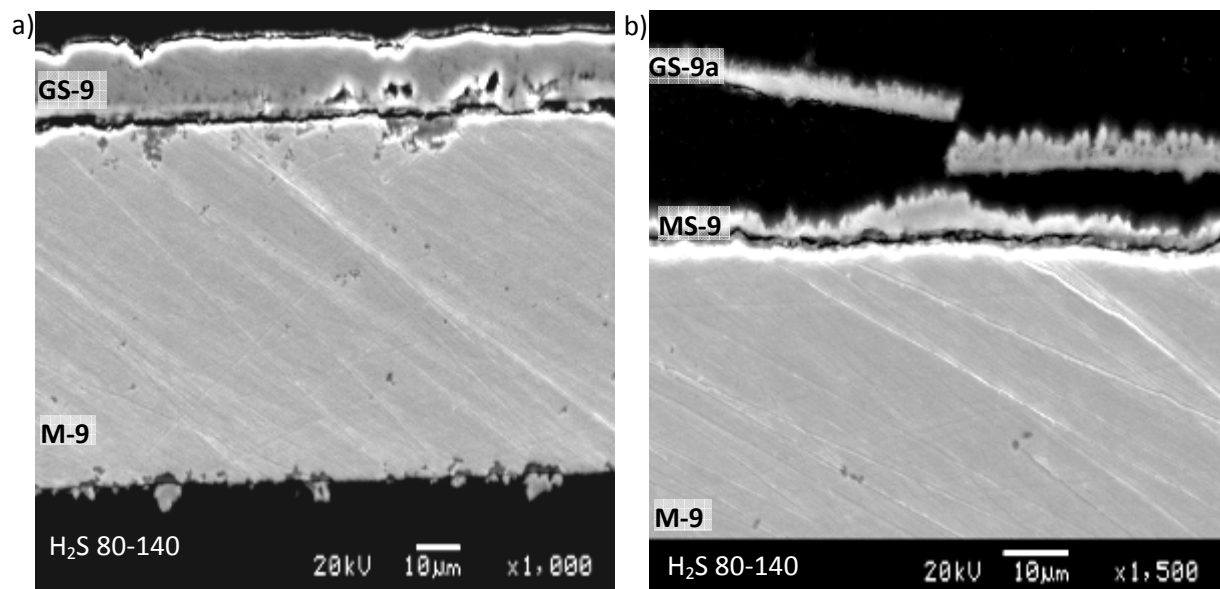
Table 56: EDS area analysis of copper foil after exposure to H₂S at 80°C-140°C

Figure 57	SEM composition (wt %)			
H₂S 80-140	**S-K**	**Cu-K**	**Stoichiometry**	**Phases**
GS –9	32.66	67.34	CuS	Covellite
GS –9a	32.20	67.80	CuS	Covellite
*MS –9	28.94	71.06	Cu₉S₈	Yarrowite
M –9	0	100	Cu	Copper
*Yarrowite weight composition is 69.03% Cu and 30.97% S, the composition of MS-9 is slightly different from the yarrowite composition but yarrowite is the closest sulphide to match this composition.				

Table 57: XRD analyses of a copper foil corrosion product after exposure to H₂S at 80°C to 140°C (wt %)

Phase	**Stoichiometry**	**Semi-quantitative (%)**	**Structure**
Covellite	CuS	9.9	Orthorhombic
Low chalcocite	Cu₂S	50.5	Monoclinic
High chalcocite	Cu₂S	24.8	Hexagonal
Copper	Cu	14.9	Cubic

A coherent chalcocite was the sulphide phase detected by XRD and EDS on the corrosion product formed after exposing copper foil to a hydrogen sulphide gas at 140°C. Covellite was detected by EDS as the major phase in the corrosion layer, which formed when the temperature was varied from 80°C to 140°C with a thin inner layer of yarrowite in contact with the foil. No chalcocite was detected by EDS in this sample (H₂S 80-140), while XRD detected covellite and chalcocite as major phases. The XRD samples were only scanned on the surface of the corrosion product because the powder sample could not be prepared, since the corrosion product was so coherent on the foil it could not be separated from the foil residue. This may cause the discrepancy on the EDS and XRD results.

It has been observed that when the temperature of the copper cooler surface is varied, the resulting corrosion product has a different morphology than when the copper cooler surface is at a constant temperature. Only chalcocite was detected in a copper foil corrosion product after exposure to hydrogen sulphide at 140°C; when the temperature was raised from 80°C to 140°C, a layer of covellite was also detected.

7.6.2.5. Summary: Effect of gas composition on phase composition of the corrosion product

Copper foil samples which were exposed to different gas compositions, such as sulphur gas, sulphur gas + HCl, sulphur gas + H_2O and hydrogen sulphide, depicted different morphologies at the same copper foil surface temperature. This finding indicates that the morphology of the copper corrosion product is a function of a corroding gas composition. Copper foil samples which were exposed to sulphur vapour at different copper foil surface temperatures varied in phase composition. Covellite and sulphur were the major phases when the copper foil surface was operated at 80°C. Covellite and yarrowite were observed when the copper foil surface temperature was 110°C. Yarrowite, digenite and molten sulphur formed after exposure of copper foil to sulphur when the copper foil was at 140°C.

These findings indicate that if the copper cooler surface temperature is below 110°C, covellite and powder sulphur will form in the presence of sulphur in high sulphur concentrations. At a copper surface temperature between 110°C and 140°C there is a transition in sulphide phases from covellite to yarrowite and digenite.

The addition of HCl vapour at a copper foil surface temperature of 140°C changes the phase chemical composition of the corrosion product from yarrowite and digenite to covellite. Tolbachite ($CuCl_2$) was detected as a minor phase in this corrosion product.

Covellite and copper oxysulphate formed when copper foil was exposed to sulphur and water vapour at a copper foil surface temperature of 80°C to 140°C. The addition of water vapour to sulphur vapour at a copper foil surface temperature of 140°C changes the phase chemical composition of the corrosion product from yarrowite and digenite to covellite.

The addition of water vapour and that of HCl have the same effect on the corrosion product's chemical composition in that it yield a corrosion product with less Cu:S atomic ratio 1:1. The chemical composition of the corrosion product formed when copper was exposed to S_2 at 140°C has a higher Cu:S atomic ratio

(1.8:1). This observation implies that the addition of HCl and water vapour in a Cu-S system affects the phase relations in such a system.

High chalcocite and low chalcocite were the major phases formed when copper foil was exposed to a hydrogen sulphide gas at a copper foil surface temperature of 140°C. Varying the copper foil surface temperature from 80°C to 140°C resulted in the formation of low chalcocite, high chalcocite and covellite.

8. SUMMARY AND CONCLUSIONS

8.1. Mag-chrome brick post-mortem sample

The corrosion of copper coolers in PGM smelters was studied through analysis of the post-mortem samples of the PGM smelter refractory wall. It was observed that at the slag/feed interface the mag-chrome brick had completely corroded, leaving a 10cm thick freeze lining in front of the copper cooler. At the slag zone there was some brick left. The samples were therefore collected behind the freeze lining, behind the brick and on top of a copper cooler.

The freeze lining had two textures, a porous cracked hot face and a dense cold face in contact with the copper cooler. The freeze lining consisted of augite, diopside, forsterite and chromite, which constituted the slag. CuCl, element sulphur and a mixture of silicon, calcium and chlorine were detected at the cold face of the freeze lining. Base metal sulphides such as iron sulphide, copper sulphide, digenite, millerite and chalcopyrite were detected as minor phases in this sample. Behind the freeze lining (freeze lining-copper cooler interface) digenite and covellite were major phases detected by XRD. The analysis profile performed by EDS from the freeze lining-copper cooler interface to 20 mm towards the copper cooler revealed that the phase composition of the corrosion product changes with depth towards the copper cooler. Furthest from the cooler was a layer of sulphur with chalcocite-digenite solid solution, nickel sulphide, arsenic sulphide and covellite adjacent to the sulphur, while closest to the cooler were chalcocite, covellite and a non-stoichiometric copper-deficient copper sulphide ($Cu_{1.3}S$). At the mag-chrome brick-copper cooler interface were covellite, elemental sulphur and atacamite in small amounts.

Two wear mechanisms could be identified:

- In one mechanism the copper cooler reacted with base metal sulphides such as nickel sulphide and copper iron sulphide, which infiltrated the porous freeze lining.

Sulphidation of copper coolers in PGM smelters

- The other mechanism involved copper cooler reactions with the furnace gases, such as sulphur and chlorine, which resulted in the formation of covellite, atacamite and nantokite (behind the brick).

8.2. Graphite block post-mortem sample

No significant wear of the graphite block was observed at the slag-feed interface. The depth of infiltration of graphite block by sulphides was higher at the cold face than at the hot face. The hot face of the graphite block had 2mm thick freeze lining which had pentlandite, chalcopyrite, augite, enstatite, forsterite, pyrrhotite and millerite as minor phases. The cold face had copper-rich chalcocite, covellite, digenite and minor amounts of atacamite, chalcanthite and nantokite. G-lid had atacamite, nantokite and chalcanthite as major phase. Nukundamite and chalcopyrite were detected at G-bottom cold face. No element sulphur was observed in any of the graphite samples. The amounts of the corrosion products and matte were less in the graphite block cold face compared to the amount of the corrosion product observed behind the freeze lining when mag-chrome brick was used.The green growth observed after storing the sample for four months has atacamite and chalcanthite as major phases. This observation suggests that the formation of hydrated chloride and copper sulphate species are associated with water vapour, either in the furnace or under atmospheric conditions after sampling. It was concluded that the permeation path for the gases and furnace melt is through the graphite-graphite interface and not through the graphite block itself.

8.3. Base metal sulphides in the post-mortem samples

The base metal sulphides detected behind the freeze lining were also observed in the hot and cold face of the graphite block, although some compounds differed in compositions, e.g. no millerite was observed in the graphite block but pentlandite was observed, which is also a nickel containing sulphide. Significant amounts of element sulphur were detected behind the freeze lining of the mag-chrome post-mortem sample while in the graphite no elemental sulphur but pure copper was observed at the cold face of the graphite block. Andrews [2008] reported that pentlandite $(Fe,Ni)_9S_8$, troilite (FeS), pyrrhotite $(Fe_{1-x}S)$ and copper

iron sulphides are the phases identified in the entrained matte. Similar phases were detected in the graphite block, especially in the hot face. It can be concluded that the base metal sulphides that become entrained in the slag contribute significantly to the amount of matte that penetrates to the cold face of the refractory lining, e.g. graphite.

Corrosion of copper coolers progresses by the gaseous attack by sulphur and chlorine.

8.4. Laboratory sulphidation of copper

The laboratory test work was performed to investigate the conditions under which different copper sulphides form (covellite and digenite). It was confirmed that phase composition in the copper-sulphur system is dependent on the temperature and atmospheric conditions. When copper is exposed to sulphur at 80°C the resulting sulphide is covellite with loose sulphur powder at the gas-sulphide interface if there is excess sulphur. If the copper foil is at 110°C the resulting sulphides are covellite and yarrowite or digenite. At a copper temperature of 140°C yarrowite is a major phase with covellite and molten sulphur forming at the gas-sulphide interface. The addition of HCl and water vapour at a copper foil temperature of 140°C results in the formation of covellite as a major phase and tolbachite ($CuCl_2$) when HCl is added and covellite and dolerophane ($Cu_2O(SO_4)$) when water vapour is added. Corrosion of copper by hydrogen sulphide forms chalcocite (Cu_2S).

It was concluded that in the presence of sulphur a copper cooler at temperatures below 110°C will form covellite and a loose sulphur powder, which was observed in the post-mortem sample behind the mag-chrome brick. In the presence of hydrogen sulphide a copper cooler will react to form chalcocite.

Experiments in which copper foil was exposed to sulphur vapour at different temperatures indicated that the corrosion rate of an annealed copper foil is a function of temperature from 80°C to 110°C. An average corrosion rate of 54 mm/y was observed at 80°C while at 110°C a rate of 80 mm/y was observed. Above 112°C the slope of the corrosion rate dropped to almost zero. This

indicated the effect of the phase transition on a copper-sulphur system coupled with a phase transition from solid to liquid sulphur and formation of a porous layer at the metal-scale interfcae. This observation indicates that if the copper cooler surface temperature is operated between 80°C and 110°C, severe corrosion should be expected in the presence of elemental sulphur.

The addition of chlorine changed the corrosion kinetics below 110°C from linear to parabolic. Above 112°C the corrosion rate kinetics became linear. The addition of HCl vapour in a sulphur vapour corroding gas will enhance the corrosion rate at temperatures above 112°C. The foil residue after exposure to a gas with HCl was perforated which suggest that the presence of HCl introduces pitting corrosion.

The sulphide phases formed during all the experiments exhibited highly non-adherent and friable characteristics except for the chalcocite that formed when the copper foil was exposed to hydrogen sulphide. At long exposure times the sulphide layer cracked exposing new metal surface which resulted in an increase in corrosion rate. The sulphide layer will not protect the copper cooler from further corroding since it is prone to cracking and is non adherent.

9. CONCLUDING REMARKS

The sulphidation of copper coolers in primary PGM smelters has been a major problem since they were used by the platinum industry.

A post-mortem analysis of a mag-chrome lined furnace wall revealed the presence of elemental sulphur, covellite, digenite and base metal sulphides such as iron sulphide, iron nickel sulphide and nickel sulphide. It can be concluded that copper cooler corrosion observed at the slag-feed interface when the mag-chrome brick was used progressed through two wear mechanisms, one mechanism was the reaction of the copper cooler with sulphur which resulted in the formation of covellite, yarrowite and deposition of sulphur as observed on the laboratory test work. The other mechanism identified behind the freeze lining was a copper cooler reaction with the base metal sulphides such as NiS and $(CuFe)_xS$ which infiltrated through the porous freeze lining.

Heat transfer calculations indicate that the copper cooler surface temperature can range from 48.1°C to 109.2°C behind the mag-chrome brick based on a rammable thickness of 1mm to 5mm. When a mag-chrome brick is totally consumed the copper cooler temperature can reach 153.6°C.

The post-mortem analysis performed on a graphite block removed from the same smelter indicated that graphite inhibits the corrosion of copper coolers by limiting the permeation path of the gases and furnace melt from the furnace to the copper cooler surface. The gases and the furnace melt diffuse through the gaps at the graphite-graphite interface, as base metal sulphides were observed at the graphite-graphite interface. Graphite block had no significant wear on the hot face and very low amounts of corrosion products were observed compared to the mag-chrome brick post mortem sample. It is not clear how graphite efficiently minimize the deposition of elemental sulphur at the hot and the cold face but no sulphur was observed in any of the graphite samples.

Increased amounts of the hydrated chloride (atacamite) and sulphate (chalcanthite) phases were observed on the graphite block samples after 4 months of storage. This implies that the formation of hydrated phases take place

under atmospheric conditions (either outside the furnace or inside the furnace after shutdown).

Sulphur vapour is the main gaseous species given off during sulphide smelting under reducing conditions. According to the laboratory tests performed, reaction products between copper and sulphur include covellite and sulphur powder at 80°C, covellite and yarrowite at 110°C and yarrowite, covellite, molten sulphur and digenite at 140°C. Sulphur formed the outer layer followed by covellite and the copper rich sulphide formed adjacent to the copper foil exhibiting high porosity and non adherent properties. Chalcocite forms when copper react with hydrogen sulphide gas. The phase composition of the corrosion product is a function of both the temperature and the corroding gas composition.

The presence of chlorine induces pitting corrosion which was confirmed by the perforation observed on the copper foil residue. Chlorine also reacts with the copper to form CuCl and $CuCl_2$. The addition of water vapour together with S_2 at 140°C changes the morphology of the corrosion product from smooth dense copper rich sulphide to dendrites of covellite and minor amounts of copper oxysulphate.

Corrosion rates ranging from 25mm/y to as high as 80mm/y can be observed when a copper cooler surface is operated respectively between 65°C and 110°C. The corrosion rate decreases significantly above the melting point of sulphur. Sulphidation is a strong effect and can cause severe corrosion even at moderate temperatures. The corrosion rate observed in the laboratory tests matches the corrosion rates observed in the smelter slag-feed interface when the mag-chrome brick was used. The presence of chlorine induces a transition from linear to parabolic rate behaviour below 112°C. Above 112°C the chlorine enhances the corrosion rate significantly.

The corrosion observed in the PGM smelters can occur through the base metal sulphides reacting with copper and also through sulphur which evaporates from the furnace contents through the freeze lining and mag-chrome brick to the copper cooler surface where sulphur gets deposited as powder below 112°C and as molten sulphur above 112°C. The sulphides that form from the reaction of

Sulphidation of copper coolers in PGM smelters

copper and sulphur are friable and non adherent which makes the sulphide prone to cracking and peeling off, exposing the metal surface for further reaction. The corrosion behaviour in short exposure times is linear and cannot be accurately extrapolated to long exposure times, as there are factors that affect corrosion, e.g. scale properties (thickness, adhesion, porosity and physical disruption).

Sulphidation of copper coolers in PGM smelters

10. RECOMMENDATIONS FOR FUTURE WORK

The copper cooler is cast and consists of 97 wt% copper; the copper foil used in this study was 98% annealed. There is a variety of specifications on copper foils, e.g. degree of annealing, purity and oxygen content. It will be worthwhile to perform similar corrosion tests on different foils and compare the corrosion behaviour of foils based on foil purity and treatment.

There was no significant amount of element sulphur in the graphite block, while in the post-mortem refractory sample collected when using refractory mag-chrome bricks, the rammable was covered with element sulphur. Determining the interaction between sulphurous gases and graphite will enhance the understanding of the effect of graphite on copper cooler corrosion.

On the graphite hot face it was mostly matte that remained attached to the graphite, understanding the wettability of the graphite by matte will be beneficial in understanding the interactions between the graphite and the furnace melts.

11. REFERENCES

Andrews, L., Base metal losses to furnace slag during processing of Platinum bearing concentrates, Master's Thesis, University of Pretoria, 2008.

Baker, H., ASM Handbook volume 3, Alloy phase diagrams. ASM International, 1992.

Bale, C.W., Chartrand, P., Degterov, S.A., Eriksson, G., Hack, K., Ben Mahfoud, R., Melancon, J., Pelton, A.D. and Petersen, S., Factsage thermochemical software and databases. *CALPHAD*, 2002, **26(2)**, 189-228.

Bartkowicz, I. and Stoklosa, A., Kinetics of copper sulphidation at temperatures 570K-1123K. *Oxidation of metals*, 1986, **25(5/6)**, 305-319.

Bartkowicz, I. and Stoklosa, A., Kinetics of copper, nickel, cobalt and iron sulfidation by a modified "pellet" method. The effect of reaction at metal/scale interface. *Solid State Ionics*, 1987, **23**, 51-59.

Blachnik, R. and Muller, A., The formation of Cu_2S from the elements II copper used in form of foils. *Thermochimica Acta,* 2001, **366***, 47-59.*

Brooks, S. and Meadowcroft, D.B., The role of chlorine in the corrosion of Mild and low Alloy steels in low pO_2, high pS_2 environments*. High Temperature Corrosion in Energy Systems Proceedings of the Symposium.* 1985*, 515-527.*

Cramer, L.A., The extractive metallurgy of South Africa's platinum ores. *Journal of Metals*, 2001, 14-18.

De Kieviet, A., Gaunguly, S., Dennis, P. and Pieters, T., Monitoring and control of furnace 1 freeze lining at Tasminian electro-metallurgical company. *Proceedings: Tenth International Ferroalloys Congress*; Cape Town, South Africa, 2004, 477 - 487.

Sulphidation of copper coolers in PGM smelters

Fereday, F., Submerged Arc Furnaces. Electric Power Research Institute. Industrial and Agricultural technologies and services, published by Epricentre for materials production, 1996.

Fornasiero, D., Fullston, D., Li, C. and Ralston, J., Separation of enargite and tennantite from non-arsenic copper sulfide minerals by selective oxidation or dissolution. *International Journal of Minerals Processing*, 2001, **61**, 109-119.

Furer, J., Lambertin, L. and Colson, J., Morphological and kinetic study of copper corrosion when covered with digenite sulphide layer in sulphur under covellite formation conditions. *Corrosion Science*, 1977, **17**, 625-632.

Gesmundo, F., Niu, Y., Castello, P., Viani, F., Huntz, A.M. and Wu, W.T.*,* The sulphidation of two-phase Cu-Ag Alloys in H_2-H_2S mixtures at 550-750°C. *Corrosion Science,* 1996, *38(8),* 1295-1317.

Graedel, T.E., Franey, J.P., Kammlott, G.W. and Vandenberg, J.M., The atmospheric sulfidation of copper single crystals. *Journal of Electrochemical Society, Electrochemical Science and Technology,* 1987, **134(7)**, 1632-1635.

Gudyanga, F. P., Mahlangu, T., Chifamba, J. and Simbi, D.J., Reductive decomposition of galena (PbS) using Cr(II) ionic species in an aqueous chloride medium for silver (Ag) recovery. *Minerals Engineering*, 1999, **12(7)**, 787-797.

Haywood, J., Sarvinis, J., Monaghan, A. and Baker, P.W., Intensive sidewall cooling in Hall Heroult cells. *COM light Metals*, 2003, 77-90.

Hopt, M. and Rossouw, E., New opportunities – exhaustive monitored copper coolers for submerged arc furnaces. *The Journal of the Southern African Institute of Mining and Metallurgy*, 2006, **106**, 373 – 378.

Hundermark, R., de Villiers, B. and Ndlovu, J., Process description and short history of Polokwane smelter. Southern African Pyrometallurgy, *The*

Sulphidation of copper coolers in PGM smelters

Southern African Institute of Mining and Metallurgy, Johannesburg, 2006, 35-42.

Jones, R.T., Platinum smelting in South Africa. *South African Journal of Science*, 1999, **95**, 525-534.

Kammlott, G.W., Franey, J.P., Graedel, T.E., Atmospheric sulfidation of copper Alloys. *Journal of Electrochemical Society*, 1984, **131(3)**, 505-511.

Klein, C., Cornelius, S. and Hurlbut, J., Manual of Mineralogy, 21st Edition revised, after James Dana, 1937.

Lambertin, M. and Colson, J., The mechanism and kinetics of central cavity formation during the growth of thick layers of copper sulphides on metal. *Oxidation of metals*, 1973, **7(3)**, 163-171.

Larson, R. S., A physical and mathematical model for the atmospheric sulphidation of copper by hydrogen sulphide. *Journal of Electrochemical Society*, 2002, **149(2)**, B40-B46.

Lenahan, W.C. and Murray-Smith, R. de L., Assay and Analytical Practice in the South African Mining Industry. *The Southern African Institute of Mining and Metallurgy* Monograph series M6.2001, 176-177.

Logue, R., Sirota, D. and Troxtell, K., Deposition rate control during silicon pitaxy. Semiconductor International, 2004.

Loubser, M. and Verryn, S., Combining XRF and XRD analyses and sample preparation to solve mineralogical problems. *South African Journal of Geology*, 2008, **111**, 229-238.

Love, A., Middleman, S. and Hochberg A.K., The dynamics of bubblers as vapor delivery systems. *Journal of Crystal Growth*, 1993, **129**, 119-133.

Mabiza, L., An overview of PGM smelting in Zimbabwe-Zimplats Operations. Southern African Pyrometallurgy, *The Southern African Institute of Mining and Metallurgy*, Johannesburg, 2006, 63-75.

Martinez, A. and Toesca, S., Reactivity of Copper-doped, brass plated steel cords with hydrogen sulphide. *Reactivity of Solids*, 1986, **1**, 263-273.

Marx, F., Shapiro, M., Mitchell, D. and Delport, D., Developments in Copper Cooler Design for Pyrometallurgical Applications. *The Journal of the Southern African Institute of Mining and Metallurgy*, 2007, 677-684.

Matyas, A.G., Francki, R.C., Donaldson, K.M. and Wasmund, B., Application of new technology in the design of high power electric smelting furnaces. *The Proceedings of the International Symposium on Non-Ferrous Pyrometallurgy*: Trace Metals, Furnace Practices and Energy Efficiency, Edmonton, Alberta, 31st: Conference of metallurgists of the metallurgical society of CIM: *Canadian Institute of Mining metallurgy and Petroleum*, Canada, 1993, **86(972)**, 92-99.

Middleman, S., Some problems related to the performance of an evaporator as a vapor delivery system. *Journal of Crystal Growth*, 1991, **114**, 13-21.

Nell, J., Melting of Platinum concentrates in South Africa. VII International Conference on Molten slags fluxes and salts, *The Southern African Institute of Mining and Metallurgy*, 2004, 165-170.

Nelson, L.R., Geldenhuis, J.M.A., Emery, B., de Vries, M., Joiner, K., Sarvinis, J., Stober F.A., Sullivan, R., Voermann, N., Walker, C. and Wasmund, B., Hatch Developments in furnace design in conjunction with smelting plants in Africa. *The Southern African Institute of Mining and Metallurgy*, 2006, 417- 436.

Patnik, P., Handbook of Inorganic Chemicals, McGraw-Hill, 2003.

Perry, R.H., Chilton, C.H. and Kirkpatrick S.D., Perry's Chemical Engineer's Handbook, 4th Edition. McGraw-Hill, 1963, 3-43.

Pistorius, C., Confidential Report, University of Pretoria, 2004.

Pistorius, C., Confidential Report, University of Pretoria, 2006.

Plascencia, G., Utigard T.A. and Jaramillo, D., Extending the life of water-cooled copper cooling fingers for furnace refractories. *Journal of Metals*, 2005, 44-48.

Reid, M., Punch, J., Garfias-Mesias, L.F., Shannon, K., Belochapkine, S. and Tanner, D.A., Study of mixed flowing gas exposure of copper. *Journal of the Electrochemical Society*, 2008, **155(4)**, C147- C153.

Sarvinis, J., de Vries, S., Joiner, K., van Mierlo, C., Voermann, N., Stober, F., Rule, C. and Majoko, P., Improvements to BHP Hartley Platinum's smelting furnace. Copper 99 - Cobre 99; Fourth International Conference; Phoenix, AZ; USA; 1999, 613-628.

Schacht, C.A., Ed.: *Refractories Handbook.* Marcel Dekker, Inc, 2004, 42-47.

Schuster, C. E., Vangel, M.G. and Schafft, H.A., Improved estimation of the resistivity of pure copper and electrical determination of thin copper film dimensions. *Micro Electronics Reliability*, 2001, **41**, 239-252.

Sesselmann, W. and Chuang, T.J., The interaction of chlorine with copper II bulk diffusion. *Surface Science*, 1986, **176**, 67-90.

Steinhogl, W., Schindler, G., Steinlesberger, G., Training, M. and Engelhardt, M., Comprehensive study of the resistivity of copper wires lateral dimensions of 100nm and smaller. Journal of Applied Physics, 2005, **97**, 023706-1 to 023706-2.

Swinbourne, D. R. and Harris, B., Kinetics of copper(I)sulphide chlorination. *Institution of Mining and Metallurgy transaction C*, 1979, **88**, 93-98.

Tezuka, K. T., Sheets, W.C., Kurihara, R., Shan, Y. J., Imoto, H., Marks, T. J. and Poeppelmeier, K. R., Synthesis of covellite (CuS) from the Elements. *Solid State Science,* 2007, **9**, 95-99.

Sulphidation of copper coolers in PGM smelters

Tran, T.T.M., Fiaud, C. and Sutter, E.M.M., Oxide and sulphide layers on copper exposed to H_2S containing moist air. *Corrosion Science,* 2005, **47**, 1724-1737.

Tran, T.T.M., Fiaud, C. and Villanova, A., The atmospheric corrosion of copper by hydrogen sulphide in underground conditions. *Corrosion Science,* 2003, **45**, 2787-2802*.*

Uchechukwu, V.A., Protection of copper coolers. Graduate Department of Metallurgy and Materials Science, Master's Thesis, University of Toronto, 2000.

Van Manen, P.K., Furnace Energy efficiency at Polokwane smelter. Third international platinum conference 'platinum in transformation', *The Southern African Institute of Mining and Metallurgy*, 2008, 191-196.

Vaughan, D. J. and Craig, J. R., Mineral chemistry of metal sulfides. Cambridge University, 1978.

Verlag, S. Slag Atlas, 2nd Edition. Communications, 1995, 593-599.

Verscheure, K., Kyllo, A.K., Filzwieser, A., Blanpain, B. and Wollants, P., Furnace cooling technology in pyrometallurgical processes. Sohn International Symposium: *Advanced Processing of Metals and Materials*, - New Improved and Existing Technologies: non Ferrous Materials Extraction and Processing, TMS (The Minerals, Metals & Materials Society), 2006, **4**, 139-154.

Voermann, N., Ham, F., Merry, J., Veenstra, R. and Hutchinson, K., Furnace cooling design for modern high-intensity pyrometallurgical processes. Copper 99-Cobre 99 Volume V: Smelting Operations and Advances, International conference, Phoenix Arizona, 1999, 573-582.

Vracar, R. Z. and Cerovic, K.P., Thermodynamic analysis of copper (I) sulphide chlorination by calcium chloride in the presence of oxygen. *Journal of the Serbian Chemical Society*, 1999, **64(5-6)**, 365-374.

Woollacott, L.C. and Eric, R.H., Mineral and Metal Extraction an Overview. *The Southern African Institute of Mining and Metallurgy*, 1994.

Sulphidation of copper coolers in PGM smelters

12. APPENDIX

Appendix A: Data sheets of the refractory brick and rammable material and XRF analyses of the plant (post mortem) sample.

Table A 1: Chemical composition of chemically bonded Chrome-Alumina ramming refractory material as reported in data sheet from the supplier

Compound	SiO_2	$Al_2O_3+P_2O_5$	Fe_2O_3	TiO_2	CaO+MgO	K_2O+Na_2O	Cr_2O_3
%	1.0	68.3	0.2	0.1	0.2	0.2	30.0

PCE Orton Cone	+34	
Maximum Service Temperature	1750	°C
Maximum Particle Size	5,6	mm
Dry Shrinkage	0,1	%
Mass Required	3240	kg/m^3
Bulk Density	3150	kg/m^3
Dried @ 110°C	2920	kg/m^3
Fired to 1000°C		
Cold Crushing Strength	40,0	MPa
Dried @ 110°C	60,0	MPa
Fired to 1500°C		
Moisture Content	5,5	%
Permanent Linear Change	-0,2	%
Fired to 1000°C		
Thermal Conductivity @ 1000°C	1,4	W/mK
Workability	20,0	%

Table A 2: Chemical composition of Magnesia-chrome brick as reported in Data sheet from the supplier

Compound	MgO	Cr_2O_3	Fe_2O_3	Al_2O_3	CaO	SiO_2
%	57,0	23,0	12,0	6,5	0,6	0,5

Physical	data					
Bulk	density	3,34		g/cm³	EN	993-1
Apparent	porosity	14,0		vol%	EN	993-1
Cold	crushing	strength		80,0	N/mm²	EN	993-5
Thermal	conductivity	(500°C)		3,10	W/mK	DR.	KLASSE
Thermal	conductivity	(750°C)		2,90	W/mK	DR.	KLASSE
Thermal	conductivity	(1000°C)		2,80	W/mK	DR.	KLASSE
Thermal	conductivity	(1200°C)		2,80	W/mK	DR.	KLASSE
lin.	thermal	expansion	(500°C)	0,41	%	-
lin.	thermal	expansion	(750°C)	0,65	%	-
lin.	thermal	expansion(1000°C)	0,90	%	-
lin.	thermal	expansion(1200°C)	1,20	%	-
lin.	thermal	expansion(1400°C)	1,47	%	-

Description
Magnesia-chromite brick with fused MgCr grain, high fired, very good hot strength and corrosion resistance

The freeze lining samples were ground to <75m in a Tungsten Carbide milling vessel, roasted at 1000ºC to determine Loss On Ignition value and after adding 1g sample to 9g Li2B4O7 fused into a glass bead. Major element analyses were executed on the fused bead using the ARL9400XP+ spectrometer. Another aliquot of the sample was pressed in a powder briquette for trace element analyses.

Table A 3: XRF analysis of the Freeze Lining (front, middle and back face)

	*FLA (hot face)	*FLA (middle)	*FLA (cold face)	**FLB (hot face)	**FLB (cold face)
SiO_2	39.76	37.84	34.83	38.45	31.18
TiO_2	0.37	0.26	0.23	0.26	0.24
Al_2O_3	3.95	5.02	14.48	4.17	16.64
Fe_2O_3	20.83	17.03	13.22	20.85	11.86
MnO	0.23	0.26	0.21	0.19	0.14
MgO	16.71	16.26	12.91	14.95	11.46
CaO	6.29	8.78	7.07	7.19	6.80
Na_2O	0.00	0.00	0.00	0.00	0.00
K_2O	0.00	0.20	0.00	0.00	0.00
P_2O_5	0.00	0.00	0.00	0.00	0.17
Cr_2O_3	3.76	5.28	9.23	5.07	10.53
NiO	3.01	2.52	1.17	2.88	1.05
V_2O_5	0.00	0.00	0.00	0.00	0.00
ZrO_2	0.00	0.00	0.00	0.00	0.00
SO_3	0.44	0.46	0.46	0.53	0.43
Cl	0.03	0.54	0.27	0.51	0.41
CuO	1.79	1.42	3.34	1.69	5.13
ZnO	0.06	0.00	0.04	0.32	0.06
LOI	2.29	3.32	3.32	1.77	3.43
Total	99.52	99.19	100.8	98.83	99.52

Two different freeze lining samples were submitted for analysis, Freeze Lining A (FLA) and Freeze Lining B (FLB).
*FLA was divided into 3 portions (hot, middle and cold) face.
**FLB was divided into two portions (hot face and cold face). An average of FLA and FLB was used in the text.

The refractory post-mortem samples were prepared as pressed powder briquettes and introduced to the ARL 9400XP+ XRF spectrometer. Analyses were executed using the UniQuant software. The software analyse for all elements in the periodic table between Na and U, but only elements found above the detection limits were reported. The values were normalised, as no LOI was done to determine crystal water and oxidation state changes. All elements were expressed as oxides, except for Zn, Fe, Pb, Mn, Cu and Cd that are usually associated with S as sulphides.

Table A 4: XRF analyses of the plant samples

	StdErr	*FBC	**TBC (Blue)	**TBC (white)	**TBC (Black)	#FLC
S	0.194	6.45	0.00	0.00	0.00	20.36
SO_3	0.330	20.16	42.79	41.57	39.92	0.00
CaO	0.045	0.12	0.05	0.14	0.03	0.07
MgO	0.077	0	0.83	0.00	0.15	0.00
SiO_2	0.154	1.13	1.68	0.90	0.28	0.66
Fe	0.097	0.22	0.99	0.32	0.15	3.40
Pb	0.000	0.01	0.00	0.00	0.00	0.12
Mn	0.000	0.01	0.02	0.00	0.01	0.02
Al_2O_3	0.150	21.80	1.55	13.45	2.15	17.80
Cu	0.173	27.60	36.78	32.92	42.74	35.00
K_2O	0.000	0.02	0.11	0.05	0.16	0.02
Cl	0.063	2.89	0.76	1.27	2.79	2.40
P_2O_5	0.000	0.02	0.03	0.14	0.02	0.11
TiO_2	0.009	0.03	0.06	0.61	0.02	0.03
V_2O_5	0.009		0.02	0.00	0.00	0.00
NiO	0.018	0.07	0.03	0.03	0.00	1.28
Cr_2O_3	0.091	12.01	4.52	0.03	0.68	6.62
As_2O_3	0.010	0.18	0.00	0.00	0.00	0.74
Tl_2O_3	0.009	0.02	0.00	0.00	0.00	0.42
TeO_2	0.001	0.08	0.00	0.00	0.00	0.24
Total before normalisation:		95.40%	93.40%	92.10%	94.40%	98.40%

*FBC: sample collected between the front brick and the cooler
**TBC: sample collected between the top brick and the cooler
#FLC: sample collected between the freeze lining and the cooler

UNIVERSITEIT VAN PRETORIA
UNIVERSITY OF PRETORIA
YUNIBESITHI YA PRETORIA Sulphidation of copper coolers in PGM smelters

Appendix B: XRD scans of all the plant samples (corrosion products), graphite samples and the copper foil samples.
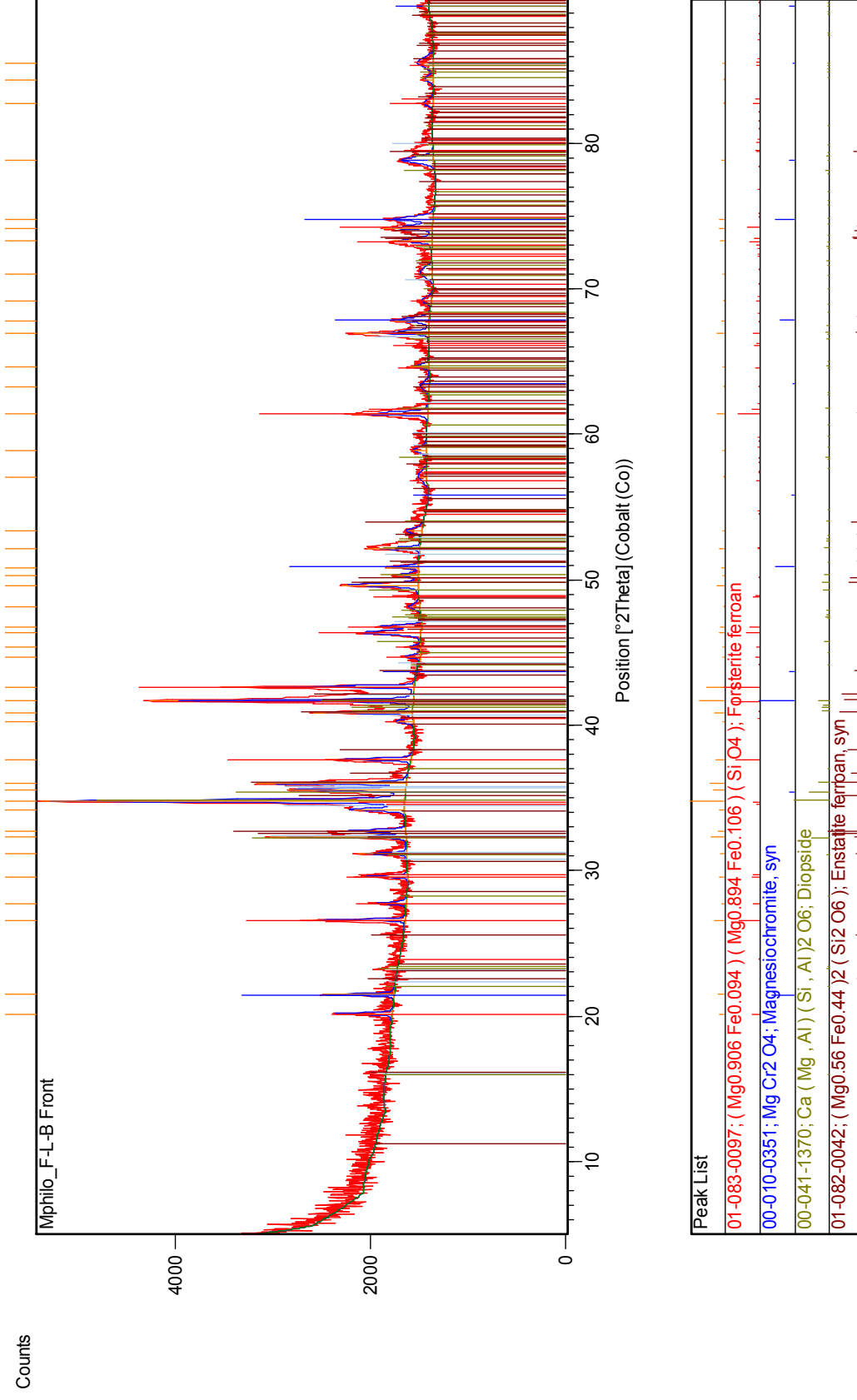
Figure B 1: XRD scan of the freeze lining front (hot face).

Sulphidation of copper coolers in PGM smelters
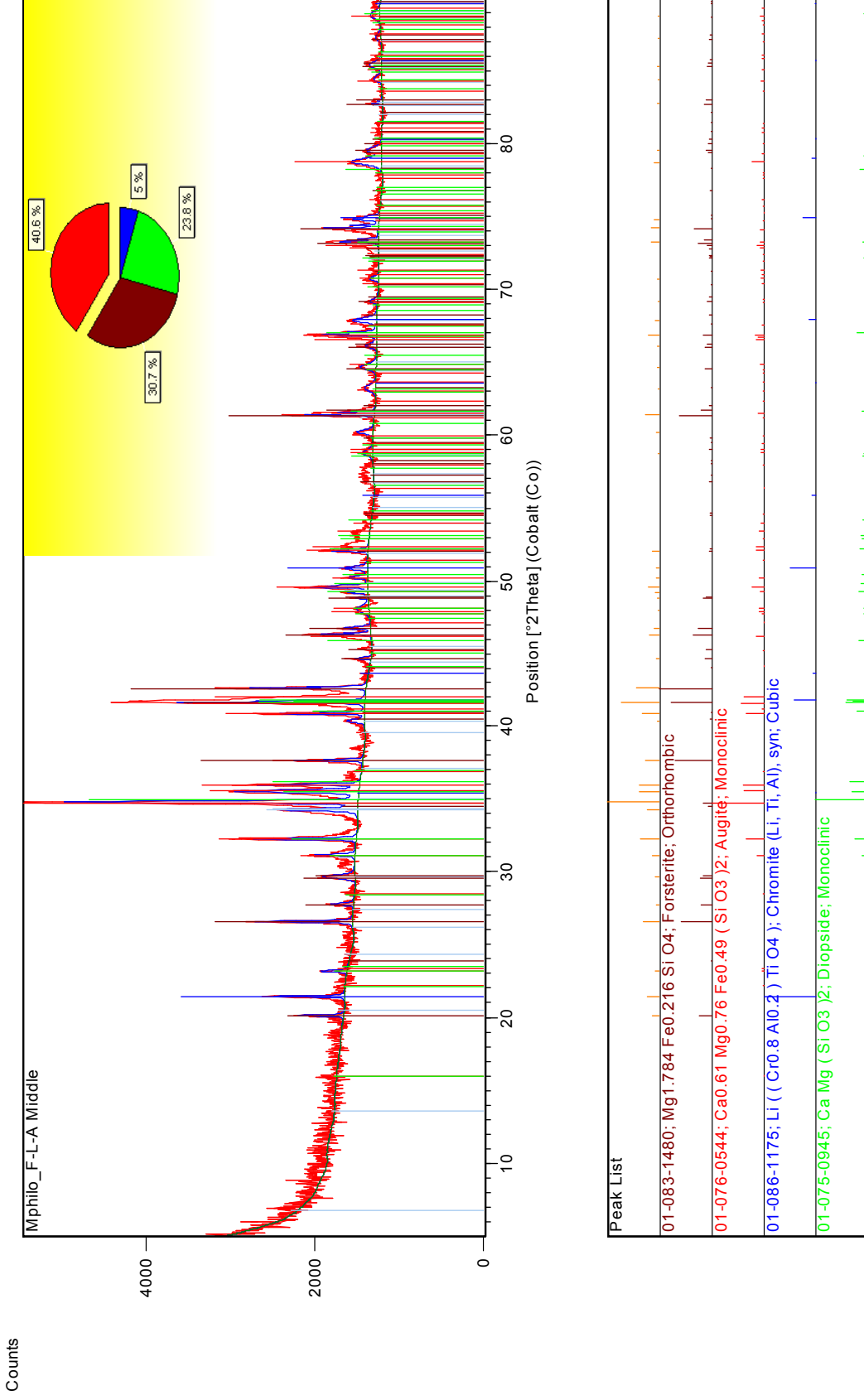
Figure B 2: XRD scan of the freeze lining middle.

Sulphidation of copper coolers in PGM smelters
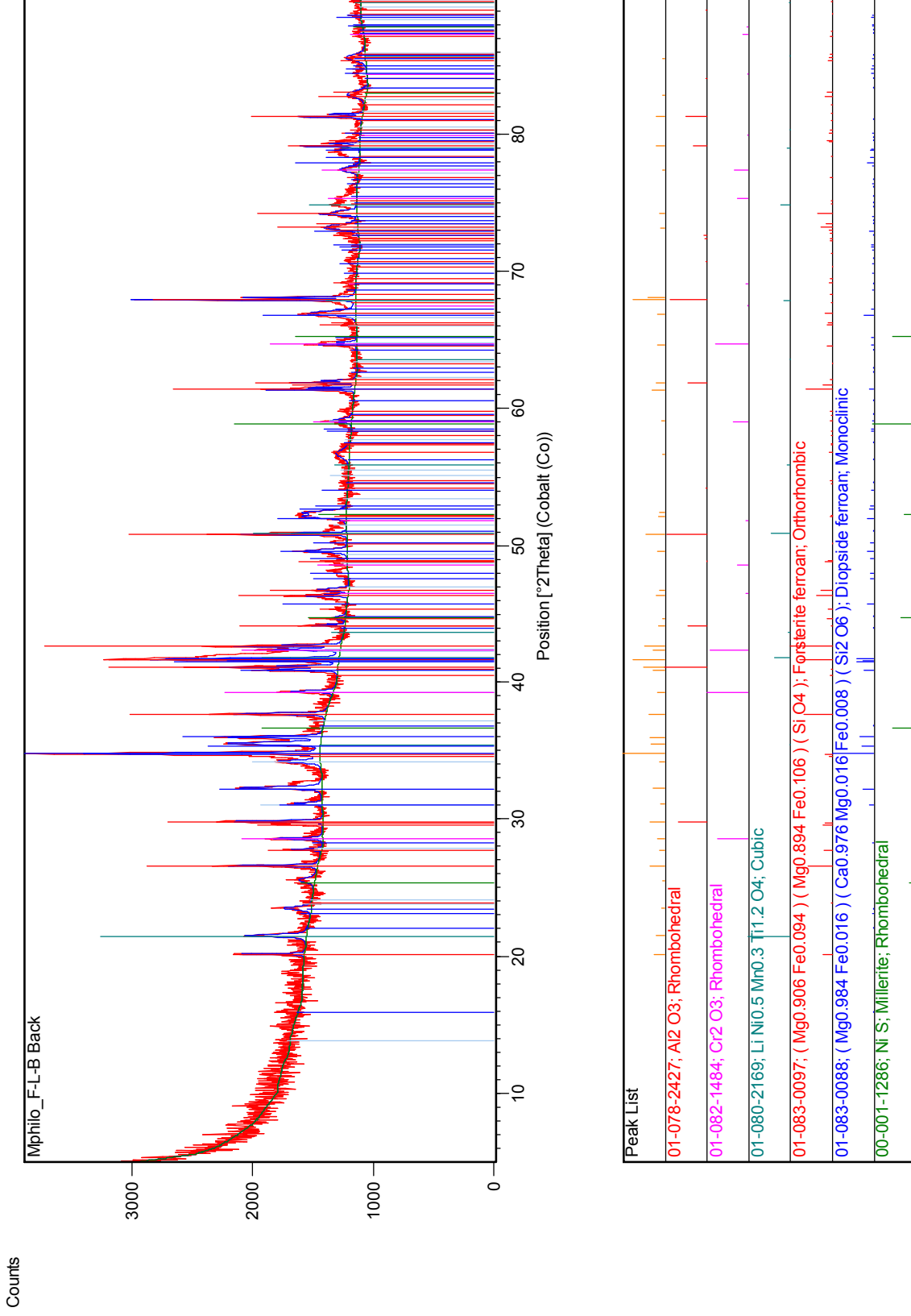
Figure B 3: XRD scan of the freeze lining back (cold) face.
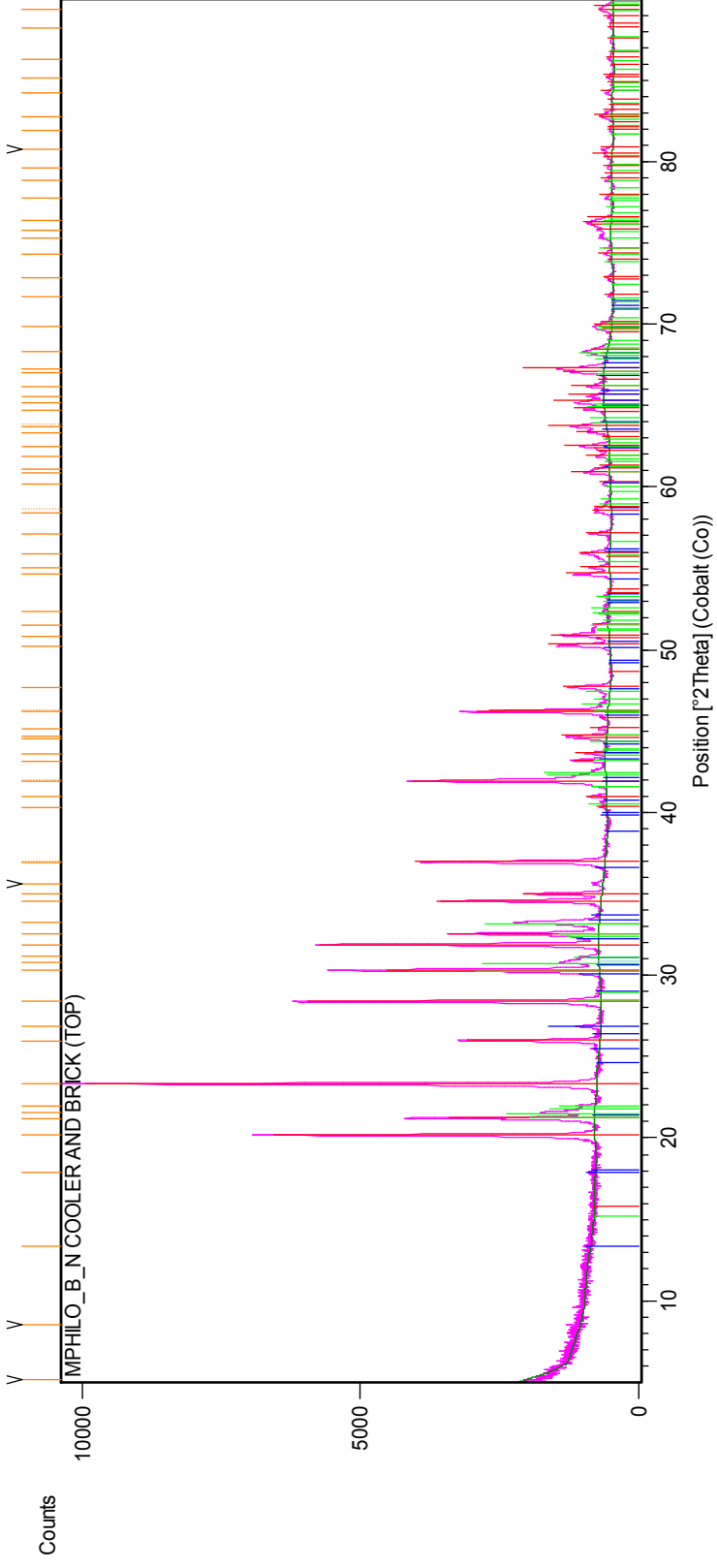
Sulphidation of copper coolers in PGM smelters

Figure B 4: XRD scan of the corrosion product collected between the top brick and the cooler.

Sulphidation of copper coolers in PGM smelters

UNIVERSITEIT VAN PRETORIA
UNIVERSITY OF PRETORIA
YUNIBESITHI YA PRETORIA
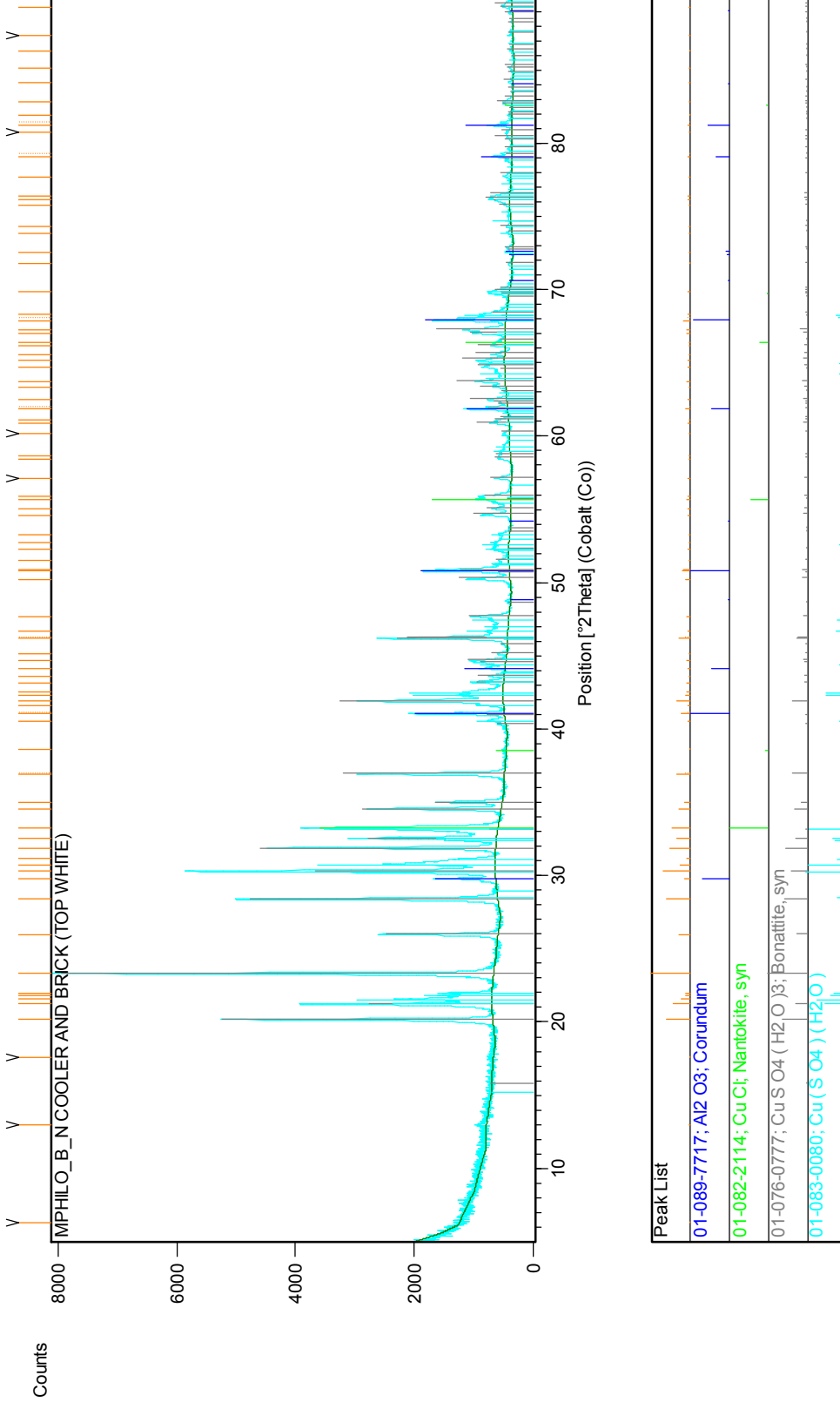
Figure B 5: XRD scan of the corrosion product collected between the top brick and the cooler (white).

Sulphidation of copper coolers in PGM smelters
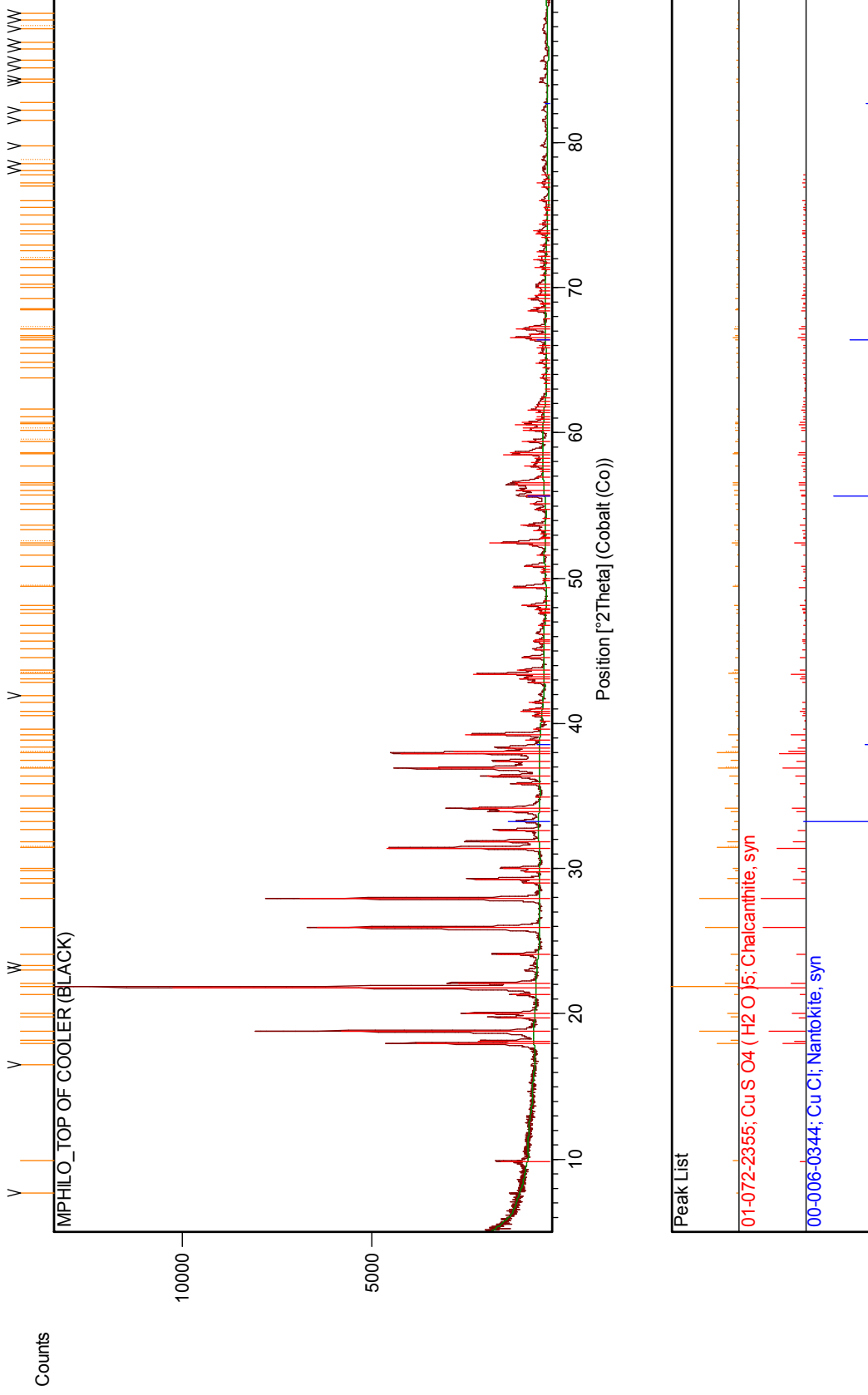
Figure B 6: XRD scan of the corrosion product collected between the top brick and the cooler (black).

Sulphidation of copper coolers in PGM smelters
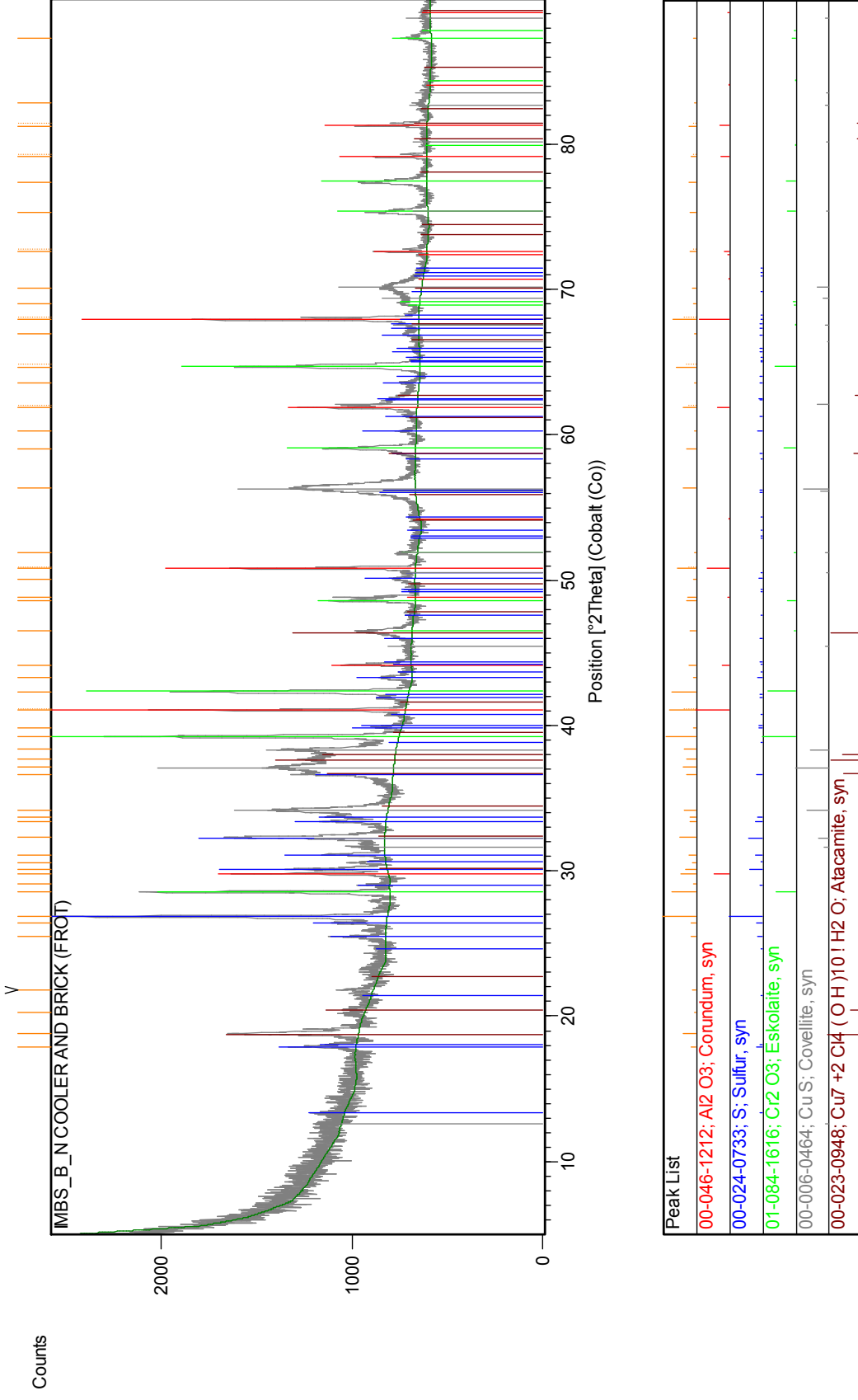
Figure B 7: XRD scan of the corrosion product collected between the front brick and the cooler.

Sulphidation of copper coolers in PGM smelters
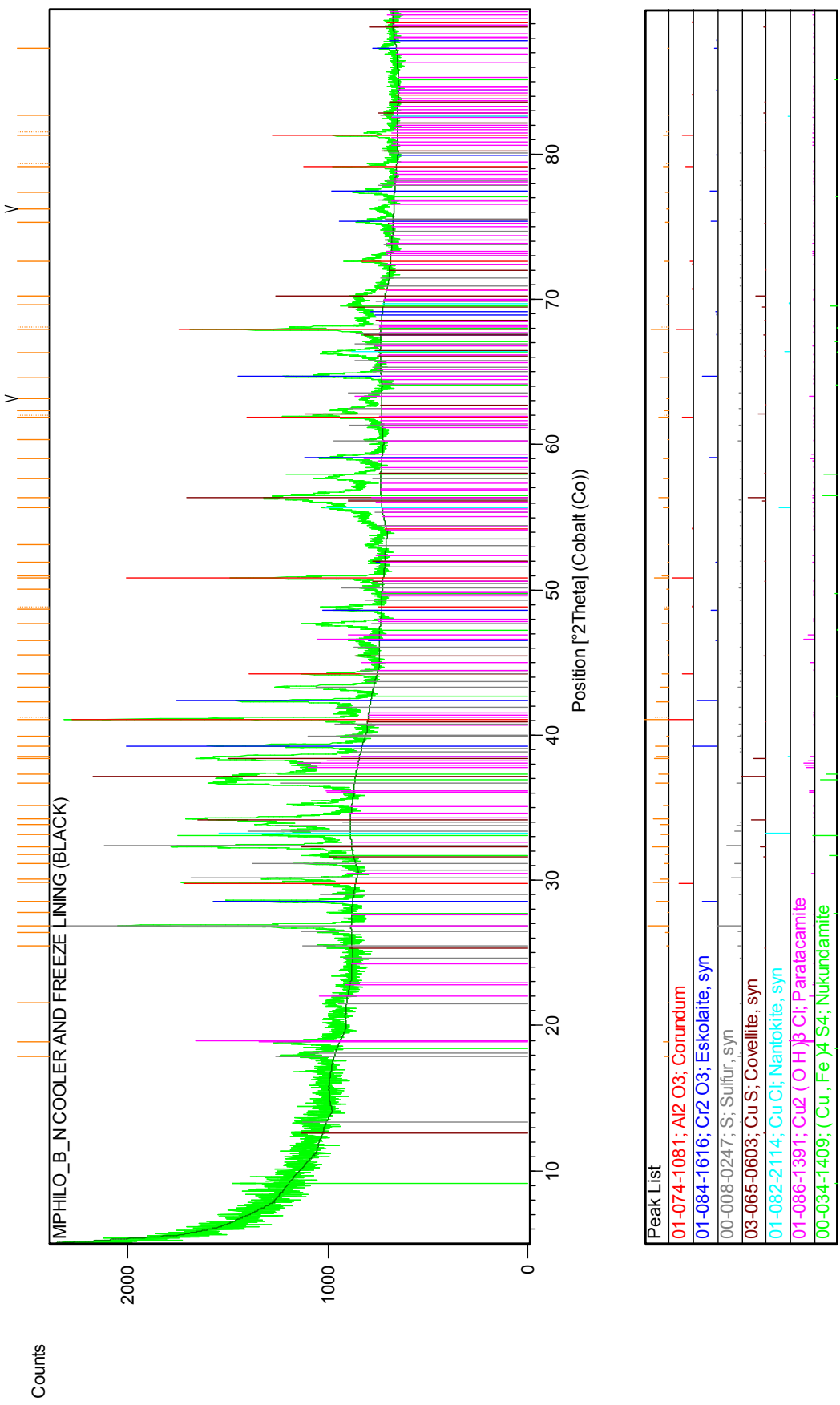
Figure B 8: XRD scan of the corrosion product collected between the freeze lining and the cooler (black).

Sulphidation of copper coolers in PGM smelters
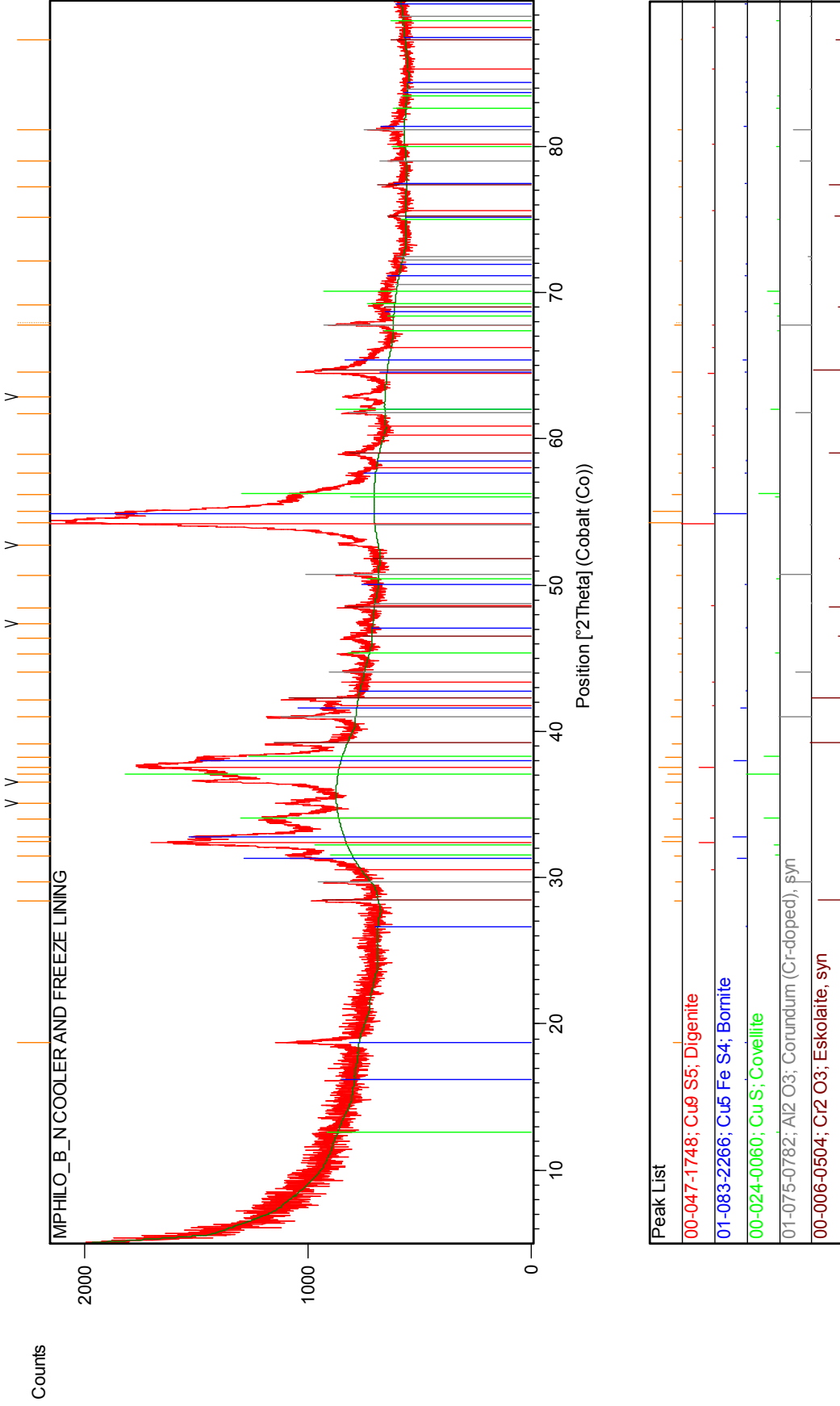
Figure B 9: XRD scan of the corrosion product collected between the freeze lining and the cooler (composite).

Sulphidation of copper coolers in PGM smelters

Figures B10 to B24 depict the XRD scans of the post mortem samples of the graphite block.
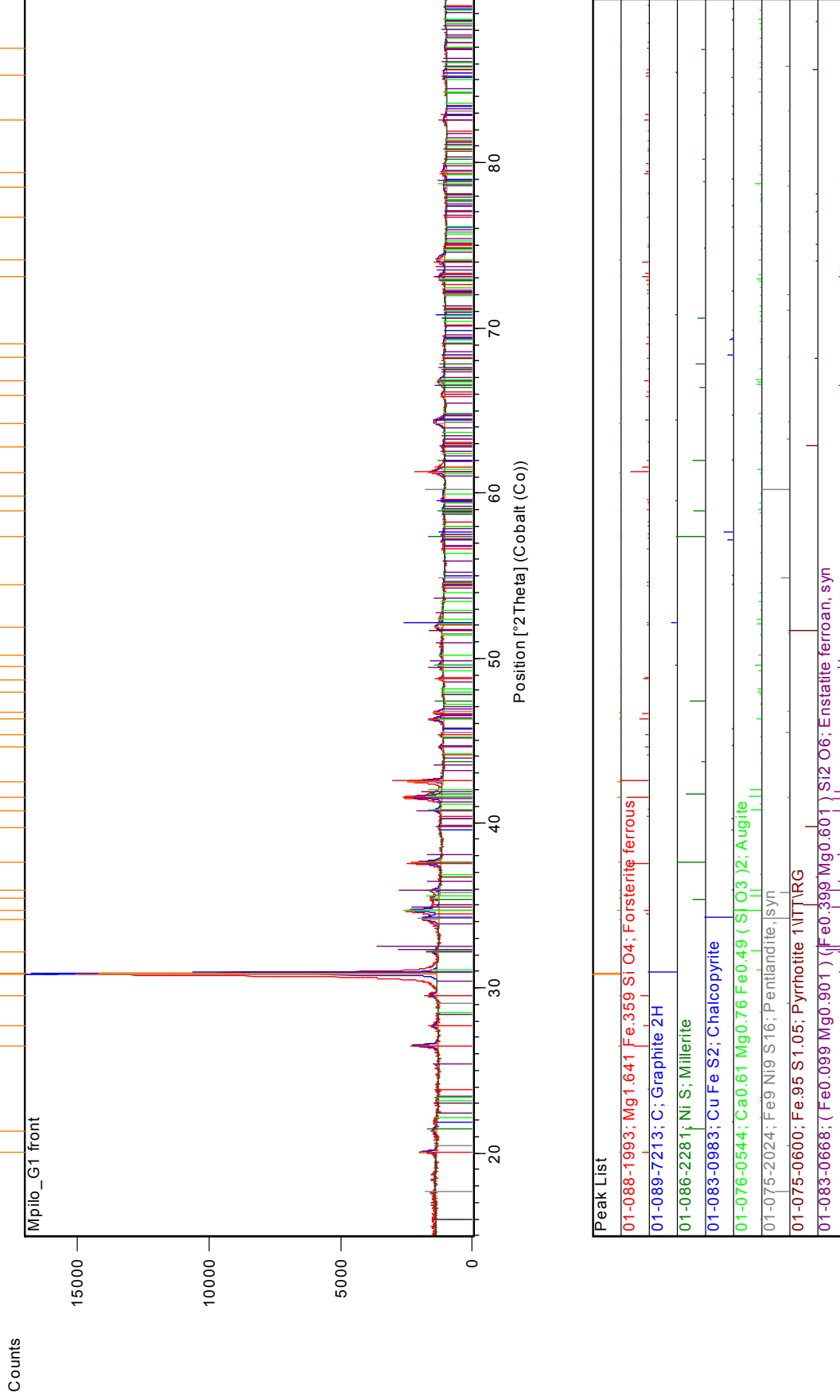
Figure B 10: XRD scan of sample G1 front.
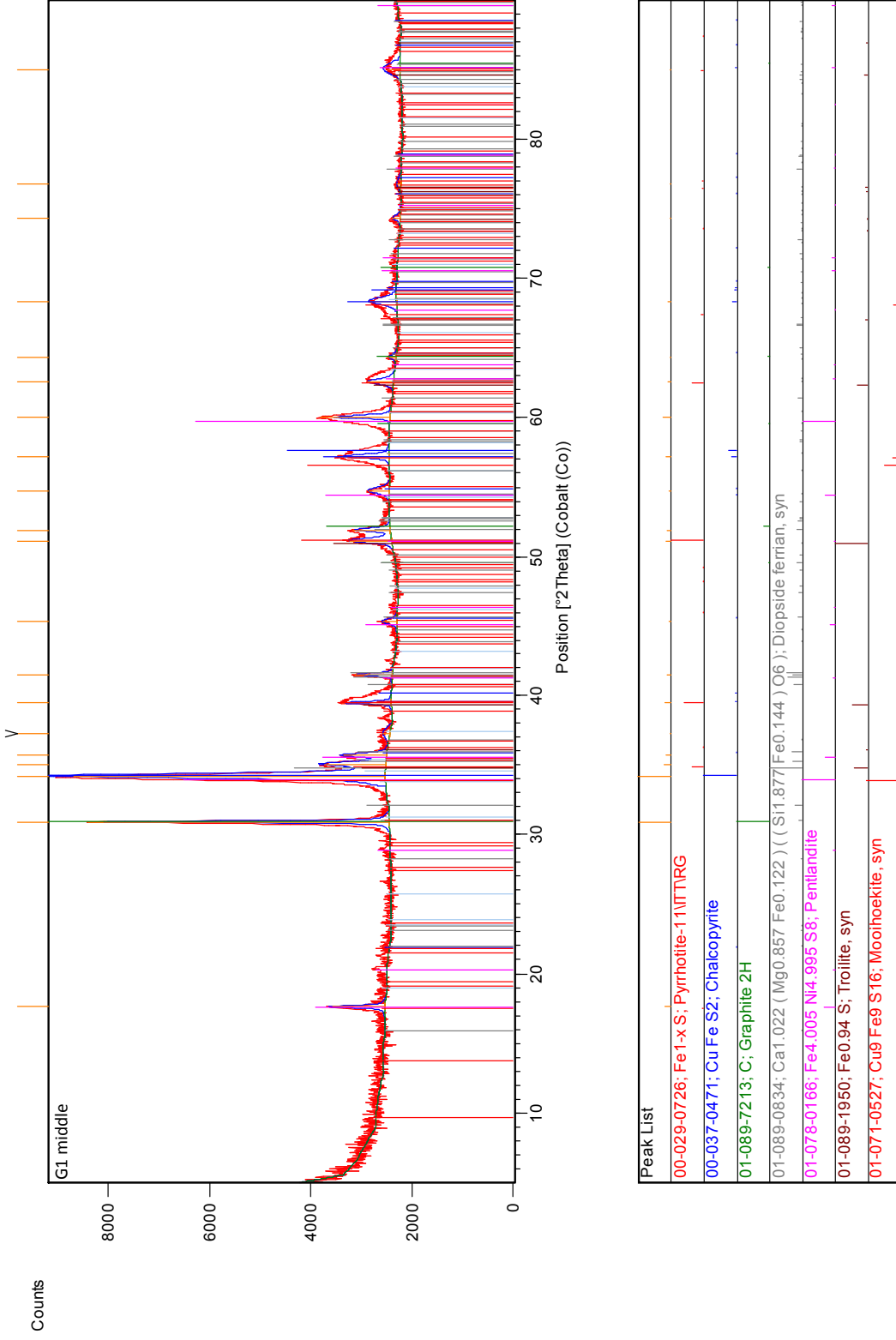
Figure B 11: XRD scan of sample G1 middle.

Mpilo_G1 back

Counts

Position [°2Theta] (Cobalt (Co))

Peak List

01-085-1326; Cu; Copper
00-011-0646; Cu+2 S O4 !5 H2 O; Chalcanthite, syn
01-089-7213; C; Graphite 2H
01-082-2114; Cu Cl; Nantokite, syn
01-083-1462; Cu2 S; Chalcocite
01-088-2158; Cu9 S5; Digenite
01-077-0116; Cu Cl2 (Cu (O H)2)3; Atacamite
01-072-0617; Cu7 S4; Anilite
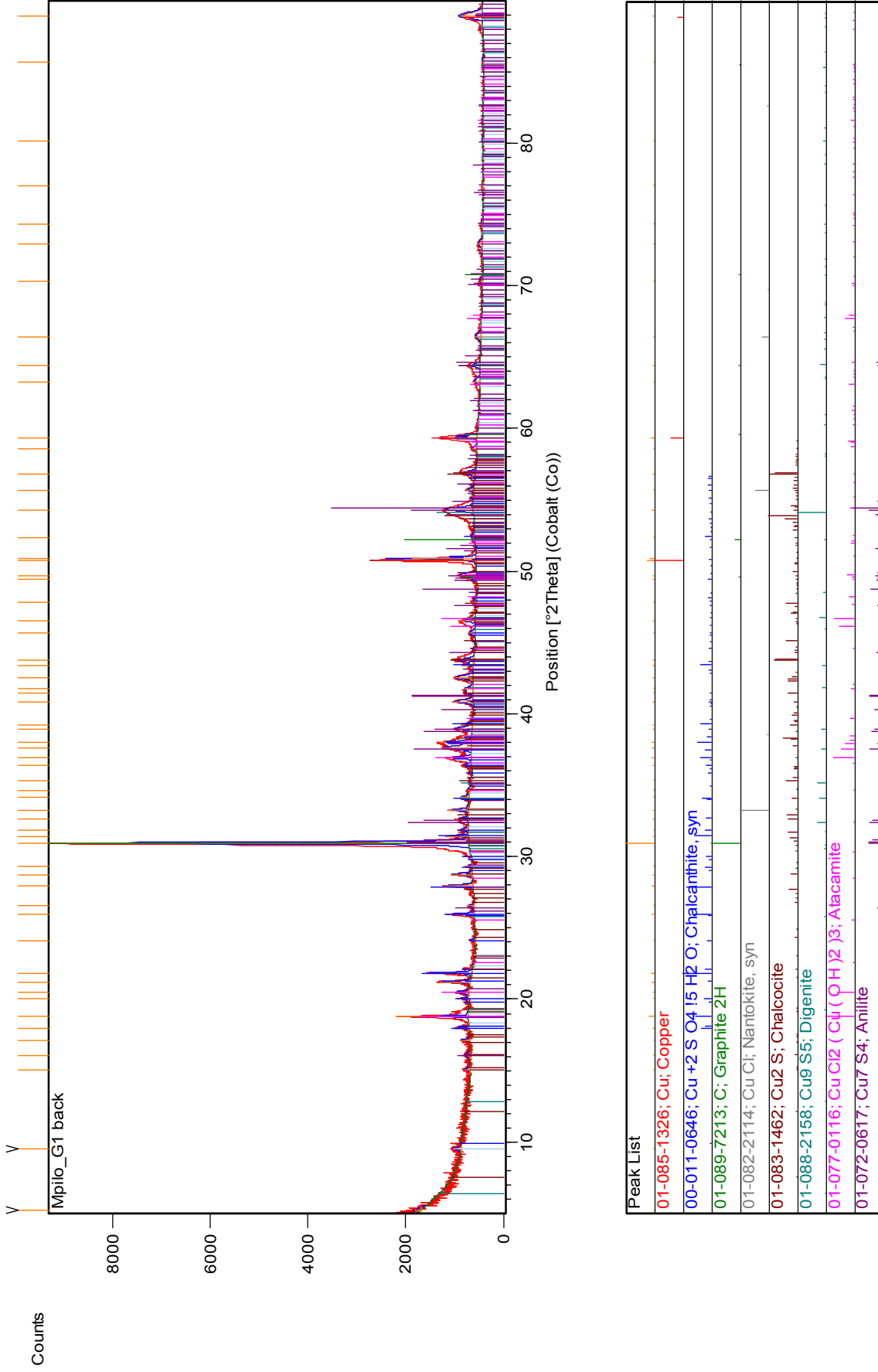
Figure B 12: XRD scan of sample G1 back.

UNIVERSITEIT VAN PRETORIA
UNIVERSITY OF PRETORIA
YUNIBESITHI YA PRETORIA   Sulphidation of copper coolers in PGM smelters

G-1 green

Peak List

00-023-0948; Cu7 +2 Cl4 (O H)10 ! H2 O; Atacamite, syn

01-072-2355; Cu S O4 (H2 O)5; Chalcanthite, syn

01-089-7213; C; Graphite 2H

01-077-2383; Cu Cl; Nantokite, syn

01-071-2288; Cu Cl2 (H2 O)2; Eriochalcite, syn

Counts

Position [°2Theta] (Cobalt (Co))
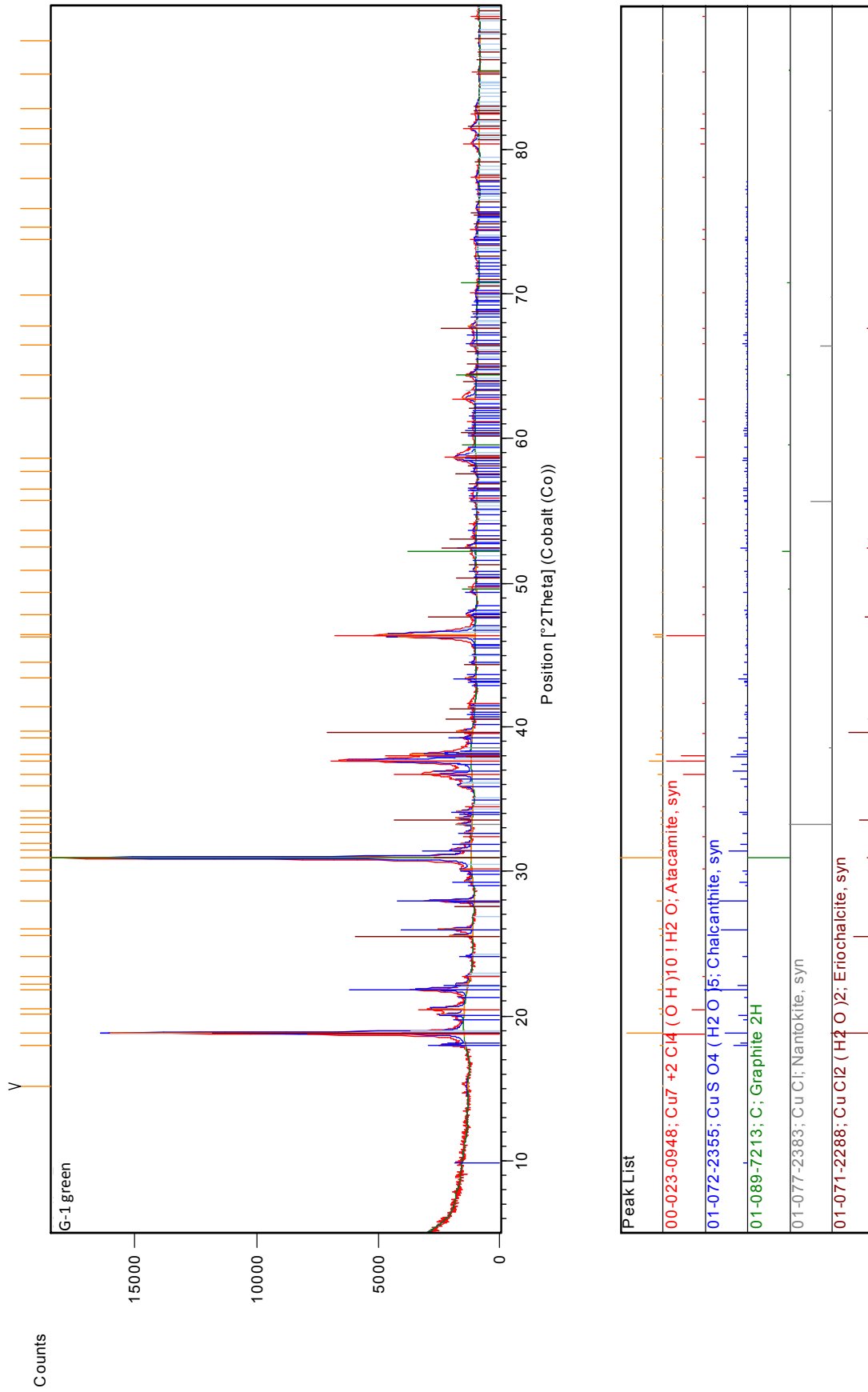
Figure B 13: XRD scan of sample G1 green.

Counts

Mpilo_G3 front

Position [°2Theta] (Cobalt (Co))

Peak List

01-080-1631; (Mg1.626 Fe0.37) (Si O4); Forsterite

01-089-7213; C; Graphite 2H

01-076-0544; Ca0.61 Mg0.76 Fe0.49 (Si O3)2; Augite

01-070-2127; Mg1.1 Fe0.87 Ca0.03 Si2 O6; Enstatite ferroan

01-086-2280; Ni S; Millerite
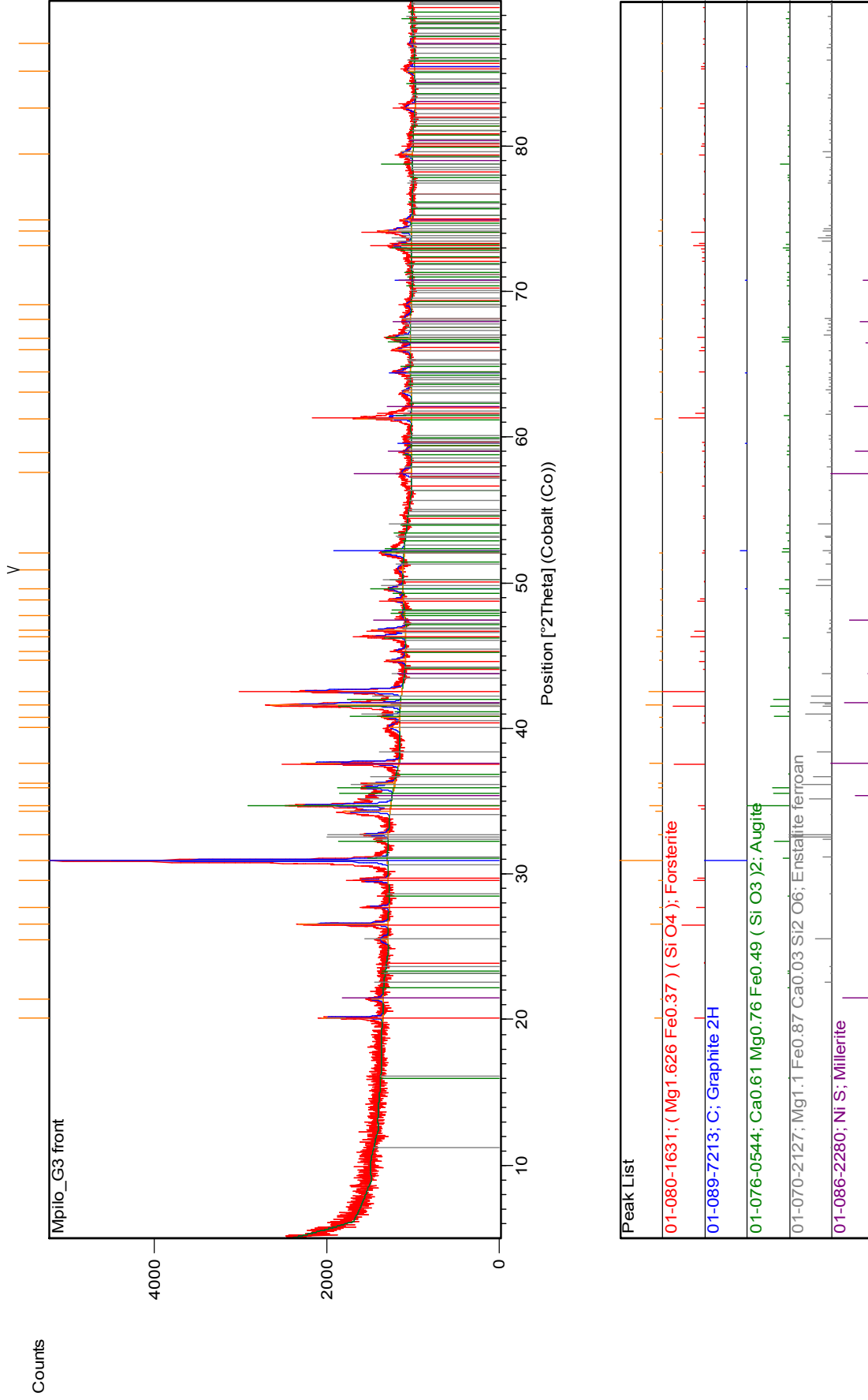
Figure B 14: XRD scan of sample G3 front.

Sulphidation of copper coolers in PGM smelters
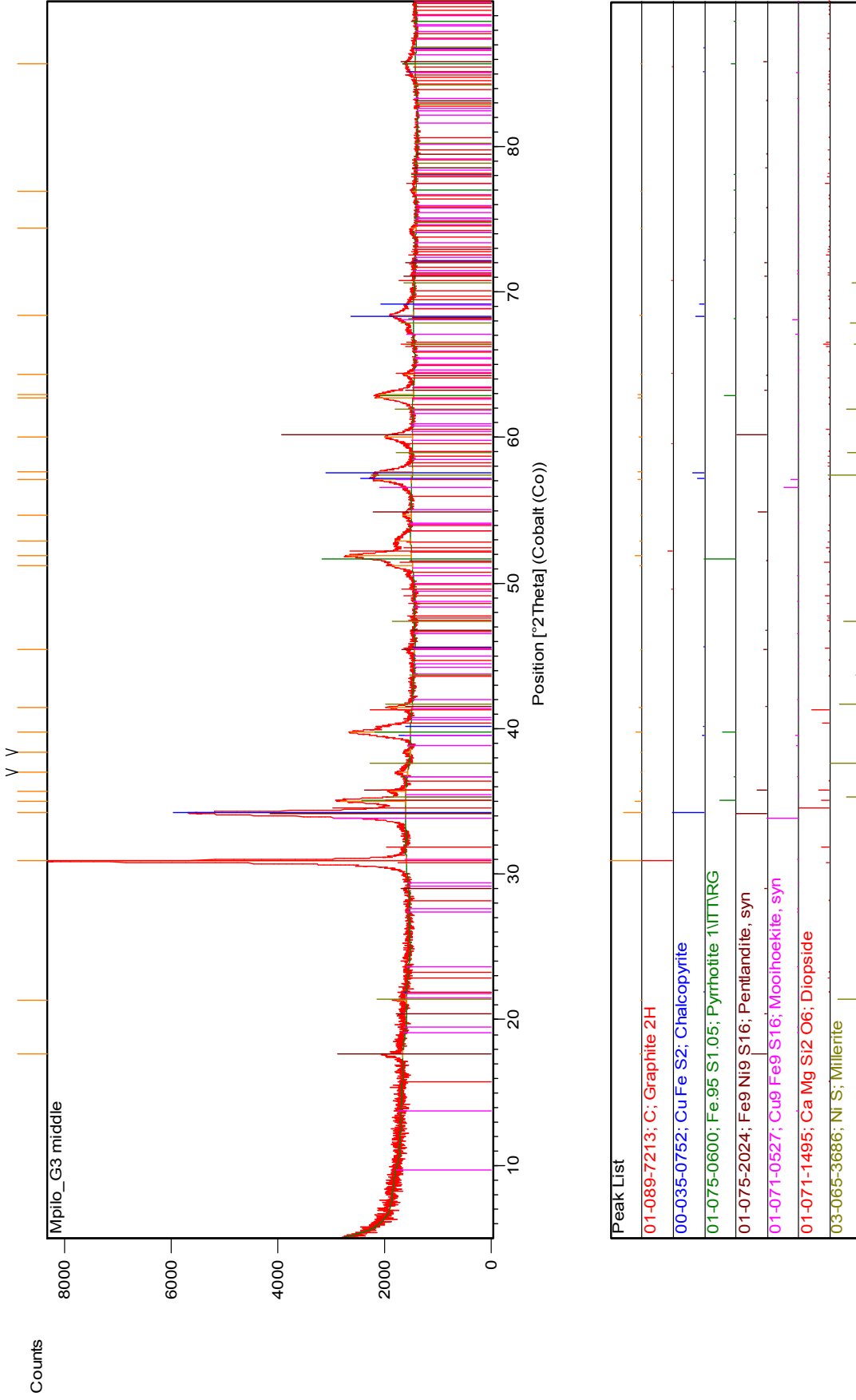
Figure B 15: XRD scan of sample G3 middle.

Sulphidation of copper coolers in PGM smelters
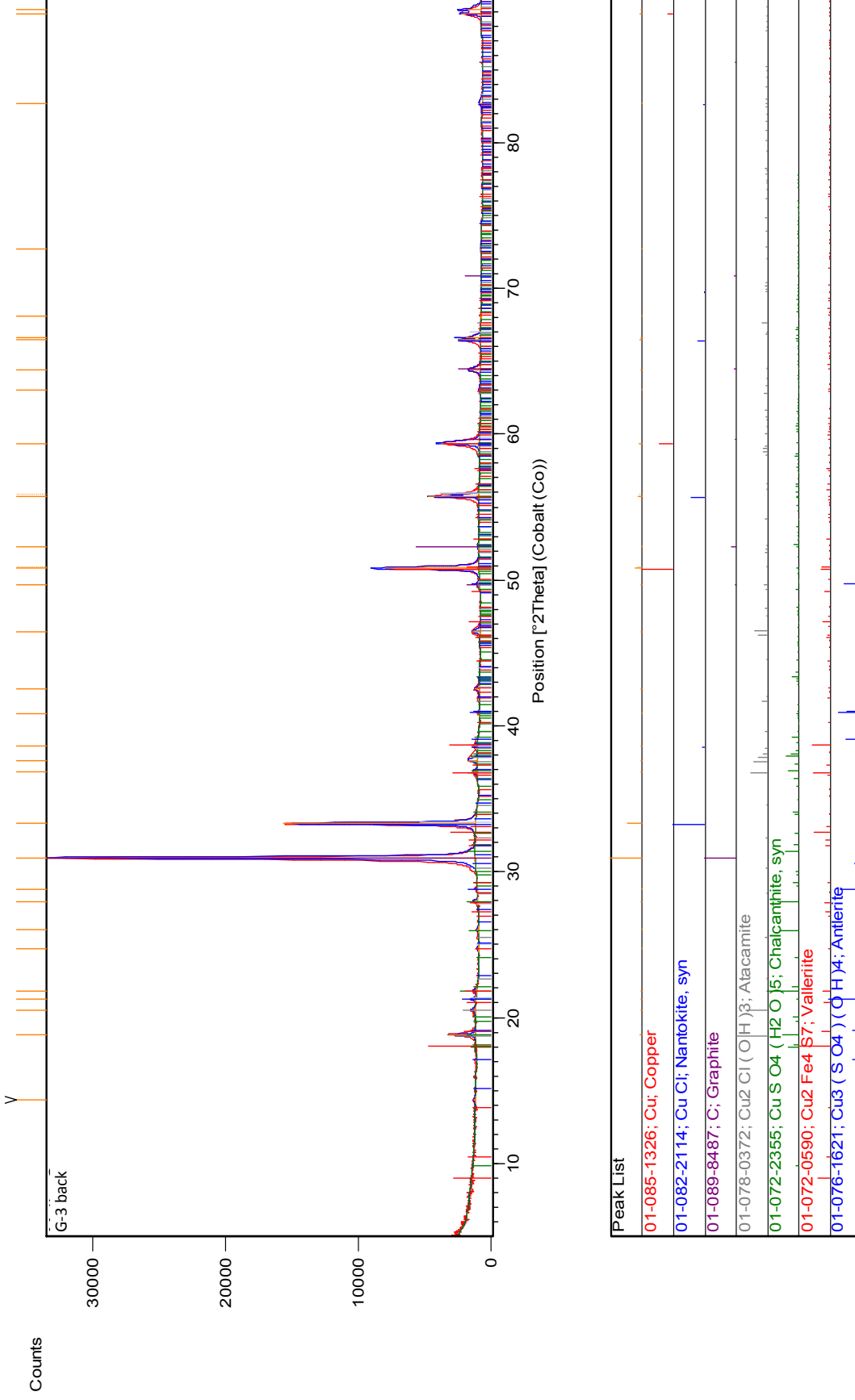
Figure B 16: XRD scan of sample G3 back.

Sulphidation of copper coolers in PGM smelters
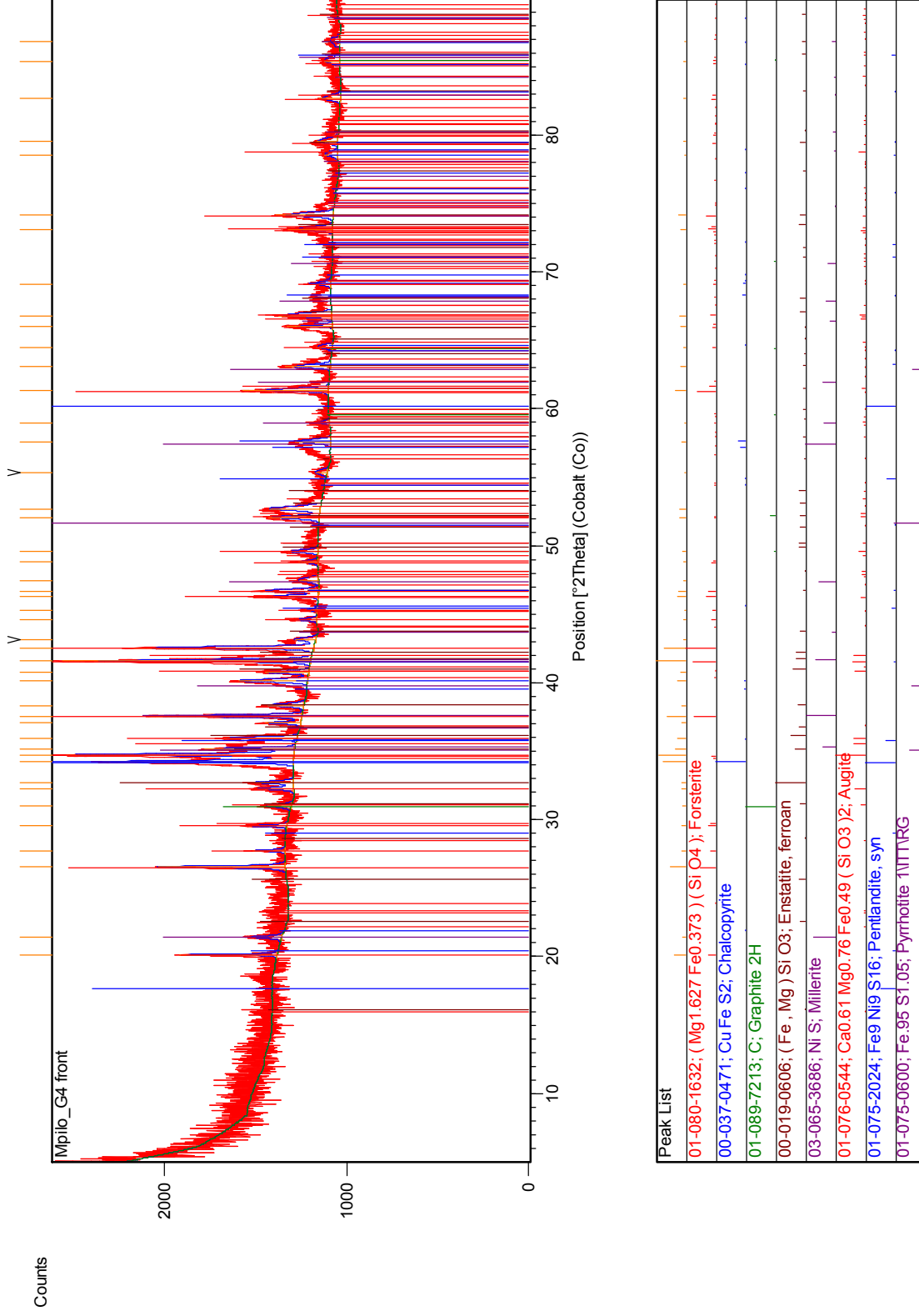
Figure B 17: XRD scan of sample G4 front.

Sulphidation of copper coolers in PGM smelters

Figure B 18: XRD scan of sample G4 middle.

Sulphidation of copper coolers in PGM smelters

Figure B 19: XRD scan of sample G5 front.

Sulphidation of copper coolers in PGM smelters
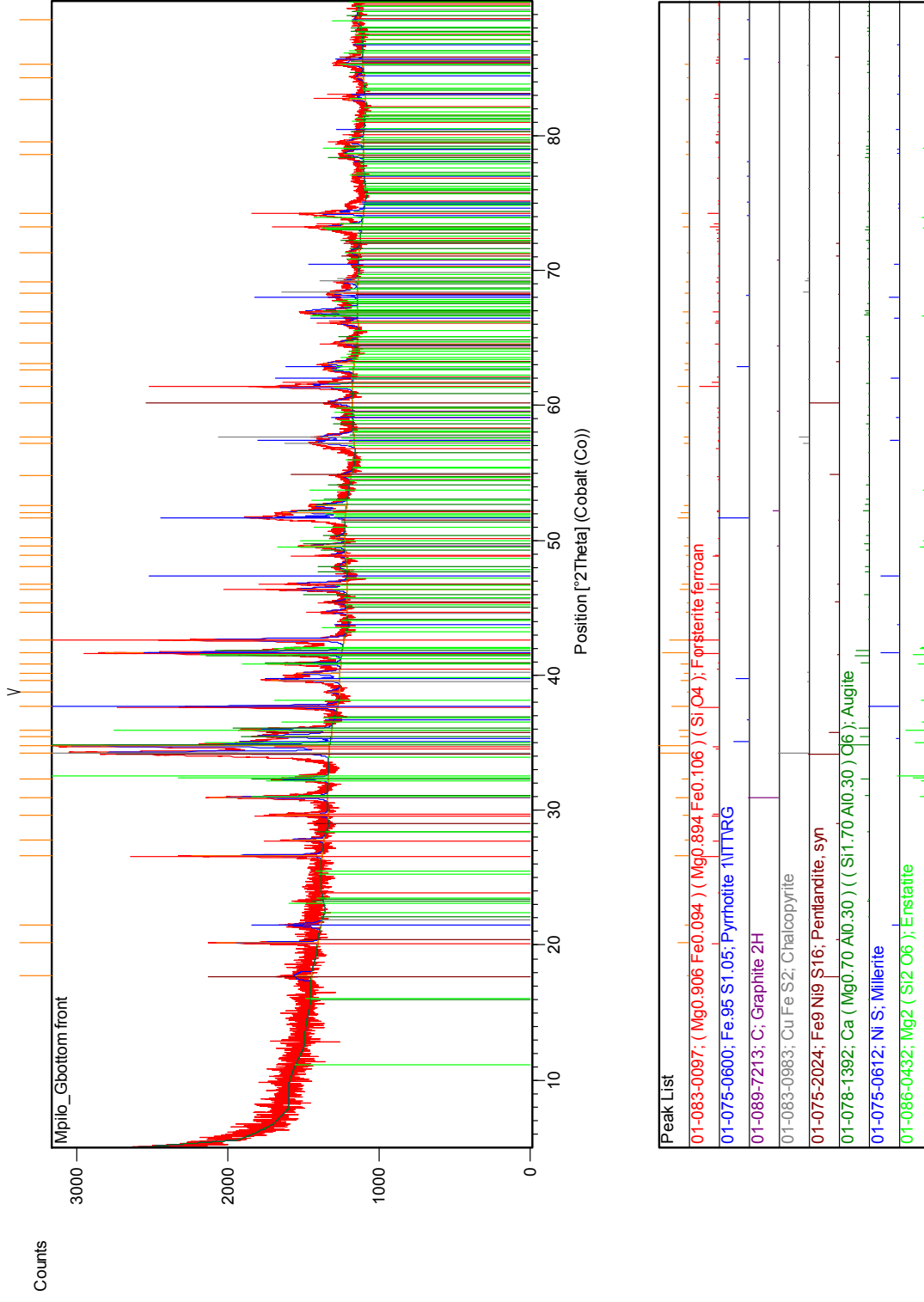
Figure B 20: XRD scan of sample G-bottom front.

Sulphidation of copper coolers in PGM smelters
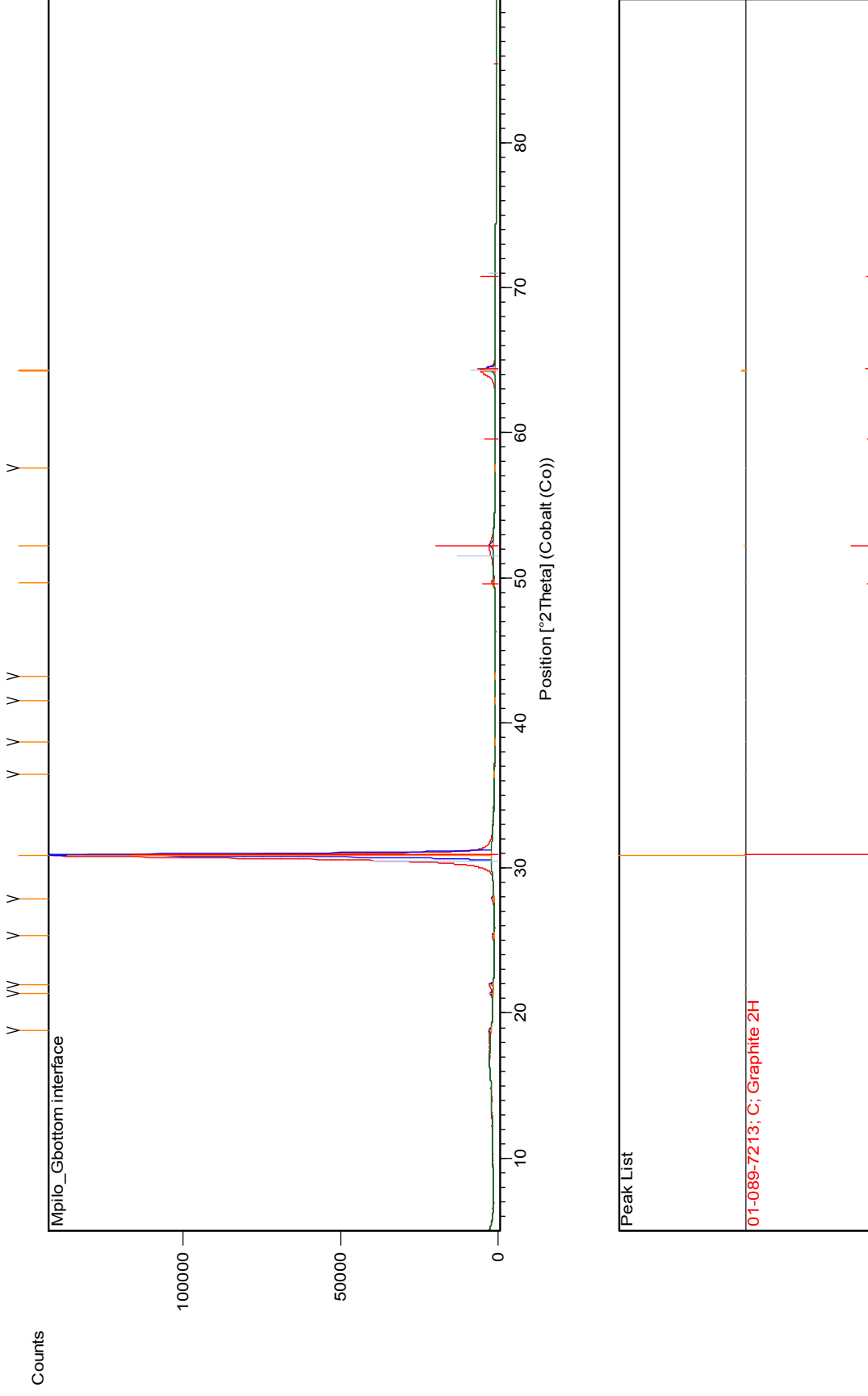
Figure B 21: XRD scan of sample G-bottom_castable interface.

G-bottom back

Counts

Position [°2Theta] (Cobalt (Co))
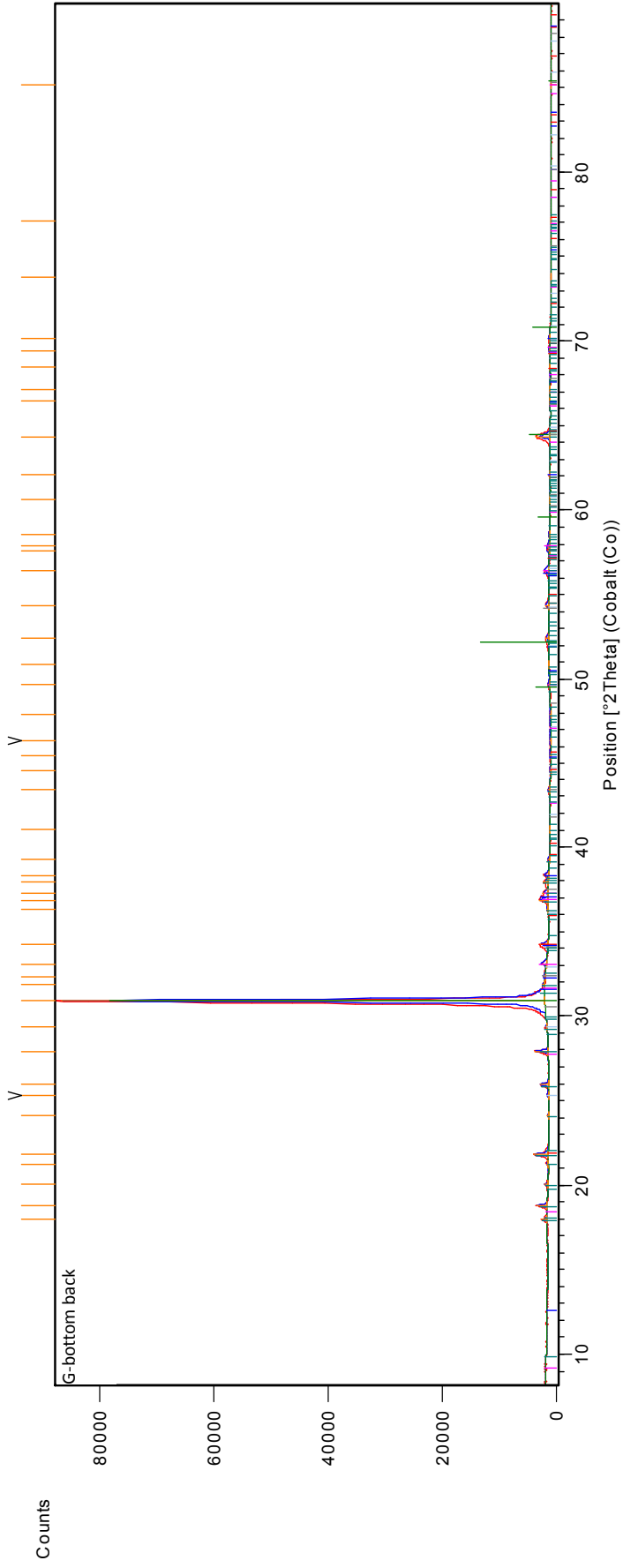
Peak List

01-083-0983; Cu Fe S2; Chalcopyrite

00-006-0464; Cu S; Covellite, syn

01-089-7213; C; Graphite 2H

00-047-1748; Cu9 S5; Digenite

01-083-1809; Cu3.39 Fe0.61 S4; Nukundamite

01-070-1823; Cu S O4 (H2 O)5; Chalcanthite

Figure B 22: XRD scan of sample G-bottom back.
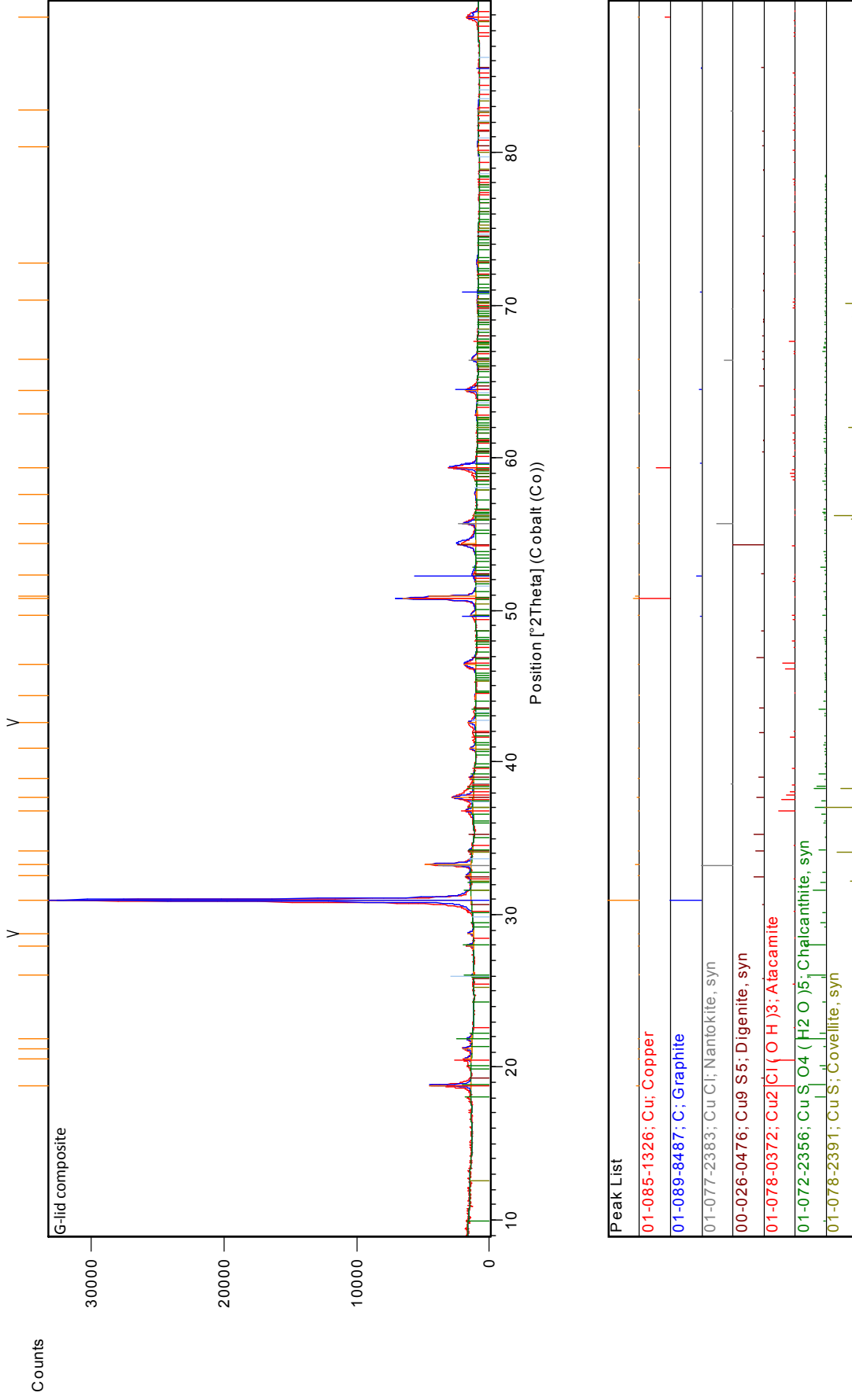
Figure B 23: XRD scan of sample G-lid.

Peak List

01-085-1326; Cu; Copper
01-089-8487; C; Graphite
01-077-2383; Cu Cl; Nantokite, syn
00-026-0476; Cu9 S5; Digenite, syn
01-078-0372; Cu2 Cl (O H)3; Atacamite
01-072-2356; Cu S O4 (H2 O)5; Chalcanthite, syn
01-078-2391; Cu S; Covellite, syn

Figure B 24: XRD scan of sample G-lid green.

Sulphidation of copper coolers in PGM smelters

Figures B25 to B33 depict the XRD scans of the corrosion products from the sulphidation laboratory tests performed on a copper foil.
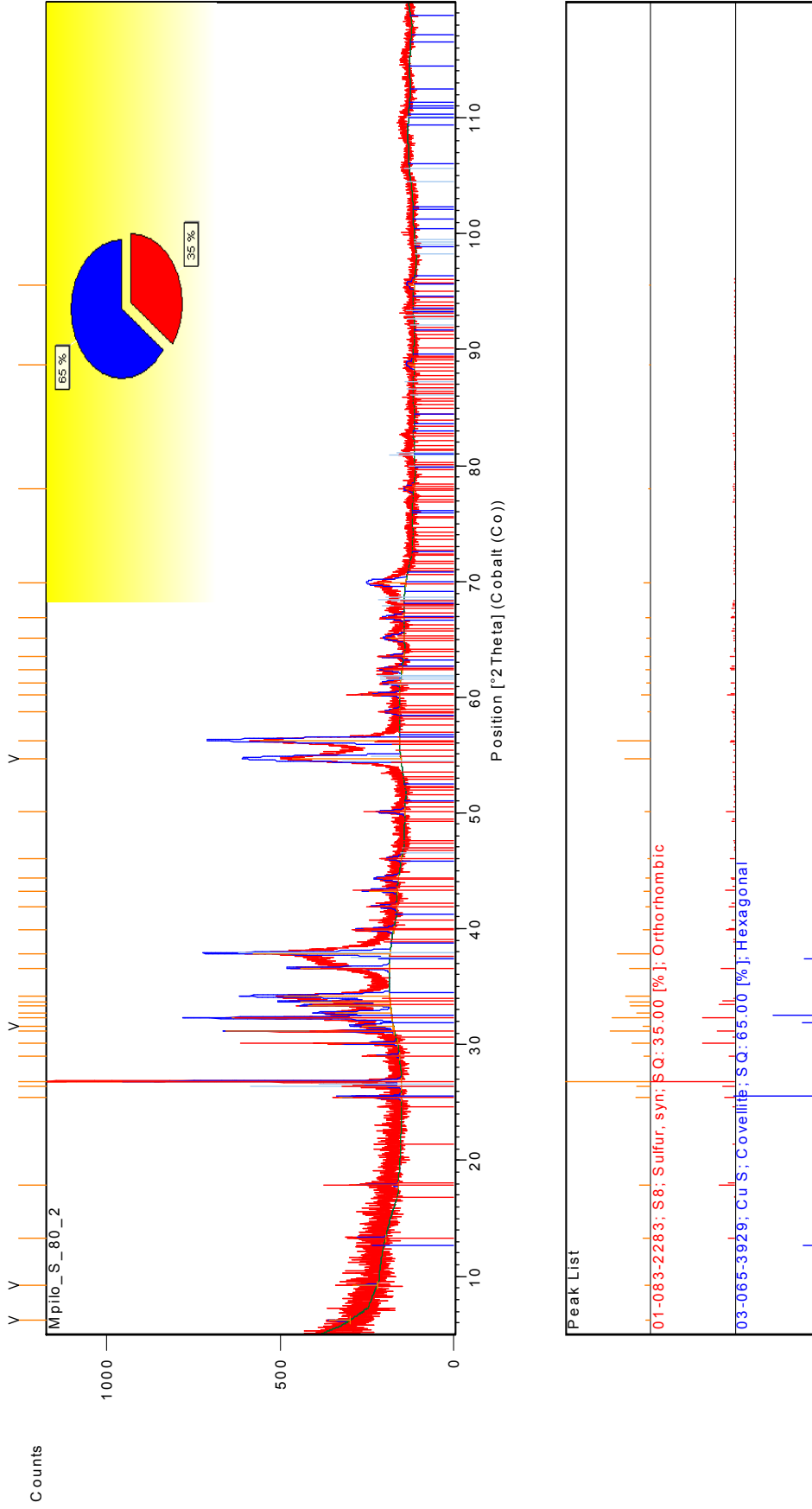
Figure B 25: XRD scan of a copper foil after exposure to sulphur vapour at 80°C.

Sulphidation of copper coolers in PGM smelters
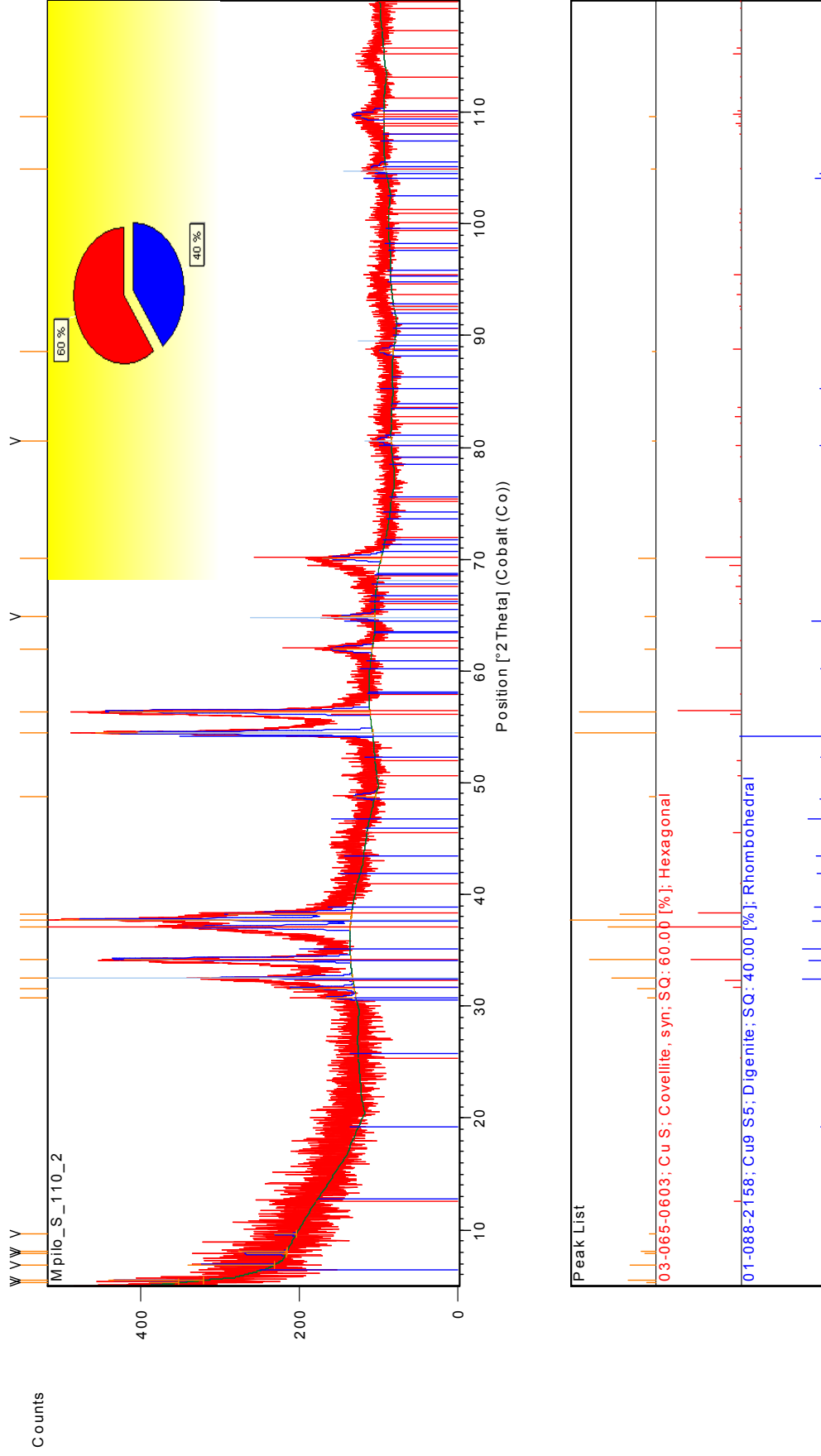
Figure B 26: XRD scan of a copper foil after exposure to sulphur vapour at 110°C.

Sulphidation of copper coolers in PGM smelters
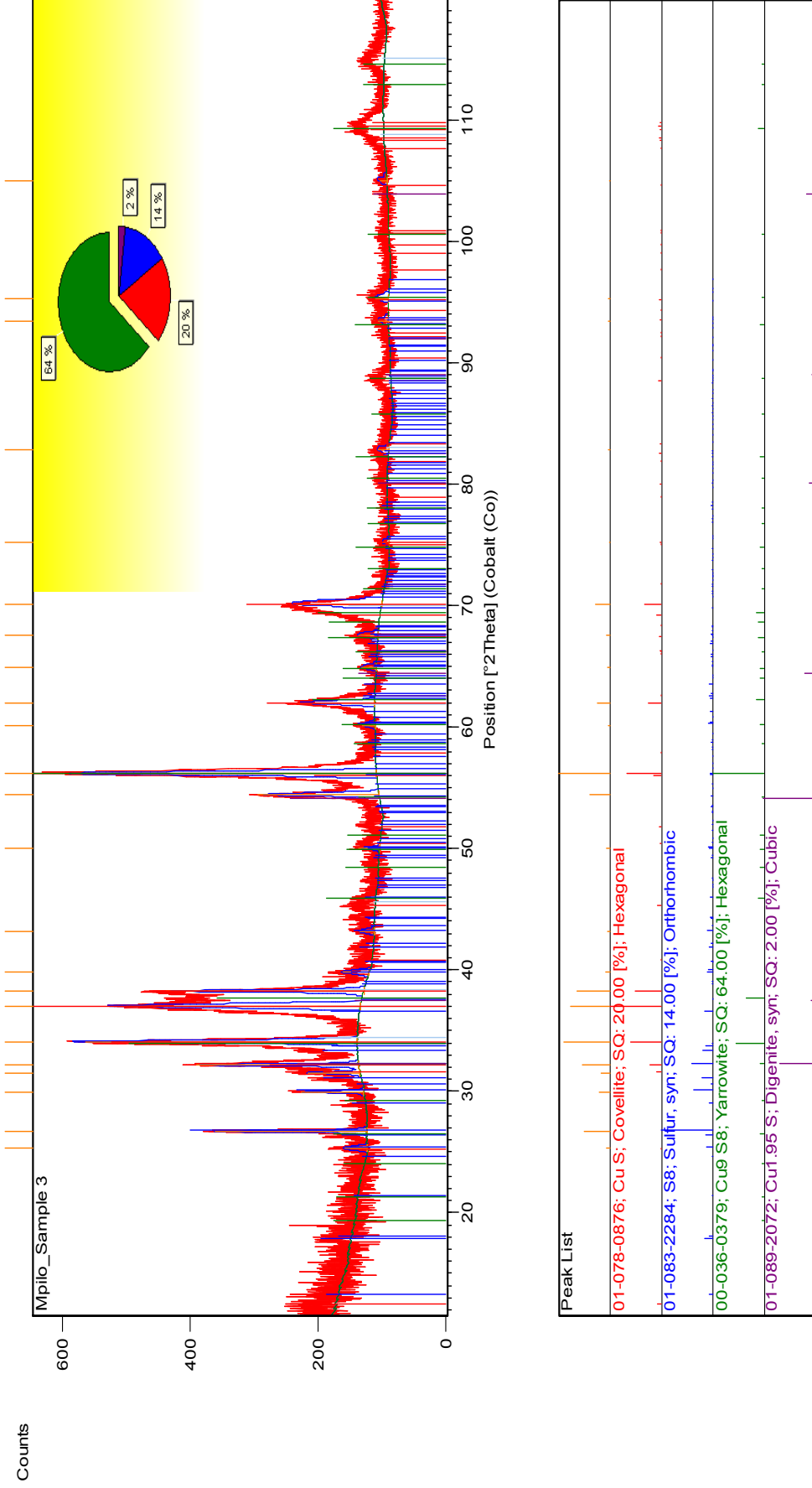
Figure B 27: XRD scan of a copper foil after exposure to sulphur vapour at 140°C.
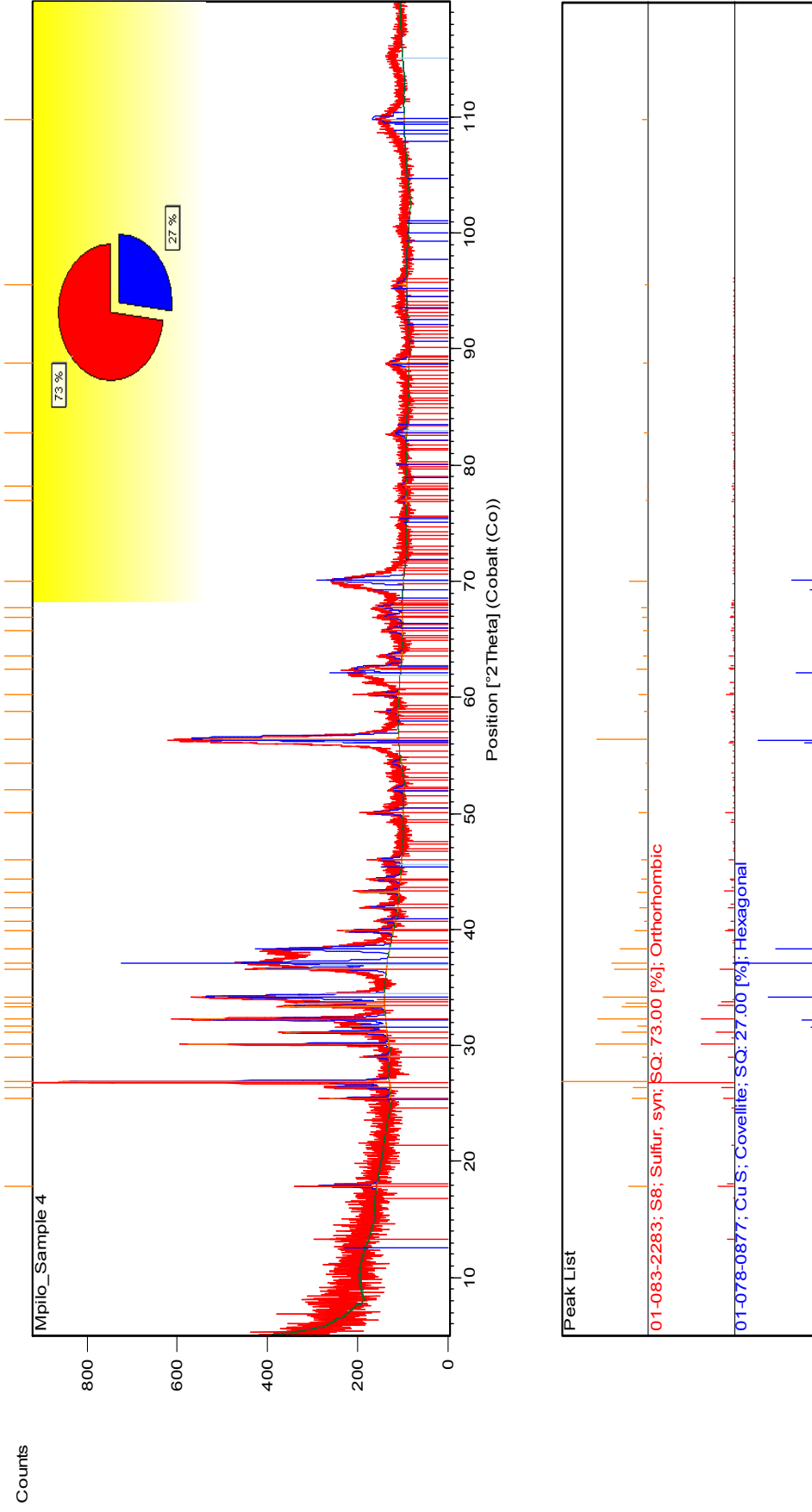
Sulphidation of copper coolers in PGM smelters

Figure B 28: XRD scan for a copper foil after exposure to sulphur vapour at temperatures from 80°C to 140°C.

Sulphidation of copper coolers in PGM smelters
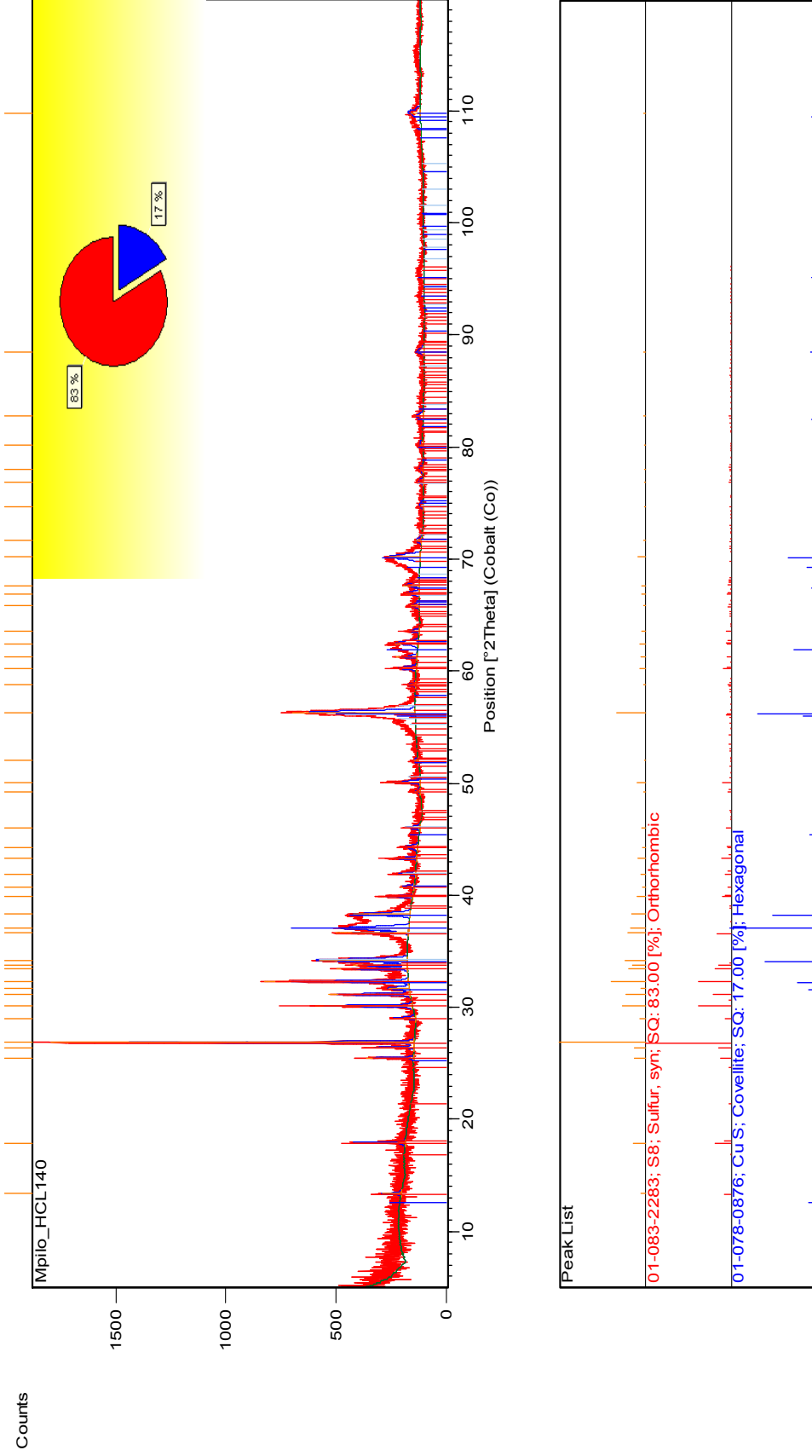
Figure B 29: XRD scan of a copper foil after exposure to sulphur and HCl vapour at 140°C.
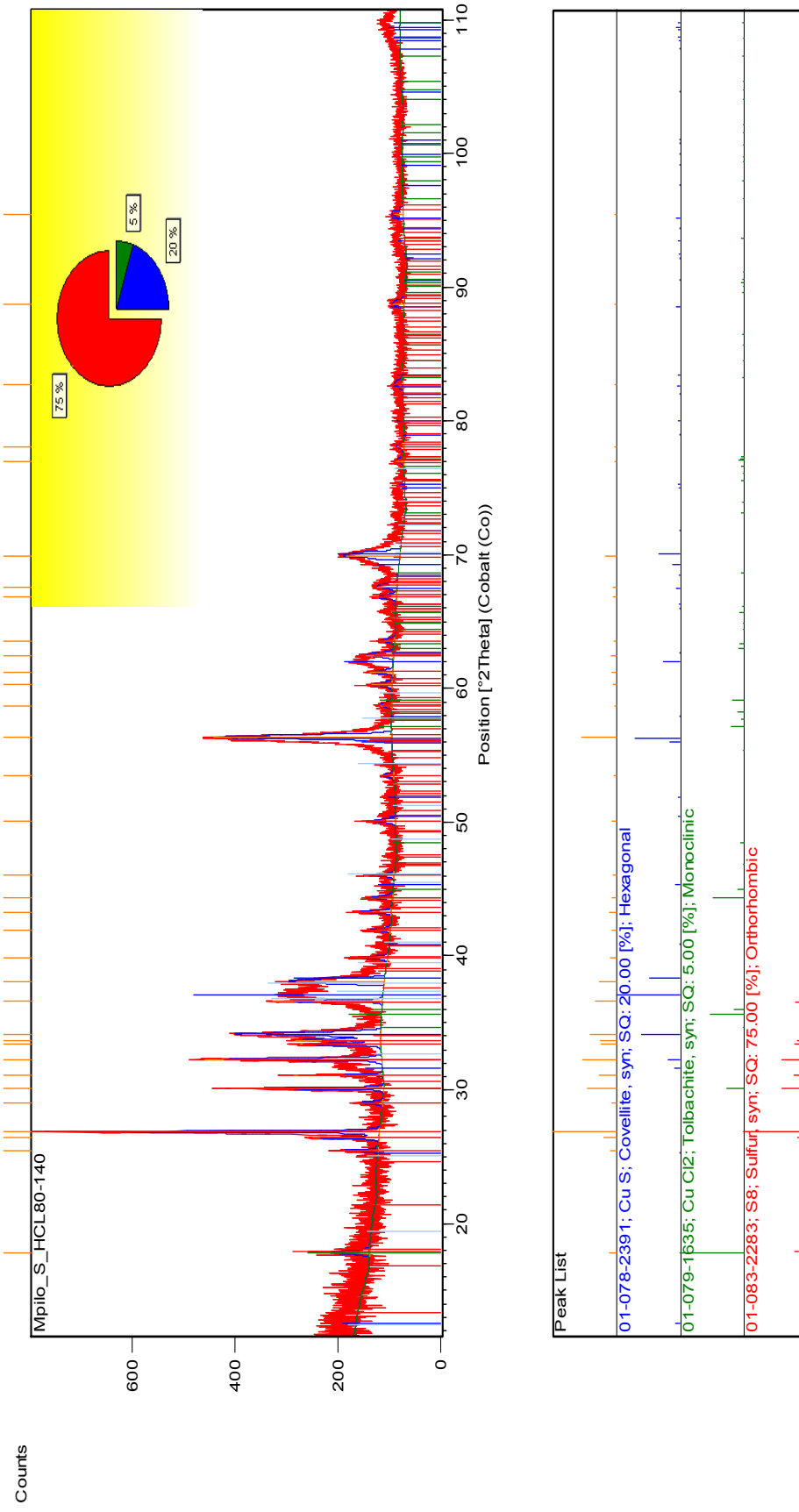
Sulphidation of copper coolers in PGM smelters

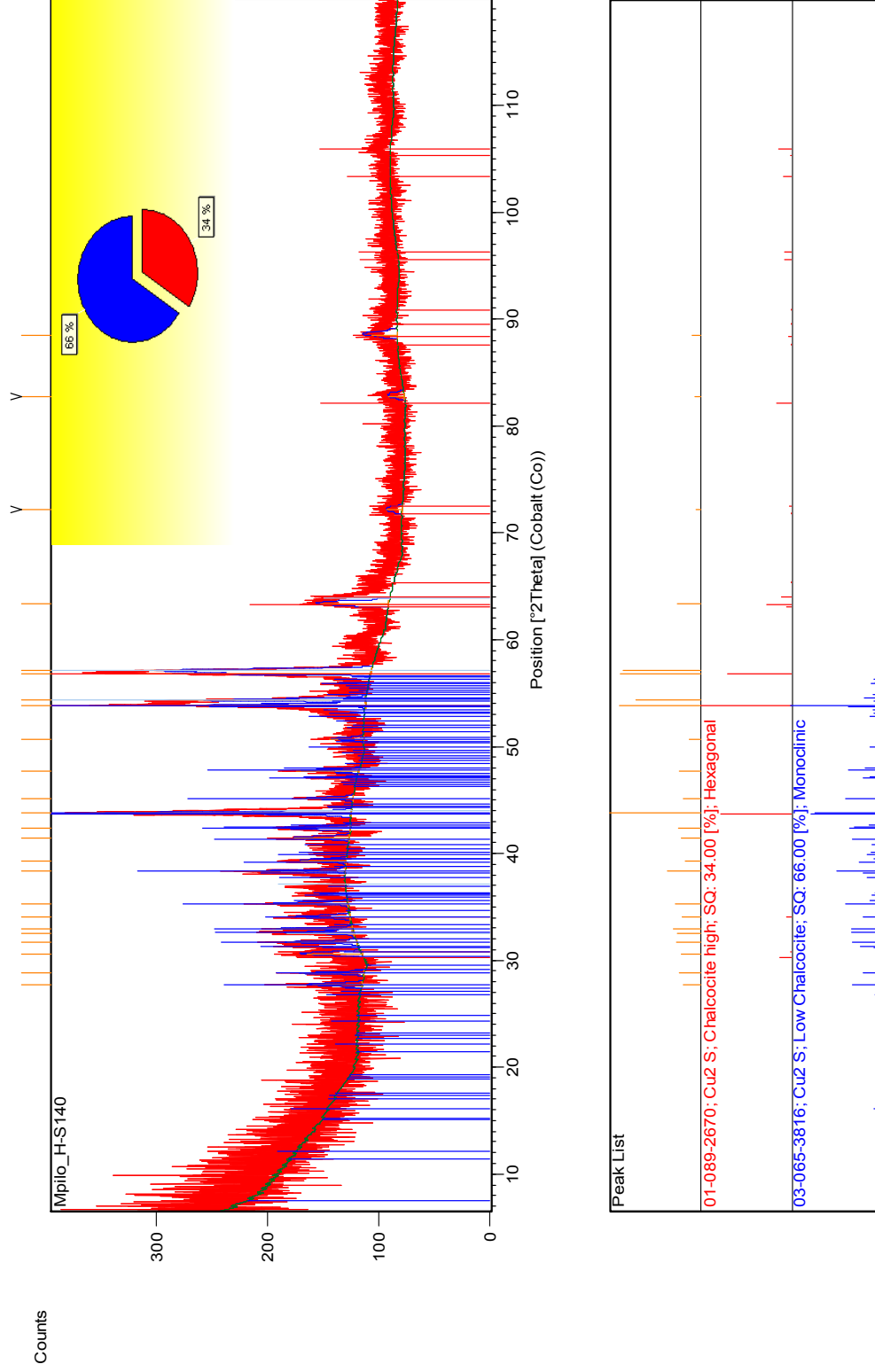*Figure B 30: XRD scan of a copper foil after exposure to sulphur and HCl vapour at temperatures from 80°C to 140°C.*

Sulphidation of copper coolers in PGM smelters

Figure B 31: XRD scan of a copper foil after exposure to hydrogen sulphide vapour at 140°C.

Sulphidation of copper coolers in PGM smelters

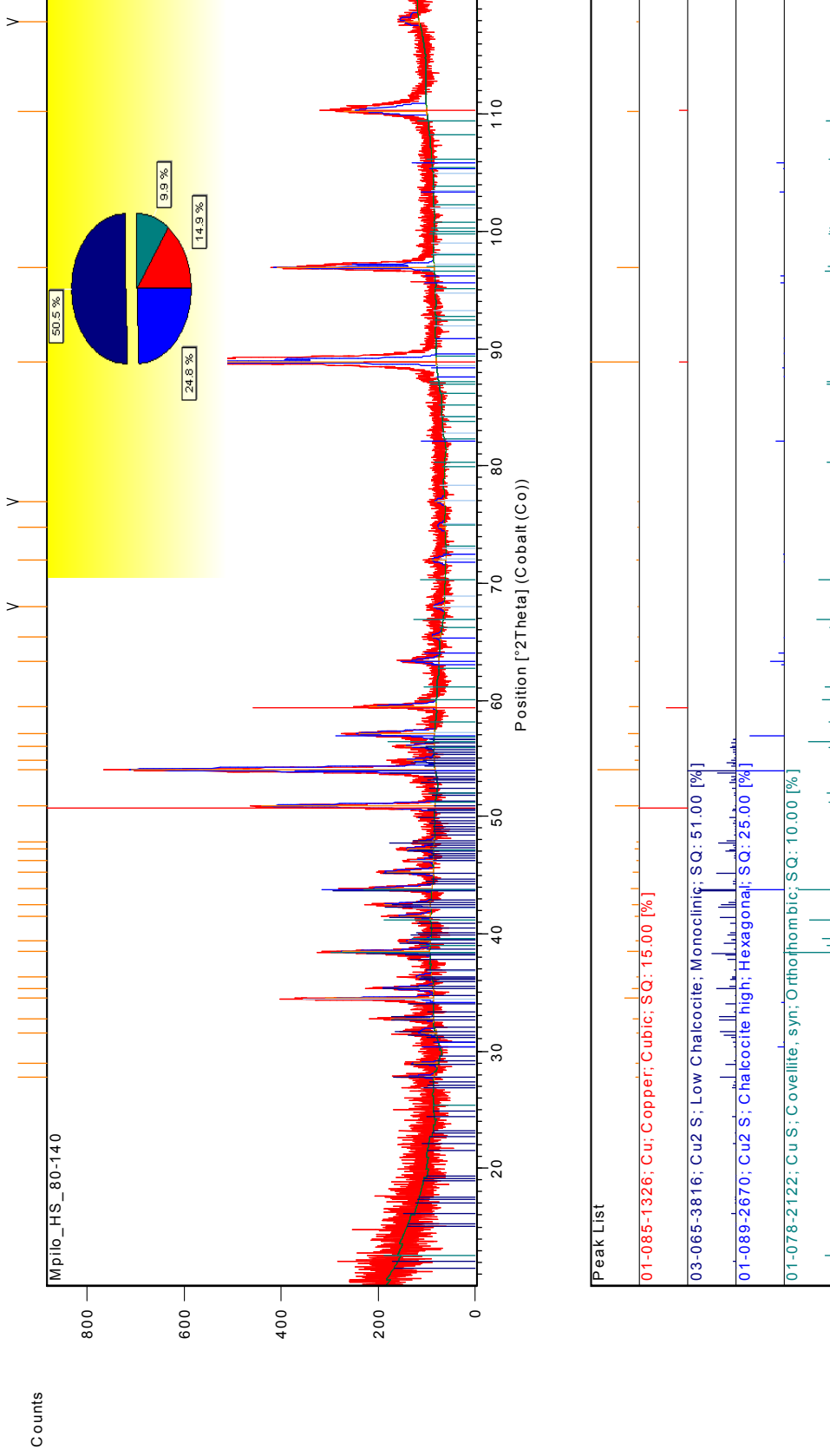*Figure B 32: XRD scan of a copper foil after exposure to hydrogen sulphide vapour at temperatures from 80°C to 140°C.*
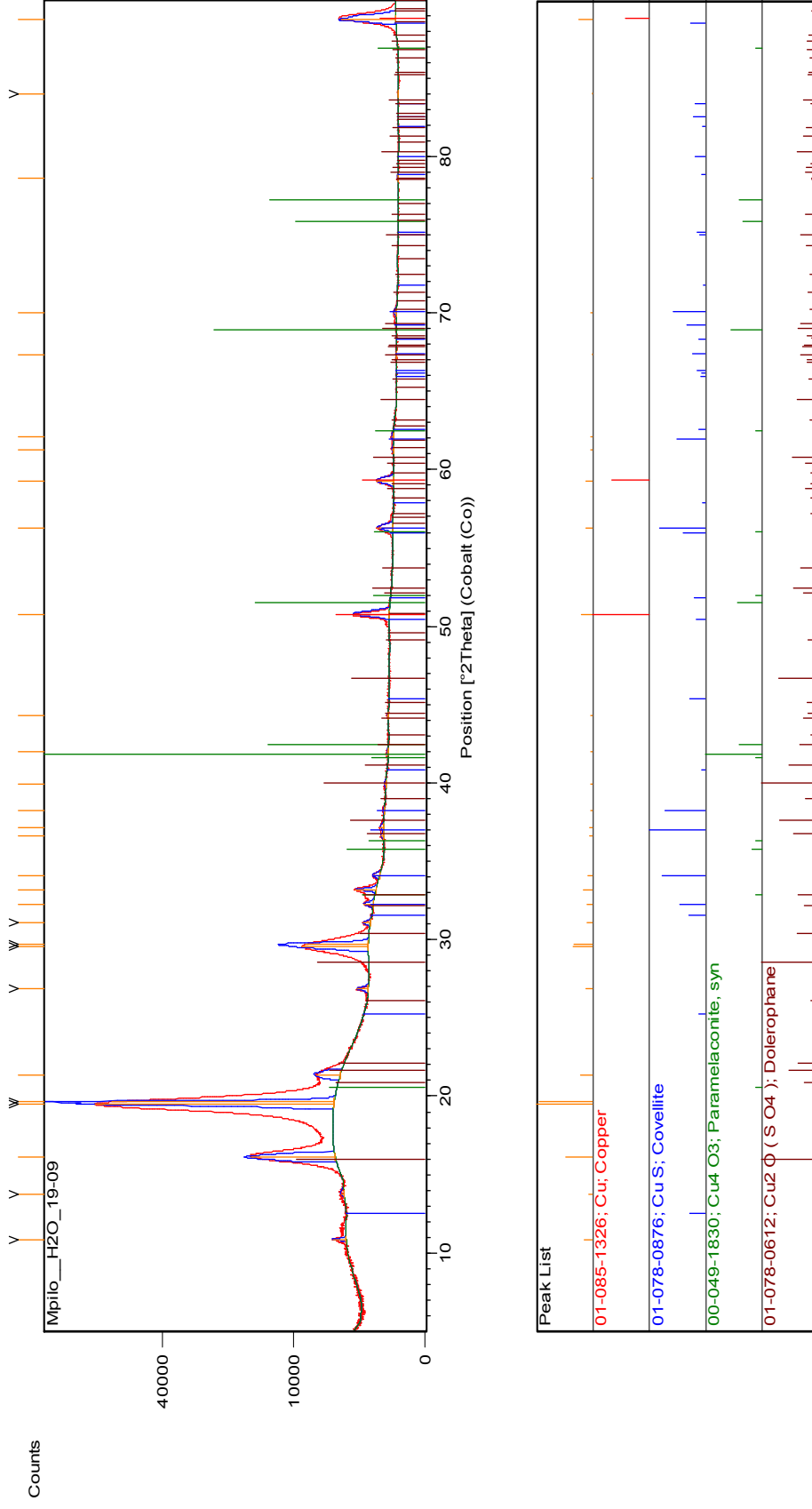
Sulphidation of copper coolers in PGM smelters

Figure B 33: XRD scan of a copper foil after exposure to sulphur vapour with water vapour additions at 80°C to 140°C.

Sulphidation of copper coolers in PGM smelters

Appendix C: Calibration curves for argon flow meter and the thermocouple
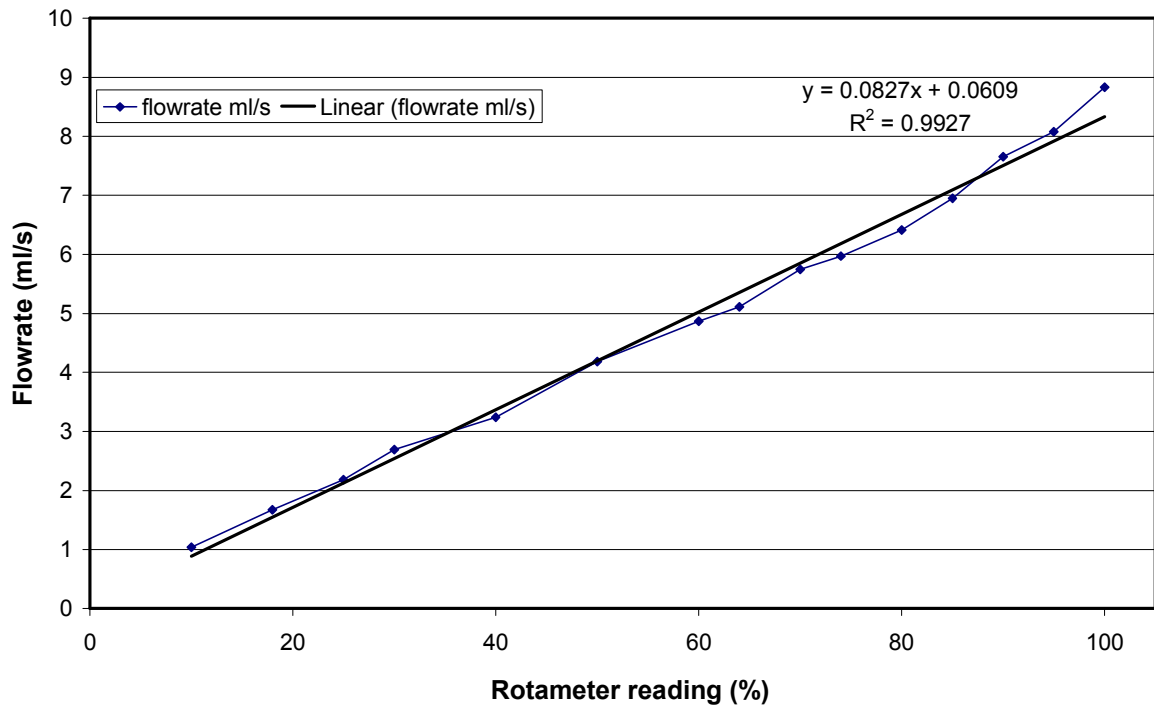
Figure C 1: Calibration curve for the argon flow rate.

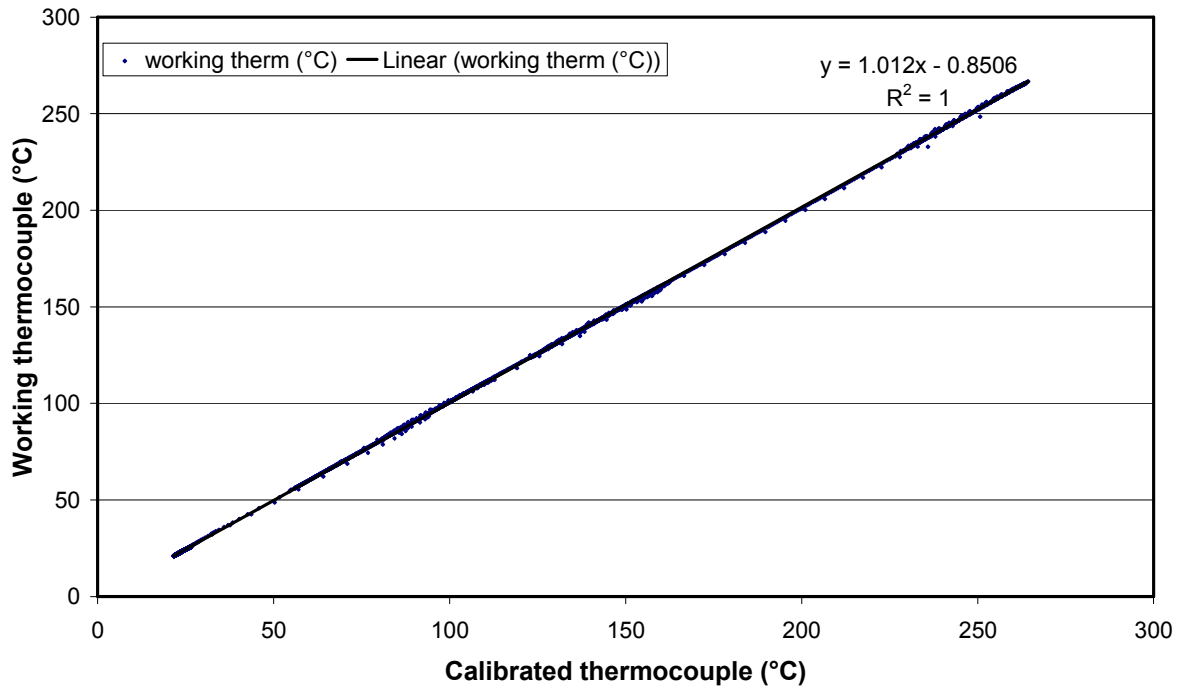Sulphidation of copper coolers in PGM smelters

Figure C 2: Calibration curve for a thermocouple.

Sulphidation of copper coolers in PGM smelters

Appendix D

Appendix D: Graphical presentation of the ICP graphite block and the ash analyses.

Elements are plotted separately and the elements contents are from the top graphite portion (G1) to the bottom portion (Gbottom) plotted as a function of position (hot, middle or cold face) in which the sample was taken.
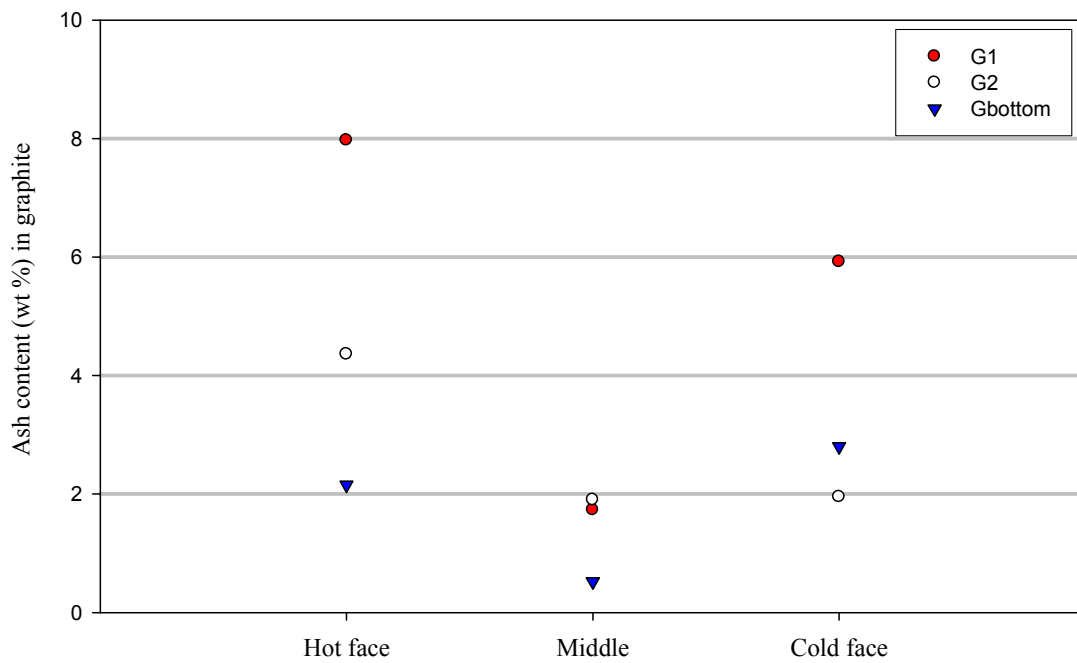

Figure D 1: Ash content (wt %) in a graphite sample.

Sulphidation of copper coolers in PGM smelters
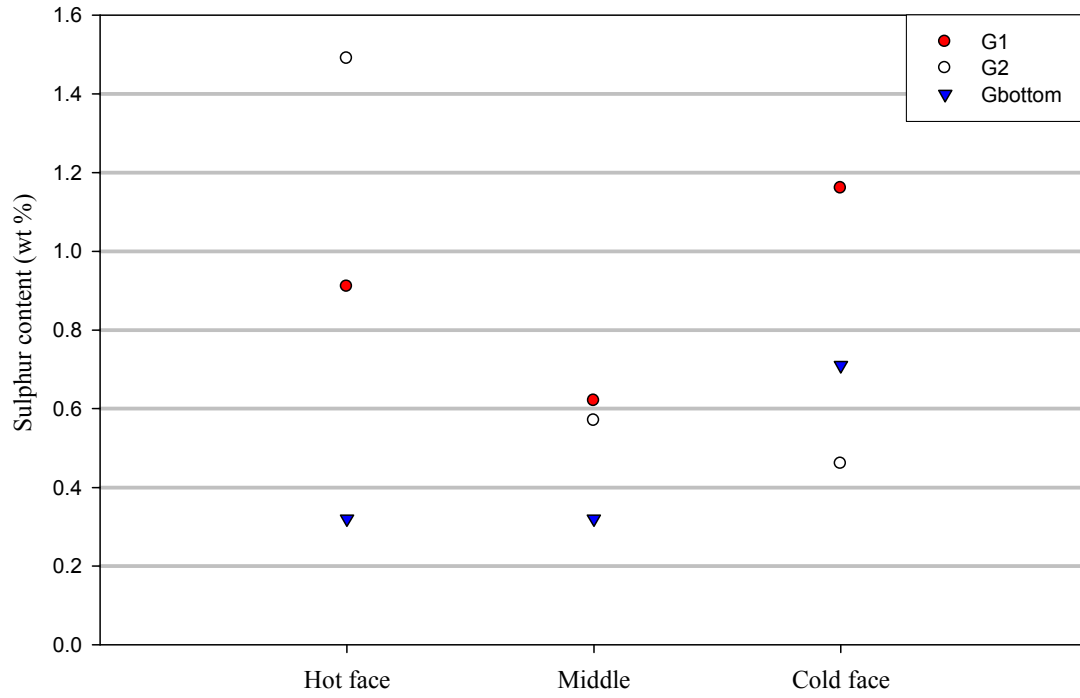
Figure D 2: Sulphur content (wt %) in a graphite sample.

Sulphidation of copper coolers in PGM smelters
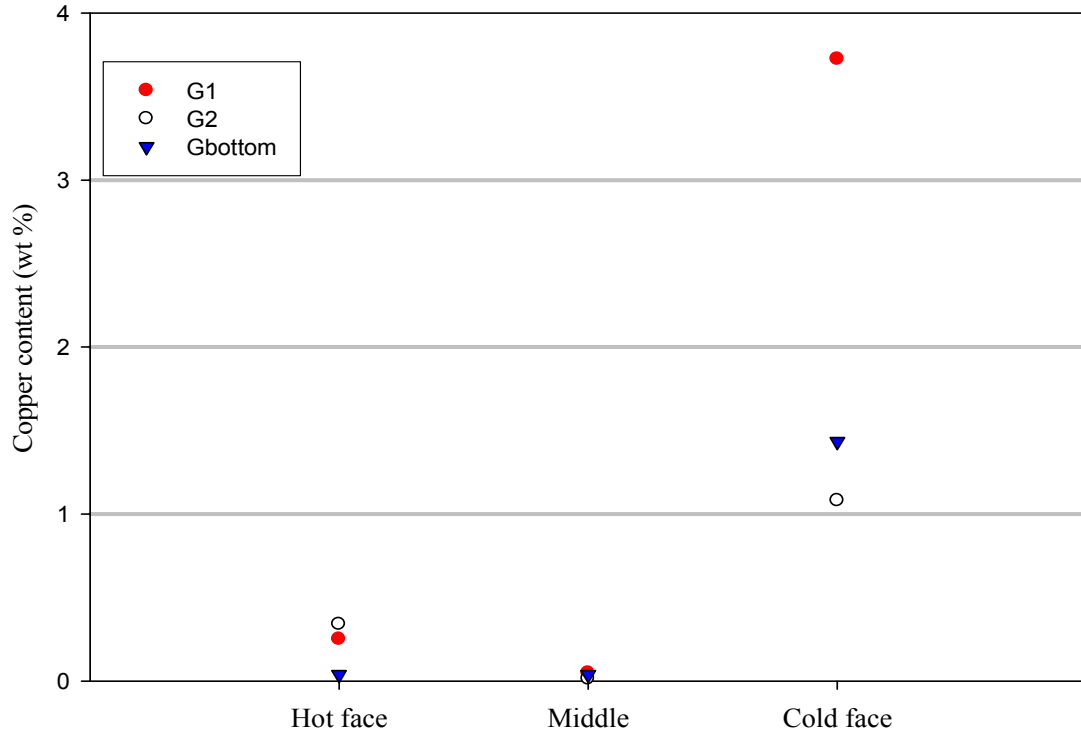
Figure D 3: Copper content (wt %) in a graphite sample.

Figure D 4: Copper content (wt %) in Ashed graphite sample.

Sulphidation of copper coolers in PGM smelters

Figure D 5: Nickel content (wt %) in a graphite sample.

Figure D 6: Nickel content (wt %) in Ashed graphite sample.

Figure D 7: Iron (total) content (wt %) in a graphite sample.

Figure D 8: Iron (total) content (wt %) in Ashed graphite sample.

Figure D 9: SiO₂ content (wt %) in a graphite sample.

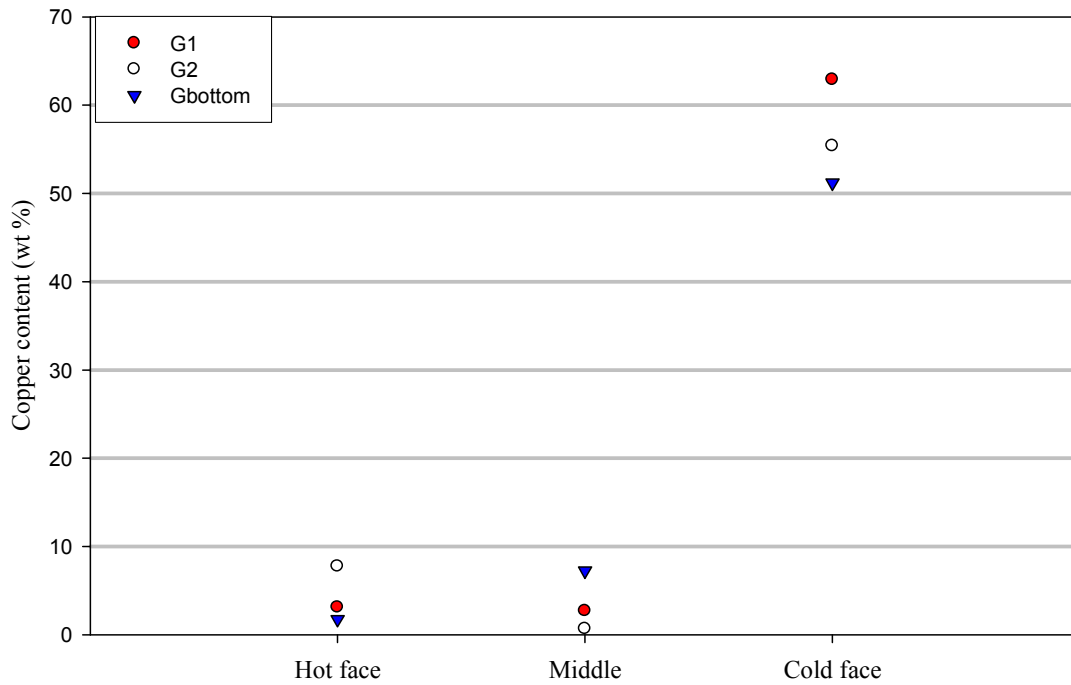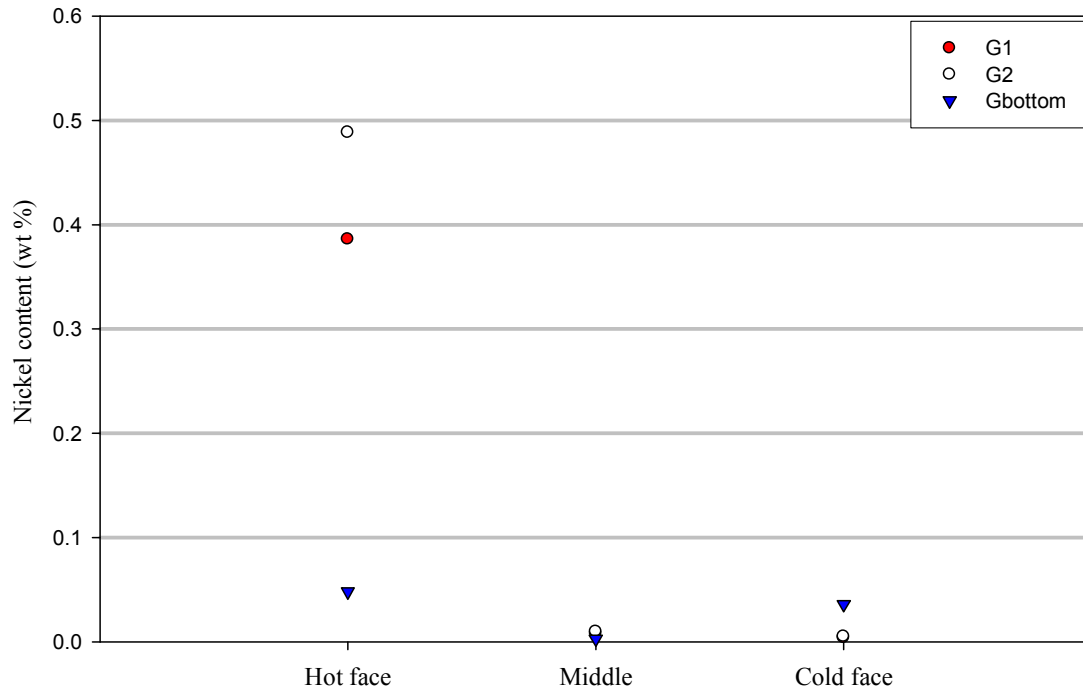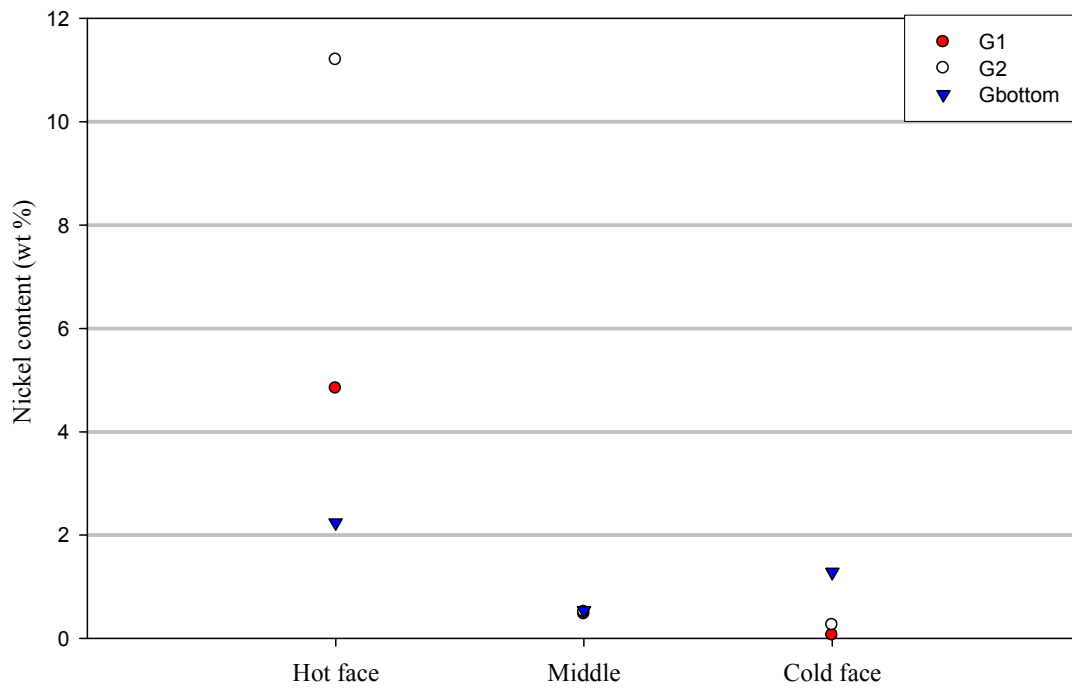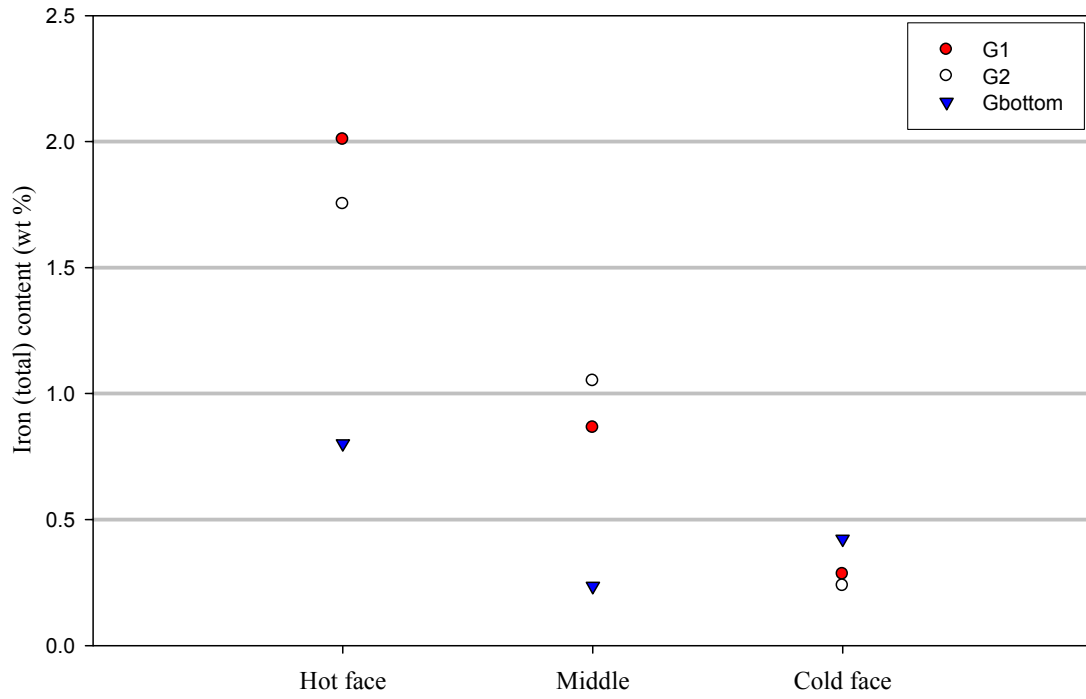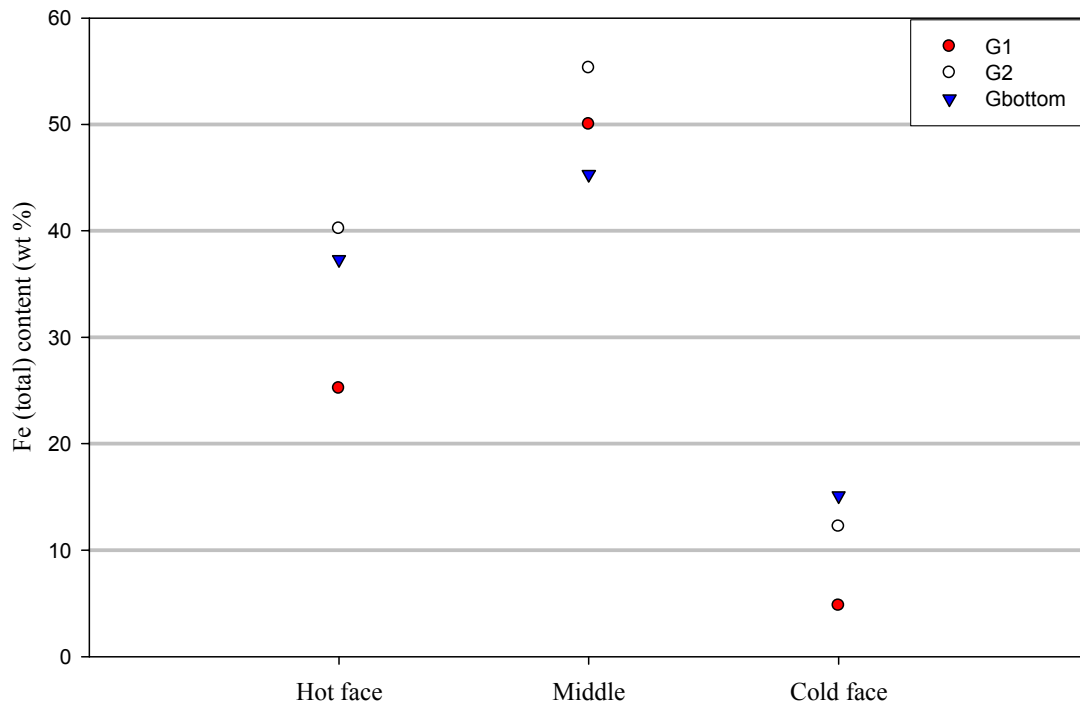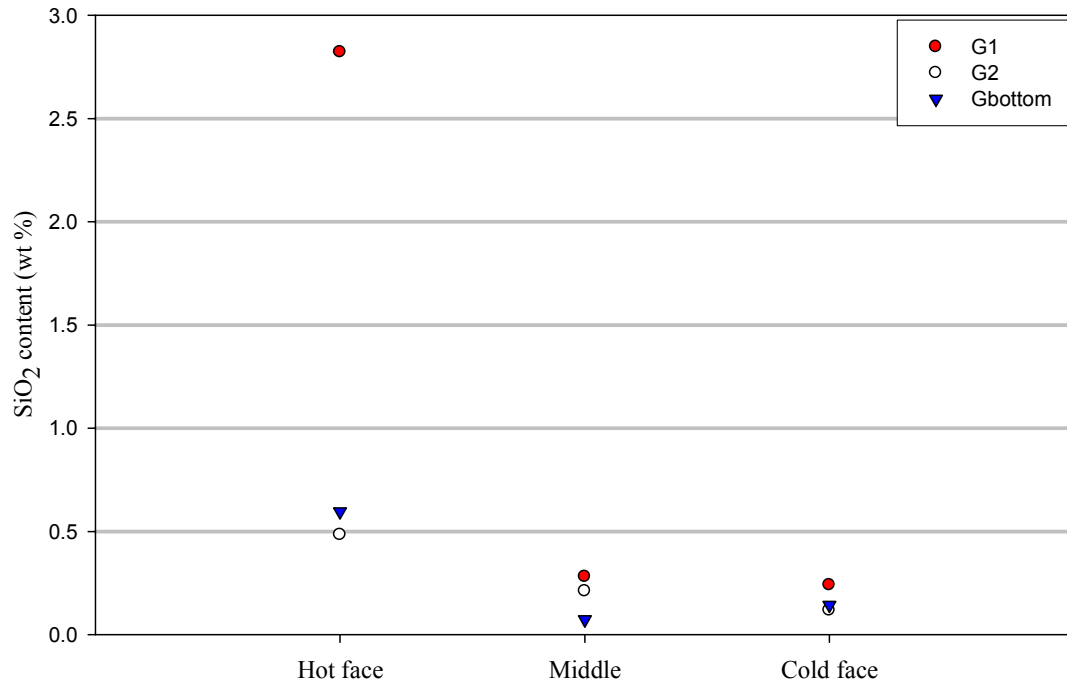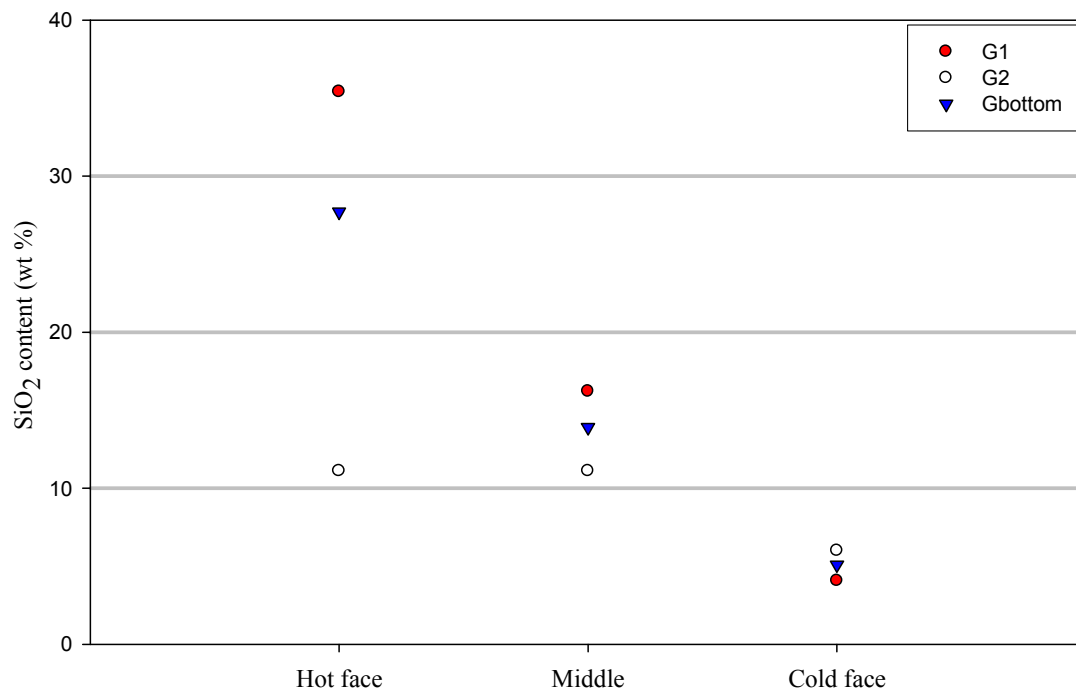*Figure D 10: SiO₂ content (wt %) in Ashed graphite sample.*

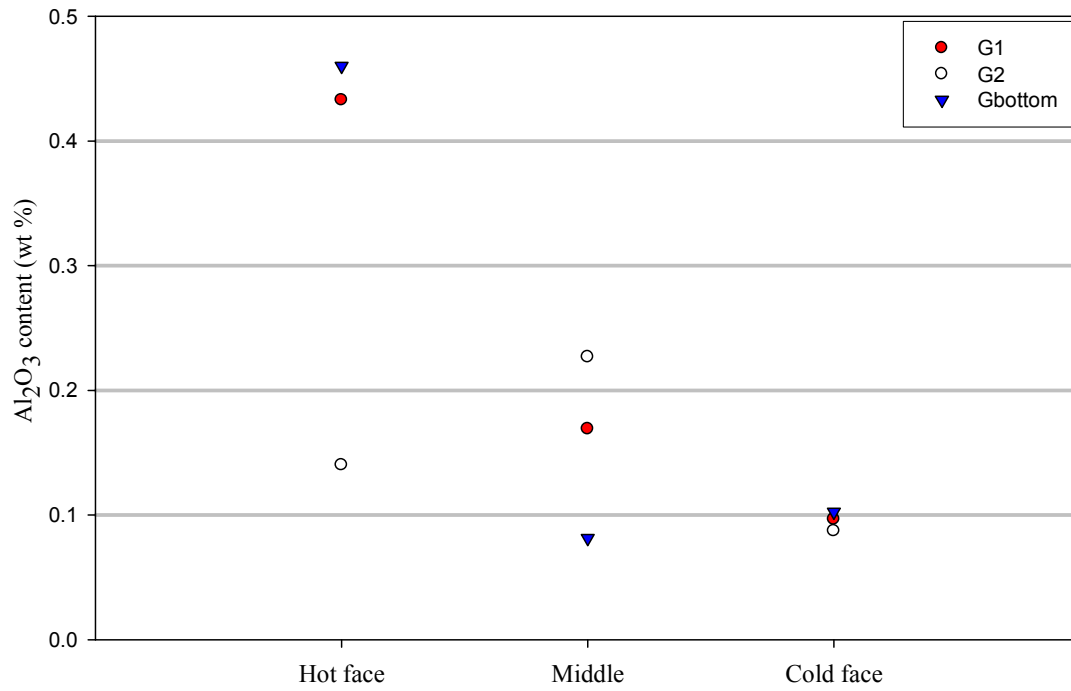Sulphidation of copper coolers in PGM smelters

Figure D 11: Al₂O₃ content (wt %) in a graphite sample.
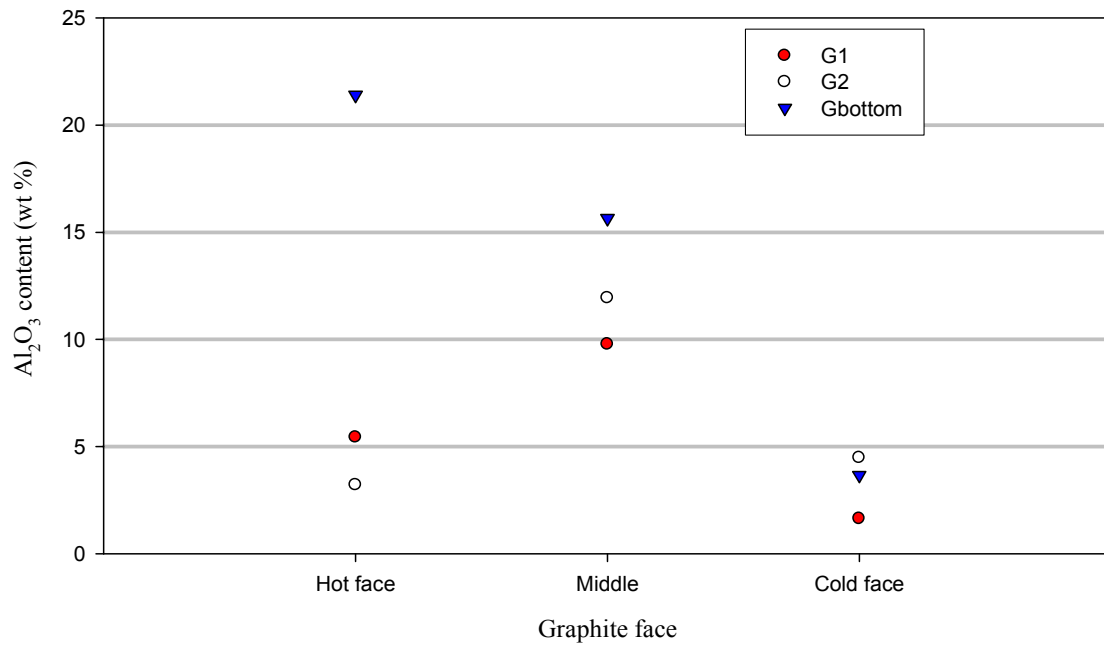
Figure D 12: Al₂O₃ content (wt %) in Ashed graphite sample.

Appendix E

Appendix E outlines the procedures used to quantify the gases synthesised in this test work, i.e. hydrogen chloride gas (HCl), water vapour (H_2O) and hydrogen sulphide gas (H_2S).

<u>Determination of the amount of HCl vapour in the argon stream</u>

HCl vapour was added with the sulphur gas during the sulphidation laboratory tests to determine the effect of HCl additions on the corrosion rate of copper and on the product morphology.

To determine the amount of HCl vapour added with argon stream, Equation E 1 (Antoinne equation) and Equation E 2 were used [Middleman 1991, Love et al. 1992 and Logue et al. 2004]. Vapour pressure of the HCl was calculated from Equation E 1, where A, B and C are thermodynamic coefficients of HCl vapour [Love et al. 1992 and Logue et al. 2004].

$$\log_{10} P = A - \frac{B}{C+T}$$ 	Equation E 1

where P is the vapour pressure of HCl and T is the temperature of the gas stream, which was 25°C in this study. The summary of the calculated values of HCl vapour pressure and flow rate is in Table E1. HCl flow rate was calculated from Equation E 2:

$$F_{HCl} = F_{Ar} \frac{P_{HCl}}{P_{atm} - P_{HCl}}$$ 	Equation E 2

where F_{HCl} is the HCl molar flow rate, F_{Ar} the molar flow rate of a carrier gas (argon), P_{HCl} is the vapour pressure of water calculated from Equation E 1, P_{atm} is the bubbler pressure which in this case is atmospheric.

F_{Ar} was calculated from the equation in Figure D, which was determined from the calibration curve and the argon meter reading, which was 50. Calculated values of flow rate and partial pressure are depicted in Table E 1.

Sulphidation of copper coolers in PGM smelters

Table E 1: HCl vapour pressure and flow rate calculated data

Parameters	values	Units
Temp	25	°C
Ar flow rate	0.252	l/min
HCl partial pressure	32.5	mm Hg
HCl partial pressure	0.043	atm
HCl flow rate	0.011	l/min
HCl flow rate	0.675	l/h

Determination of the amount of water in the argon stream

Water vapour was added with the sulphur gas during sulphidation laboratory tests to determine the effect of water vapour on the corrosion product morphology. To determine the amount of water vapour added, the procedure used to determine the HCl vapour was used. The vapour pressure of the liquid water was calculated from Equation E 1, where A, B and C are thermodynamic coefficients of (water) and where P is the vapour pressure of the water and T is the temperature of the bubbler, which was controlled at 80°C in this study [Love et al. 1992; Logue et al. 2004].

The summary of the calculated values of water vapour pressure and flow rate is in Table E 2. The water vapour flow rate was calculated from Equation E 3:

$$F_{H_2O} = F_{Ar} \frac{P_{H_2O}}{P_{atm} - P_{H_2O}}$$ Equation E 3

where F_{H_2O} is the water molar flow rate, F_{Ar} the molar flow rate of a carrier gas (argon), P_{H_2O} is the vapour pressure of water calculated from Equation E 1, P_{atm} is the bubbler pressure, which in this case is atmospheric.

F_{Ar} was calculated from the equation in Figure D, which was determined from the calibration curve and the argon meter reading, which was 50.

$$F_{Ar}(ml/s) = 0.0827x + 0.0609$$

$$F_{Ar}(ml/s) = 0.0827 \times 50 + 0.0609 = 4.1959 \ ml/s$$

$$F_{Ar} = 0.252 \ l/\min$$

Table E 2: Water vapour pressure and flow rate calculated data

Parameters	Values	Units
A	8.07	
B	1730.63	
C	233.42	
Temp	80	°C
Ar flow rate	0.252	l/min
H_2O partial pressure	354.53	mm Hg
H_2O partial pressure	0.47	atm
H_2O flow rate	0.22	l/min
H_2O flow rate	13.22	l/h

Determination of the amount of hydrogen sulphide synthesised

A schematic diagram of the setup used to determine the amount of H$_2$S synthesised is depicted in Figure E1 [Gudyanga et al. 1999]. Stage I was synthesis of H$_2$S gas by reacting synthetic FeS with dikute sulphuric acid solution according to Equation E1.

The H$_2$S was bubbled through a potassium dichromate solution in which the H$_2$S gas is oxidised by the chromate ions forming Cr(III). Ferrous sulphate solution was titrated by a chrome sulphide solution (from stage II) to determine the amount of Cr(III) formed in Stage II. Diphylamine indicator was used for the titration; the end point was indicated by a change in solution colour from light green to pink [Gudyanga et al. 1999].
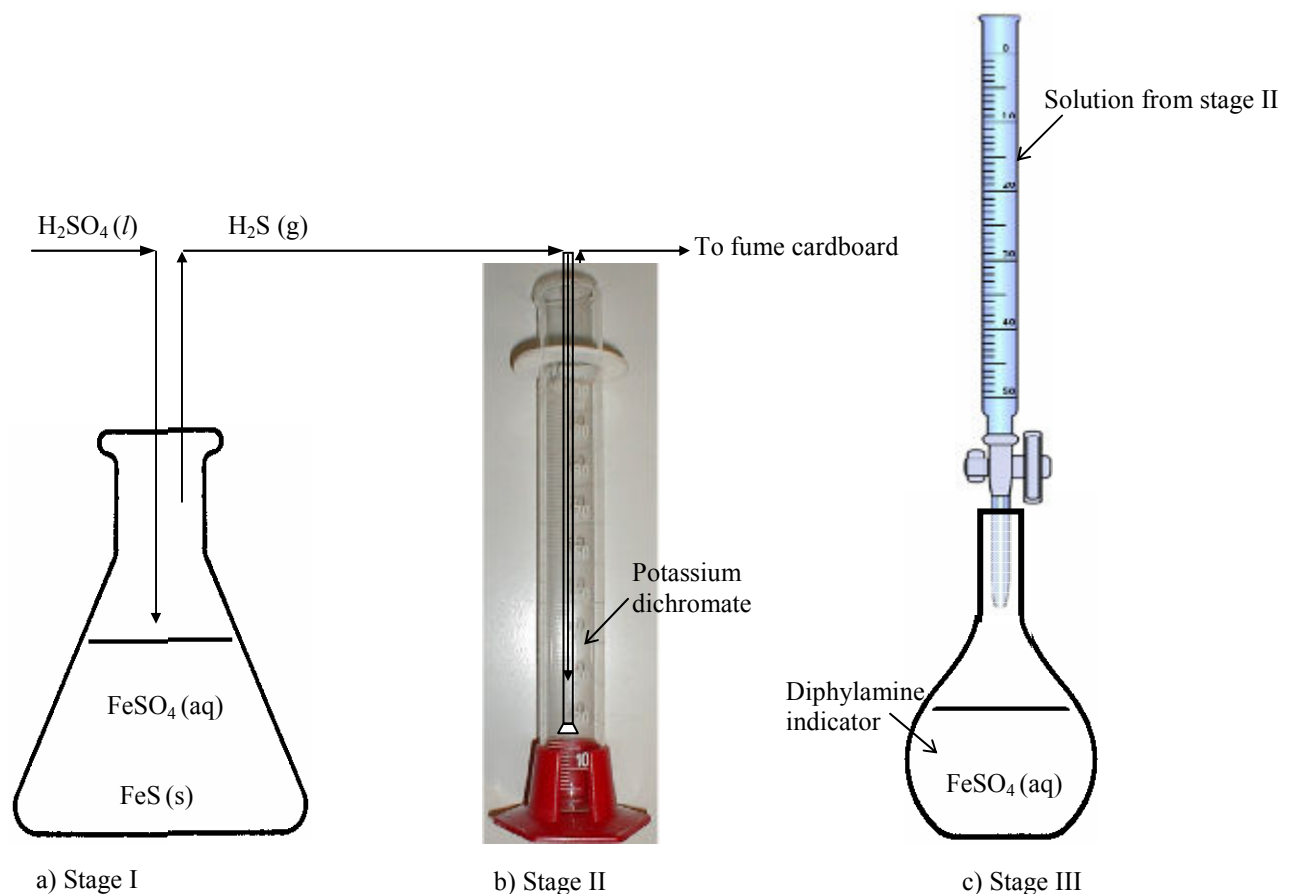
Figure E 1: Schematic diagram of the H$_2$S gas detection setup.

$$4Cr_2O_7^{2-} + 3H_2S + 29H^+ = 8Cr^{3+} + 3HSO_4^- + 16H_2O \qquad \text{Equation E 4}$$

Sulphidation of copper coolers in PGM smelters

$$Cr_2O_7^{2-} + 14H^+ + 6Fe^{2+} = 2Cr^{3+} + 6Fe^{3+} + 7H_2O \qquad \text{Equation E 5}$$
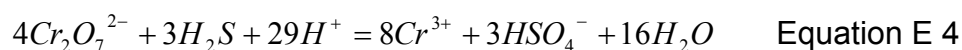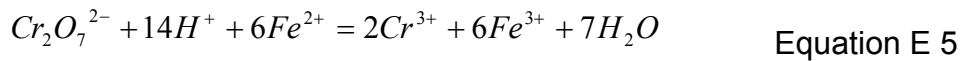
From the volume determined in stage III it was possible to calculate the amount of Cr (III) generated in Equation E 2 and hence the amount of hydrogen sulphide evolved from stage I, Equation E 1

The calculated values of moles and titration volumes are summarised in Table E3. According to the titration results only 0.05 moles of H_2S reacted with the dichromate which is 50% of the moles that were theoretically formed in Equation E4. This implies that the scrubbling process was not efficient or less H_2S was formed in Equation 4. Scrubbing could be improved by using a longer flask e.g 2 litre flask instead of 1 litre which was used in this test work. To improve the efficiency of the process in Equation 4 an inert gas should be bubbled through the acid (H_2SO_4) prior to reacting the gas with FeS, inert gas will reduce the oxygen in the acid and this favours the formation H_2S.

Density H_2S (g/L) =	1.36
Mass H_2S (g) =	3.88
Volume H_2S (L) =	2.84
PV=nRT	
n (mol) =	0.11
R (J/mol.K =	8.31
T (K) =	298.0
V (L) =	2.84
P (kPa) =	95.92

Table E 3: Summary of the calculated data for the H₂S determination

(stoichiometry)	FeS(s)	+	H₂SO₄(aq)	+	5H₂O	=	FeSO₄(aq)	+	H₂S(g)
mass (g)	10		11.16		10.24		17.28		3.88
Molar mass (g/mol)	87.92		98.08		18		151.91		34.08
mols	0.11		0.11		0.57		0.11		0.11
g:ml			1.84						
volume (ml)			6.06		30				

(stoichiometry)	4K₂Cr₂O₇	+	3H₂S	+	6H⁺	=	K₂SO₄	+	2CrCl₃	+	3H₂O	+	H⁺
	4		3		6		1		2		3		1

(stoichiometry)	K₂Cr₂O₇	+	6FeSO₄.7H₂O	+	14H⁺	=	2Cr³⁺	+	6Fe³⁺	+	7H₂O
	1		6								
volume (ml)	2000		25.0								
mass (g)	50		2								
Molar mass (g/mol)	294.18		277.91								
mols	0.17		0.0072								
concentrate (mol/L)	0.085		0.0072								

Before H₂S was bubbled through the dichromate

Before H₂S was bubbled through the dichromate

volume fresh sample dichromate	0.38	ml
conc fresh sample dichromate	0.07986	mol/L

dichromate residue volume	1.70	ml
concentrate residue dichromate	0.01764	mol/L
Moles of dichromate consumed	0.05	mol/L
% H₂S scrubbed	50%	

Sulphidation of copper coolers in PGM smelters

Sulphidation of copper coolers in PGM smelters